ISSN: 2152-7385 Volume 2, Number 12, December 2011

Scientific Research

Applied Mathematics

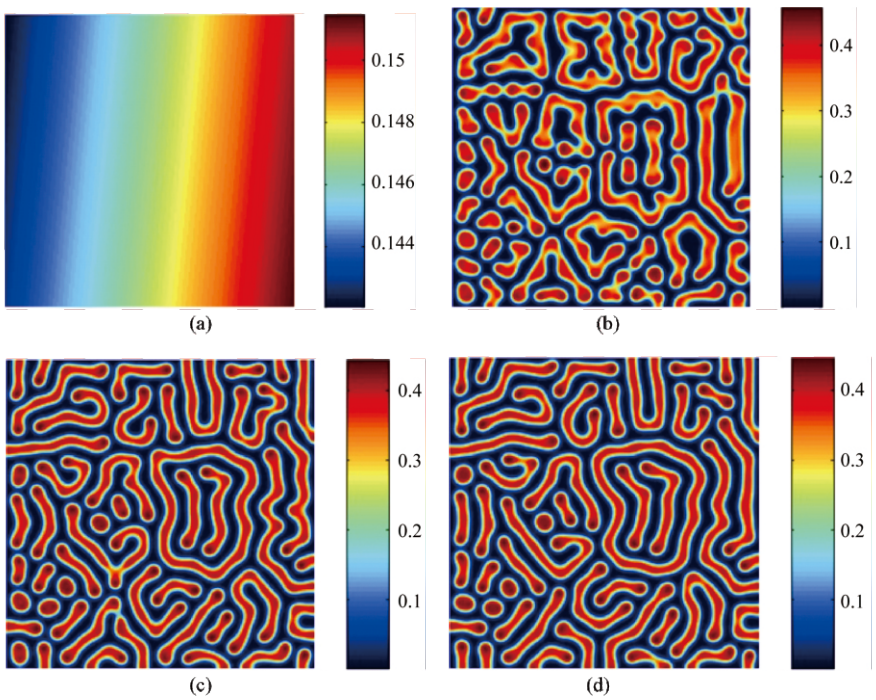

ISSN: 2152-7385

www.scirp.org/journal/am

Journal Editorial Board

ISSN Print: 2152-7385 ISSN Online: 2152-7393

http://www.scirp.org/journal/am

Editor in Chief

Editorial Board

Editorial Assistant

Applied Mathematics, 2011, 2, 1425-1550
Published Online December 2011 in SciRes (http://www.SciRP.org/journal/am/)

TABLE OF CONTENTS

Volume 2 Number 12 December 2011

Applied Mathematics, **2011, 2, 1425-1550**
Published Online December 2011 in SciRes (http://www.SciRP.org/journal/am/)

The figure on the front cover is from the article published in Applied Mathematics, 2011, Vol. 2, No. 12, pp. 1507-1514, by Dawit Melese and Sunita Gakkhar.

Applied Mathematics (AM)

Journal Information

SUBSCRIPTIONS

The *Applied Mathematics* (Online at Scientific Research Publishing, www.SciRP.org) is published monthly by Scientific Research Publishing, Inc., USA.

Subscription rates:

Print: $59 per issue.
To subscribe, please contact Journals Subscriptions Department, E-mail: sub@scirp.org

SERVICES

Advertisements
Advertisement Sales Department, E-mail: service@scirp.org

Reprints (minimum quantity 100 copies)
Reprints Co-ordinator, Scientific Research Publishing, Inc., USA.
E-mail: sub@scirp.org

COPYRIGHT

PRODUCTION INFORMATION

For manuscripts that have been accepted for publication, please contact:
E-mail: am@scirp.org

Applied Mathematics, 2011, 2, 1425-1431
doi:10.4236/am.2011.212201 Published Online December 2011 (http://www.SciRP.org/journal/am)

The Physical Transient Spectrum for a Multi-Photon V-Type Three-Level Atom Interacting with a Squeezed Coherent Field in the Presence of Nonlinearities

Fahmy K. Faramawy[1], Abd El-Hameed Abd-Riheem Eied[2]
[1]*Mathematics Department, Faculty of Science, Al-Azhar University, Cairo, Egypt*
[2]*Department of Mathematics, Faculty of Science, Shaqra University, Shaqra, Saudi Arabia*
E-mail: fkf54@yahoo.com
Received May 24, 2011; *revised June* 22, 2011; *accepted July* 1, 2011

Abstract

We study the interaction of a multi-photon three-level atom with a single mode field in a cavity, taking explicitly into account the existence of forms of nonlinearities of both the field and the intensity-dependent atom-field coupling. The analytical forms of the emission spectrum is calculated using the dressed states of the system. The effects of photon multiplicities, mean photon number, detuning, Kerr-like medium and the intensity-dependent coupling functional on the emission spectrum are analyzed.

Keywords: Emission Spectrum, Nonlinearities, Multi-Photon Process

1. Introduction

The spectrum of spontaneous emission of a V-configuration three-level atom, whose two upper levels are coupled by a classical field and their energy spacing is much larger than the spontaneous emission widths has been investigated [1]. It has been shown that the spontaneously generated interference can induce the spectrum to exhibit six peaks and depend on the phase of the classical field. The effects of a broadband squeezed vacuum on three-level atoms at different configurations (Λ, V and Ξ configurations) have also been investigated [2-5]. Further work has also been done to study the resonance fluorescence spectra of three-level atoms interacting with two coherent lasers and two independent squeezed vacuum [3-5]. The fluorescence spectrum for a strongly driven three-level system in which one of the two photon transition is coupled to a finite-bandwidth squeezed vacuum field has been examined [4]. Quantum interference effects in resonance fluorescence and absorption spectra of a V-type three-level atom damped by a broadband squeezed vacuum, studied in [6].

In recent years, there has been tremendous progress in the ability to generate states of the electromagnetic field with manifestly quantum or nonclassical characteristics experimentally [7-9]. Squeezed states of light are nonclassical states for which the fluctuations in one of two quadrature phase amplitudes of the electromagnetic field drop below the level of fluctuations associated with the vacuum state of the field. Squeezed states therefore provide a field which is in some sense quieter than the vacuum state and hence can be employed to improve measurement precision beyond the standard quantum limits.

The goal of this paper is to shed some light on the emission spectrum for a general three-level system. The model we shall consider is consisting of a single V-type three level atom interacting with a multi-photon one mode field in a perfect cavity, including acceptable kinds of nonlinearities of both the field and the intensity-dependent atom-field coupling. To reach our goal it is more convenient to use exact expression for the unitary operator $U(t)$ in the frame of the dressed state formalism. This will be considered in Section 2. In Section 3 we employ the analytical results obtained to find an analytical expression for the emission spectrum by using the finite double-Fourier transform of the two-time field correlation function. By a numerical computation, we examine the influence of photon multiplicities, mean photon number, detuning parameters,the functional dependence of the coupling as well as the nonlinearity parameter on the emission spectrum in Section 4. Finally the conclusions are summarized in Section 5.

2. Formulation of the Problem

The Hamiltonian of the system in the rotating-wave app-

roximation is of the form ($\hbar = 1$)

$$H = H_0 + H_{in} \tag{1}$$

$$H_0 = \sum_{j=1}^{3} \omega_j \sigma_{j,j} + \Omega \hat{a}^{+} \hat{a} \tag{2}$$

The operators $\hat{a}$ and $\hat{a}^{+}$ are the boson operators for the field satisfying $[\hat{a}, \hat{a}^{+}] = 1$. Where ω_1, ω_2 and ω_3 are the atomic levels energies ($\omega_1 > \omega_2 > \omega_3$) and Ω is the field frequency, with the detuning parameters Δ_1 and Δ_2 (as shown in **Figure 1**) given by

$$\Delta_1 = -k\Omega + (\omega_1 - \omega_3), \Delta_2 = -k\Omega + (\omega_2 - \omega_3) \tag{3}$$

The interaction part of the Hamiltonian in the presence of an arbitrary nonlinear medium, via multi-photon process k can be written as

$$\begin{aligned} H_{in} = {} & \Re(\hat{a}^{\dagger}\hat{a}) + \lambda_1 \left(\sigma_{13} f_1(\hat{a}^{\dagger}\hat{a}) \hat{a}^{k} + \hat{a}^{+k} f_1(\hat{a}^{\dagger}\hat{a}) \sigma_{31} \right) \\ & + \lambda_2 \left(\sigma_{23} f_2(\hat{a}^{\dagger}\hat{a}) \hat{a}^{k} + \hat{a}^{+k} f_2(\hat{a}^{\dagger}\hat{a}) \sigma_{32} \right). \end{aligned} \tag{4}$$

$\Re(\hat{a}^{\dagger}\hat{a})$ and $f(\hat{a}^{\dagger}\hat{a})$ are Hermitian operators functions of photon number operators, such that $\lambda_1 f_1(\hat{a}^{\dagger}\hat{a})$ and $\lambda_2 f_2(\hat{a}^{\dagger}\hat{a})$ represents an arbitrary intensity-dependent atom-field coupling, while $\Re(\hat{a}^{\dagger}\hat{a})$ denotes the one-mode field nonlinearity which can model Kerr-like medium nonlinearity as will be discussed later. The operators σ_{ij} satisfy the following commutation relations $[\sigma_{ij}, \sigma_{\kappa l}] = \sigma_{il}\delta_{j\kappa} - \sigma_{\kappa j}\delta_{il}$, $[\hat{a}, \sigma_{ij}] = 0$.

The initial state $|\Psi(0)_{AF}\rangle$ of the combined atom-field system may be written as

$$|\Psi(0)_{AF}\rangle = |\Psi(0)_A\rangle \otimes |\Psi(0)_F\rangle \tag{5}$$

where $|\Psi(0)_A\rangle = |1\rangle\langle 1|$ the initial state of the atom and $|\Psi(0)_F\rangle = |\Theta\rangle\langle\Theta|$ is the initial state of the field. The initial state $|\Theta\rangle = \sum p^{(n)} |n\rangle$ where the probability amplitude $p^{(n)}$ is defined in the usual manner as $p^n = \langle n | \Theta \rangle$.

The time evolution between the atom and the field is defined by the unitary evolution operator generated by H. Thus $U(t)$ is given by:

$$U(t) \equiv \exp(-iHt).$$

This unitary operator $U(t)$ is written as

$$\begin{aligned} U(t) = {} & \sum_{s=0}^{k-1} \exp(-iE_{03}^{(s)} t) |\Phi^{(s)}\rangle\langle\Phi^{(s)}| \\ & + \sum_{n=k}^{\infty} \sum_{j=1}^{3} \exp(-iE_j^{(n)} t) |\Psi_j^{(n)}\rangle\langle\Psi_j^{(n)}| \end{aligned} \tag{6}$$

where j = 1, 2, 3 and the eigenvalues

$$E_{03}^{(s)} = \omega_3 + \Omega s + \Re(s), (s = 0, 1, \cdots, k-1)$$

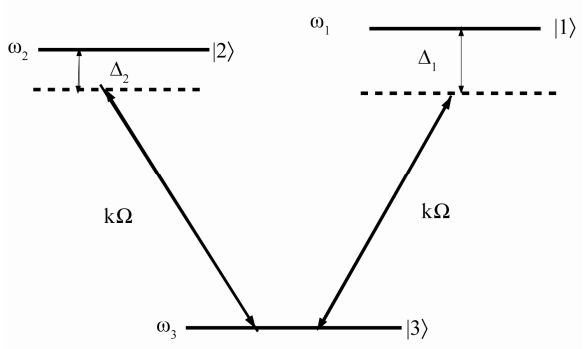

Figure 1. Energy level diagram for a *V*-type three-level atom with *k*-photon detuning Δ_1, Δ_2.

$$E_j^{(n)} = -\frac{X_1}{3} + \frac{2}{3}\left(\sqrt{X_1^2 - 3X_2}\right)\cos(\theta_j) \tag{7}$$

and

$$\theta_j = \left(\frac{1}{3}\cos^{-1}\left[\frac{9X_1X_2 - 2X_1^3 - 27X_3}{2\left(X_1^2 - 3X_2\right)^{\frac{3}{2}}} \right] + (j-1)\frac{2\pi}{3} \right), \tag{8}$$

with

$$\begin{aligned} X_1 &= -(r_1 + r_2 + r_3) \\ X_2 &= -\left[V_1^2 + V_2^2 - r_1 r_2 - r_1 r_3 - r_2 r_3 \right] \\ X_3 &= r_2 V_1^2 + r_1 V_2^2 - r_1 r_2 r_3 \\ r_1 &= \omega_1 + \Omega n + \Re(n) \\ r_2 &= \omega_2 + \Omega n + \Re(n) \\ r_3 &= \omega_3 + \Omega(n+k) + \Re(n+k) \\ V_1 &= \lambda_1 f_1(n) \sqrt{\frac{(n+k)!}{n!}}, V_2 = \lambda_2 f_2(n) \sqrt{\frac{(n+k)!}{n!}} \end{aligned} \tag{9}$$

and $|\Phi^{(s)}\rangle$, $|\Psi_j^{(n)}\rangle$ are the dressed states of the system associated with the eigenvalues $E_{03}^{(s)}$ and $E_j^{(n)}$, (j = 1, 2, 3).

$$\begin{aligned} |\Phi^{(s)}\rangle &= |s, 3\rangle, (s = 0, 1, \cdots, k-1) \\ |\Psi_j^{(n)}\rangle &= \alpha_j^{(n)} |n, 1\rangle + \beta_j^{(n)} |n, 2\rangle + \gamma_j^{(n)} |n+k, 3\rangle \end{aligned} \tag{10}$$

where

$$\begin{pmatrix} \alpha_j^{(n)} \\ \beta_j^{(n)} \\ \gamma_j^{(n)} \end{pmatrix} = \frac{1}{M} \begin{pmatrix} -V_1\left(r_2 - E_j^{(n)}\right) \\ -V_2\left(r_1 - E_j^{(n)}\right) \\ \left(r_1 - E_j^{(n)}\right)\left(r_2 - E_j^{(n)}\right) \end{pmatrix} \tag{11}$$

$$M = \sqrt{(r_1 - E_j^{(n)})^2 (r_2 - E_j^{(n)})^2 + V_1^2 (r_2 - E_j^{(n)})^2 + V_2^2 (r_1 - E_j^{(n)})^2} \tag{12}$$

Having obtained the explicit form of the unitary operator $U(t)$, the eigenvalues and the eigenfunctions for the system under consideration, we are therefore in a position to discuss any property related to the atom or the field.

3. The Physical Transient Spectrum

In this section we derive the physical transient spectrum $S(\nu)$ by calculating the Fourier transform of the time averaged dipole-dipole correlation function $\left\langle \left(\sigma_{13}(t_1) + \sigma_{23}(t_1)\right)\left(\sigma_{31}(t_2) + \sigma_{32}(t_2)\right)\right\rangle$, The physical spectrum $S(\nu)$ of radiation field emitted by a cavity-bound atom is given by the expression [10].

$$S(\nu) = \Gamma \int_0^T \mathrm{d}t_1 \int_0^T \mathrm{d}t_2 \exp\left[-(\Gamma - i\nu)(T - t_1) - (\Gamma + i\nu)(T - t_2)\right] \times \left\langle \left(\sigma_{13}(t_1) + \sigma_{23}(t_1)\right)\left(\sigma_{31}(t_2) + \sigma_{32}(t_2)\right)\right\rangle. \tag{13}$$

where T is the interaction time and Γ is the bandwidth of the filter. After carrying out the various operations we get

$$\begin{aligned} S(\nu) = {} & \Gamma \sum_{s=0}^{k-1} \sum_{j=1}^{3} \left|p^{(s)}\right|^2 \left|\alpha_j^{(s)}\right|^2 \Upsilon(E_{03}^{(s)}, E_j^{(s)}) \\ & \times \left[\left|\alpha_j^{(s)}\right|^2 + \alpha_j^{*(s)} \beta_j^{(s)} + \alpha_j^{(s)} \beta_j^{*(s)} + \left|\beta_j^{(s)}\right|^2\right] \\ & + \Gamma \sum_{n=k}^{\infty} \sum_{i=1}^{3} \sum_{j=1}^{3} \left|p^{(n)}\right|^2 \left|\alpha_j^{(n)}\right|^2 \left|\gamma_i^{(n-k)}\right|^2 \Upsilon(E_i^{(n-k)}, E_j^{(n)}) \\ & \times \left[\left|\alpha_j^{(n)}\right|^2 + \alpha_j^{*(n)} \beta_j^{(n)} + \alpha_j^{(n)} \beta_j^{*(n)} + \left|\beta_j^{(n)}\right|^2\right] \end{aligned} \tag{14}$$

where

$$\Upsilon(x, y) = \left[\frac{1 + \exp(-2\Gamma T) - 2\exp(-\Gamma T)\cos(\nu + x - y)T}{\Gamma^2 + (\nu + x - y)^2}\right] \tag{15}$$

Thus the time averaged spectrum consists of resonant structures which arise from transitions among different dressed states. The final structure of the time averaged spectrum will depend on the form of the input photon distribution $p^{(n)}$. Due to the quantum interference between component states the oscillations in the cavity field become composed of different component states.

4. Results and Discussion

On the basis of the analytical solution presented in a previous section, we shall study numerically the physical transient spectrum in a a squeezed coherent initial field. The photon number distribution for a squeezed coherent state [11] can be written as

$$\left|P_n\right|^2 = s \frac{(\tanh r)^n}{2^n n! \cosh r} \left| H_n\left(\frac{\varepsilon}{\sqrt{2\cosh r \sinh r}}\right)\right|^2 \times \exp\left[-\left|\varepsilon\right|^2 + \tanh r \; Re(\varepsilon)^2\right], \tag{16}$$

where, $\varepsilon = \alpha \cosh r + \alpha^* \sinh r$, $\alpha = \left|\alpha\right| \exp(i\varsigma)$ and H_n is the Hermite polynomial. We suppose here the minor axis of the ellipse, representing the direction of squeezing, parallel to the coordinate of the field oscillator. The initial phase ς of α is the angle between the direction of coherent excitation and the direction of squeezing. The mean photon number of this field is equal to $\bar{n} = \left|\alpha\right|^2 + \sinh^2 r$. Putting $r = 0$ we get the photon distribution for an initial coherent state with $\bar{n} = \left|\alpha\right|^2$ whereas for $\alpha = 0$ the photon distribution for an initial squeezed vacuum state with $\bar{n} = \sinh^2 r$ is recovered. The latter distribution is oscillatory with zeros for odd n.

By means of dressed atom states, and quantum beats we know that when the number n changes by k unit, this coupling describes the spontaneous emission of k photon with a frequency close to Ω. Since the dressed state $\left|\Psi_3^{(n-k)}\right\rangle$ is totally decoupled from the other dressed states, it can not be populated [12,13]. Then the field can only couple such transitions where the final states are either $\left|\Psi_1\right\rangle$ or $\left|\Psi_2\right\rangle$ but not $\left|\Psi_3\right\rangle$ [12,14]. So, there are only six possible allowed spontaneous decays from the three perturbed states of $E^{(n)}$ (where $E^{(n)} = \left\{\left|\Psi_1^{(n)}\right\rangle, \left|\Psi_2^{(n)}\right\rangle, \left|\Psi_3^{(n)}\right\rangle\right\}$) to lower multiplicities $E_j^{(n-k)}$ [15,16]. Generally they are asymmetric, because the intensities of the symmetrically placed sidebands are not equal. While at exact resonance the spectrum becomes symmetric [16]. Due to the non population of the dressed state $\left|\Psi_3\right\rangle$ the two transitions $\left|\Psi_3\right\rangle \rightarrow \left|\Psi_1\right\rangle$ and $\left|\Psi_3\right\rangle \rightarrow \left|\Psi_2\right\rangle$ vanish [12-14]. Hence, the emission spectrum of V-type three-level atom for a single cavity field has four-peak structure. In what follows we shall consider the effect of men photon number, detuning parameters Δ_1, Δ_2, intensity dependent coupling $f_i(n)$ and the nonlinear Kerr medium parameter χ on the spectrum of the system under consideration.

4.1. Effect of Multiplicity and Mean Photon Number

For $k = 1$ small $\bar{n}$ Rabi vacuum peaks dominate the spectrum see **Figure 2.1(a)**. While by increasing the

mean photon number of the cavity field the effect of the vacuum state diminishes and we note that there is a central deep gap surrounded by two symmetric spikes beside a two symmetric peaks however with structure appear as one moves away from the center as shown in **Figure 2.2(a)**. This is due to that the central two peaks located at $\left(\nu + E_1^{(n-k)} - E_1^{(n)}\right)$ and $\left(\nu + E_2^{(n-k)} - E_2^{(n)}\right)$ coalescence into each other, giving a single double peak at the center of the spectrum, while the other two peaks giving the symmetric sidebands around the central structure (see **Figure 2.2(a)**). With further increase in the mean photon number and hence the variance the spectrum not only become quite rich, and the gap depth and width decrease because the central two peaks coalescence into each other further but also, the sidebands move away from the central line, and its height decreases while it gets wider and wider as long as the mean photon number $\bar{n}$ increases. Hance, at sufficiently large mean photon number the central two peaks merge to a single peak leading to a three-peak structure. In **Figure 2(b)** where $k=2$ the situation is completely changed, we note the appearance of two wall separated central spikes surrounded by two symmetric groups of small spikes, which their heights having a maximum for the small middle spikes. Also, the central structure which observed at $k=1$ disappearing here. The two central spikes which nearest to the center becomes higher and narrower as the mean photon number increase. But for $k=3$ the spectra dived in to two symmetric groups of spikes located around the center. By increasing the values of $\bar{n}$ the spectrum is quite rich. Also, we can observe that the side peaks move away from the central line, and its height decrease by increasing the mean photon number see **Figure 2.2(c)**. Finally, as the photon multiplicities number increase, the number of allowed transition between the dressed states increase and hence number of peaks appearing in the spectrum increase as *k* increase (compare frames in **Figures 2.1** and **2.2**).

4.2. Effect of Detuning

As we compare the figure **Figure 3** and **Figure 2.2** where the case of absence of detuning is considered, we generally may say that detuning adds asymmetry to the spectrum and the shape of the spectrum is changed on both sides of the central line. The left spikes is suppressed on changing Δ_1, Δ_2, while the right spikes is moving away from the resonant frequency and becomes higher as the values of the detuning parameters Δ_1, Δ_2 increase (compare frames 1, 2 in **Figure 3**. Also, the peaks at the left hand side decrease gradually, so that it disappear for a large values of the detuning parameters Δ_1, Δ_2 as shown in **Figure 3.2**. But, these phenomena takes place in a faster way as k decrease (compare frames a,b,c in **Figure 3.2**. Finally, not only the number of peaks, there position and there maximum heights depends on the detuning parameters Δ_1, Δ_2 but, also the photon number multiplicity *k*.

4.3. Effect of Kerr Medium

Now we will turn our attention to the effect on the spectrum $S(\nu)$ of the nonlinearity of the field with a Kerr-type medium due to the term $\Re(n)$ being taken in

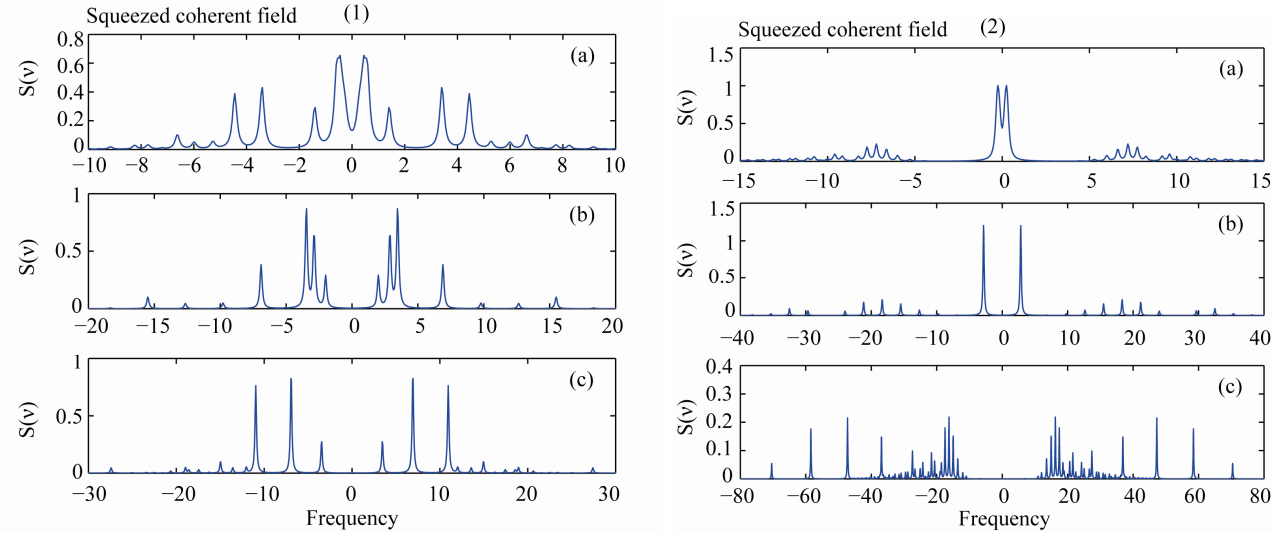

Figure 2. The evolution of the function $S(\nu)$ in a perfect cavity as a function of $(\nu - k\Omega)/\sqrt{\lambda_1\lambda_2}$ with $\lambda_{1,2}=1$, $\Delta_{1,2}=0$, $\chi=0$, $\Gamma=0.1$, $\varsigma=0$, $f_{1,2}(n)=1$, $T=100$ and (*a*) $k=1$; (*b*) $k=2$; (*c*) $k=3$ with (1) $r=1$, $a=1$; (2) $r=1.1$, $\alpha=\sqrt{5}$.

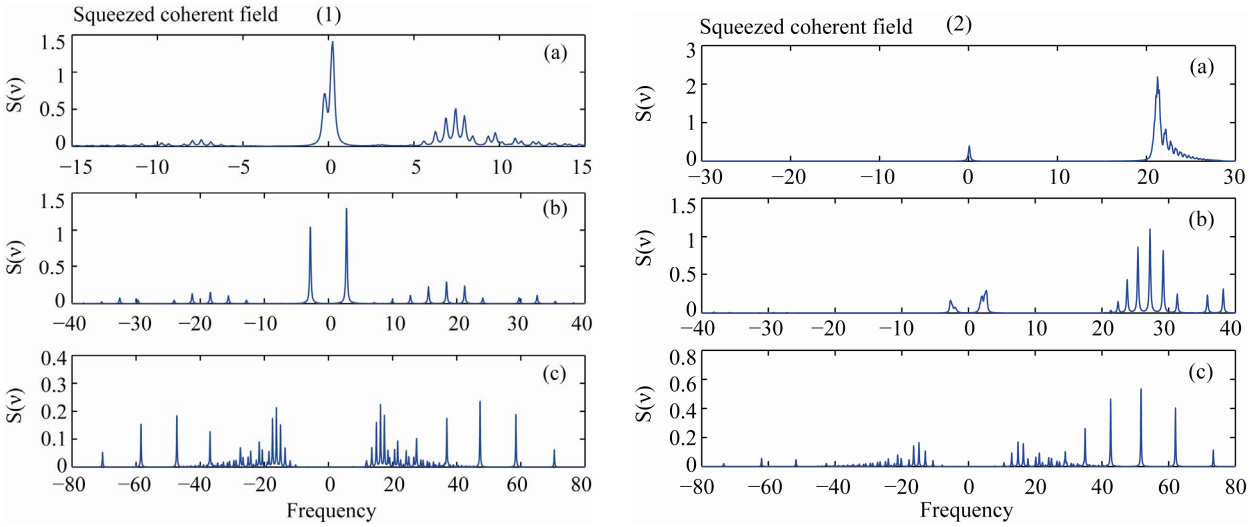

Figure 3. The same as Figure 2.2 but with, (1) $\Delta_1 = 5$, $\Delta_2 = 4$; (2) $\Delta_1 = \Delta_2 = 20$.

the form $\chi n(n-1)$, where χ is related to the third-order nonlinear susceptibility. In fact the optical Kerr effect is one of the most extensively studied phenomenon in the field of nonlinear optics because of its applications. The addition of the Kerr-like medium parameter to the problem adds asymmetry to the spectrum that can be seen from comparison of the cases considered in **Figure 4** with **Figures 2.2**. The right side peaks are suppressed while the left side peaks gain height and becomes narrower gradually as the values of χ increased see **Figure 4.2**. So that the right side hand peaks nearly disappear for a large values of χ see **Figure 4.2**. But this phenomena takes place in a slow way as k increase. We may conclude that, the effect of the Kerr-like medium is opposite to the effect of detuning. Furthermore, the effect of the nonlinear medium on the spectrum of the emitted light is the shift of the spectrum to the left and changing the amplitudes of the peaks depending on the value of χ, k. The maximum height of peaks increase as χ increases for all values of k. While the maximum height of peaks decrease as k increases for all values of χ.

4.4. Effect of Intensity Dependent Coupling Functional

In **Figure 5** we study the effect of different functionals of intensity dependent coupling $f_1(n), f_2(n)$ on the emission spectrum $S(\nu)$. When $f_1(n) = f_2(n) = \sqrt{n+1}$ the range of the spectrum is extended due to the larger stepwise excitation than that for $f_1(n) = f_2(n) = 1$. Also, the spectra divided into two groups of peaks which are symmetrically located around the central frequency for all values k (see **Figure 5.1**. Furthermore, not only the maximum height of peaks decrease but, the number of these peaks increases as k increase. When we consider $f_1(n) = f_2(n) = \frac{1}{\sqrt{n+1}}$ the stepwise excitation becomes smaller than that in the case $f_1(n) = f_2(n) = 1$. So that the sidebands become closer to each other, hence the number of peaks and the range of the spectrum decreases for all values of k see **Figure 5.2**. For $k = 1$ we get a situation similar to a Mollow spectrum (*i.e* only three peaks appears)which one gets in semiclassical fields see **Figure 5.2(a)**. While for $k = 2$ we note a deep gap between two higher wall spikes at the center surrounded by two lower side bands see **Figure 5.2(b)**. For $k = 3$ the two wall spikes which nearest to the center gain height (compare **Figure 5.2(c)** with **Figure 2.2(c)**). Finally, the spectrum can be controlled by choosing the right intensity-dependent coupling functional.

5. Conclusions

We have investigated the emission spectrum for a multi-photon V-type three-level atom, taking into account arbitrary forms of nonlinearities of both the field and the intensity-dependent atom-field coupling. The spectrum is calculated when the field initially in a squeezed coherent state. We have explored the influence of various parameters of the system on the emission spectrum. It is observed that

- For $k = 1$ the spectrum of V-type three-level atom for the cavity field has four-peak structure. But for sufficiently large values of the mean photon number the spectrum tends to a three peak structure.
- As the photon multiplicities number increase, the number of allowed transition between the dressed states increase and hence number of peaks increase as k icrease.

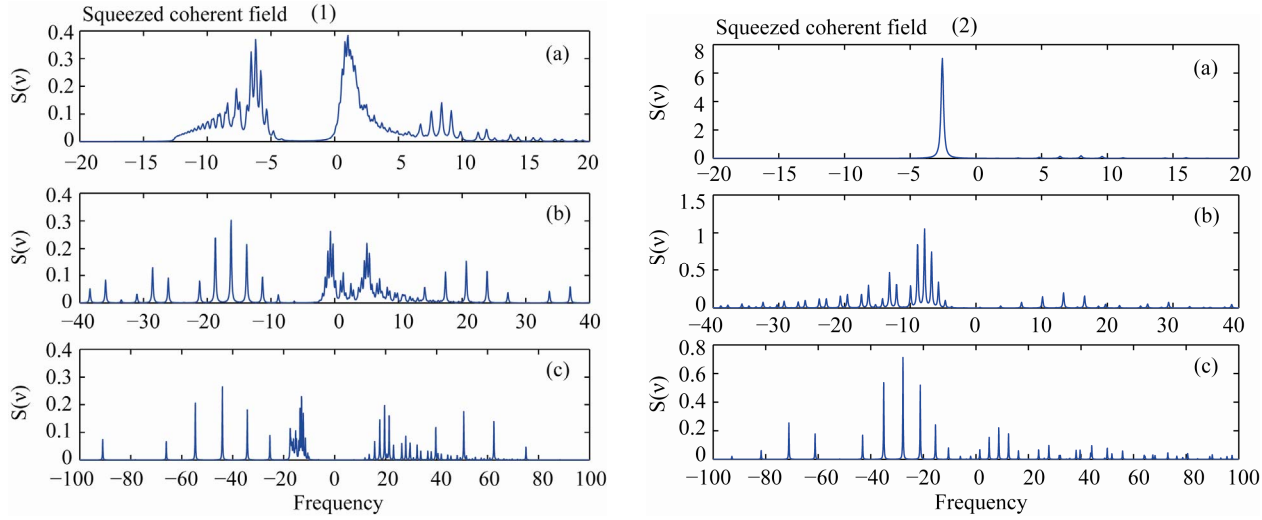

Figure 4. The same as Figure 2.2 but with, (1) $\chi = 0.1$; (2) $\chi = 0.8$.

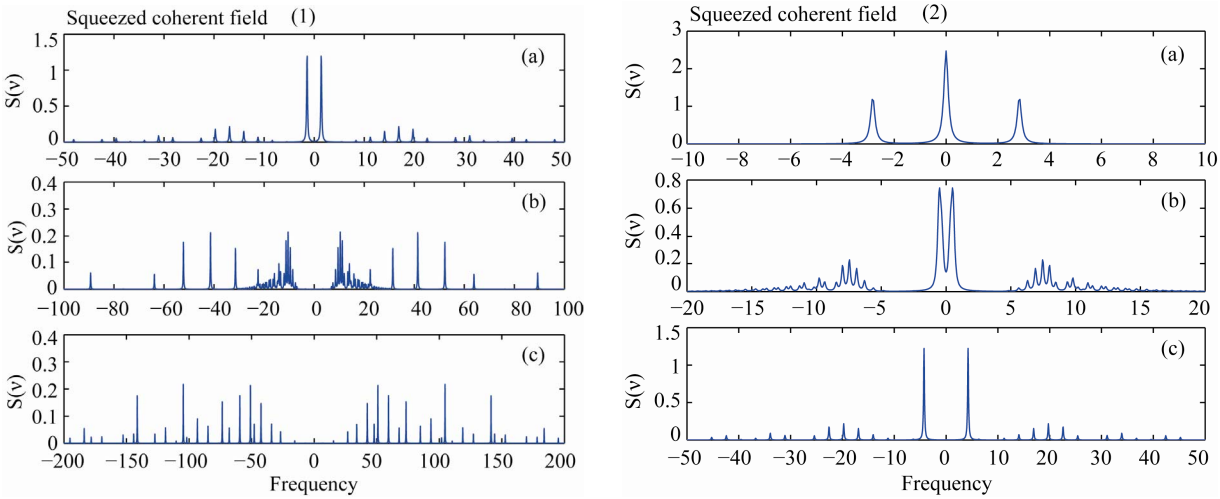

Figure 5. The same as Figure 2.2 but (1) $f_1(n) = f_2(n) = \sqrt{n}$; (2) $f_1(n) = f_2(n) = \frac{1}{\sqrt{n+1}}$.

- The peak position is associated with not only the photon number $(\bar{n})$ and the photon multiplicity number k but also the intensity-dependent atom-field coupling constant $\lambda_i f_i(n)$.
- The heights of the spectrum components becomes shorter and the distances between them is larger as the mean photon number increased.
- The symmetry shown in the standard three-level atom model for the spectra is no longer present once Kerr effect or detuning is considered.
- The effect of detuning on the spectrum of the emitted light is twofold. The first effect is the shift of the spectrum to the right side. The second effect is the dependence of the amplitudes and heights of the peaks on Δ_i.
- The Kerr medium has an effect opposite to the effect of the detuning, where the earlier has shorter elements. Also, the heights and widths of the peaks not only depend on the photon multiplicity but also on the value of χ. Consequently, changes in the detuning and the Kerr medium parameters can show in the spectra, and hence the heights of the peaks, their shifts and widths are altered compared with the case of resonance.
- The strong field effects can be produced by choosing the right parameters for these nonlinearities.

6. References

[1] C. Hooijer, G.-X. Li, K. Allaart and D. Lenstra, "Spontaneous emission in a V-Type Three-Level Atom Driven by a Classical Field," *Physics Letters A*, Vol. 263, No. 4-6, 1999, pp. 250-256.

doi:10.1016/S0375-9601(99)00718-5

[2] Z. Ficek and P. D. Drummond, "Three-Level Atom in a Broadband Squeezed Vacuum Field. I. General Theory," *Physical Review A*, Vol. 43, No. 11, 1991, pp. 6247-6257. doi:10.1103/PhysRevA.43.6247

[3] S. Smart and S. Swain, "Three-Level Atom in a Squeezed Vacuum II. Resonance Fluorescence," *Journal of Modern Optics*, Vol. 41, No. 6, 1994, pp. 1055-1077. doi:10.1080/09500349414551021

[4] B. J. Dalton, M. R. Ferguson and Z. Ficek, "Resonance Fluorescence Spectra of Three-Level Atoms in a Squeezed Vacuum," *Physical Review A*, Vol. 54, No. 3, 1996, pp. 2379-2390. doi:10.1103/PhysRevA.54.2379

[5] B. J. Dalton M. Bostick and Z. Fizec, "Probe Absorption Spectra for Driven Atomic Systems in a Narrow Bandwidth Squeezed Vacuum," *Physical Review A*, Vol. 53, No. 6, 1996, pp. 4439-4439. doi:10.1103/PhysRevA.53.4439

[6] O. G. Calderon, F. Carreno and M. A. Anton, "Quantum Interference Effects in Resonance Fluorescence and Absorption Spectra of a-Type Three-Level Atom Damped by a Broadband Squeezed Vacuum," *Optics Communications*, Vol. 221, No. 4-6, 2003, pp. 365-385. doi:10.1016/S0030-4018(03)01490-1

[7] D. F. Walls and G. J. Milburn, "Quantum Optics," Springer-Verlag, Berlin, 1994.

[8] C. M. Caves and B. L. Schumaker, "New Formalism for Two-Photon Quantum Optics. I. Quadrature Phase and Squeezed States," *Physical Review A*, Vol. 31, No. 5, 1985, pp. 3068-3092. doi:10.1103/PhysRevA.31.3068

[9] V. V. Dodonov, "Nonclassical States in Quantum Optics: A Squeezed Review of the First 75 Years," *Journal of Optics B*, Vol. 4, No. 1, 2002, p. R1. doi:10.1088/1464-4266/4/1/201

[10] J. H. Eberly and K. Wodkiewicz, "The Time-Dependent Physical Spectrum of Light," *Journal of the Optical Society of America*, Vol. 67, No. 9, 1977, pp. 1252-1261. doi:10.1364/JOSA.67.001252

[11] R. Loudon, "Quantum Statistics of Linear and Nonlinear Optical Phenomena," *Optica Acta*: *International Journal of Optics*, Vol. 31, No. 8, 1984, pp. 847-852. doi:10.1080/713821593

[12] S.-Y. Zhu, R. C. F. Chan and C. P. Lee, "Spontaneous Emission from a Three-Level Atom," *Physical Review A*, Vol. 52, No. 1, 1995, pp. 710-716. doi:10.1103/PhysRevA.52.710

[13] G. X. Li, K. Allaart, C. Hooijer and D. Lenstra, "Spontaneous Emission in a V-Type Three-Level Atom Driven by a Classical Field," *Physics Letters A*, Vol. 263, No. 4-6, 1999, pp. 250-256. doi:10.1016/S0375-9601(99)00718-5

[14] P. Dong and S. H. Tang, "Absorption Spectrum of a V-Type Three-Level Atom Driven by a Coherent Field," *Physical Review A*, Vol. 65, 2002, Article ID 033816, 10 Pages.

[15] C. Cohen-Tannoudji and S. Reynaud, "Dressed-Atom Description of Resonance Fluorescence and Absorption Spectra of a Multi-Level Atom in an Intense Laser Beam," *Journal of Physics B*, Vol. 10, No. 3, 1977, p. 345. doi:10.1088/0022-3700/10/3/005

[16] C. Cohen-Tannoudji and S. Reynaud, "Simultaneous Saturation of Two Atomic Transitions Sharing a Common Level," *Journal of Physics B*, Vol. 10, No. 12, 1977, p. 2311. doi:10.1088/0022-3700/10/12/010

Applied Mathematics, 2011, 2, 1432-1436
doi:10.4236/am.2011.212202 Published Online December 2011 (http://www.SciRP.org/journal/am)

Approximate Analytical Solutions for the Nonlinear Brinkman-Forchheimer-Extended Darcy Flow Model

Basant K. Jha[1], Muhammad L. Kaurangini[2*]
[1]*Department of Mathematics, Ahmadu Bello University, Zaria, Nigeria*
[2]*Department of Mathematical Sciences, Kano University of Science and Technology, Wudil, Nigeria*
E-mail: [*]*kaurangini@yahoo.com*
Received September 6, 2011; *revised November* 6, 2011; *accepted November* 13, 2011

Abstract

New approximate analytical solutions for steady flow in parallel-plates channels filled with porous materials governed by non-linear Brinkman-Forchheimer extended Darcy model for three different physical situations are presented. These results are compared with those obtained from an implicit finite-difference solution of the corresponding time dependent flow problem. It is seen that the time dependent flow solutions yield the almost same steady state values as obtained by using the new approximate analytical solutions

Keywords: Non-Linear, Darcy, Time Dependent Flow, Steady State

1. Introduction

The behaviour of fluid flow in porous media has achieved considerable attention due to its important practical applications. Applications include packed-bed catalytic reactor, geothermal reservoir, drying of porous solids, shell-side flow model in shell-and tube heat exchanger, petroleum resources and many others. Reference [1] and [2] studied the mixed convection flow problems in porous media based on the model of Darcy law. For flow through the porous media with solid boundary, [3] proposed the classical boundary term in addition to Darcy's law. This Brinkman-extended Darcy model analyzed the no slip boundary condition at the wall and showed that although the wall shear resistance has little influence on the pressure drop, it has drastic effects on stream-wise velocity component and heat transfer rate at the interface between porous media and solid boundary.

In many modern applications, porous media are characterized by high velocities, *i.e*., the Reynolds number based on mean pore size is grater than unity. In such cases, it is necessary to account for deviation from linearity in the momentum equation for porous media. This deviation is accounted for by the Forchheimer term representing the quadratic drag which is essential for large particle Reynolds numbers. From the physical point quadratic drag appears in the momentum equation for porous media because of large filtration velocities, the form drag due to the solid obstacles becomes comparable with the surface drag due to friction [4].

Reference [5] also presented a closed form solution of the Brinkman-Forchheimer-extended Darcy momentum equation and the associated heat transfer equation for the case of fully developed flow with uniform heat flux at the boundary. They assumed a boundary-layer-type developed flow and as a consequence their solution is inaccurate when the inertia parameter is small and Darcy number approaches and exceeds the value of unity. Reference [6] reconsidered the analysis presented in [5] without invoking their boundary-layer assumption and derived a more general theoretical solution.

Recent results on the model (Brinkman-Forchheimer extended Darcy) presented are in [7-10]. In all the results presented above, no attempt was made to solve the nonlinear equations analytically.

In the present work, flow formation in a parallel plate channels filled with a fluid saturated porous media is analyzed analytically and numerically. The flow is described by the Brinkman-Forchheimer extended Darcy equation.

2. Mathematical Model

The physical problem under consideration consists of a steady laminar fully developed flow between two infinitely long horizontal parallel plates filled with porous material. The flow formation is caused either by pressure gradient or (and) by the movement of one of the bounding plates. The fluid is assumed to be Newtonian with uniform properties and the porous medium is isotropic

and homogeneous. The x'-axis is taken along one of the plate while y'-axis is normal to it. Under the above mentioned assumption and using the dimensionless parameters given in the nomenclature, the equation of motion in porous media which accounts for the boundary and non-linear inertia term is

$$\gamma \frac{\mathrm{d}^2 u}{\mathrm{d}y^2} - \frac{u}{Da} - \frac{C}{\sqrt[4]{Da^n}} u^n + G = 0, \qquad (1)$$

The first term in the left-hand side of Equation (1) is the Brinkman term, second is the Darcy and third is the Forchheimer term $(n=2)$, hence the momentum transfer in the porous media is governed by steady Brinkman-Forchheimer extended Darcy model.

The boundary conditions in dimensionless form are:

$$\begin{aligned} u &= B \quad \text{at} \quad y = 0 \\ u &= 0 \quad \text{at} \quad \mathrm{y} = 1 \end{aligned} \qquad (2)$$

The above equations have been rendered in dimensionless form by using the non-dimensional parameters defined in nomenclature.

3. Analytical Solutions

By introducing the assumption $\alpha = u^{n-1}$ into Equation (1) it becomes

$$\gamma \frac{\mathrm{d}^2 u}{\mathrm{d}y^2} - \frac{u}{Da} - \frac{C\alpha}{\sqrt[4]{Da^n}} u + G = 0 \qquad (3)$$

Equation (3) has the solutions in Subsections 3.1-3.3.

3.1. Couette Flow [*G* = 0.0 and *B* = 1.0]

$$u(y) = \frac{\mathrm{Sinh}\left(\lambda(1.-y)\right)}{\mathrm{Sinh}(\lambda)} \qquad (4)$$

where $\lambda = \frac{1}{\sqrt{\gamma}} \sqrt{\frac{1}{Da} + \frac{C\alpha}{\sqrt[4]{Da^n}}}$

3.2. Pressure Driven Flow [*B* = 0 and *G* ≠ 0.0]

$$u(y) = \frac{G}{\gamma\lambda^2}\left[\frac{\mathrm{Sinh}(\lambda y) - \mathrm{Sinh}(1.-y)}{\mathrm{Sinh}(\lambda)} + 1.\right] \qquad (5)$$

3.3. Generalized Couette Flow [*B* = 1.0 and *G* ≠ 0.0]

$$\begin{aligned} u(y) = {} & \frac{\mathrm{Sinh}\left(\lambda(1.-y)\right)}{\mathrm{Sinh}(\lambda)} \\ & - \frac{G}{\gamma\lambda^2}\left[\frac{\mathrm{Sinh}\left(\lambda(1.-y)\right)}{\mathrm{Sinh}(\lambda)} + \frac{\mathrm{Sinh}(\lambda y)}{\mathrm{Sinh}(\lambda)} - 1.\right] \end{aligned} \qquad (6)$$

The Equations (4) to (6) can be used to find the values of the dimensionless velocity u as a function of dimensionless distance y in the interval [0,1] at the iteration $(i+1)$ in terms of value of λ at the iteration i. It should be noted here that λ is function of α which really stands for $u_i(y)$. Thus Equations (4) to (6) can be written in the following algorithmic form

$$u_{i+1}(y) = F\left(y, u_i(y)\right) \qquad (7)$$

4. Numerical Solution

The analytical solutions of the previous section are valid for steady state momentum transfer in porous medium containing Darcy, Brinkman and Forchheimer terms. To explore the limits of validity of these analytical solutions and to extend our investigation to time dependent momentum transfer in porous medium, numerical solution of the time dependent problem is obtained using implicit finite difference approach.

Consider the dimensionless form of time dependent momentum equation

$$\frac{\partial u}{\partial t} = \gamma \frac{\partial^2 u}{\partial y^2} - \frac{u}{Da} - \frac{C}{\sqrt[4]{Da^n}} u^n + G = 0 \qquad (8)$$

The first term in the right-hand side of Equation (8) is the Brinkman term, second is the Darcy and third is the Forchheimer term $(n=2)$, hence the momentum transfer in the porous media is governed by time dependent Brinkman-Forchheimer extended Darcy model.

The initial and boundary conditions in dimensionless form for the present problem are:

$$\begin{aligned} & u = 0, \quad \text{for all } y \text{ when } t \le 0, \\ & \text{at } y = 0: \ u = B, \\ & \text{at } y = 1: \ u = 0, \quad \text{for } t > 0 \end{aligned} \qquad (9)$$

The equations above also have been rendered in dimensionless form by using the non-dimensional parameters defined in nomenclature.

The numerical solution of Equation (8) using the initial and boundary conditions (9) is obtained by discretization of the momentum Equation (8) into the finite deference equation at the grid points (i, j). They are in order as follows:

$$\begin{aligned} \frac{u(i,j) - u(i,j-1)}{\Delta t} = {} & \gamma \frac{u(i+1,j) - 2u(i,j) + u(i,j-1)}{(\Delta y)^2} \\ & - \frac{u(i,j)}{Da} - \frac{C\left(u(i,j)\right)^n}{\sqrt[4]{Da^n}} + G \end{aligned} \qquad (10)$$

Here the index *i* refers to *y* and *j* to *t*. The partial time derivative is approximated by the backward difference

formula, while the second-order partial space derivative is approximated by the central difference formula. The above equation is solved by Thomas algorithm by manipulating into a system of linear algebraic equations in the tri-diagonal form.

In each time step, the process of numerical integration for every dependent variable starts from the first neighboring grid point of the plate at $y = 0$ and proceeds towards the another plate using the tri-diagonal form of the finite difference Equation (10) until it reaches at immediate grid point of the plate at $y = 1$.

In each time step the velocity field is obtained. The process of computation is advanced until a steady state is approached by satisfying the following convergence criterion:

$$\frac{\sum \left| A_{i,j+1} - A_{i,j} \right|}{M \left| A \right|_{\max}} < 10^{-6} \tag{12}$$

with respect to velocity field.

Here $A_{i,j}$ represents the velocity field, M is the number of interior grid points and $\left| A \right|_{\max}$ is the maximum absolute value of $A_{i,j}$.

In the numerical computation special attention is needed to specify Δt to get a steady state solution as rapidly as possible, yet small enough to avoid instabilities.

It is set, which is suitable for present computation, as

$$\Delta t = Stabr \times \left(\Delta y \right)^2 \tag{13}$$

The parameter *Stabr* is determined by numerical experimentation in order to achieve convergence and stability of the solution procedure. Numerical experiments show that the value 2 is suitable for numerical computations.

5. Results and Discussion

For the Brinkman-Forchheimer extension of Darcy equation to model the flow in a porous media (n = 2), B = 1.0, γ = 1.0, C = 0.52, Da = 0.01, and G = + 10.0, 0.0 and –10.0, the solutions of Equation (1) have been compared with the implicit finite-difference solution of Equation (8) in **Tables 1**, **2** and **3**, for Couette flow, pressure driven flow and generalized Couette flow respectively.

Table 1. B = 1.0, γ = 1.0, Da = 0.01, G = 0.0 & C = 0.52.

y	ANALYTICAL SOLUTION	NUMERICAL SOLUTION (IMPLICIT FINITE-DIFFERENCE SOLUTION)
0.0	1.00000	1.00000
0.1	0.36443	0.36457
0.2	0.13439	0.13381
0.3	0.04959	0.04923
0.4	0.01828	0.01813
0.5	0.00673	0.00668
0.6	0.00248	0.00246
0.7	0.00091	0.00090
0.8	0.00033	0.00032
0.9	0.00011	0.00010
1.0	0.00000	0.00000

Table 2. B = 0.0, γ = 1.0, Da = 0.01 & C = 0.52.

G = 10.0	y	ANALYTICAL SOLUTION	NUMERICAL SOLUTION (IMPLICIT FINITE-DIFFERENCE SOLUTION)
	0.0	0.00000	0.00000
	0.1	0.06306	0.06296
	0.2	0.08611	0.08606
	0.3	0.09450	0.09448
	0.4	0.09745	0.09744
	0.5	0.09817	0.09816
	0.6	0.09745	0.09744
	0.7	0.09450	0.09448
	0.8	0.08611	0.08606
	0.9	0.06306	0.06296
	1.0	0.00000	0.00000

$G = -10.0$			
	0.0	0.00000	0.00000
	0.1	–0.06335	–0.06331
	0.2	–0.08676	–0.08671
	0.3	–0.09536	–0.09532
	0.4	–0.09840	–0.09837
	0.5	–0.09915	–0.09912
	0.6	–0.09840	–0.09837
	0.7	–0.09536	–0.09532
	0.8	–0.08676	–0.08671
	0.9	–0.06335	–0.06331
	1.0	0.00000	0.00000

Table 3. $B = 1.0$, $\gamma = 1.0$, $Da = 0.01$ & $C = 0.52$.

$G = 10.0$	y	ANALYTICAL SOLUTION	NUMERICAL SOLUTION (IMPLICIT FINITE-DIFFERENCE SOLUTION)
	0.0	1.00000	1.00000
	0.1	0.42608	0.42646
	0.2	0.21942	0.21891
	0.3	0.14532	0.14313
	0.4	0.11546	0.11527
	0.5	0.10478	0.10470
	0.6	0.09988	0.09983
	0.7	0.09539	0.09536
	0.8	0.08643	0.08637
	0.9	0.06316	0.06306
	1.0	0.00000	0.00000
$G = -10.0$			
	0.0	1.00000	1.00000
	0.1	0.30250	0.30234
	0.2	0.04874	0.04808
	0.3	–0.04517	–004548
	0.4	–0.07984	–0.07992
	0.5	–0.09229	–0.09229
	0.6	–0.09587	–0.09584
	0.7	–0.09443	–0.09439
	0.8	–0.08643	–0.08637
	0.9	–0.06324	–0.06320
	1.0	0.00000	0.00000
$Gr = 0.0$			
	0.0	1.00000	1.00000
	0.1	0.36443	0.36457
	0.2	0.13439	0.13381
	0.3	0.04959	0.04923
	0.4	0.01828	0.01813
	0.5	0.00673	0.00668
	0.6	0.00248	0.00246
	0.7	0.00091	0.00090
	0.8	0.00033	0.00032
	0.9	0.00011	0.00010
	1.0	0.00000	0.00000

From the results presented in Tables, it can be noticed that the approximate analytical solutions presented in this work, though it is simple, it gives good and accurate results, and hence it can be efficiently used to solve this class of nonlinear differential equation models.

6. References

[1] W. J. Minkowycz, P. Cheng and R. N. Hirschberg, "Non-similar Boundary Layer Analysis of Mixed Convection about a Horizontal Heated Surface in a Fluid—Saturated Porous Medium," *International Communications in Heat and Mass Transfer*, Vol. 11, 1984, pp. 127-141. doi:10.1016/0735-1933(84)90017-4

[2] M. P. Cheng and C. H. Chang, "Mixed Convection about a Nonisothermal Cylinder and Sphere in a Porous Medium," *Numerical Heat and Mass Transfer*, Vol. 8, 1985, pp. 349-359.

[3] H. C. Brinkman, "A Calculation of the Viscous Force Exerted by a Flowing Fluid on a Dence Swarm of Particles," *Applied Scientific Research*, Vol. 1, No. 1, 1949, pp. 727-734.

[4] D. A. Nield and A. Bejan, "Convection in Porous Media," Springer-Verlag, New York, 1992.

[5] K. Vafai and S. J. Kim, "Forced Convection in a Channel filled with a Porous Medium: An Exact Solution," *Transactions of the ASME* (*American Society of Mechanical Engineers*) *Series C*: *Journal of Heat Transfer*, Vol. 111, No. 4, 1989, pp. 1103-1106. doi:10.1115/1.3250779

[6] D. A. Nield, S. L. M. Junqueira and J. L. Lage, "Forced Convection in a Fluid-Saturated Porous-Medium Channel with Isothermal or Iso-Flux Boundaries," *Journal of Fluid Mechanics*, Vol. 322, 1996, pp. 201-214. doi:10.1017/S0022112096002765

[7] M. A. Al-Nimr and T. K. Aldoss, "The Effect of the Macroscopic Local Inertial Term on the Non-Newtonian Fluid Flow in Channels Filled with Porous Medium," *International Journal of Heat and Mass Transfer*, Vol. 47, 2004, pp. 125-133. doi:10.1016/S0017-9310(03)00382-X

[8] B. A. Abu-Hijleh and M. A. Al-Nimr, "The Effect of the Local Inertial Term on the Fluid Flow in Channels Partially Filled with Porous Material," *International Journal of Heat Mass Transfer*, Vol. 44, No. 8, 2001, pp. 1565-1572. doi:10.1016/S0017-9310(00)00207-6

[9] A. F. Khadrawi and M. A. Al-Nimr, "The Effect of the Local Inertial Term on the Free Convection Fluid Flow in Vertical Channels Partially Filled with Porous Media," *Journal of Porous Media*, Vol. 6, No. 1, 2003, pp. 1-12. doi:10.1615/JPorMedia.v6.i1.40

[10] M. L. Kaurangini and B. K. Jha, "Effect of Inertial on Generalized Couette Flow in Composite Parallel Plates with Uniform Porous Medium in the Presence of Suction and Injection," *International Journal of Modelling, Simulation and Control* (*AMSE*), 2011, Article in Press.

Nomenclature

$\frac{\mathrm{d}p}{\mathrm{d}x}$ = axial pressure gradient

G = dimensionless pressure gradient, $\left(-\frac{H^3}{\rho\nu^2}\frac{\mathrm{d}p}{\mathrm{d}x}\right)$

H = total width of the channel

y' = dimensional co-ordinate

y = dimensionless co-ordinate, $\left(\frac{y'}{H}\right)$

n = index

C^* = inertia coefficient

C = dimensionless inertia coefficient, $\left(C^*\nu^{n-2}H^{\left[3-\frac{3n}{2}\right]}\right)$

U_0 = motion of the channel wall at $y' = 0$

B = dimensionless motion of the channel wall at $y' = 0$

K = permeability of the porous medium

Da = Darcy number, $\left(\frac{K}{H^2}\right)$

u' = velocity of the fluid

u = dimensionless velocity of the fluid, $\left(\frac{u'H}{\nu}\right)$

t' = dimensional time

t = dimensionless time, $\left(\frac{t'\nu}{H^2}\right)$

Greek symbols

ν_{eff} = effective kinematics viscosity of porous medium

ν = kinematics viscosity of fluid

γ = ratio of kinematics viscosity

G = dimensionless axial pressure gradient

Applied Mathematics, **2011, 2, 1437-1442**
doi:10.4236/am.2011.212203 Published Online December 2011 (http://www.SciRP.org/journal/am)

Scientific Research

On *p* and *q*-Horn's Matrix Function of Two Complex Variables

Ayman Shehata
Department of Mathematics, *Faculty of Science*, *Assiut University*, *Assiut*, *Egypt*
E-mail: *drshehata2006@yahoo.com*
Received September 24, 2011; *revised October* 25, 2011; *accepted November* 3, 2011

Abstract

The main aim of this paper is to define and study of a new Horn's matrix function, say, the *p* and *q*-Horn's matrix function of two complex variables. The radius of regularity on this function is given when the positive integers *p* and *q* are greater than one, an integral representation of ${}^{p}\mathrm{H}_{2}^{q}(A,A',B,B';C;z,w)$ is obtained, recurrence relations are established. Finally, we obtain a higher order partial differential equation satisfied by the *p* and *q*-Horn's matrix function.

Keywords: Hypergeometric Matrix functions, *p* and *q*-Horn's Matrix Function, Contiguous Relations, Matrix Functions, Matrix Differential Equation, Differential Operator

1. Introduction

Many special functions encountered in mathematical physics, theoretical physics, engineering and probability theory are special cases of hypergeometric functions [1]. Hypergeometric series in one and more variables occur naturally in a wide variety of problems in applied mathematics, statistics [2-4], and operations research and so on [5]. In [6,7], the hypergeometric matrix function has been introduced as a matrix power series and an integral representation. Moreover, Jódar and Cortés introduced, studied the hypergeometric matrix function $F(A,B;C;z)$, the hypergeometric matrix differential equation in [8] and the explicit closed form general solution of it has been given in [9]. Upadhyaya and Dhami have earlier studied the generalized Horn's functions of matrix arguments with real positive definite matrices as arguments [10] and this function H_7 also [11], while the author has earlier studied the Horn's matrix function H_2 of two complex variables under differential operators [7]. In [12, 13], extension to the matrix function framework of the classical families of *p*-Kummer's matrix functions and *p* and *q*-Appell matrix functions have been proposed.

Our purpose here is to introduce and study an extension of the matrix functions of two variables. This paper is organized as follows: Section 2 contains the definition of the *p* and *q*-Horn's matrix function of two variables, its radius of regularity and integral relation of the *p* and *q*-Horn's matrix function is given. Some matrix recurrence relations are established in Section 3. Finally, the effect of differential operator on this function is investigated and *p* and *q*-Horn's matrix partial differential equation are obtained in Section 4.

Throughout this paper D_0 will denote the complex plane cut along the negative real axis. The spectrum of a matrix A in $C^{N\times N}$, denoted by $\sigma(A)$ is the set of its eigenvalues of A. If A is a matrix in $C^{N\times N}$, its two-norm denoted by $\|A\|_2$ is defined by [14]

$$\|A\|_2 = \sup_{x\neq 0}\frac{\|Ax\|_2}{\|x\|_2}$$

where for a vector y in C^N, $\|y\|_2 = \left(y^T y\right)^{\frac{1}{2}}$ is the Euclidean norm of *y*.

If *f*(*z*) and *g*(*z*) are holomorphic functions of complex variables *z*, defined in an open set Ω of the complex plane, and if A and B are a matrix in $C^{N\times N}$ with $\sigma(A)\subset\Omega$ and $\sigma(B)\subset\Omega$ also and if $AB=BA$, then from the properties of the matrix functional calculus [15], it follows that

$$f(A)g(B) = g(B)f(A). \tag{1.1}$$

The reciprocal gamma function denoted by $\Gamma^{-1}(z)=\frac{1}{\Gamma(z)}$ is an entire function of the complex variable z. Then for any matrix A in $C^{N\times N}$, the image of $\Gamma^{-1}(z)$ acting on *A* denoted by $\Gamma^{-1}(A)$ is a welldefined

matrix. Furthermore, if

$$\begin{aligned} &A+nI \text{ is invertible for every} \\ &\text{non negative integer } n \end{aligned} \tag{1.2}$$

where I is the identity matrix in $C^{N\times N}$, then $\Gamma(A)$ is invertible, its inverse coincides with $\Gamma^{-1}(A)$ and one gets [8]

$$\begin{aligned} (A)_n &= A(A+I)\cdots(A+(n-1)I) \\ &= \Gamma(A+nI)\Gamma^{-1}(A); n \geq 1; (A)_0 = I. \end{aligned} \tag{1.3}$$

Jódar and Cortés have proved in [16], that

$$\Gamma(A) = \lim_{n\to\infty}(n-1)![(A)_n]^{-1}n^A. \tag{1.4}$$

Let P and Q be two positive stable matrices in $C^{N\times N}$. The gamma matrix function $\Gamma(P)$ and the beta matrix function $B(P,Q)$ have been defined in [16], as follows

$$\Gamma(P) = \int_0^\infty e^{-t}t^{P-I}\mathrm{d}t; t^{P-I} = e^{(P-I)\ln t} \tag{1.5}$$

and

$$B(P,Q) = \int_0^1 t^{P-I}(1-t)^{Q-I}\mathrm{d}t. \tag{1.6}$$

Let P and Q be commuting matrices in $C^{N\times N}$ such that the matrices $P+nI$, $Q+nI$ and $P+Q+nI$ are invertible for every integer $n \geq 0$. Then according to [8], we have

$$B(P,Q) = \Gamma(P)\Gamma(Q)\left[\Gamma\left(P+Q\right)\right]^{-1}. \tag{1.7}$$

2. Definition of *p* and *q*-Horn's Matrix Function

Suppose that p and q are positive integers. The p and q-Horn's matrix function ${}^p\mathrm{H}_2^q(A,A',B,B';C;z,w)$ of two complex variables is written in the form

$$\begin{aligned} &{}^p\mathrm{H}_2^q(A,A',B,B';C;z,w) \\ &= \sum_{m,n=0}^{\infty}\frac{(A)_{m-n}(A')_m(B)_n(B')_n[(C)_m]^{-1}}{(pm)!(qn)!}z^m w^n \end{aligned} \tag{2.1}$$

where $U_{m,n}(z,w) = V_{m,n}z^m w^n$ and

$$V_{m,n} = \frac{(A)_{m-n}(A')_m(B)_n(B')_n[(C)_m]^{-1}}{(pm)!(qn)!}.$$

For simplicity, we can write the ${}^p\mathrm{H}_2^q(A,A',B,B';C;z,w)$ in the form ${}^p\mathrm{H}_2^q$, ${}^p\mathrm{H}_2^q(A+I,A',B,B';C;z,w)$ in the form ${}^p\mathrm{H}_2^q(A\pm)$, $\cdots$, ${}^p\mathrm{H}_2^q(A,A',B,B';C+I;z,w)$ in the form ${}^p\mathrm{H}_2^q(C\pm)$.

We begin the study of this function by calculating its radius of regularity R of such function for this purpose we recall relation (1.3.10) of [17,18] and keeping in mind that $1 \leq \sigma_{m,n} \leq 2^{\frac{m+n}{2}}$. We define the radius of regularity of the function ${}^p\mathrm{H}_2^q(A,A',B,B';C;z,w)$ as

$$\begin{aligned} \frac{1}{R} &= \limsup_{m+n\to\infty}\left(\frac{\|V_{m,n}\|}{\sigma_{m,n}}\right)^{\frac{1}{m+n}} \\ &= \limsup_{m+n\to\infty}\left(\frac{\left\|(A)_{m-n}(A')_m(B)_n(B')_n[(C)_m]^{-1}\right\|}{(pm)!(qn)!\sigma_{m,n}}\right)^{\frac{1}{m+n}} \\ &= \limsup_{m+n\to\infty}\left\|\left(\frac{(m-n)^{-A}(A)_{m-n}}{(m-n-1)!}(m-n-1)!(m-n)^A\frac{m^{-A'}(A')_m}{(m-1)!}(m-1)!m^{A'}\frac{n^{-B}(B)_n}{(n-1)!}(n-1)!n^B\frac{n^{-B'}(B')_n}{(n-1)!}(n-1)!\right.\right. \\ &\qquad \left.\left.n^{B'}\frac{m^C[(C)_m]^{-1}}{(m-1)!}(m-1)!m^{-C}\right)\right\|^{\frac{1}{m+n}}\left(\frac{1}{(pm)!(qn)!\sigma_{m,n}}\right)^{\frac{1}{m+n}} \\ &= \limsup_{m+n\to\infty}\left\|\left(\frac{\Gamma(C)\Gamma^{-1}(A)\Gamma^{-1}(A')\Gamma^{-1}(B)\Gamma^{-1}(B')}{(m-n)^A m^{A'-C}n^{B+B'}}\right)\right\|^{\frac{1}{m+n}}\left(\frac{(m-n-1)!(n-1)!(n-1)!}{(pm)!(qn)!\sigma_{m,n}}\right)^{\frac{1}{m+n}} \end{aligned}$$

where $\sigma_{m,n} = \begin{cases}\left(\frac{m+n}{m}\right)^{\frac{m}{2}}\left(\frac{m+n}{n}\right)^{\frac{n}{2}}, m,n \neq 0; \\ 1, \qquad\qquad m,n = 0.\end{cases}$

Using Stirling formula and take $m = \mu n$ is a positive integer, then

$$\frac{1}{R} \le \limsup_{n\to\infty} \left\| \left([n(\mu-1)]^{A} (\mu n)^{A'-C} n^{B+B'} \right) \right\|^{\frac{1}{n(\mu+1)}} \left(\frac{(\mu n-n-1)!(n-1)!(n-1)!}{(p\mu n)!(qn)!} \right)^{\frac{1}{n(\mu+1)}}$$

$$= \limsup_{n\to\infty} \left(\frac{(\mu n-n-1)!(n-1)!(n-1)!}{(p\mu n)!(qn)!} \right)^{\frac{1}{n(\mu+1)}} = \limsup_{n\to\infty} \left(\frac{\sqrt{2\pi(\mu n-n-1)} \left(\frac{\mu n-n-1}{e} \right)^{\mu n-n-1}}{\sqrt{2\pi p\mu n} \left(\frac{p\mu n}{e} \right)^{p\mu n}} \frac{2\pi(n-1) \left(\frac{n-1}{e} \right)^{2(n-1)}}{\sqrt{2\pi qn} \left(\frac{qn}{e} \right)^{qn}} \right)^{\frac{1}{n(\mu+1)}}$$

$$= \limsup_{n\to\infty} \left(\frac{(\mu n-n-1)^{\frac{\mu-1}{\mu+1}} (n-1)^{\frac{2}{\mu+1}}}{n^{\frac{q+p\mu}{\mu+1}} q^{\frac{q}{\mu+1}} (p\mu)^{\frac{p\mu}{\mu+1}}} \right) = 0.$$

Summarizing, the following result has been established. As a conclusion, we get the following result.

Theorem 2.1. Let A, A', B, B' and C be matrices in $C^{N\times N}$ such that $C+mI$ are invertible for all integer $m \ge 0$. Then, the *p* and *q*-Horn's matrix function is an entire function in the case that, at least, one of the integers *p* and *q* are greater than one.

If $p=q=1$, then the function is convergence in $|z| \le r$, $|w| \le s$ and $(r+1)s=1$ in [5,19].

Integral form of the *p* and *q*-Horn Matrix Function

Suppose that A' and C are matrices in the space $C^{N\times N}$ of the square complex matrices, such that $A'C=CA'$, A', C and $C-A'$ are positive stable matrices.

By (1.3), (1.4) and (1.7) one gets

$$\begin{aligned} &(A')_m \left[(C)_m\right]^{-1} \\ &= \Gamma\left(A'+mI\right)\Gamma(C)\Gamma^{-1}(A')\Gamma^{-1}\left(C+mI\right) \\ &= \Gamma^{-1}(A')\Gamma^{-1}\left(C-A'\right)\Gamma(C)\int_0^1 t^{A'+(m-1)I}\left(1-t\right)^{C-A'-I}\,\mathrm{d}t. \end{aligned} \tag{2.2}$$

Substituting from (2.1) and (2.2), we see that

$$\begin{aligned} &{}^{p}\mathrm{H}_2^{q}(A,A',B,B';C;z,w) \\ &= \sum_{m,n=0}^{\infty} \frac{(A)_{m-n}(B)_n(B')_n}{(pm)!(qn)!} z^m w^n \\ &\quad \cdot \Gamma^{-1}(A')\Gamma^{-1}(C-A')\Gamma(C)\int_0^1 t^{A'+(m-1)I}(1-t)^{C-A'-I}\,\mathrm{d}t \\ &= \Gamma^{-1}(A')\Gamma^{-1}(C-A')\Gamma(C) \\ &\quad \cdot \int_0^1 t^{A'-I}\left(1-t\right)^{C-A'-I} {}^{p}_{3}\mathrm{F}_0^{q}(A,B,B';-;zt,w)\,\mathrm{d}t. \end{aligned}$$

Therefore, the following result has been established.

Theorem 2.2. Let A, A', B, B' and C be matrices in $C^{N\times N}$. Then the *p* and *q*-Horn's matrix function of two complex variables satisfies the following integral form

$$\begin{aligned} &{}^{p}\mathrm{H}_2^{q}(A,A',B,B';C;z,w) \\ &= \Gamma^{-1}(A')\Gamma^{-1}(C-A')\Gamma(C) \\ &\quad \cdot \int_0^1 t^{A'-I}\left(1-t\right)^{C-A'-I} {}^{p}_{3}\mathrm{F}_0^{q}(A,B,B';-;zt,w)\,\mathrm{d}t \end{aligned} \tag{2.3}$$

where

$${}^{p}_{3}\mathrm{F}_0^{q}(A,B,B';-;zt,w) = \sum_{m,n=0}^{\infty} \frac{(A)_{m-n}(B)_n(B')_n}{(pm)!(qn)!}(zt)^m w^n .$$

3. Matrix Recurrence Relations

Some recurrence relation are carried out on the *p* and *q*-Horn's matrix function. In this connection the following contiguous functions relations follow, directly by increasing or decreasing one in original relation

$$\begin{aligned} &{}^{p}\mathrm{H}_2^{q}(\mathrm{A}+) \\ &= \sum_{m,n=0}^{\infty} \frac{(A+I)_{m-n}(A')_m(B)_n(B')_n\left[(C)_m\right]^{-1}}{(pm)!(qn)!} z^m w^n \\ &= \sum_{m,n=0}^{\infty} A^{-1}(A+(m-n)I) \\ &\quad \cdot \frac{(A+I)_{m-n}(A')_m(B)_n(B')_n\left[(C)_m\right]^{-1}}{(pm)!(qn)!} \\ &= \sum_{m,n=0}^{\infty} A^{-1}(A+(m-n)I)U_{m,n}(z,w) \end{aligned} \tag{3.1}$$

and

$$\begin{aligned} {}^{p}\mathrm{H}_2^{q}(\mathrm{A}-) &= \sum_{m,n=0}^{\infty} \frac{(A-I)_{m-n}(A')_m(B)_n(B')_n\left[(C)_m\right]^{-1}}{(pm)!(qn)!} z^m w^n \\ &= \sum_{m,n=0}^{\infty} (A-I)[(A+(m-n-1)I)]^{-1}U_{m,n}(z,w). \end{aligned} \tag{3.2}$$

Similarly

$$
\begin{aligned}
&{}^{p}\mathrm{H}_2^q(A'+)=\sum_{m,n=0}^{\infty}A'^{-1}\left(A'+mI\right)U_{m,n}(z,w),\\
&{}^{p}\mathrm{H}_2^q(A'-)=\sum_{m,n=0}^{\infty}\left(A'-I\right)\left[\left(A'+\left(m-1\right)I\right)\right]^{-1}U_{m,n}(z,w),\\
&{}^{p}\mathrm{H}_2^q(B+)=\sum_{m,n=0}^{\infty}B^{-1}\left(B+nI\right)U_{m,n}(z,w),\\
&{}^{p}\mathrm{H}_2^q(B-)=\sum_{m,n=0}^{\infty}\left(B-I\right)\left[\left(B+\left(n-1\right)I\right)\right]^{-1}U_{m,n}(z,w),\\
&{}^{p}\mathrm{H}_2^q(B'+)=\sum_{m,n=0}^{\infty}B'^{-1}\left(B'+nI\right)U_{m,n}(z,w),\\
&{}^{p}\mathrm{H}_2^q(B'-)=\sum_{m,n=0}^{\infty}\left(B'-I\right)\left[\left(B'+\left(n-1\right)I\right)\right]^{-1}U_{m,n}(z,w),\\
&{}^{p}\mathrm{H}_2^q(\mathrm{C}+)=\sum_{m,n=0}^{\infty}C^{-1}\left(C+mI\right)U_{m,n}(z,w),\\
&{}^{p}\mathrm{H}_2^q(\mathrm{C}-)=\sum_{m,n=0}^{\infty}\left(C-I\right)\left[\left(C+\left(m-1\right)I\right)\right]^{-1}U_{m,n}(z,w).
\end{aligned}
\tag{3.3}
$$

4. The *p* and *q*-Horn's Matrix Function under the Differential Operator

Consider the differential operator D on the p and q-Horn's matrix function of two complex variables, defined in [7, 17] as

$$
D=\begin{cases}d_1+d_2, & m,n\geq 1\\ 1, & \text{otherwise}\end{cases}
$$

where $d_1=z\dfrac{\partial}{\partial z}$ and $d_2=w\dfrac{\partial}{\partial w}$. This operator has the property $Dz^m w^n=(m+n)z^m w^n$.

For the p and q-Horn's matrix function the following relations hold

$$
\begin{aligned}
&(DI+A)\ {}^{p}\mathrm{H}_2^q\\
&=\sum_{m,n=0}^{\infty}\left(A+\left(m+n\right)I\right)\\
&\qquad\cdot\frac{(A)_{m-n}(A')_m(B)_n(B')_n[(C)_m]^{-1}}{(pm)!(qn)!}z^m w^n\\
&=A^{p}\mathrm{H}_2^q(A+)+2d_2\,{}^{p}\mathrm{H}_2^q
\end{aligned}
\tag{4.1}
$$

and

$$
\begin{aligned}
&\left(d_1I+A'\right)\ {}^{p}\mathrm{H}_2^q\\
&=\sum_{m,n=0}^{\infty}\left(A'+mI\right)\frac{(A)_{m-n}(A')_m(B)_n(B')_n[(C)_m]^{-1}}{(pm)!(qn)!}z^m w^n\\
&=A'^{p}\mathrm{H}_2^q(A'+).
\end{aligned}
\tag{4.2}
$$

By the same way, we have

$$
\begin{aligned}
&\left(d_2I+B\right)^{p}\mathrm{H}_2^q=B^{p}\mathrm{H}_2^q(B+),\\
&\left(d_2I+B'\right)^{p}\mathrm{H}_2^q=B'^{p}\mathrm{H}_2^q(B'+),\\
&\left(d_1I+C-I\right)^{p}\mathrm{H}_2^q=(C-I)^{p}\mathrm{H}_2^q(C-).
\end{aligned}
\tag{4.3}
$$

From (4.1), (4.2) and (4.3), we get

$$
\begin{aligned}
\left(A-A'-B\right)^{p}\mathrm{H}_2^q&=A^{p}\mathrm{H}_2^q(A+)+2d_2\,{}^{p}\mathrm{H}_2^q\\
&\quad-A'^{p}\mathrm{H}_2^q(A'+)-B^{p}\mathrm{H}_2^q(B+),\\
\left(A-A'-B\right)^{p}\mathrm{H}_2^q&=A^{p}\mathrm{H}_2^q(A+)+2d_2\,{}^{p}\mathrm{H}_2^q\\
&\quad-A'^{p}\mathrm{H}_2^q(A'+)-B'^{p}\mathrm{H}_2^q(B'+).
\end{aligned}
\tag{4.4}
$$

From (4.1), (4.3) and (4.4), we have

$$
\begin{aligned}
\left(A-B-C\right)^{p}\mathrm{H}_2^q&=A^{p}\mathrm{H}_2^q(A+)+2d_2\,{}^{p}\mathrm{H}_2^q\\
&\quad-(C-I)^{p}\mathrm{H}_2^q(C-)+{}^{p}\mathrm{H}_2^q-B^{p}\mathrm{H}_2^q(B+),\\
\left(A-B'-C\right)^{p}\mathrm{H}_2^q&=A^{p}\mathrm{H}_2^q(A+)+2d_2\,{}^{p}\mathrm{H}_2^q\\
&\quad-\left(C-I\right)^{p}\mathrm{H}_2^q(C-)+{}^{p}\mathrm{H}_2^q-B'^{p}\mathrm{H}_2^q(B'+).
\end{aligned}
\tag{4.5}
$$

Also from (4.2), (4.3) and (4.4), we see that

$$
\begin{aligned}
&\left(A'-C\right)^{p}\mathrm{H}_2^q\\
&=A'^{p}\mathrm{H}_2^q(A'+)-\left(C-I\right)^{p}\mathrm{H}_2^q(C-)-{}^{p}\mathrm{H}_2^q,\\
&\left(B-B'\right)^{p}\mathrm{H}_2^q=B^{p}\mathrm{H}_2^q(B+)-B'^{p}\mathrm{H}_2^q(B'+),\\
&\left(A'-C-B+B'\right)^{p}\mathrm{H}_2^q\\
&=A'^{p}\mathrm{H}_2^q(A'+)-\left(C-I\right)^{p}\mathrm{H}_2^q(C-)\\
&\quad-{}^{p}\mathrm{H}_2^q-B^{p}\mathrm{H}_2^q(B+)+B'^{p}\mathrm{H}_2^q(B'+).
\end{aligned}
\tag{4.6}
$$

Now, we append this section by introducing the differential operator $d_1=z\dfrac{\partial}{\partial z}$ and $d_2=w\dfrac{\partial}{\partial w}$ to the entire functions in successive manner as follows;

$$\left[d_1\left(d_1-\frac{1}{p}\right)\left(d_1-\frac{2}{p}\right)\ldots\left(d_1-\frac{p-1}{p}\right)+d_2\left(d_2-\frac{1}{q}\right)\left(d_2-\frac{2}{q}\right)\ldots\left(d_2-\frac{q-1}{q}\right)\right]\ {}^{p}\mathrm{H}_2^{q}$$

$$=\sum_{m=1,n=0}^{\infty} m\left(m-\frac{1}{p}\right)\left(m-\frac{2}{p}\right)\ldots\left(m-\frac{p-1}{p}\right)\frac{(A)_{m-n}(A')_m(B)_n(B')_n[(C)_m]^{-1}}{(pm)!(qn)!}z^m w^n$$

$$+\sum_{m=0,n=1}^{\infty} n\left(n-\frac{1}{q}\right)\left(n-\frac{2}{q}\right)\ldots\left(n-\frac{q-1}{q}\right)\frac{(A)_{m-n}(A')_m(B)_n(B')_n[(C)_m]^{-1}}{(pm)!(qn)!}z^m w^n$$

$$=\frac{1}{p^p}\sum_{m=1,n=0}^{\infty} mp\left(\frac{pm-1}{p}\right)\left(\frac{pm-2}{p}\right)\ldots\left(\frac{pm-p+1}{p}\right)\frac{(A)_{m-n}(A')_m(B)_n(B')_n[(C)_m]^{-1}}{(pm)!(qn)!}z^m w^n$$

$$+\frac{1}{q^q}\sum_{m=0,n=1}^{\infty} nq\left(\frac{qn-1}{q}\right)\left(\frac{qn-2}{q}\right)\ldots\left(\frac{qn-q+1}{q}\right)\frac{(A)_{m-n}(A')_m(B)_n(B')_n[(C)_m]^{-1}}{(pm)!(qn)!}z^m w^n$$

$$=\frac{1}{p^p}\sum_{m=1,n=0}^{\infty}\frac{(A)_{m-n}(A')_m(B)_n(B')_n[(C)_m]^{-1}}{(pm-p)!(qn)!}z^m w^n+\frac{1}{q^q}\sum_{m=0,n=1}^{\infty}\frac{(A)_{m-n}(A')_m(B)_n(B')_n[(C)_m]^{-1}}{(pm)!(qn-q)!}z^m w^n$$

$$=\frac{1}{p^p}\sum_{m,n=0}^{\infty}\frac{(A)_{m-n+1}(A')_{m+1}(B)_n(B')_n[(C)_{m+1}]^{-1}}{(pm)!(qn)!}z^{m+1}w^n+\frac{1}{q^q}\sum_{m,n=0}^{\infty}\frac{(A)_{m-n-1}(A')_m(B)_{n+1}(B')_{n+1}[(C)_m]^{-1}}{(pm)!(qn)!}z^m w^{n+1}$$

$$=\frac{z}{p^p}\sum_{m,n=0}^{\infty}(A+(m-n+1)I)(A'+mI)\left[(C+mI)\right]^{-1}\frac{(A)_{m-n+1}(A')_{m+1}(B)_n(B')_n[(C)_{m+1}]^{-1}}{(pm)!(qn)!}z^m w^n$$

$$+\frac{w}{q^q}\sum_{m,n=0}^{\infty}\left[\left(A+(m-n-1)I\right)\right]^{-1}(B+nI)(B'+nI)$$

$$\frac{(A)_{m-n+1}(A')_m(B)_{n+1}(B')_{n+1}\left[(C)_m\right]^{-1}}{(pm)!(qn)!}z^m w^n$$

$$=\frac{z}{p^p}AA'[(C)]^{-1}\,{}^{p}\mathrm{H}_2^{q}(A+,A'+,B,B';C+;z,w)+\frac{w}{q^q}\left[(A-I)\right]^{-1}BB'\,{}^{p}\mathrm{H}_2^{q}(A-,A',B+,B'+;C;z,w)$$

i.e.,

$$\left[d_1\left(d_1-\frac{1}{p}\right)\left(d_1-\frac{2}{p}\right)\ldots\left(d_1-\frac{p-1}{p}\right)+d_2\left(d_2-\frac{1}{q}\right)\left(d_2-\frac{2}{q}\right)\ldots\left(d_2-\frac{q-1}{q}\right)\right]\ {}^{p}\mathrm{H}_2^{q}$$

$$=\frac{z}{p^p}AA'[(C)]^{-1}\,{}^{p}\mathrm{H}_2^{q}(A+,A'+,B,B';C+;z,w)+\frac{w}{q^q}\left[(A-I)\right]^{-1}BB'\,{}^{p}\mathrm{H}_2^{q}(A-,A',B+,B'+;C;z,w)$$

We can written the ${}^{p}\mathrm{H}_2^{q}(A,A',B,B';C;z,w)$, then

$$\left[d_1\left(d_1-\frac{1}{p}\right)\left(d_1-\frac{2}{p}\right)\ldots\left(d_1-\frac{p-1}{p}\right)(d_1I+C-I)+d_2\left(d_2-\frac{1}{q}\right)\left(d_2-\frac{2}{q}\right)\ldots\left(d_2-\frac{q-1}{q}\right)(d_2I-I)\right]\ {}^{p}\mathrm{H}_2^{q}$$

$$=\frac{1}{p^p}\sum_{m=1,n=0}^{\infty}\frac{\left(C+(m-1)I\right)(A)_{m-n}(A')_m(B)_n(B')_n[(C)_m]^{-1}}{(pm-p)!(qn)!}z^m w^n+\frac{1}{q^q}\sum_{m=0,n=1}^{\infty}\frac{(n-1)(A)_{m-n}(A')_m(B)_n(B')_n[(C)_m]^{-1}}{(pm)!(qn-q)!}z^m w^n$$

$$=\left[\frac{z}{p^p}(DI+A)(d_1I+A')-\frac{2z}{p^p}d_2(d_1I+A')+\frac{w}{q^q}(DI+A)d_2I-\frac{w}{q^q}(d_1I+A')d_2I\right]\ {}^{p}\mathrm{H}_2^{q}.$$

Therefore, the following result has been established.

Theorem 4.1. Let A, A', B, B' and C be matrices in $C^{N\times N}$. Then the ${}^{p}\mathrm{H}_2^{q}(A,A',B,B';C;z,w)$ is a solution for the following differential equation

$$\left[d_1\left(d_1-\frac{1}{p}\right)\left(d_1-\frac{2}{p}\right)\ldots\left(d_1-\frac{p-1}{p}\right)\left(d_1I+C-I\right)+d_2\left(d_2-\frac{1}{q}\right)\left(d_2-\frac{2}{q}\right)\ldots\left(d_2-\frac{q-1}{q}\right)\left(d_2I-I\right) \right.$$
$$\left. -\frac{z}{p^p}(DI+A)(d_1I+A')+\frac{2z}{p^p}d_2(d_1I+A')-\frac{w}{q^q}(DI+A)d_2I+\frac{w}{q^q}(d_1I+A)d_2I \right] \ {}^{p}\mathrm{H}_2^{q} \qquad (4.7)$$
$$=0.$$

5. Acknowledgements

The Author expresses his sincere appreciation to Dr. M. S. Metwally, (Department of Mathematics, Faculty of Science (Suez), Suez Canal University, Egypt) for his kind interest, encouragements, help, suggestions, comments and the investigations for this series of papers.

6. References

[1] H. M. Srivastava and P. W. Karlsson, "Multiple Gaussian Hypergeometric Series," Ellis-Horwood, Chichester, 1985.

[2] A. G. Constantine and R. J. Mairhead, "Partial Differential Equations for Hypergeometric Functions of Two Argument Matrices," *Journal of Multivariate Analysis*, Vol. 2, No. 3, 1972, pp. 332-338. doi:10.1016/0047-259X(72)90020-6

[3] A. M. Mathai, "A Handbook of Generalized Spcial Functions for Statistical and Physical Sciences," Oxford University Press, Oxford, 1993.

[4] A. M. Mathai, "Jacobians of Matrix Transformations and Functions of Matrix Argument," World Scientific Publishing, New York, 1997.

[5] H. M. Srivastava and H. L. Manocha, "A Treatise on Generating Functions," Ellis Horwood, New York, 1984.

[6] M. T. Mohamed and A. Shehata, "A Study of Appell's Matrix Functions of Two Complex Variables and Some Properties," *Journal Advances and Applications in Mathematical Sciences*, Vol. 9, No. 1, 2011, pp. 23-33.

[7] A. Shehata, "A Study of Some Special Functions and Polynomials of Complex Variables," Ph.D. Thesis, Assiut University, Assiut, 2009.

[8] L. Jódar and J. C. Cortés, "On the Hypergeometric Matrix Function," *Journal of Computational and Applied Mathematics*, Vol. 99, No. 1-2, 1998, pp. 205-217. doi:10.1016/S0377-0427(98)00158-7

[9] L. Jódar and J. C. Cortés, "Closed form General Solution of the Hypergeometric Matrix Differential Equation," *Mathematical and Computer Modelling*, Vol. 32, No. 9, 2000, pp. 1017-1028. doi:10.1016/S0895-7177(00)00187-4

[10] L. M. Upadhyaya and H. S. Dhami, "Generalized Horn's Functions of Matrix Arguments," *Bulletin Pure and Applied Sciences*: *Section E. Mathematics and Statistics*, Vol. 29E, No. 2, 2010, pp. 353-364.

[11] L. M. Upadhyaya, "A Summation Formula for a Horn's Double Hypergeometric Function-II," *Bulletin Pure and Applied Sciences: Section E. Mathematics and Statistics*, Vol. 2E, No. 2, 2010, pp. 279-286.

[12] Z. M. G. Kishka, M. A. Saleem, S. Z. Radi and M. Abul-Dahab, "On the *p* and *q*-Appell Matrix Function," *Southeast Asian Bulletin of Mathematics*, Vol. 35, 2011, pp. 807-818.

[13] M. S. Metwally, "On *p*-Kummers Matrix Function of Complex Variable under Differential Operators and Their Properties," *Southeast Asian Bulletin of Mathematics*, Vol. 35, 2011, pp. 1-16.

[14] G. Golub and C. F. Van Loan, "Matrix Computations," The Johns Hopkins University Press, Baltimore, 1989.

[15] N. Dunford and J. Schwartz, "Linear Operators, Part I," Interscience, New York, 1955.

[16] L. Jódar and J. C. Cortés, "Some Properties of Gamma and Beta Matrix Functions," *Applied Mathematics Letter*s, Vol. 11, No. 1, 1998, pp. 89-93. doi:10.1016/S0893-9659(97)00139-0

[17] K. A. M. Sayyed, "Basic Sets of Polynomials of Two Complex Variables and Convergence Properties," Ph.D. Thesis, Assiut University, Assiut, 1975.

[18] K. A. M. Sayyed, M. S. Metwally and M. T. Mohamed, "Certain Hypergeometric Matrix Function," *Scientiae Mathematicae Japonicae*, Vol. 69, No. 3, 2009, pp. 315-321. http://www.jams.or.jp/notice/scmjol/2009.html#2009-21

[19] A. Erdélyi, W. Magnus, F. Oberhettinger and G. Tricomi, "Higher Tanscendental Functions," McGraw-Hill Book Co., New York, Vol. 1, 1953.

Applied Mathematics, **2011, 2, 1443-1445**
doi:10.4236/am.2011.212204 Published Online December 2011 (http://www.SciRP.org/journal/am)

Inverse Eigenvalue Problem for Generalized Arrow-Like Matrices

Zhibin Li, Cong Bu, Hui Wang
College of Mathematics, Dalian Jiaotong University, Dalian, China
E-mail: *lizhibinky*@163.*com*
Received October 14, 2011; *revised November* 15, 2011; *accepted November* 23, 2011

Abstract

This paper researches the following inverse eigenvalue problem for arrow-like matrices. Give two characteristic pairs, get a generalized arrow-like matrix, let the two characteristic pairs are the characteristic pairs of this generalized arrow-like matrix. The expression and an algorithm of the solution of the problem is given, and a numerical example is provided.

Keywords: Generalized Arrow-Like Matrices, Characteristic Value, Inverse Problem, Unique

1. Introduction

The Inverse eigenvalue problem for matrices in the problems involved in the field of structural design, pattern recognition, parameter recognition, automatic control and so on, it has a good engineering background, and its research has obvious significance [1]. Many experts and scholars have addressed more extensively and in-depth studied, get a lot of conclusions about inverse eigenvalue problem for Jacobi matrices [2], but there is less research about the inverse eigenvalue problem for arrow- like matrices [3,4]. This paper researches the following inverse eigenvalue problem for generalized arrow-like matrices.

Generalized arrow-like matrices refer to the matrix as follows:

$$J=\begin{pmatrix} a_1 & b_1 & \cdots & b_{m-1} & b_m & & & \\ c_1 & a_2 & & & & & & \\ \vdots & & \ddots & & & & & \\ c_{m-1} & & & a_m & & & & \\ c_m & & & & a_{m+1} & b_{m+1} & & \\ & & & & c_{m+1} & a_{m+2} & \ddots & \\ & & & & & \ddots & \ddots & b_{n-1} \\ & & & & & & c_{n-1} & a_n \end{pmatrix} \quad (1)$$

When $m=1$, J becomes generalized Jacobi matrix [1]; when $m=n$, J is an arrow-like matrice. This article studies the following characteristic value inverse:

Question IEPGAM. Given two real numbers $\lambda,\mu(\lambda\neq\mu)$ and two nonzero real vectors $x=(x_1,x_2,\cdots,x_n)^{\mathrm{T}}\in R^n$, $y=(y_1,y_2,\cdots,y_n)^{\mathrm{T}}\in R^n$.

Find the $n\times n$ real generalized arrow-like matrice J, such that $Jx=\lambda x, Jy=\mu y$.

The expression and an algorithm of the solution of the problem is given in Section 2, and a numerical example is provided in Section 3.

2. The Solution of Question IEPGAM

Because (λ,x) and (μ,y) are two characteristic pairs of the generalized arrow-like matrices J,

In it,

Let:

$$x_0=x_{n+1}=y_0=y_{n+1}=b_0=b_n=c_0=c_n=0, \quad (2)$$

$$D_i=\begin{vmatrix} x_i & y_i \\ x_{i+1} & y_{i+1} \end{vmatrix}(i=0,1,\cdots,n), \quad (3)$$

$$E_i=\begin{vmatrix} x_1 & x_i \\ y_1 & y_i \end{vmatrix}(i=2,3,\cdots,m+1) \quad (4)$$

So

$$a_1x_1+b_1x_2+\cdots+b_{m-1}x_m+b_mx_{m+1}=\lambda x_1, \quad (5\text{-}1)$$

$$c_1x_1+a_2x_2=\lambda x_2, \quad (5\text{-}2)$$

$$\cdots$$

$$c_{m-1}x_1+a_mx_m=\lambda x_m, \quad (5\text{-}m)$$

$$c_mx_1+a_{m+1}x_{m+1}+b_{m+1}x_{m+2}=\lambda x_{m+1}, \quad (5\text{-}m{+}1)$$

$$c_{m+1}x_{m+1}+a_{m+2}x_{m+2}+b_{m+2}x_{m+3}=\lambda x_{m+2}, \quad (5\text{-}m{+}2)$$

$$\cdots$$

$$c_{n-2}x_{n-2}+a_{n-1}x_{n-1}+b_{n-1}x_n=\lambda x_{n-1}, \quad (5\text{-}n\text{–}1)$$
$$c_{n-1}x_{n-1}+a_n x_n=\lambda x_n. \quad (5\text{-}n)$$
$$a_1y_1+b_1y_2+\cdots+b_{m-1}y_m+b_m y_{m+1}=\mu y_1, \quad (6\text{-}1)$$
$$c_1y_1+a_2y_2=\mu y_2, \quad (6\text{-}2)$$
$$\cdots$$
$$c_{m-1}y_1+a_m y_m=\mu y_m, \quad (6\text{-}m)$$
$$c_m y_1+a_{m+1}y_{m+1}+b_{m+1}y_{m+2}=\mu y_{m+1}, \quad (6\text{-}m\text{+}1)$$
$$c_{m+1}y_{m+1}+a_{m+2}y_{m+2}+b_{m+2}y_{m+3}=\mu y_{m+2}, \quad (6\text{-}m\text{+}2)$$
$$\cdots$$
$$c_{n-2}y_{n-2}+a_{n-1}y_{n-1}+b_{n-1}y_n=\mu y_{n-1}, \quad (6\text{-}n\text{–}1)$$
$$c_{n-1}y_{n-1}+a_n y_n=\mu y_n. \quad (6\text{-}n)$$

- For inverse $b_i, c_i (i=m+1,m+2,\cdots,n-1)$, $a_i (i=m+2,m+3,\cdots,n)$.

From (5) and (6), we can get

$$c_{i-1}x_{i-1}+a_i x_i+b_i x_{i+1}=\lambda x_i (i=m+2,m+3,\cdots,n), \quad (7)$$
$$c_{i-1}y_{i-1}+a_i y_i+b_i y_{i+1}=\mu y_i (i=m+2,m+3,\cdots,n). \quad (8)$$

In order to eliminate a_i, multiply by y_i on both sides of (7), multiply by x_i on both sides of (8), then cut on both sides, we can get

$$b_i D_i=(\mu-\lambda)x_i y_i+c_{i-1}D_{i-1} (i=m+2,m+3,\cdots,n). \quad (9)$$

To problem *A*, because $c_i=kb_i, (i=2,3,\cdots,n-1)$, so (9) become

$$b_i D_i=(\mu-\lambda)x_i y_i+kb_{i-1}D_{i-1} \quad (i=m+2,m+3,\cdots,n) \quad (10)$$

Let $i=n$, because $D_n=0$, so

$$b_{n-1}D_{n-1}=\frac{x_n y_n}{k}(\lambda-\mu),$$

Let $i=n-1$, $b_{n-2}D_{n-2}=(\lambda-\mu)\left[\frac{x_n y_n}{k^2}+\frac{x_{n-1}y_{n-1}}{k}\right]$;

……

Let $i=m+2$,

$$b_{m+1}D_{m+1}=(\lambda-\mu)\left[\frac{x_n y_n}{k^{n-(m+1)}}+\frac{x_{n-1}y_{n-1}}{k^{n-(m+2)}}+\cdots+\frac{x_{m+2}y_{m+2}}{k}\right]$$

Under normal circumstances,

$$b_j D_j=(\lambda-\mu)\sum_{s=0}^{n-(j+1)}\frac{x_{n-s}y_{n-s}}{k^{n-(s+j)}} (j=m+1,m+2,\cdots,n-1). \quad (11)$$

If $D_j\neq 0$ $(j=m+1,m+2,\cdots,n-1)$, then x_i, y_i can not be zero at the same time ,so

$$b_j=\frac{(\lambda-\mu)}{D_j}\sum_{s=0}^{n-(j+1)}\frac{x_{n-s}y_{n-s}}{k^{n-(s+j)}} (j=m+1,m+2,\cdots,n-1), \quad (12)$$

$$c_j=kb_j, (j=m+1,m+2,\cdots,n-1), \quad (13)$$

$$a_j=\begin{cases}\dfrac{\lambda x_j-c_{j-1}x_{j-1}-b_j x_{j+1}}{x_j}, x_j\neq 0;\\ \dfrac{\mu y_j-c_{j-1}y_{j-1}-b_j y_{j+1}}{y_j}, y_j\neq 0\end{cases}. \quad (14)$$
$$(j=m+2,m+3,\cdots,n)$$

- For inverse a_{m+1}, c_m, b_m.

From (5) and the $m+1$ equation of (6),

$$c_m E_{m+1}=(\lambda-\mu)x_{m+1}y_{m+1}+b_{m+1}D_{m+1}, \quad (15)$$
$$a_{m+1}E_{m+1}=\mu x_1 y_{m+1}-\lambda x_{m+1}y_1-b_{m+1}E_{m+2}, \quad (16)$$
$$b_m=\frac{c_m}{k}. \quad (17)$$

- For inverse $c_1, c_i, b_i (i=2,3,\cdots,m-1)$, $a_i (i=2,3,\cdots,m)$.

From (5) and 2 to m equation of (6),

$$c_{i-1}x_1+a_i x_i=\lambda x_i (i=2,3,\cdots,m), \quad (18)$$
$$c_{i-1}y_1+a_i y_i=\mu y_i (i=2,3,\cdots,m). \quad (19)$$

From (18) and (19), we can get

$$c_{i-1}E_i=(\lambda-\mu)x_i y_i (i=2,3,\cdots,m), \quad (20)$$
$$a_i E_i=\mu x_1 y_i-\lambda x_i y_1 (i=2,3,\cdots,m), \quad (21)$$
$$b_i=\frac{c_i}{k} (i=2,3,\cdots,m-1). \quad (22)$$

- For inverse a_1, b_1.

From (5) and (6), we can get

$$a_1x_1+b_1x_2=\lambda x_1-\sum_{s=2}^{m}b_s x_{s+1}, \quad (23)$$
$$a_1y_1+b_1y_2=\mu y_1-\sum_{s=2}^{m}b_s y_{s+1}. \quad (24)$$

If $D_1\neq 0$, from (23) and (24), then we can get

$$a_1=\frac{\lambda x_1y_2-\mu x_2y_1-\sum_{s=2}^{m}b_s(x_{s+1}y_2-x_2y_{s+1})}{D_1}, \quad (25)$$

$$b_1=\frac{(\mu-\lambda)x_1y_1-\sum_{s=2}^{m}b_s(y_{s+1}x_1-y_1x_{s+1})}{D_1}. \quad (26)$$

According to the above analysis, to question IEPGAM, we can get the follow theorem.

Theorem. If the following conditions are satisfied:

1) $D_1\neq 0$;
2) $D_i\neq 0$ $(i=m+1,m+2,\cdots,n-1)$;
3) $E_i\neq 0$ $(i=2,3,\cdots,m+1)$

Then question IEPGAM has the unique solution, and

$$b_j = \frac{(\lambda-\mu)}{D_j}\sum_{s=0}^{n-(j+1)}\frac{x_{n-s}y_{n-s}}{k^{n-(s+j)}}\ (j=m+1,m+2,\cdots,n-1) \quad (27)$$

$$a_j = \begin{cases} \dfrac{\lambda x_j - c_{j-1}x_{j-1} - b_j x_{j+1}}{x_j}, x_j \neq 0; \\ \dfrac{\mu y_j - c_{j-1}y_{j-1} - b_j y_{j+1}}{y_j}, y_j \neq 0 \end{cases}, \quad (28)$$

$$(j=m+2,m+3,\cdots,n)$$

$$b_m = \frac{(\lambda-\mu)x_{m+1}y_{m+1} + b_{m+1}D_{m+1}}{kE_{m+1}}, \quad (29)$$

$$a_{m+1} = \frac{\mu x_1 y_{m+1} - \lambda x_{m+1}y_1 - b_{m+1}E_{m+2}}{E_{m+1}}, \quad (30)$$

$$b_j = \frac{(\lambda-\mu)x_{j+1}y_{j+1}}{kE_{j+1}}(i=2,3,\cdots,m-1), \quad (31)$$

$$b_1 = \frac{(\mu-\lambda)x_1y_1 - \sum_{s=2}^{m} b_s(y_{s+1}x_1 - y_1x_{s+1})}{D_1} \quad (32)$$

$$a_j = \frac{\mu x_1 y_j - \lambda x_j y_1}{E_j}(j=2,3,\cdots,m), \quad (33)$$

$$a_1 = \begin{cases} \lambda - \dfrac{\sum_{s=1}^{m} b_s x_{s+1}}{x_1}, x_1 \neq 0; \\ \mu - \dfrac{\sum_{s=1}^{m} b_s y_{s+1}}{y_1}, y_j \neq 0 \end{cases} \quad (34)$$

$$c_j = kb_j, (i=2,3,\cdots,n-1), \quad (35)$$

$$c_1 = \frac{(\lambda-\mu)x_2y_2}{E_2}. \quad (36)$$

3. Numerical Examples

Example 1. Give $\lambda=1,\mu=2,k=2,m=2,n=5$, $x=(1,1,1,1,1)^{\mathrm{T}}, y=(1,0,2,-1,0)^{\mathrm{T}}$.

It is easy to be calculated

$$D_1=-1\neq 0, D_2=-3\neq 0, D_4=1\neq 0;$$

$$E_2=-1\neq 0, E_3=1\neq 0, E_4=-2.$$

From Theorem, the question IEPGAM has the unique solution. And

$$b_3=\frac{\lambda-\mu}{D_3}\left[\frac{x_5y_5}{k^2}+\frac{x_4y_4}{k}\right]=-\frac{1}{6},$$

$$b_2=\frac{1}{kE_3}\left[(\lambda-\mu)x_3y_3+b_3D_3\right]=-\frac{3}{4},$$

$$b_4=\frac{\lambda-\mu}{D_4}\left[\frac{x_5y_5}{k}\right]=0,$$

$$b_1=\frac{(\mu-\lambda)x_1y_1-b_2(y_3x_1-y_1x_3)}{D_1}=-\frac{7}{4};$$

$$c_2=kb_2=-\frac{3}{2},$$

$$c_3=kb_3=-\frac{1}{3},$$

$$c_4=kb_4=0,$$

$$c_1=\frac{(\lambda-\mu)x_2y_2}{E_2}=0;$$

$$a_1=\lambda-\frac{b_1x_2+b_2x_3}{x_1}=\frac{7}{2},$$

$$a_2=\frac{\mu x_1y_2-\lambda x_2y_1}{E_2}=1,$$

$$a_3=\frac{\mu x_1y_3-\lambda x_3y_1-b_3E_4}{E_3}=\frac{8}{3},$$

$$a_4=\frac{\lambda x_4-c_3x_3-b_4x_5}{x_4}=\frac{4}{3},$$

$$a_5=\frac{\lambda x_5-c_4x_4-b_5x_6}{x_5}=1.$$

So

$$J=\begin{pmatrix} \frac{7}{2} & \frac{-7}{4} & \frac{-3}{4} & 0 & 0 \\ 0 & 1 & 0 & 0 & 0 \\ \frac{-3}{2} & 0 & \frac{8}{3} & \frac{-1}{6} & 0 \\ 0 & 0 & \frac{-1}{3} & \frac{4}{3} & 0 \\ 0 & 0 & 0 & 0 & 1 \end{pmatrix}$$

and $Jx=\lambda x, Jy=\mu y$.

4. References

[1] D. J. Wang, "Inverse Eigenvalue Problem in Structural Dynamics," *Journal of Vibration and Shock*, No. 2, 1988, pp. 31-43.

[2] H. Dai, "Inverse Eigenvalue Problem for Jacobi Matrices," *Computation Physics*, Vol. 11, No. 4, 1994, pp. 451-456.

[3] C. H. Wu and L. Z. Lu, "Inverse Eigenvalue Problem for a Kind of Special Matrix," *Journal of Xiamen University* (*Natural Science*), No. 1, 2009, pp. 22-26.

[4] Q. X. Yin, "Generalized Inverse Eigenvalue Problem for Arrow-Like Matrices," *Journal of Nan Jing University of Aeronautics & Astronautics*, Vol. 34, No. 2, 2002, pp. 190-192.

Applied Mathematics, 2011, 2, 1446-1447
doi:10.4236/am.2011.212205 Published Online December 2011 (http://www.SciRP.org/journal/am)

Extension of Range of MINRES-CN Algorithm

Mojtaba Ghasemi Kamalvand
Department of Mathematics, Lorestan University, Khorramabad, Iran
E-mail: *m_ghasemi*98*@yahoo.com*
Received January 20, 2011; *revised May* 10, 2011; *accepted May* 18, 2011

Abstract

MINRES-CN is an iterative method for solving systems of linear equations with conjugate-normal coefficient matrices whose conspectra are located on algebraic curves of a low degree. This method was proposed in a previous publication of author and KH. D. Ikramov. In this paper, the range of applicability of MINRES-CN is extended in new direction. These are conjugate normal matrices that are low rank perturbations of Symmetric matrices. Examples are given that demonstrate a higher efficiency of MINRES-CN for this class of systems compared to the well-known algorithm GMRES.

Keywords: Conjugate-Normal Matrices, MINRES-CN Algorithm, MINRES-CN2 Algorithm

1. Introduction and Preliminaries

Suppose that one needs to solve the system of linear equations

$$Ax = b \tag{1}$$

with a conjugate-normal $n \times n$-matrix A. In the context of this paper, conjugate-normality means that

$$AA^* = \overline{A^*A} \tag{2}$$

A particular example of conjugate-normal matrices are symmetric matrices.

The method proposed in [1] is a minimum residual algorithm for the subspaces, which are the finite segments of the sequence

$$x, \bar{A}\bar{x}, A^*\bar{x}, \bar{A}Ax, \bar{A}A^Tx, A^*A^Tx, \bar{A}A\bar{A}\bar{x}, \cdots, \tag{3}$$

Unlike GMRES, this method, called MINRES-CN, is described by a recursion whose (fixed) length depends on the degree m of Γ (the conspectrum (you can see definition of conspectrum in [2]) of A belongs to an algebraic curve Γ of a low degree)). For instance, the length of the recursion is six in the case $m = 2$, which is given the most attention in [1].

2. Extension of Range

In this section, the range of applicability of MINRES-CN is extended in new direction.

We examine the behavior of MINRES-CN for new class of matrices A that can be considered as low rank perturbations of Symmetric matrices.

Let us first recall that any square complex matrix A can be uniquely represented in the form (see [3])

$$A = S + K, S = S^T, K = -K^T \tag{4}$$

We consider the class of conjugate-normal matrices A distinguished by the condition,

$$k = rankK < \frac{k-1}{2} \tag{5}$$

where n is the order of A. The conspectrum of such a matrix belongs to the union of the real axis and (at most) k lines that are parallel to the imaginary axis, *i.e.*, to a degenerate algebraic curve whose degree does not exceed $k + 1$. Hence, MINRES-CN is applicable to matrices of this type.

3. Numerical Results

Therefore, we can apply MINRES-CN to solving systems with conjugate normal coefficient matrices satisfying conditions (4) and (5).

The efficiency of the method is illustrated by several examples where band systems were solved. The performance of MINRES-CN2 (which is a specialization of MINRES-CN for conjugate normal matrices whose conspectra belong to a second-degree curve) in these examples is compared with that of the Matlab library program implementing GMRES.

In examples, we used the Matlab library function gmres for GMRES and a specially designed Matlab procedure for MINRES-CN2. The same stopping criterion

was used for both methods; namely,

$$\|r\|_2 < \epsilon \quad (6)$$

where r is the current residual, while a positive scalar ϵ should be given by the user. For the example under discussion, we set $\epsilon = 10^{-8}$.

In all of our experiments, the order of systems was 2000. The right hand sides were generated as pseudo-random vectors with components distributed uniformly on (0, 1). The calculations were performed on a 2 Duo E630 OEM 1.86 GHz PC with core memory of 1024 Mb.

Example 3.1. Suppose that, $A = (a_{ij})_{n\times n}$, where $a_{ij} \in [10,14]$, for $i = 1, 2, \cdots, n-2$, and $a_{n-1,n-1} = a_{n,n} = 0, a_{n-1,n} = -11, a_{n,n-1} = 11$ (where $A = S + K$ and $rankK = 2$), another entries of matrix A are zero. The conspectrum is located on the coordinate axes; *i.e.*, it belong to the second-degree curve,

$$xy = 0 \quad (7)$$

It follows that a system with the matrix A can be processed by MINRES-CN2.

MINRES-CN2 converges faster than GMRES (8 iteration steps and t = 0.02 s against 11 steps and t = 0.09 s).

Example 3.2. Suppose that $A = (a_{ij})_{n\times n}$, where $a_{ij} \in [10,14]$, for $i = 1, 2, \cdots, n-2$, and $a_{n-1,n-1} = a_{n,n} = 12, a_{n-1,n} = -11, a_{n,n-1} = 11$ (where $A = S + K$ and $rankK = 2$), another entries of matrix A are zero. The conspectrum is located on the real axis and the line x = 2; *i.e.*, it belong to the second-degree curve,

$$(x-12)y = 0.$$

It follows that a system with the matrix A can be processed by MINRES-CN2.

MINRES-CN2 needs 10 steps and t = 0.02 s, while GMRES requires 12 steps and the time 0.09 s.

Example 3.3. Suppose that $A = (a_{ij})_{n\times n}$, where $a_{ij} \in [40,45]$, for $i = 1, 2, \cdots, n-4$, and $a_{n-1,n} = -43, a_{n,n-1} = 43, a_{n-3,n-4} = -41, a_{n-4,n-3} = 41$ (where $A = S + K$ and $rankK = 4$), another entries of matrix A are zero. The conspectrum is located on the coordinate axes; *i.e.*, it belongs to the second-degree curve (7). It follows that a system with the matrix A can be processed by MINRES-CN2. 7 iteration steps and t = 0.02 s for MINRES-CN2 against 12 steps and t = 0.08 s for GMRES.

4. References

[1] M. G. Kamalvand and Kh. D. Ikramov, "A Method of the Congruent Type for Linear Systems with Conjugate-Normal Coefficient Matrices," *Computational Mathematics and Mathematical Physics*, Vol. 49, No. 2, 2009, pp. 203-216. doi:10.1134/S0965542509020018

[2] H. Fassbender and Kh. D. Ikramov, "Some Observations on the Youla Form and Conjugate-Normal Matrices," *Linear Algebra and Its Applications*, Vol. 422, No. 1, 2007, pp. 29-38. doi:10.1016/j.laa.2006.09.004

[3] R. A. Horn and C. R. Johnson, "Matrix Analysis," Cambridge University Press, Cambridge, 1985.

Applied Mathematics, 2011, 2, 1448-1452
doi:10.4236/am.2011.212206 Published Online December 2011 (http://www.SciRP.org/journal/am)

Degree of Approximation of Conjugate of Signals (Functions) by Lower Triangular Matrix Operator

Vishnu Narayan Mishra[1], Huzoor H. Khan[2], Kejal Khatri[1]
[1]*Department of Mathematics, S. V. National Institute of Technology, Surat, India*
[2]*Department of Mathematics, Aligarh Muslim University, Aligarh, India*
E-mail: *vishnu_narayanmishra@yahoo.co.in, huzoorkhan@yahoo.com, kejal*0909*@gmail.com*
Received May 4, 2011; *revised October* 25, 2011; *accepted November* 5, 2011

Abstract

In the present paper, an attempt is made to obtain the degree of approximation of conjugate of functions (signals) belonging to the generalized weighted $W(L_P, \xi(t))$, $(p \geq 1)$-class, by using lower triangular matrix operator of conjugate series of its Fourier series.

Keywords: Conjugate Fourier Series, Generalized Weighted $W(L_P, \xi(t))$-Class, Degree of Approximation and Lower Triangular Matrix Means

1. Introduction

Let f be a 2π-periodic signal (function) and let $f \in L_1[0, 2\pi] = L_1$. Then the Fourier series of a function (signal) f at any point x is given by

$$f(x) \approx \frac{a_0}{2} + \sum_{k=1}^{\infty}(a_k \cos kx + b_k \sin kx) \equiv \sum_{k=0}^{\infty} u_k(f;x), \tag{1.1}$$

with partial sums $s_n(f;x)$—a trigonometric polynomial of degree (or order) n, of the first $(n+1)$ terms.

The conjugate series of Fourier series (1.1) of f is given by

$$\sum_{k=1}^{\infty}(b_k \cos kx - a_k \sin kx) \equiv \sum_{k=1}^{\infty} v_k(f;x) \tag{1.2}$$

with partial sums $\tilde{s}_n(f;x)$.

If f is Lebesgue integrable and $p \geq 1, f \in Lip(\xi(t), p)$, then

$$2\pi\tilde{f}(x) = -\int_0^{\pi}\psi(t)\cot(t/2)\mathrm{d}t = -\lim_{h\to 0}\int_h^{\pi}\psi(t)\cot(t/2)\mathrm{d}t,$$

exists for all x Zygmund [1, p. 131], $\tilde{f}(x)$ is called the conjugate function of $f(x)$.

The matrix $\mathrm{T} \equiv (a_{n,k})$, in which $a_{n,k}$ is the element in n-th row and k-th column is usually called the matrix of T. Matrices T such that $a_{n,k} = 0$, for $k > n$, are called lower triangular.

Let $\mathrm{T} \equiv (a_{n,k})$ be an infinite lower triangular matrix satisfying Töeplitz [2] conditions of regularity, *i.e.*

$\sum_{k=0}^{n}|a_{n,k}| \leq M$, where M is a finite constant independent of n,

$\lim_{n\to\infty} a_{n,k} = 0$, for each $k > n$ and $\lim_{n\to\infty}\sum_{k=0}^{n} a_{n,k} = 1$.

Let $\sum_{n=0}^{\infty} u_n$ be an infinite series whose $(k+1)^{th}$ partial sum $s_k = \sum_{n=0}^{k} u_n$.

The sequence-to-sequence transformation

$$\tau_n = \sum_{k=0}^{\infty} a_{n,k}\, s_k = \sum_{k=0}^{\infty} a_{n,n-k}\, s_{n-k},\ n = 0,1,2,\cdots,$$

defines the sequence $\{\tau_n\}$ of lower triangular matrix summability means of sequence $\{s_n\}$ generated by the sequence of coefficients $(a_{n,k})$. The transforms τ_n are called linear means or matrix means (determined by the matrix T) of the sequence $\{s_n\}$.

An infinite series Σu_n is said to be summable to s by lower triangular matrix T-method, if $\lim_{n\to\infty}\tau_n$ exists and is equal to s Zygmund [1, p. 74] and we write $\tau_n \to s(T)$, as $n \to \infty$ The summability matrix T or the sequence-to-sequence transformation τ_n is said to be regular, if $\lim_{n\to\infty} s_n = s \Rightarrow \lim_{n\to\infty}\tau_n = s$.

A function (signal) $f(x) \in Lip\,\alpha$, for $0 < \alpha \leq 1$, if $|f(x+t) - f(x)| = \mathrm{O}(t^{\alpha})$.

A function (signal) $f(x) \in Lip(\alpha, p)$ for $p \geq 1,\ 0 < \alpha \leq 1$, Fadden [3], if

$$\left\{\int_0^{2\pi} \left|f(x+t) - f(x)\right|^p \mathrm{d}x\right\}^{1/p} = \mathrm{O}(t^{\alpha}),$$

Given a positive increasing function $\xi(t)$ and an integer $p \geq 1,\ f(x) \in Lip(\xi(t), p)$, Khan [4], if

$$\left\{\int_0^{2\pi} \left|f(x+t) - f(x)\right|^p \mathrm{d}x\right\}^{1/p} = \mathrm{O}(\xi(t)).$$

In case $\xi(t) = t^{\alpha}, 0 < \alpha \leq 1$, then $Lip(\xi(t), p)$ coincides with the class $Lip(\alpha, p)$. If $p \to \infty$ in $Lip(\alpha, p)$ class then this class reduces to $Lip\,\alpha$.

For a given positive increasing function $\xi(t)$, an integer $p \geq 1, f(x) \in W(L_p, \xi(t))$, Khan [4], if

$$\left\{\int_0^{2\pi} \left|\{f(x+t) - f(x)\}\sin^{\beta} x\right|^p \mathrm{d}x\right\}^{1/p} = \mathrm{O}(\xi(t)), (\beta \geq 0).$$

We note that, if $\beta = 0$ then the generalized weighted $W(L_p, \xi(t)), (p \geq 1)$-class coincide with the class $Lip(\xi(t), p)$.

Also we observe that

$$Lip\,\alpha \subseteq Lip(\alpha,\ p) \subseteq Lip(\xi(t),\ p) \subseteq W(L_p, \xi(t))$$

for $0 < \alpha \leq 1,\ p \geq 1$, Mishra [5].

The L_p-norm is defined by

$$\|f\|_p = \left(\int_0^{2\pi} |f(x)|^p \mathrm{d}x\right)^{1/p}, \quad p \geq 1.$$

The L_{∞}-norm of a function $f : R \to R$ is defined by

$$\|f\|_{\infty} = \sup\{|f(x)| : x \in R\},$$

and the degree of approximation $E_n(f)$ of a function $f : R \to R$ is given by

$$E_n(f) = \min_n \|f(x) - \tau_n(f; x)\|_p,$$

in terms of n, where $\tau_n(f; x)$ is a trigonometric polynomial of degree (order) n. This method of approximation is called trigonometric Fourier Approximation (tfa) Mishra [6]. Riesz-Hölder Inequality states that if p and q be non-negative extended real numbers such that $1/p + 1/q = 1$. If $f \in L^p[a,b]$ and $g \in L^q[a,b]$, then $f.g \in L^1[a,b]$ and

$$\int_a^b |f\,g| \leq \|f\|_p \|g\|_q.$$

Equality holds if and only if, for some non-zero constants A and B, we have $A|f|^p = B|g|^q$ *a.e.*

Second Mean Value theorem for integration states that if $G : [a,b] \to R$ is a positive monotonically decreasing function and $\phi : [a,b] \to R$ is an integrable function, then $\exists$ a number $x \in (a,b)$ such that

$$\int_a^b G(t)\,\phi(t)\mathrm{d}t = G(a+0)\int_a^x \phi(t)\mathrm{d}t\ .$$

Here $G(a+0)$ stands for $\lim_{a+} G$, the existence of which follows from the conditions. Note that it is essential that the interval (a, b] contains b. A variant not having this requirement is:

If $G : [a,b] \to R$ is a monotonic (not necessarily decreasing and positive) function and $\phi : [a,b] \to R$ is an integrable function, then $\exists$ a number $x \in (a,b)$ such that

$$\int_a^b G(t)\phi(t)\mathrm{d}t = G(a+0)\int_a^x \phi(t)\mathrm{d}t + G(b-0)\int_x^b \phi(t)\mathrm{d}t.$$

We use the following notations:

$$\psi(t) = f(x+t) - f(x-t),$$

$$A_{n,k} = \sum_{r=k}^{n} a_{n,r},\ A_{n,0} = 1, \forall n \geq 0,$$

$M_n(t) = \dfrac{1}{2\pi}\sum_{k=0}^{n} \dfrac{a_{n,k}\cos(k+1/2)t}{\sin(t/2)}$, $\tau = [1/t]$—the greatest integer not exceeding of $1/t$.

Furthermore C will denote an absolute positive constant, not necessarily the same at each occurrence. Throughout this paper, we take $a_{n,k} \geq 0\ (0 \leq k \leq n)$, and $A_{n,0} = 1 \forall n$.

2. Main Result

It is well known that the theory of approximations *i.e.*, tfa, which originated from a well known theorem of Weierstrass, has become an exciting interdisciplinary field of study for the last 130 years. These approximations have assumed important new dimensions due to their wide applications in signal analysis, in general and in digital signal processing [5] in particular, in view of the classical Shannon sampling theorem.

This has motivated by various investigators such as Qureshi ([7,8]), Khan ([4,9]) Chandra [10], Leindler [11] Mishra [5] discussed the degree of approximation of signals (functions) belonging to $Lip\alpha, Lip(\alpha, p), Lip(\xi(t), p)$ and $W(L_p, \xi(t))$-classes by using Cesàro and Nörlund means of an infinite series. Qureshi ([12,13]) have determined the degree of $\tilde{f}(x)$, conjugate of a function $f(x) \in Lip\alpha$ and $Lip(\alpha, p)$ by Nörlund means of conjugate series of a Fourier series.

The purpose of this paper is to determine the degree of approximation of $\tilde{f}(x)$, conjugate of a function $f(x) \in W(L_p, \xi(t)), (p \geq 1)$, by lower triangular matrix means.

We prove:

***Theorem* 2.1.** *Let* $T \equiv (a_{n,k})$ *be an infinite regular*

lower triangular matrix such that the elements $(a_{n,k})$ be non-negative, non-decreasing with $k \le n$. *If* $f:R \to R$ *is a* 2π*-periodic*, *Lebesgue integrable and belonging to the generalized weighted* $W(L_p, \xi(t)), p \ge 1$*-class*, *then the degree of approximation of* $\tilde{f}(x)$, *conjugate of* $f(x) \in W(L_p, \xi(t))$, *by lower triangular matrix means* $\tilde{\tau}_n(f;x)$ *is given by*

$$\left\|\tilde{\tau}_n(f;x) - \tilde{f}(x)\right\|_p = O\left(n^{\beta+1/p}\xi(1/n)\right) \quad \forall n > 0, \qquad (2.1)$$

provided $\xi(t)$ *is positive increasing function of t satisfying the following conditions*

$$\left\{\int_0^{\pi/n}\left(\frac{t|\psi(t)|}{\xi(t)}\right)^p \sin^{\beta p} t\,\mathrm{d}t\right\}^{1/p} = O(n^{-1}) \qquad (2.2)$$

$$\left\{\int_{\pi/n}^{\pi}\left(\frac{t^{-\delta}|\psi(t)|}{\xi(t)}\right)^p \mathrm{d}t\right\}^{1/p} = O(n^{\delta}) \qquad (2.3)$$

and $$\frac{\xi(t)}{t} \text{ is decreasing in } t \qquad (2.4)$$

where δ *is an arbitrary number such that* $q(1-\delta+\beta)-1>0$, q *the conjugate index of p and conditions* (2.2), (2.3) *hold uniformly in x and* $p^{-1}+q^{-1}=1$.

Note 1. Condition (2.4) implies $\xi(\pi/n) \le \pi\xi(1/n)$, for $(\pi/n) \ge (1/n)$

Note 2. Also for $\beta = 0$ our Theorem (2.1) reduces to one of the theorem of Lal and Kushwaha [14].

3. Lemmas

In order to prove our Theorem 2.1, we require the following lemma.

Lemma 3.1. Under the conditions of our Theorem 2.1 on $(a_{n,k})$, we have

$$M_n(t) = O\left(\frac{A_{n,\tau}}{t}\right), \quad \text{for } \frac{\pi}{n} < t \le \pi.$$

Proof. For $\pi n^{-1} < t \le \pi$, $(\sin t)^{-1} \le \pi/2t$, for $0 < t \le \pi/2$, $\tau \le n$, we have

$$\begin{aligned}
&|M_n(t)| \\
&= \left|\frac{1}{2\pi}\sum_{k=0}^{n-\tau-1} a_{n,k}\frac{\cos(k+1/2)t}{\sin(t/2)} + \frac{1}{2\pi}\sum_{k=n-\tau}^{n} a_{n,k}\frac{\cos(k+1/2)t}{\sin(t/2)}\right| \\
&\le \frac{1}{2t}\left|\sum_{k=0}^{n-\tau-1} a_{n,k}\cos(k+1/2)t\right| + \frac{1}{2t}\left|\sum_{k=n-\tau}^{n} a_{n,k}\cos(k+1/2)t\right| \\
&\le \frac{1}{2t}\left[2a_{n,n-\tau-1}\max_{0\le r\le n-\tau-1}\left|\sum_{k=0}^{r}\cos(k+1/2)t\right|\right. \\
&\qquad \left. + \sum_{k=n-\tau}^{n} a_{n,k}\left|\cos(k+1/2)t\right|\right] \\
&= \frac{1}{2t}\left[O\left(\frac{a_{n,n-\tau-1}}{t}\right) + A_{n,\tau}\right],
\end{aligned}$$

and

$$\begin{aligned}
A_{n,\tau} &= \sum_{k=n-\tau}^{n} a_{n,k} \\
&= a_{n,n-\tau} + a_{n,n-\tau+1} + \cdots + a_{n,n} \\
&\ge a_{n,n-\tau-1} + a_{n,n-\tau-1} \cdots + a_{n,n-\tau-1} \\
&= (\tau+1)a_{n,n-\tau-1} \\
&= \left(\frac{1}{t}+1\right)a_{n,n-\tau-1} \\
&\ge \left(\frac{a_{n,n-\tau-1}}{t}\right)
\end{aligned}$$

Therefore, $|M_n(t)| = O\left(\frac{A_{n,\tau}}{t}\right)\cdots$ This completes the proof of Lemma 3.1.

4. Proof of Theorem 2.1

The k^{th} partial sum of the conjugate series of the Fourier series (1.2) is given by

$$\begin{aligned}
\tilde{s}_n(f;x) &= -\frac{1}{2\pi}\int_0^{\pi}\cot(t/2)\psi(t)\mathrm{d}t \\
&\quad + \frac{1}{2\pi}\int_0^{\pi}\frac{\cos(n+1/2)t}{\sin(t/2)}\psi(t)\mathrm{d}t
\end{aligned}$$

$$\tilde{s}_n(f;x) - \left(-\frac{1}{2\pi}\int_0^{\pi}\cot(t/2)\psi(t)\mathrm{d}t\right)$$

$$= \frac{1}{2\pi}\int_0^{\pi}\frac{\cos(n+1/2)t}{\sin(t/2)}\psi(t)\mathrm{d}t$$

Then

$$\sum_{k=0}^{n} a_{n,k}\left\{\tilde{s}_n(f;x) - \left(-\frac{1}{2\pi}\int_0^{\pi}\cot(t/2)\psi(t)\mathrm{d}t\right)\right\}$$

$$= \frac{1}{2\pi}\int_0^{\pi}\left(\sum_{k=0}^{n} a_{n,k}\frac{\cos(n+1/2)t}{\sin(t/2)}\right)\psi(t)\mathrm{d}t$$

or,

$$\tilde{\tau}_n(f;x) - \tilde{f}(x) = I_1 + I_2 \qquad (4.1)$$

Using Riesz-Hölder's inequality, condition (2.2), (2.4), note 1, the fact that $(\sin t)^{-1} \le \frac{\pi}{2t}$, for $0 < t \le \pi/2$, $p^{-1}+q^{-1}=1$ and the second mean value theorem for integrals, we find

$$|I_1| \le \left[\int_0^{\pi/n}\left(\frac{t|\psi(t)|}{\xi(t)}\sin^{\beta} t\right)^p \mathrm{d}t\right]^{1/p} \cdot \left[\int_0^{\pi/n}\left\{\frac{\xi(t)}{t\sin^{\beta} t}|M_n(t)|\right\}^q \mathrm{d}t\right]^{1/q}$$

$$\le \left[\int_0^{\pi/n}\left(\frac{t|\psi(t)|}{\xi(t)}\sin^{\beta} t\right)^p \mathrm{d}t\right]^{1/p} \cdot \left[\int_0^{\pi/n}\left\{\frac{\xi(t)|\cos(k+1/2)t|}{t\sin^{\beta} t|\sin(t/2)|}\right\}^q \mathrm{d}t\right]^{1/q}$$

$$= O\left(\frac{1}{n}\right)\left[\int_0^{\pi/n} O\left\{\frac{\xi(t)}{t^2\sin^{\beta} t}\right\}^q \mathrm{d}t\right]^{1/q}$$

$$= O\left(\frac{1}{n}\right)\left[\left(\frac{\pi/n}{\sin(\pi/n)}\right)^{\beta q}\int_h^{\pi/n} O\left\{\frac{\xi(t)}{t^{2+\beta}}\right\}^q \mathrm{d}t\right]^{1/q}; h\to 0$$

$$= O\left(\frac{1}{n}\right)\left[\int_h^{\pi/n}\left\{\frac{\xi(t)}{t^{2+\beta}}\right\}^q \mathrm{d}t\right]^{1/q}; \quad h\to 0$$

$$= O\left(\frac{1}{n}\right)O\left(\xi\left(\frac{\pi}{n}\right)\right)\left[\left(\int_h^{\pi/n} t^{-(2+\beta)q}\mathrm{d}t\right)^{1/q}\right]$$

$$= O\left(n^{-1}\xi\left(\frac{1}{n}\right)\right)O\left(n^{2+\beta-1/q}\right)$$

$$= O\left(n^{\beta+1/p}\xi\left(\frac{1}{n}\right)\right) \tag{4.2}$$

Now by Riesz-Hölder's inequality, conditions (2.3), (2.4), note 1, Lemma 3.1, the fact that $(\sin t)^{-1} \le \frac{\pi}{2t}$, for $0 < t \le \pi/2$, $p^{-1}+q^{-1}=1$, we obtain

$$|I_2| = \left|\int_{\pi/n}^{\pi} |\psi(t)||M_n(t)|\mathrm{d}t\right|$$

$$\le \left\{\int_{\pi/n}^{\pi}\left|\frac{t^{-\delta}\psi(t)\sin^{\beta} t}{\xi(t)}\right|^p \mathrm{d}t\right\}^{1/p}\left\{\int_{\pi/n}^{\pi}\left|\frac{\xi(t)M_n(t)}{t^{-\delta}\sin^{\beta} t}\right|^q \mathrm{d}t\right\}^{1/q}$$

$$= \left\{\int_{\pi/n}^{\pi}\left(\frac{t^{-\delta}|\psi(t)||\sin^{\beta} t|}{\xi(t)}\right)^p \mathrm{d}t\right\}^{1/p} \cdot \left\{\int_{\pi/n}^{\pi}\left(\frac{\xi(t)}{t^{-\delta}\sin^{\beta} t}O\left(\frac{A_{n,\tau}}{t}\right)\right)^q \mathrm{d}t\right\}^{1/q}$$

$$= O\left(n^{\delta}\right)\left\{\int_{\pi/n}^{\pi}\left(\frac{\xi(t)A_{n,\tau}}{t^{-\delta+\beta+1}}\right)^q \mathrm{d}t\right\}^{1/q}$$

$$= O\left(n^{\delta}\right)\left\{\int_{1/\pi}^{\pi/n}\left(\frac{\xi(1/y)}{y^{\delta-\beta-1}}\right)^q \frac{\mathrm{d}y}{y^2}\right\}^{1/q}$$

$$= O\left(n^{\delta}\,\frac{\xi(\pi/n)}{\pi/n}\right)\left\{\int_{1/\pi}^{\pi/n}\left(\frac{\mathrm{d}y}{y^{\delta q-\beta q+2}}\right)\right\}^{1/q}$$

$$= O\left(n^{\delta+1}\,\xi\left(\frac{1}{n}\right)\right)\left\{\frac{\left(\frac{n}{\pi}\right)^{q(-\delta+\beta)-1} - \left(\frac{1}{\pi}\right)^{q(-\delta+\beta)-1}}{q(-\delta+\beta)-1}\right\}^{1/q}$$

$$= O\left(n^{\delta+1}\,\xi\left(\frac{1}{n}\right)\right)O\left(n^{-\delta+\beta-1/q}\right)$$

$$= O\left(n^{\beta+1-1/q}\,\xi(1/n)\right) = O\left(n^{\beta+1/p}\,\xi(1/n)\right). \tag{4.3}$$

Combining I_1 and I_2 yields

$$\left|\tilde{\tau}_n(f;x)-\tilde{f}(x)\right| = O\left(n^{\beta+1/p}\xi(1/n)\right).$$

Now, using the L_p-norm, we get

$$\left\|\tilde{\tau}_n(f;x)-\tilde{f}(x)\right\|_p = \left\{\int_0^{2\pi}\left|\tilde{\tau}_n(f;x)-\tilde{f}(x)\right|^p \mathrm{d}x\right\}^{1/p}$$

$$= O\left\{\int_0^{2\pi}\left(n^{\beta+1/p}\xi(1/n)\right)^p \mathrm{d}x\right\}^{1/p}$$

$$= O\left\{n^{\beta+1/p}\xi(1/n)\left(\int_0^{2\pi}\mathrm{d}x\right)^{1/p}\right\}$$

$$= O\left(n^{\beta+1/p}\xi(1/n)\right).$$

This completes the proof of our Theorem 2.1.

5. Applications

The following corollaries can be derived from our Theorem 2.1.

Corollary 5.1. If $\beta = 0$ and $\xi(t) = t^{\alpha}$, $0 < \alpha \le 1$, then the generalized weighted class $W\left(L_p, \xi(t)\right)$ reduces to class $Lip(\alpha, p)$ and the degree of approximation of a function $f(x) \in Lip(\alpha, p)$ is given by $\left\|\tilde{\tau}_n(f;x)-\tilde{f}(x)\right\|_p = O\left(n^{-\alpha+1/p}\right)$.

Proof of corollary 5.1. From our Theorem 2.1 for $\beta = 0$, we have

$$\left\|\tilde{\tau}_n(f;x)-\tilde{f}(x)\right\|_p = \left(\int_0^{2\pi}\left|\tilde{\tau}_n(f;x)-\tilde{f}(x)\right|^p \mathrm{d}x\right)^{1/p}$$

$$= O\left(n^{1/p}\xi(1/n)\right) = O\left(\frac{1}{n^{\alpha-1/p}}\right), p \ge 1.$$

This completes the proof of corollary 5.1.

Corollary 5.2. If $p \to \infty$ in corollary 5.1, then for

$0<\alpha<1$, $\left\|\tilde{\tau}_n(f;x)-\tilde{f}(x)\right\|_p=O\left(n^{-\alpha}\right)$.

Corollary 5.3. If $a_{n,k}=p_{n-k}P_n^{-1}, P_n\neq 0, \xi(t)=t^{\alpha}$ then the degree of approximation of $\tilde{f}(x)$, conjugate of $f\in Lip(\alpha,p)$ by Nörlund means $\tilde{\tau}_n(f;x)=P_n^{-1}\sum_{k=0}^{n}p_{n-k}\tilde{s}_k(f;x)$ of the conjugate series of Fourier series is given by

$$\left\|\tilde{\tau}_n(f;x)-\tilde{f}(x)\right\|_p=O\left(n^{-\alpha+1/p}\right).$$

Corollary 5.4. If $a_{n,k}=p_{n-k}P_n^{-1}, P_n\neq 0, \xi(t)=t^{\alpha}, p\to\infty$ then the degree of approximation of $\tilde{f}(x)$, conjugate of $f\in Lip\ \alpha$ by Nörlund means $\tilde{\tau}_n=P_n^{-1}\sum_{k=0}^{n}p_{n-k}\tilde{s}_k$ of the conjugate series of Fourier series is given by

$$\left\|\tilde{\tau}_n-\tilde{f}\right\|_{\infty}=\begin{cases}O\left((n+1)^{-\alpha}\right), 0<\alpha<1,\\ O\left(\log(n+1)\pi e/(n+1)\right), \alpha=1.\end{cases}\quad(5.1)$$

Corollary 5.5. If $a_{n,k}=p_{n-k}q_kR_n^{-1}$ such that $R_n=\sum_{k=0}^{n}p_{n-k}q_k\neq 0, R_y y^{-\alpha}$ is monotonic non-decreasing then the degree of approximation of $\tilde{f}(x)$, conjugate of a function $f\in Lip\,\alpha$, by generalized Nörlund means $\tilde{\tau}_n(f;x)=R_n^{-1}\sum_{k=0}^{n}p_{n-k}q_k\tilde{s}_k(f;x)$ of the conjugate series (1.2) satisfies equation (5.1).

6. Remarks

Remark 6.1. Lal and Kushwaha [14]. The degree of approximation $\left\|\tilde{\tau}_n(f;x)-\tilde{f}(x)\right\|_p=O\left(n^{-\alpha+1/p}\right)$. determined by Qureshi [13, p. 561, L. 12] tends to ∞ if $0<\alpha<3^{-1}<1$ and $p=2$ and also for other values. Therefore, this deficiency has encouraged to investigate degree of approximation of conjugate of functions belonging to $Lip(\alpha,p)$ considering $p^{-1}<\alpha<1$.

7. Acknowledgements

The authors are grateful to his beloved parents for their encouragement to his work. The authors are grateful to the referee for his valuable suggestions and useful comments for the improvement of this paper. The authors are also thankful to the AM Editor in chief Prof. Chris Cannings, University of Sheffield, UK and AM Editorial Assistant Ms. Tian Huang, Scientific Research Publishing, USA for their kind cooperation during communication.

8. References

[1] A. Zygmund, "Trigonometric Series Vol. I," Cambridge University Press, Cambridge, 1959.

[2] O. Töeplitz, "Über Allgemeine Lineare Mittelbildungen," *Prace Matematyczno—Fizyczne Journal*, Vol. 22, 1913, pp. 113-119. http://www.zentralblatt-math.org/zmath/en/journals/search/?an=00003590

[3] L. McFadden, "Absolute Nörlund Summability," *Duke Mathematical Journal*, Vol. 9, 1942, pp. 168-207. doi:10.1215/S0012-7094-42-00913-X

[4] H. H. Khan, "On the Degree of Approximation to a Function Belonging to Weighted (L^P, $\xi(t)$) Class," *Aligarh Bulletin of Mathematics*, Vol. 3-4, 1973-1974, pp. 83-88.

[5] V. N. Mishra, "Some Problems on Approximations of Functions in Banach Spaces," Ph.D. Thesis, Indian Institute of Technology, Roorkee, 2007.

[6] V. N. Mishra, "On the Degree of Approximation of Signals (Functions) Belonging to the Weighted $W(L_P, \xi(t))$, ($p \geq 1$)-Class by Almost Matrix Summability Method of Its Conjugate Fourier Series," *International Journal of Applied Mathematics and Mechanics*, Vol. 5, No. 7, 2009, pp. 16-27.

[7] K. Qureshi, "On the Degree of Approximation of a Function Belonging to *Lip*α," *Indian Journal of Pure and Applied Mathematics*, Vol. 13, No. 8, 1982, pp. 898-903.

[8] K. Qureshi, "On the Degree of Approximation of a Function Belonging to the Class *Lip*(α,*p*)," *Indian Journal of Pure and Applied Mathematics*, Vol. 13, No. 4, 1982, pp. 466-470.

[9] H. H. Khan, "On the Degree of Approximation to a Function by Triangular Matrix of Its Conjugate Fourier Series II," *Indian Journal of Pure and Applied Mathematics*, Vol. 6, 1975, pp. 1473-1478.

[10] P. Chandra, "Trigonometric Approximation of Functions in L_P-Norm," *Journal of Mathematical Analysis and Applications*, Vol. 275, 2002, pp. 13-26. doi:10.1016/S0022-247X(02)00211-1

[11] L. Leindler, "Trigonometric Approximation in L_P-Norm," *Journal of Mathematical Analysis and Applications*, Vol. 302, 2005, pp. 129-136. doi:10.1016/j.jmaa.2004.07.049

[12] K. Qureshi, "On the Degree of Approximation of Conjugate of Function Belonging to the Lipschitz Class by Means of Conjugate Series," *Indian Journal of Pure and Applied Mathematics*, Vol. 12, No. 9, 1981, pp. 1120-1123.

[13] K. Qureshi, "On the Degree of Approximation of Conjugate of Function Belonging to the Class *Lip*(α,*p*) by Means of Conjugate Series," *Indian Journal of Pure and Applied Mathematics*, Vol. 13, No. 5, 1982, pp. 560-563.

[14] S. Lal, and J. K. Kushwaha, "Approximation of Conjugate of Functions Belonging to the Generalized Lipschitz class by Lower Triangular Matrix Means," *International Journal of Mathematical Analysis*, Vol. 3, No. 21, 2009, pp. 1031-1041.

Applied Mathematics, **2011, 2, 1453-1461**
doi:10.4236/am.2011.212207 Published Online December 2011 (http://www.SciRP.org/journal/am)

Propagation of Torsional Surface Waves under the Effect of Irregularity and Initial Stress

Shishir Gupta, Dinesh K. Majhi, Sumit K. Vishwakarma, Santimoy Kundu
Department of Applied Mathematics, Indian School of Mines, Dhanbad, India
E-mail: *shishir_ism@yahoo.com*
Received August 24, 2011; *revised October* 14, 2011; *accepted October* 23, 2011

Abstract

The present paper has been framed to study the influence of irregularity, initial stress and porosity on the propagation of torsional surface waves in an initially stressed anisotropic poro-elastic layer over a semi-infinite heterogeneous half space with linearly varying rigidity and density due to irregularity at the interface. The irregularity has been taken in the half-space in the form of a parabola. It is observed that torsional surface waves propagate in this assumed medium. In the absence of irregularity the velocity of torsional surface wave has been obtained. Further, it has been seen that for a layer over a homogeneous half space, the velocity of torsional surface waves coincides with that of Love waves.

Keywords: Irregularity, Torsional Surface Waves, Anisotropic, Initial Stress

1. Introduction

The study of surface waves in a half-space is important to seismologists due to its possible applications in Geophysical prospecting and in understanding the cause and estimation of damage due to earthquakes. Surface waves carry the greatest amount of energy from shallow shocks and are of primary cause of destruction that can result from earthquakes. The propagation of surface waves in detail are well documented in the text book literature (Achenbach, J. D. [1], Ewing, W. M., Jardetzky, W. S., Press, F. [2], Bath, M. [3]). One type of surface wave may be available in non-homogeneous earth known as torsional surface waves. These waves are horizontally polarized but give a twist to the medium when it propagates. Although much information is available on the propagation of surface waves such as Rayleigh waves, Love waves and Stonely waves etc., the torsional wave has not drawn much attention and very little literature is available on the propagation of this wave. Some papers have been published on the propagation of torsional waves in elastic medium with different types of inhomogeneity. Lord Rayleigh [4] in his remarkable paper showed that the isotropic homogeneous elastic half-space does not allow a torsional surface wave to propagate, in this connection Georgiadis *et al*. [5] have examined the torsional surface wave in a linear gradient-elastic half-space. Meissner [6] pointed out that in an inhomogeneous elastic half-space with quadratic variation of shear modulous and density varying linearly with depth, torsional surface waves do exist. Vardoulakis, I. [7] has studied the problem on torsional surface waves in inhomogeneous elastic media. Also S. Dey *et al.* [8] studied the propagation of torsional waves in a homogeneous substratum over a heterogeneous half-space.

The study of porous medium in recent time has acquired prime interest. The layer of the earth usually of such materials and the medium is generally dealt under the name of poro-elastic medium. Investigation on propagation of waves in liquid saturated porous solids are relevant to geophysical prospecting methods, survey techniques are very useful in oil industry. While deriving the mechanics of such medium it is assumed that the pore sizes are small and macroscopially speaking their average distribution is uniform. The role of pore water in seismology has been emphasized in many studies. Biot [9] has established the theory of the propagation of elastic waves in a porous elastic solid saturated by a viscous fluid. Under the assumption of dynamic coupling between solid and fluid mass, Biot [10] has developed the mathematical theory for the propagation of elastic waves in a fluid saturated porous medium. Based on this theory, many problems of surface waves in poro-elastic materials have been studied in the past years by Buckingham, M. J. [11], Sharma, M. D. and Gogna, M. L. [12], Sharma, M. D., Kumar, R. and Gogna, M. L. [13], Sharma, M. D., Kumar, R. and Gogna, M. L. [14].

The development of initial stresses in the medium is

due to many reasons, for example resulting from the difference of temperature, process of quenching, shot peening and cold working, slow process of creep, differential external forces, gravity variations etc. These stresses have a pronounced influence on the propagation of waves as shown by Biot [15]. The earth is also an initially stressed medium. It is therefore of much interest to study the influence of these stresses on the propagation of torsional surface wave. The study of surface waves in an initially stressed medium is of interest not for theoretical taste only but for practical purposes too. Based on the pioneering work of Biot [15] on pre-stressed solids, various studies of body and surface wave propagation in the pre-stressed solids have been carried out by many researchers such as Chattopadhyay *et al.* [16], Kar, B. K. and Kalyani, V. K. [17] and Dey, S. and Addy, S. K. [18] .

The study of wave propagation in elastic medium with different irregularities is of great importance to seismologists as well as to geophysicists to understand and predict the seismic behavior at the different margins of earth. This fact leads us towards this study. The present paper discusses the possibility of existence of torsional surface wave in an initially stressed anisotropic poro-elastic layer over a semi-infinite heterogeneous half space with linearly varying rigidity and density due to irregularity at the interface. The irregularity has been taken in the half-space in the form of a parabola. It is observed that torsional surface waves propagate in this assumed medium. Irregularity and initial stress play an important role in the seismic wave propagation. This paper has been framed out to show the effect of irregularity at the interface in the parabolic form and initial stress on the propagation of torsional surface wave. As the porosity parameter decreases, the half-space will become an elastic solid with less pores and the velocity of torsional surface waves decreases and ultimately vanishes when the medium is elastic solid. The effect of irregularity and the initial stresses are very prominent on the propagation of torsional surface waves. The presence of initial compressive stress reduces the velocity of torsional surface waves. As the initial compressive stress increases, the velocity of propagation decreases. It is also observed that in the limiting case if the porous medium changes to a liquid layer then a torsional surface wave don't exist. It is interesting to note that in a poro-elastic medium over a homogeneous half-space the torsional wave mode changes to Love wave mode. Parabolic irregularity is mostly found in the earth so the present study can help the seismologists to understand and predict the seismic behaviour at different margins of the earth.

2. Formulation of the Problem

Let us Consider a model which consists of a water saturated porous layer M_1 of thickness H with anisotropy of Weiskopf type under compressive initial stresses $P' = -s'_{rr}$ along the radial direction and with one parabolic irregularity on the interface between the layer and a semi-infinite non-homogeneous elastic half-space M_2 as shown in **Figure 1**. The heterogeneity has been considered both in density and rigidity. We assume that the irregularity is of the form of a parabola with span of length 2 *m* and depth *h*.

Assuming the origin of the cylindrical co-ordinate system at the middle point of the interface irregularity and the z-axis downward positive, the following variation in rigidity and density has been taken

1) for the layer, $\mu = \mu_o, \rho = \rho_0$

2) for the half-space, $\mu = \mu_1(1+az), \rho = \rho_1(1+bz)$

where μ and ρ are rigidity and density of the media respectively and a, b are constants having dimensions that are inverse of length.

The equation of irregularity has been taken as

$$z = \varepsilon F(r), \text{where } F(r) = \begin{cases} h\left(1-\dfrac{r^2}{m^2}\right) \text{ for } |r| \le m \\ 0 \text{ for } |r| > m \end{cases}$$

and $\varepsilon = \dfrac{h}{2m}$ and $\varepsilon \ll 1$.

3. Solution of the Problem

3.1. Solution for Porous Layer

The dynamical equations of initially stressed poroelastic medium is obtained by suitably coupling Biot's [19] dynamical equations of an initially stressed medium with the equations of poro-elasticity given by Weiskopf [20] and Biot [9,10]. Those are

$$\frac{\partial s'_{rr}}{\partial r} + \frac{1}{r}\frac{\partial s'_{r\theta}}{\partial \theta} + \frac{\partial s'_{rz}}{\partial z} + \frac{s'_{rr} - s'_{\theta\theta}}{r} - P'\frac{\partial \omega'_\theta}{\partial z} = \frac{\partial^2}{\partial t^2}\left(\rho_{rr}u'_r + \rho_{r\theta}U'_r\right) \tag{1}$$

$$\frac{\partial s'_{r\theta}}{\partial r} + \frac{1}{r}\frac{\partial s'_{\theta\theta}}{\partial \theta} + \frac{\partial s'_{\theta z}}{\partial z} + \frac{2}{r}s'_{r\theta} - P'\frac{\partial \omega'_z}{\partial r} = \frac{\partial^2}{\partial t^2}\left(\rho_{rr}v'_\theta + \rho_{r\theta}V'_\theta\right) \tag{2}$$

$$\frac{\partial s'_{rz}}{\partial r} + \frac{1}{r}\frac{\partial s'_{\theta z}}{\partial \theta} + \frac{\partial s'_{zz}}{\partial z} + \frac{1}{r}s'_{rz} - P'\frac{\partial \omega'_\theta}{\partial r} = \frac{\partial^2}{\partial t^2}\left(\rho_{rr}w'_z + \rho_{r\theta}W'_z\right) \tag{3}$$

and

$$\frac{\partial s'}{\partial r} = \frac{\partial^2}{\partial t^2}\left(\rho_{r\theta}u'_r + \rho_{\theta\theta}U'_r\right) \tag{4}$$

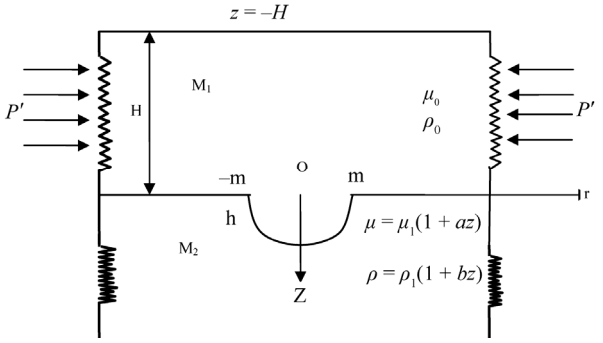

Figure 1. Geometry of the problem.

$$\frac{\partial s'}{\partial \theta} = \frac{\partial^2}{\partial t^2}\left(\rho_{r\theta} v'_\theta + \rho_{\theta\theta} V'_\theta\right) \tag{5}$$

$$\frac{\partial s'}{\partial z} = \frac{\partial^2}{\partial t^2}\left(\rho_{r\theta} w'_z + \rho_{\theta\theta} W'_z\right) \tag{6}$$

where s'_{ij} =incremental stress components;

$\left(u'_r, v'_\theta, w'_z\right)$ = components of the displacement vector of the solid;

$\left(U'_r, V'_\theta, W'_z\right)$ = components of the displacement vector of the liquid;

s' = stress in the liquid,

and

$$\begin{aligned}\omega'_r &= \frac{1}{2r}\left[\frac{\partial w'_z}{\partial \theta} - r\frac{\partial v'_\theta}{\partial z}\right], \omega'_\theta = \frac{1}{2}\left[\frac{\partial u'_r}{\partial z} - \frac{\partial w'_z}{\partial r}\right] \\ \omega'_z &= \frac{1}{2r}\left[\frac{\partial (r v'_\theta)}{\partial r} - \frac{\partial v'_\theta}{\partial \theta}\right]\end{aligned} \tag{7}$$

are the components of the rotational vector ω'.

The stress-strain relations for the water saturated anisotropic porous layer under normal initial stress P' are

$$\begin{aligned} s'_{rr} &= \left(A + P'\right)e_{rr} + \left(A - 2N + P'\right)e_{\theta\theta} + \left(F + P'\right)e_{zz} + Q_\varepsilon \\ s'_{\theta\theta} &= \left(A - 2N\right)e_{rr} + Ae_{\theta\theta} + Fe_{zz} + Q_\varepsilon \\ s'_{zz} &= Fe_{rr} + Fe_{\theta\theta} + Ce_{zz} + Q_\varepsilon \\ s'_{r\theta} &= 2Ne_{r\theta}, s'_{\theta z} = 2Ge_{\theta z}, s'_{rz} = 2Ge_{zr} \end{aligned} \tag{8}$$

where A, F, C, N and G are elastic constants of the medium. N and G are, in particular, shear moduli of the anisotropic layer in the radial and the z-direction respectively.

$$\begin{aligned} e_{rr} &= \frac{\partial u'_r}{\partial r},\ e_{\theta\theta} = \frac{1}{r}\frac{\partial v'_\theta}{\partial \theta} + \frac{u'_r}{r},\ e_{zz} = \frac{\partial w'_z}{\partial z} \\ e_{r\theta} &= \frac{1}{2}\left[\frac{1}{r}\frac{\partial u'_r}{\partial \theta} + \frac{\partial v'_\theta}{\partial r} - \frac{v'_\theta}{r}\right], e_{\theta z} = \frac{1}{2}\left[\frac{\partial v'_\theta}{\partial z} + \frac{1}{r}\frac{\partial w'_z}{\partial \theta}\right] \\ e_{zr} &= \frac{1}{2}\left[\frac{\partial w'_z}{\partial r} + \frac{\partial u'_r}{\partial z}\right] \end{aligned} \tag{9}$$

Further, Q_ε being the measure of coupling between the volume change of the solid and the liquid is a positive quantity. $\boldsymbol{s}'$ is the stress vector due to the liquid. The stress vector $\boldsymbol{s}'$ is related to the fluid pressure $\boldsymbol{P}$ by the relation

$$-\boldsymbol{s}' = f\boldsymbol{P} \tag{10}$$

where f is porosity of the layer.

The mass coefficients $\rho_{rr}, \rho_{r\theta}$ and $\rho_{\theta\theta}$ are related to the densities ρ, ρ_s, ρ_w of the layer, the solid and the water respectively by

$$\rho_{rr} + \rho_{r\theta} = (1 - f)\rho_s,\ \rho_{r\theta} + \rho_{\theta\theta} = f\rho_w \tag{11}$$

so that the mass density of the aggregate is

$$\rho' = \rho_s + f\left(\rho_w - \rho_s\right) \tag{12}$$

The above relation shows that in case the fluid of lighter density $\left(\rho_w\right)$ is filled up in the solid matrix of density $\left(\rho_s\right)$ then the density of the aggregate $\left(\rho'\right)$ will be less than the density of the solid $\left(\rho_s\right)$, there may be the case of heavier fluid such as mercury, molten metal etc. filled in the solid matrix, when the density of the aggregate will be more than that of solid. Further this relation shows that as the porosity factor f decreases from 1 to 0 *i.e.* as the volume of pores decreases, the density of the aggregate tends to the density of the solid. It has been shown by Biot that the mass coefficients obey the following inequalities also

$$\rho_{rr} > 0,\ \rho_{\theta\theta} > 0,\ \rho_{r\theta} < 0\ ,\ \rho_{rr}\rho_{\theta\theta} - \rho_{r\theta}^2 > 0 \tag{13}$$

For torsional surface waves propagating along the radial direction having displacement of the particles along θ direction we have,

$$\left.\begin{aligned} u'_r = 0, w'_z = 0, v'_\theta = v'(r, z, t) \\ U'_r = 0, W'_z = 0, V'_\theta = V'(r, z, t) \end{aligned}\right\} \tag{14}$$

The above displacements will produce $e_{\theta z}$ and $e_{r\theta}$ strain components and the other strain components will be zero. Hence the stress-strain relations are

$$s'_{\theta z} = 2Ge_{\theta z}, s'_{r\theta} = 2Ne_{r\theta} \tag{15}$$

Using (15) in (1) to (6) the equations of motion, which are not automatically satisfied, are

$$\frac{\partial s'_{r\theta}}{\partial r} + \frac{\partial s'_{\theta z}}{\partial z} + \frac{2}{r}s'_{r\theta} - P'\frac{\partial \omega'_z}{\partial r} = \frac{\partial^2}{\partial t^2}\left(\rho_{rr} v'_\theta + \rho_{r\theta} V'_\theta\right) \tag{16}$$

$$\frac{\partial^2}{\partial t^2}\left(\rho_{r\theta} v'_\theta + \rho_{\theta\theta} V'_\theta\right) = 0 \tag{17}$$

Using stress-strain relations (8), (16) may be written as

$$\begin{aligned} &\left(N - \frac{P'}{2}\right)\left(\frac{\partial^2 v'_\theta}{\partial r^2} - \frac{v'_\theta}{r^2} + \frac{1}{r}\frac{\partial v'_\theta}{\partial r}\right) + G\frac{\partial^2 v'_\theta}{\partial z^2} \\ &= \frac{\partial^2}{\partial t^2}\left(\rho_{rr} v'_\theta + \rho_{r\theta} V'_\theta\right) \end{aligned} \tag{18}$$

From (17), we have

$$\rho_{r\theta}v'_{\theta}+\rho_{\theta\theta}V'_{\theta}=d''(say)$$

$$\therefore V'_{\theta}=\frac{d''-\rho_{r\theta}v'_{\theta}}{\rho_{\theta\theta}}$$

Now,

$$\frac{\partial^2}{\partial t^2}\left(\rho_{rr}v'_{\theta}+\rho_{r\theta}V'_{\theta}\right)=d'\frac{\partial^2\left(v'_{\theta}\right)}{\partial t^2}, \tag{19}$$

where $d'=\rho_{rr}-\dfrac{\rho_{r\theta}^2}{\rho_{\theta\theta}}$

Using (19) in (18), we get

$$\left(N-\frac{P'}{2}\right)\left(\frac{\partial^2 v'_{\theta}}{\partial r^2}-\frac{v'_{\theta}}{r^2}+\frac{1}{r}\frac{\partial v'_{\theta}}{\partial r}\right)+G\frac{\partial^2 v'_{\theta}}{\partial z^2}=d'\frac{\partial^2 v'_{\theta}}{\partial t^2} \tag{20}$$

From Equation (20) it is clear that the velocity of the shear wave along radial(r) direction is $\left[\dfrac{N-\dfrac{P'}{2}}{d'}\right]^{\frac{1}{2}}$ and that along z-direction is $\left(\dfrac{G}{d'}\right)^{\frac{1}{2}}$. Now the shear wave velocity β' in the porous medium along radial direction may be expressed as,

$\beta'=\left[\dfrac{1-\zeta}{d}c_{\beta}^2\right]^{\frac{1}{2}}$, where $c_{\beta}=\sqrt{\dfrac{N}{\rho'}}$ is the velocity of the shear wave in the corresponding initial stress free non-porous anisotropic elastic medium along the radial direction, $\zeta=\dfrac{P'}{2N}$ is the non-dimensional parameter due to the initial stress P' and the density ratio,

$$d=\frac{d'}{\rho'}=\frac{1}{\rho'}\left(\rho_{rr}-\frac{\rho_{r\theta}^2}{\rho_{\theta\theta}}\right)=\gamma_{11}-\frac{\gamma_{12}^2}{\gamma_{22}}$$

where $\gamma_{11}=\dfrac{\rho_{rr}}{\rho'},\gamma_{12}=\dfrac{\rho_{r\theta}}{\rho'},\gamma_{22}=\dfrac{\rho_{\theta\theta}}{\rho'}$ are the non-dimensional parameters for the material of the porous layer as obtained by Biot.

Introducing the non-dimensional radial and depth coordinates we have

$$R=\frac{r}{L},\xi=\xi_0+\frac{z}{L},$$

ξ_0 being a constant and $\dfrac{1}{L}$ being wave number where $k=\dfrac{1}{L}$, the Equation (20) may be written as

$$\frac{\partial^2 v'_{\theta}}{\partial R^2}+\frac{1}{R}\frac{\partial v'_{\theta}}{\partial R}-\frac{v'_{\theta}}{R^2}+\frac{G}{N-\dfrac{P'}{2}}\frac{\partial^2 v'_{\theta}}{\partial \xi^2}=\frac{d'L^2}{N-\dfrac{P'}{2}}\frac{\partial^2 v'_{\theta}}{\partial t^2} \tag{21}$$

We assume a solution of Equation (21) of the form $v'_{\theta}=v'_2(\xi)J_1(R)e^{i\omega t}$, where $J_1(R)$ is the Bessel function of the first kind and $v'_2(\xi)$ is the solution of the following equation

$$\frac{d^2 v'_2}{d\xi^2}+q^2v'_2=0 \tag{22}$$

where $q^2=\dfrac{\left(\dfrac{\omega^2L^2d'}{N-\dfrac{P'}{2}}-1\right)}{\dfrac{G}{N-\dfrac{P'}{2}}}$

The solution of Equation (22) may be taken as

$$v'_2(\xi)=Ae^{iq\xi}+Be^{-iq\xi}$$

Therefore, for the torsional surface wave propagating in the radial direction, the solution of Equation (21) may be taken as

$$v'_{\theta}=J_1(R)\left(Ae^{iq\xi}+Be^{-iq\xi}\right)e^{i\omega t} \tag{23}$$

where $q^2=d\upsilon\left(\dfrac{c^2}{c_{\beta}^2}-\dfrac{1-\zeta}{d}\right)$, where $\upsilon=\dfrac{N}{G},c=\omega L$ is the phase velocity of the torsional surface wave.

3.2. Solution for Non-Homogeneous Elastic Half Space

The lower medium is considered as non-homogeneous elastic half space. The Equaiton of motion may be written as

$$\frac{\partial\sigma_{r\theta}}{\partial r}+\frac{2}{r}\sigma_{r\theta}+\frac{\partial\sigma_{z\theta}}{\partial z}=\rho\frac{\partial^2 v}{\partial t^2} \tag{24}$$

where $\sigma_{r\theta}$ and $\sigma_{z\theta}$ are stress components in the half space, $v(r,\theta,z)$ is the displacement and ρ is the density of the material of the half space.

The non-homogeneity in the medium are taken as

$$\mu=\mu_1(1+az),\rho=\rho_1(1+bz) \tag{25}$$

where, μ_1 and ρ_1 are the values of μ and ρ respectively at $z=0$, and a,b are constants having dimensions that are inverse of length.

Using the stress-strain relations

$$\sigma_{r\theta}=\mu\left[\frac{\partial v}{\partial r}-\frac{v}{r}\right],\sigma_{z\theta}=\mu\frac{\partial v}{\partial z} \tag{26}$$

and the relations (25), the Equation of motion (24) may be written as

$$\frac{\partial^2 v}{\partial r^2}+\frac{1}{r}\frac{\partial v}{\partial r}-\frac{v}{r^2}+\frac{\partial^2 v}{\partial z^2}+\frac{a}{1+az}\frac{\partial v}{\partial z}=\frac{\rho_1(1+bz)}{\mu_1(1+az)}\frac{\partial^2 v}{\partial t^2} \quad (27)$$

Introducing the non-dimensional co-ordinates

$$R=\frac{r}{L} \text{ and } \xi=\xi_0+\frac{z}{L},$$

Equation (27) takes the form as

$$\frac{\partial^2 v}{\partial R^2}+\frac{1}{R}\frac{\partial v}{\partial R}-\frac{v}{R^2}+\frac{\partial^2 v}{\partial \xi^2}+\frac{La}{\left[1+a(\xi-\xi_0)L\right]}\frac{\partial v}{\partial \xi}=\frac{\rho_1 L^2}{\mu_1}\frac{1+b(\xi-\xi_0)L}{1+a(\xi-\xi_0)L}\frac{\partial^2 v}{\partial t^2} \quad (28)$$

We assume a solution of Equation (28) of the form

$$v=v_2(\xi)J_1(R)e^{i\omega t},$$

where v_2 is the solution of the following equation

$$\frac{\mathrm{d}^2 v_2}{\mathrm{d}\xi^2}+\frac{aL}{1+a(\xi-\xi_0)L}\frac{\mathrm{d}v_2}{\mathrm{d}\xi}+\left[\frac{c^2}{c_1^2}\frac{1+b(\xi-\xi_0)L}{1+a(\xi-\xi_0)L}-1\right]v_2=0 \quad (29)$$

In the above, $c=\omega L$ is the phase velocity of the torsional surface wave and $c_1=\sqrt{\frac{\mu_1}{\rho_1}}$, velocity of shear wave in an initially stress-free elastic medium and $J_1(R)$ is the Bessel function of the first kind.

Substituting $v_2(\xi)=\frac{L^{-\frac{1}{2}}\phi(\xi)}{\left[\frac{1}{L}+a(\xi-\xi_0)\right]^{\frac{1}{2}}}$ in the Equation (29) to eliminate the term $\frac{\mathrm{d}v_2}{\mathrm{d}\xi}$,

we obtain

$$\phi''(\xi)+\left[\frac{a^2}{4\left\{\frac{1}{L}+a(\xi-\xi_0)\right\}^2}+\frac{c^2}{c_1^2}\frac{\frac{1}{L}+b(\xi-\xi_0)}{\frac{1}{L}+a(\xi-\xi_0)}-1\right]\phi(\xi)=0 \quad (30)$$

Using $\phi(\xi)=\psi(\eta)$ in (30), where $\eta=\frac{2p}{a}\left[\frac{1}{L}+a(\xi-\xi_0)\right]$ we get

$$\psi''(\eta)+\left[\frac{1}{4\eta^2}+\frac{s}{\eta}-\frac{1}{4}\right]\psi(\eta)=0 \quad (31)$$

where $s=\frac{c^2(a-b)L}{2c_1^2 pa^2L^2}$, $p^2=1-\frac{b}{a}\frac{c^2}{c_1^2}$

Equation (31) is Whittaker's equation.

We are interested in the solution of Equation (31) which is bounded and vanishes as $z\to\infty$, therefore we search for the solution which gives $v(z)\to 0$ as $z\to\infty$. This condition is equivalent to $\lim_{\eta\to\infty}\psi(\eta)\to 0$.

Therefore the solution of Equation (31) satisfying the above condition may be written as

$$v=\frac{D_1 W_{s,0}(\eta)}{L^{\frac{1}{2}}\left(\frac{a\eta}{2p}\right)^{\frac{1}{2}}}J_1(R)e^{i\omega t} \quad (32)$$

4. Boundary Conditions and Dispersion Equation

The boundary conditions are as follows

1) $\mu_0\left(\frac{\partial v'_\theta}{\partial z}\right)=0$ at $z=-H$
2) $v'_\theta=v$ at $z=\varepsilon F(r)$
3) $(\sigma_{r\theta})_0=(\sigma_{r\theta})_1$ at $z=\varepsilon F(r)$

where

$$(\sigma_{r\theta})_0=l\mu_0\frac{\partial v'_\theta}{\partial\theta}+n\mu_0\frac{\partial v'_\theta}{\partial z},$$

$$(\sigma_{r\theta})_1=l\mu_1\frac{\partial v}{\partial\theta}+n\mu_1\frac{\partial v}{\partial z}$$

and $(l,0,n)$ are components of unit normal (to the interface at $z = 0$).

$$l=0, n=1 \text{ at } z=-H$$

$$l=-\frac{\varepsilon F'}{\sqrt{1+\varepsilon^2 F'^2}}, n=\frac{1}{\sqrt{1+\varepsilon^2 F'^2}};$$

at $z=\varepsilon F(r)$

where $F'=\frac{\mathrm{d}F}{\mathrm{d}r}$

The boundary condition (3) may be written as

$$\mu_0\left(\frac{\partial v'_\theta}{\partial r}-\frac{v'_\theta}{r}\right)\left(-\frac{\varepsilon F'}{\sqrt{1+\varepsilon^2 F'^2}}\right)+\frac{1}{\sqrt{1+\varepsilon^2 F'^2}}\mu_0\frac{\partial v'_\theta}{\partial z}=\mu_1\left(\frac{\partial v}{\partial r}-\frac{v}{r}\right)\left(-\frac{\varepsilon F'}{\sqrt{1+\varepsilon^2 F'^2}}\right)+\frac{1}{\sqrt{1+\varepsilon^2 F'^2}}\mu_1\frac{\partial v}{\partial z},$$

at $z=\varepsilon F(r)$

Now, using boundary conditions (1), (2) and (3) respectively we get

$$Ae^{iq\left(\xi_0-\frac{H}{L}\right)}-Be^{-iq\left(\xi_0-\frac{H}{L}\right)}=0 \tag{33}$$

$$Ae^{iq\xi}+Be^{-iq\xi}=\frac{D_1W_{s,0}(\eta)}{\left(1+a\varepsilon F(r)\right)^{\frac{1}{2}}} \tag{34}$$

$$AM_1e^{iq\xi}-BN_1e^{-iq\xi}=D_1K_1 \tag{35}$$

where

$$\begin{aligned}K_1=\frac{\mu_1}{\mu_0}\Bigg[&\frac{W_{s,0}(\eta)}{\left(1+a\varepsilon F(r)\right)^{1/2}}\left(\frac{2rh\varepsilon}{m^2}\right)\left\{\frac{1}{L}J_1'\left(\frac{r}{L}\right)-\frac{1}{r}J_1(R)\right\}\\&+\left(\frac{2p}{aL}\right)^s J_1(R)e^{-p/aL\left(1+a\varepsilon F(r)\right)}\left(1+az\right)^{s-\frac{1}{2}}\\&\left\{\frac{a^2L}{8p}\frac{(s-0.5)^2(s+0.5)(3.5-s)}{\left(1+a\varepsilon F(r)\right)^2}\right.\\&-\frac{a^3L^2}{8p^2}\frac{(s-0.5)^2(s-1.5)^2(2.5-s)}{\left(1+a\varepsilon F(r)\right)^3}\\&+\frac{a(s-0.5)(s+1.5)}{2\left(1+a\varepsilon F(r)\right)}-\frac{p}{L}\\&\left.-\frac{a^2L}{2p}\frac{(s-0.5)^3}{\left(1+a\varepsilon F(r)\right)^2}\right\}\Bigg]\end{aligned} \tag{36}$$

Now, eliminating A, B and D_1 from Equations (33), (34) and (35) we get

$$\begin{vmatrix} e^{iq\left(\xi_0-\frac{H}{L}\right)} & -e^{-iq\left(\xi_0-\frac{H}{L}\right)} & 0\\ e^{iq\xi} & e^{-iq\xi} & -\frac{W_{s,0}(\eta)}{\left(1+a\varepsilon F(r)\right)^{\frac{1}{2}}}\\ M_1e^{iq\xi} & N_1-e^{-iq\xi} & -K_1 \end{vmatrix}=0 \tag{37}$$

Expanding the Whittaker function $W_{s,0}(\eta)$ up to linear terms in η, Equation (37) reduces to

$$\tanh q\left(\varepsilon F(r)+\mathrm{H}\right)=\frac{1}{q}\left[R_1-\frac{\mu_1}{\mu_0}\frac{R_2}{R_3}\right] \tag{38}$$

where

$$R_1=\frac{-2rh\varepsilon}{m^2}\left(1-\frac{\mu_1}{\mu_0}\right)\left(\frac{R}{4}+\frac{R^3}{96}+\frac{R^5}{1536}\right),$$

$$\begin{aligned}R_2=\Bigg(&\frac{a^2L^2}{8p}\frac{(s-0.5)^2(s+0.5)(3.5-s)}{\left(1+a\varepsilon F(r)\right)^2}\\&-\frac{a^3L^3}{8p^2}\frac{(s-0.5)^2(s-1.5)^2(2.5-s)}{\left(1+a\varepsilon F(r)\right)^3}\\&+\frac{aL(s-0.5)(s+1.5)}{2\left(1+a\varepsilon F(r)\right)}-p-\frac{a^2L^2}{2p}\frac{(s-0.5)^3}{\left(1+a\varepsilon F(r)\right)^2}\Bigg),\end{aligned}$$

$$R_3=\left(1-\frac{aL}{2p}\frac{(s-0.5)^2}{\left(1+\varepsilon F(r)\right)}+\frac{a^2L^2}{8p^2}\frac{(s-0.5)^2(s-1.5)^2}{\left(1+\varepsilon F(r)\right)^2}\right).$$

5. Particular Cases

If the medium is non-porous then $f\to 0$ and $\rho_s\to\rho'$ which leads to $\gamma_{11}+\gamma_{12}\to 1$ and $\gamma_{11}+\gamma_{12}\to 0$ and hence $\left(\gamma_{11}-\frac{\gamma_{12}^2}{\gamma_{22}}\right)\to 1$ giving $d\to 1$.

Again if $f\to 1$ then $\rho_w\to\rho'$ and the medium becomes fluid. In this case, the velocity of shear wave in the medium can not exist when $d=\left(\gamma_{11}-\frac{\gamma_{12}^2}{\gamma_{22}}\right)\to 0$.

Therefore, for a non-porous solid $d=1$, for fluid $d=0$ and for porous solid filled with liquid $0<d<1$.

5.1. Case I

If $\varepsilon\to 0, h\to 0$ *i.e.* in the absence of irregularity in the half space, then (38) reduces to

$$\tan(kqH)=\frac{\mu_1p}{\mu_0q}\frac{\left[1-\frac{aL}{2p}(s-0.5)(s+1.5)+\frac{a^2L^2}{8p^2}(s-0.5)^2(s+2.5)(s-1.5)-\frac{a^3L^3}{8p^3}(s-0.5)^2(s-1.5)^2(s-2.5)\right]}{1-\frac{aL}{2p}(s-0.5)^2+\frac{a^2L^2}{8p^2}(s-0.5)^2(s-1.5)^2}$$

which is the same velocity equation in initially stressed anisotropic heterogeneous poroelastic medium as obtained by Dey & Sarkar (2002).

5.2. Case II

If $\varepsilon\to 0, a\to 0, b\to 0$ *i.e.* when half space is free from irregularity and also half space is homogeneous then from (38) we get

$$\tan(kqH)=\frac{\mu_1p}{\mu_0q},$$

where $p^2=1-\frac{c^2}{c_1^2}$, $q^2=d\upsilon\left(\frac{c^2}{c_\beta^2}-\frac{1-\zeta}{d}\right)$

which is the dispersion equation of Love wave in an initially stressed poro-elastic medium.

5.3. Case III

If $P' \neq 0, a \to 0, b \to 0$ *i.e.* in the presence of normal initial stress and when the half-space is homogeneous then Equation (38) reduces to

$$\tan\left[kq\left(\varepsilon F(r)+H\right)\right]=\frac{\mu_1 p}{\mu_0 q},$$

$$\text{where } p^2=1-\frac{c^2}{c_1^2} \text{ and } q^2=d\upsilon\left(\frac{c^2}{c_\beta^2}-\frac{1-\zeta}{d}\right)$$

which is the velocity equation of Love wave in this case.

5.4. Case IV

If $P'=0,\ a \to 0, b \to 0$ *i.e.* in the absence of normal initial stress and when the half-space is homogeneous then from (38) we get

$$\tan\left[kq\left(\varepsilon F(r)+H\right)\right]=\frac{\mu_1 p}{\mu_0 q},$$

$$\text{where } p^2=1-\frac{c^2}{c_1^2} \text{ and } q^2=d\upsilon\left(\frac{c^2}{c_\beta^2}-\frac{1}{d}\right)$$

5.5. Case V

If $\varepsilon \to 0,\ a \to 0, b \to 0, \zeta \to 0, d \to 1$ and $N=G$ *i.e.* when the half-space is homogeneous and free from irregularity and also when the layer is initial stress free, isotropic and non-porous then (38) reduces to

$$\tan(kqH)=\frac{\mu_1 p}{\mu_0 q},$$

where

$$p^2=1-\frac{c^2}{c_1^2},\ q^2=\frac{c^2}{c_\beta^2}-1$$

$$\text{or, } \tan\left[\left(\frac{c^2}{c_\beta^2}-1\right)^{\frac{1}{2}} kH\right]=\frac{\mu_1}{\mu_0}\frac{\left(1-\frac{c^2}{c_1^2}\right)^{\frac{1}{2}}}{\left(\frac{c^2}{c_\beta^2}-1\right)^{\frac{1}{2}}}$$

which is the well-known classical result of Love wave.

6. Numerical Computation and Discussion

To study the consolidated effect of porosity, irregularity and initial stresses on the propagation of the torsional surface waves, the numerical computation of velocity c^2/c_β^2 has been made from (38) under different values of d, aL, bL, N/G, h/H, μ_1/μ_0, r/m, h/m, km, ε, ζ and $c_\beta^2/c_1^2=0.5$. The results are presented in **Figures 2** to **5**.

Figure 2 gives the dispersion curves for increasing values of kH at different sizes of the irregularity and compares the results in the medium with and without initial stresses. The curve numbers 1, 2 and 3 are for an initially stress-free medium, and the curve numbers 4, 5 and 6 are for the initially stressed medium with $\zeta=0.4$. The figure shows that the effect of the irregularity and the initial stresses are very prominent on the propagation of torsional surface waves. The presence of initial com-

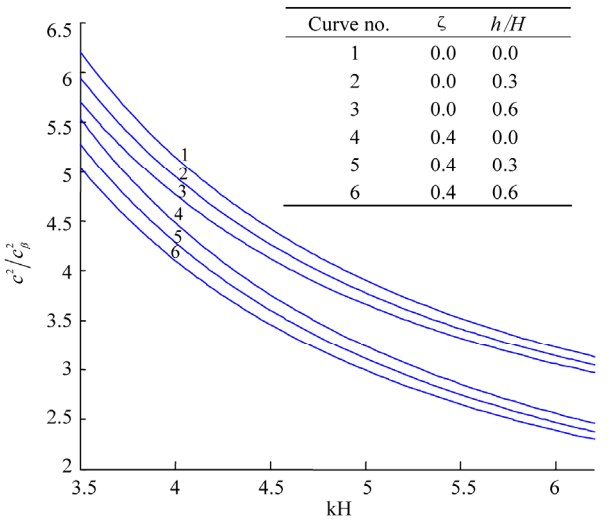

Figure 2. Torsional wave dispersion curves at different initial stresses and at different sizes of irregularity μ_1/μ_0 = 0.4, N/G = 0.3, d = 0.6, a/k = 0.1, b/k = 0.1, ε = 0.1, r/m = 0.02, h/m = 0.03, km = 0.01.

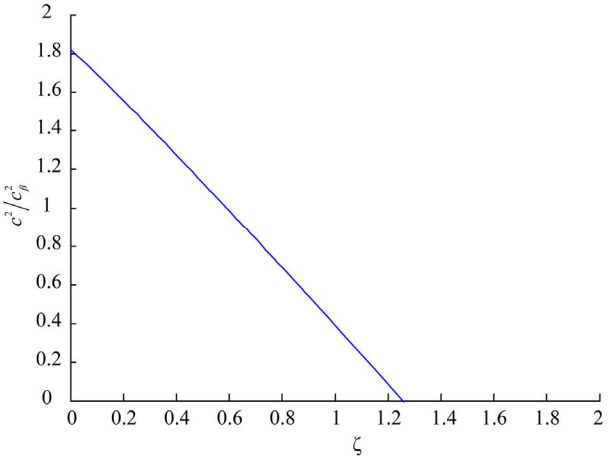

Figure 3. Variation of velocity of torsional wave with respect to initial compressive stress for kH = 0.72, N/G = 2, d = 0.6, aL = 0.1, bL = 0.1, h/H = 0.3, ε = 0.1, r/m = 0.01, h/m = 0.02, km = 0.01, μ_1/μ_0 = 0.4.

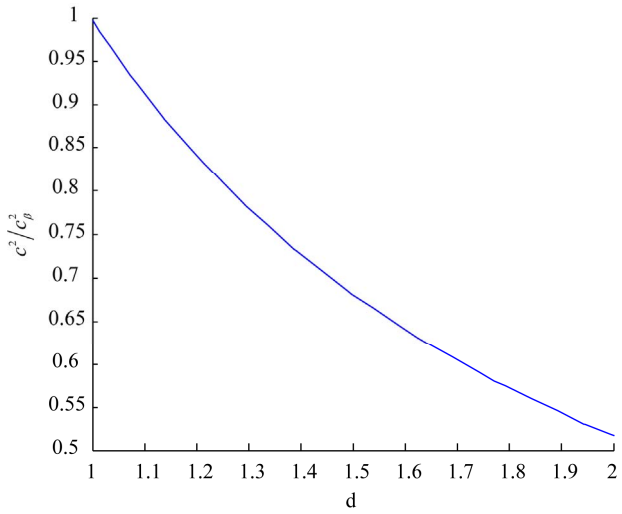

Figure 4. Variation of velocity of torsional wave with respect to porosity for kH = 0.72, N/G = 2, ζ = 0.6, aL = 0.1, bL = 0.1, h/H = 0.3, ε = 0.1, r/m = 0.01, h/m = 0.02, km = 0.01, μ_1/μ_0 = 0.4.

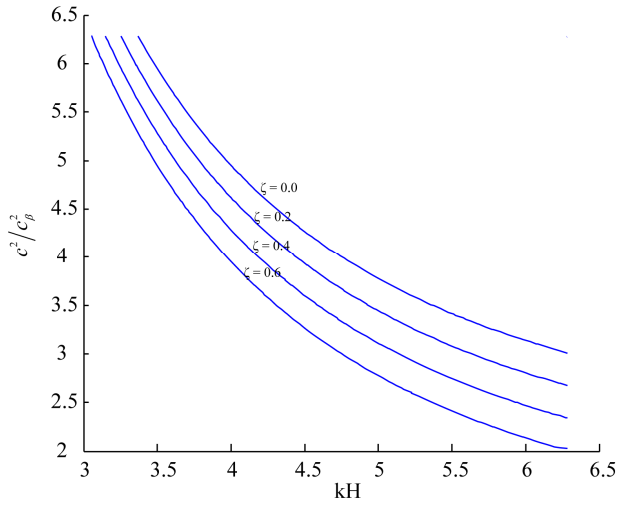

Figure 5. Effect of initial stress on the velocity of torsional wave for μ_1/μ_0 = 0.4, N/G = 0.3, d = 0.6, a/k = 0.1, b/k = 0.1, ε = 0.1, r/m = 0.02, h/m = 0.03, km = 0.01, h/H = 0.3.

pressive stress reduces the velocity of torsional surface waves. The presence of the liquid-filled pore in the medium also reduces the velocity.

Figure 3 gives a variation of velocity of torsional surface waves for the variation of ζ. The curve confirm that as the initial stress parameter increases, the velocity decreases.

Figure 4 gives a variation of velocity of torsional surface waves for the variation of porosity. The curve confirm that as the porosity increases, the velocity decreases.

Figure 5 gives the dispersion curves at different values of kH. This shows that as kH increases, the velocity drops down. Hence it is expected that after certain thickness of the layer, the torsional surface wave will not propagate in the medium. This figure also confirms that as the initial compressive stress increases, the velocity of propagation decreases.

7. Acknowledgements

The authors convey their sincere thanks to Indian School of Mines, Dhanbad, for providing JRF, Mr. Dinesh Kumar Majhi and also facilitating us with best facility.

8. References

[1] J. D. Achenbach, "Wave Propagation in Elastic Solids," North Holland Publishing Comp., New York, 1973

[2] W. M. Ewing, W. S. Jardetzky and F. Press, "Elastic Waves in LAYERED Media," McgrawHill, New York, 1957.

[3] M. Bath, "Mathematical Aspects of Seismology," Elsvier Publishing Comp., New York, 1968.

[4] L. Rayleigh, "On Waves Propagated along Plane Surface of an Elastic Solid," *Proceedings of the London Mathematical Society*, Vol. 17, No. 3, 1885, pp. 4-11. doi:10.1112/plms/s1-17.1.4

[5] H. G. Georgiadis, I. Vardoulakis and G. Lykotrafitis "Torsional Surface Waves in a Gradient-Elastic Half Space," *Wave Motion*, Vol. 31, No. 4, 2000, pp. 333-348. doi:10.1016/S0165-2125(99)00035-9

[6] E. Meissner, "Elastic Oberflachenwellen Mit Dispersion in Einem Inhomogeneous Medium," *Viertlagahrsschriftder Naturforschenden Gesellschaft, Zurich*, Vol. 66, 1921, pp. 181-195 .

[7] I. Vardoulakis, "Torsional Surface Waves in Inhomogeneous Elastic Media," *International Journal for Numerical and Analytical Methods in Geomechanics*, Vol. 8, No. 3, 1984, pp. 287-296.

[8] S. Dey, A. K. Gupta and S. Gupta, "Propagation of Torsional Surface Waves in a Homogeneous Substratum over a Heterogeneous Half-Space," *International Journal for Numerical and Analytical Methods in Geomechanics*, Vol. 20, 1996, pp. 287-294. doi:10.1002/(SICI)1096-9853(199604)20:4<287::AID-NAG822>3.0.CO;2-2

[9] M. A. Biot, "Theory of Deformation of a Porous Viscoelastic Anisotropic Solid," *Journal of Applied Physics*, Vol. 27, No. 5, 1956, pp. 459-467. doi:10.1063/1.1722402

[10] M. A. Biot, "Theory of Propagation of Elastic Waves in a Fluid-Saturated Porous Solid," *Journal of the Acoustical Society of America*, Vol. 28, No. 2, 1956, pp. 168-178. doi:10.1121/1.1908239

[11] M. J. Buckingham, "Theory of Compressional and Shear Waves in Fluid-Like Marine Sediments," *Journal of the Acoustical Society of America*, Vol. 103, No. 1, 1998, pp. 288-299. doi:10.1121/1.421091

[12] M. D. Sharma and M. L. Gogna, "Propagation of Love Waves in an Initially-Stressed Medium Consisting of

sandy Layer Lying over a Liquid Saturated Porous Solid Half-Space," *Journal of the Acoustical Society of America*, Vol. 89, No. 6, 1991, pp. 2584-2588. doi:10.1121/1.400697

[13] M. D. Sharma, R. Kumar and M. L. Gogna, "Surface Wave Propagation in a Transversely Isotropic Elastic Layer Overlying a Liquid-Saturated Porous Solid Half-Space and Lying under a Uniform Layer of Liquid," *Pure and Applied Geophysics*, Vol. 133, No. 3, 1990, pp. 523-539. doi:10.1007/BF00878003

[14] M. D. Sharma, R. Kumar and M. L. Gogna, "Surface Wave Propagation in a Liquid-Saturated Porous Layer Over-Lying a Homogeneous Transversely Isotropic Half-Space and Lying under a Uniform Layer of Liquid," *International Journal of Solids and Structures*, Vol. 27, 1991, pp. 1255-1267. doi:10.1016/0020-7683(91)90161-8

[15] M. A. Biot, "Influence of Initial Stress on Elastic Waves," *Journal of Applied Physics*, Vol. 11, No. 8, 1940, pp. 522-530. doi:10.1063/1.1712807

[16] A. Chattopadhyay, S. Bose and M. Chakraborty, "Reflection of Elastic Waves under Initial Stress at a Free Surface," *Journal of the Acoustical Society of America*, Vol. 72, No. 1, 1982, pp. 255-263. doi:10.1121/1.387987

[17] B. K. Kar and V. K. Kalyani, "Reflection and Refraction of SH-Waves Due to the Presence of a Sandwiched Initially Stressed Sandy Layer," *Geophysical research bulletin*, Vol. 25, No. 3, 1987, pp. 117-124.

[18] S. Dey and S. K. Addy, "Reflection of Plane Waves under Initial Stress at a Free Surface," *International Journal of Non-Linear Mechanics*, Vol. 12, No. 6, 1977, pp. 371-381. doi:10.1016/0020-7462(77)90038-5

[19] M. A. Biot, "Mechanics of Incremental Deformation," Wiley, New York, 1965.

[20] W. H. Weiskopf, "Stresses in Soils under a Foundation," *Journal of the Franklin Institute*, Vol. 239, No. 6, 1945, pp. 445-465. doi:10.1016/0016-0032(45)90189-X

Appendix

H : Thickness of the layer

μ : Rigidity of the medium

ρ : Density of the medium

a , b : Constants having dimensions that are inverse of length

s'_{ij} : Incremental stress components

e_{ij} : Components of strains

u'_r, v'_θ, w'_z : Displacement components of the solid in the radial, circumferential and axial directions respectively.

U'_r, V'_θ, W'_z : Displacement components of the liquid in the radial, circumferential and axial directions respectively.

s' : Stress in the liquid

$\omega'_r, \omega'_\theta, \omega'_z$: Components of the rotational vector ω' in radial, circumferential and axial directions respectively.

ω : Circular frequency

k : Wave number

f : Porosity of the layer

c : Phase velocity of the torsional surface wave

c_1 : Velocity of shear wave in an initially stress-free elastic medium.

R : Dimensionless quantity.

A, B and D_1: Arbitrary constant

Applied Mathematics, **2011, 2, 1462-1468**
doi:10.4236/am.2011.212208 Published Online December 2011 (http://www.SciRP.org/journal/am)

Scientific Research

On the Behavior of Combination High-Order Compact Approximations with Preconditioned Methods in the Diffusion-Convection Equation

Ahmad Golbabai[1*], Mahboubeh Molavi-Arabshahi[2]
[1]*Islamic Azad University, Karaj Branch, Karaj, Iran*
[2]*Faculty of Mathematics, Iran University of Science and Technology, Narmak, Iran*
E-mail: {[*]*golbabai, molavi*}*@iust.ac.ir*
Received July 20, 2011; *revised November* 20, 2011; *accepted November* 24, 2011

Abstract

In this paper, a family of high-order compact finite difference methods in combination preconditioned methods are used for solution of the Diffusion-Convection equation. We developed numerical methods by replacing the time and space derivatives by compact finite- difference approximations. The system of resulting nonlinear finite difference equations are solved by preconditioned Krylov subspace methods. Numerical results are given to verify the behavior of high-order compact approximations in combination preconditioned methods for stability, convergence. Also, the accuracy and efficiency of the proposed scheme are considered.

Keywords: Compact High-Order Approximation, Diffusion-Convection Equation, Krylov Subspace Methods, Preconditioner

1. Introduction

Recently, various powerful mathematical methods such as the homotopy perturbation method, variational iteration method, Adomian decomposition method and others [1-3] have been proposed to obtain approximate solutions in partial differential equations (PDEs). The 2-D parabolic differential equations appeared in many scientific fields of engineering and science such as neutron diffusion, heat transfer and fluid flow problems. Many computational models give rise to large sparse linear systems. For such systems iterative methods are usually preferred to direct methods which are expensive both in memory and computing requirements. Krylov subspace methods are one of the widely used and successful classes of numerical algorithms for solving large and sparse systems of algebraic equations but the speed of these methods are slow for problems which arise from typical applications. In order to be effective and obtaining faster convergence, these methods should be combined with a suitable preconditioner. The convergence rate generally depends on the condition number of the corresponding matrix. Since the preconditioner plays a critical role in preconditioned Krylov subspace methods, many preconditioner have been proposed and studied [4-6]. The ADI method is a preconditioner [7,8] that can be effective for the 2-D problems but this method is not effective for more general tri-block diagonal systems. Bhuruth and Evans [9] proposed BLAGE method as a preconditioner for a class of non-symmetric linear systems. Based on author's observations, there is not a comprehensive study for comparison of preconditioning techniques to solve linear systems. In this paper, we accomplish a comprehensive study for different preconditioners in combination with Krylov subspace methods for solving linear systems arising from the compact finite difference schemes [10, 11] for 2-D parabolic equation

$$\alpha u_{xx} + \beta u_{yy} = f(x, y, t, u, u_x, u_y, u_t) \qquad (1.1)$$

is defined in the region $W = \{x | 0 < x, y < 1, t \succ 0\}$, where α, β are positive constants. The initial conditions are:

$$u(x, y, 0) = u_0(x, y), \qquad 0 \le x, y \le 1, \qquad (1.2)$$

and boundary conditions consists of

$$u(0, y, t) = h_0(y, t), \quad u(1, y, t) = h_1(y, t), \quad t \succ 0 \qquad (1.3)$$

$$u(x, 0, t) = g_0(x, t), \quad u(x, 1, t) = g_1(x, t), \quad t \succ 0, \qquad (1.4)$$

The resulting block tri-diagonal linear system of equations is solved by using Krylov subspace methods.

Krylov subspace methods are one of the widely used and successful classes of numerical algorithms for solving large and sparse systems of algebraic equations but the speed of these methods are slow for problems which arise from typical applications [12-15]. In order to be effective and obtaining faster convergence, these methods should be combined with a suitable preconditioner. The rate of convergence generally depends on the condition number of the corresponding matrix. Since the preconditioner plays a critical role in preconditioned Krylov subspace methods, many preconditioners have been proposed and studied [6,16-18] amongst the ADI preconditioner.

In this paper, we accomplish a comprehensive study for different preconditioners in combination with Krylov subspace methods for solving linear systems arising from the compact high-order approximations. The resulting block tri-diagonal linear system of equations is solved by using Krylov subspace methods.

The outline of the paper is as follows:

In Section 2, we briefly introduce Krylov subspace methods and in Section 3, we consider some available preconditioners. In Section 4, we consider Diffusion-Convection problem arising from the compact high-order approximations. We present the results of our comparative study in the final section.

2. Krylov Subspace Methods

Consider the linear system

$$Ax = b\,, \qquad (2.1),$$

where A is a large sparse non-symmetric matrix. Let x_0 present an arbitrary initial guess to x and $r_0 = b - Ax_0$ be a corresponding residual vector. An iterative scheme for solving (2.1) is called a Krylov subspace method if for any choice of w, it produces approximate solutions of the form $x = x_0 + w$.

In Section 4, we solve our problem with well-known Krylov subspace methods such as Generalized minimal residual method GMRES (m), Quasi minimal residual method (QMR), Bi-Conjugate Gradient method (BiCG), Conjugate gradient squared method (CGS) and Bi-Conjugate Gradient Stabilized method (BiCGSTAB) for more complete explanation refer to [13-15].

3. Preconditioner

The convergence rate of iterative methods highly depends on the eigen-value distribution of the coefficient matrix. A criterion for the width of the spectrum is the Euclidean condition number for SPD matrices is

$$K = \|A\|_2 \left\|A^{-1}\right\|_2 \approx \lambda_{\max}(A)/\lambda_{\min}(A) \qquad (3.1)$$

with $\gamma = (\sqrt{K}-1)(\sqrt{K}+1)$, the distance to the exact solution x^* in the i^{th} iteration is bounded by

$$\left\|x^i - x^*\right\|_2 \le 2\sqrt{K}\gamma^i \left\|x^0 - x^*\right\|_2, \qquad (3.2)$$

the right hand side of (3.2) increases with growing condition number. Hence, lower condition numbers usually accelerate the speed of convergence. Hence we will attempt to transform the linear system into another equivalent system in the sense that it has the same solution, but has more favorable spectral properties. A preconditioner is a matrix that effects such as a transformation. If the preconditioner be as $M = M_1 M_2$ then the preconditioned system is as

$$M_1^{-1} A M_2^{-1}(M_2 x) = M_1^{-1} b\,, \qquad (3.3)$$

the matrices M_1 and M_2 are called the left and right preconditioners, respectively. Now, we briefly describe preconditioners that we use for solving linear systems and matrix A is block tri-diagonal.

3.1. Preconditioner Based on Relaxation Technique

Let $A = D + L + U$ such that D, L and U are diagonal, lower and upper triangular block matrices, respectively. A splitting of the coefficient matrix is as $A = M - N$ where the stationary iteration for solving a linear system is as

$$x_{k+1} = M^{-1}Nx_k + M^{-1}b\,. \qquad (3.4)$$

If the preconditioner M is defined as $M = D$, then this preconditioner is called Jacobi. Also, if M is defined as $M = \frac{1}{\omega}(D + \omega L)$ then we have SOR preconditioner where for $\omega = 1$, we have Gauss-Seidel preconditioner. If M is defined as $M = \frac{1}{\omega(2-\omega)}(D + \omega L)D^{-1}(D + \omega U)$, we get SSOR preconditioner. In the above notation, ω is called the relaxation parameter. We have chosen matrix M in Jacobi, G-S and SOR methods as a left preconditioner and in SSOR preconditioner, we have chosen $M_1 = \frac{1}{\omega(2-\omega)}(D + \omega L)$ as a left preconditioner and $M_2 = D^{-1}(D + \omega U)$ as a right preconditioner. Also, we take $\omega_{opt} = \frac{2}{1 + \sqrt{1 - \rho_J^2}}$ [6].

3.2. ADI Preconditioner

Let $A = H + V$ and matrix A is in the form

$$A=\begin{pmatrix} B_1 & C_1 & & & \\ A_2 & B_2 & C_2 & & \\ & \ddots & \ddots & \ddots & \\ & & A_{n-1} & B_{n-1} & C_{n-1} \\ & & & A_n & B_n \end{pmatrix}$$

where
$A_i = tridiag\{a_{1i}, b_{1i}, c_{1i}\}$, $B_i = tridiag\{a_{2i}, b_{2i}, c_{2i}\}$ and $C_i = tridiag\{a_{3i}, b_{3i}, c_{3i}\}$ of order $N \times N$ where H and V are given in the form $H = \{0.5B_i, b_{3i}, b_{1i}\}$, $V = \{0.5B_i, a_{1i}, c_{1i}, a_{3i}, c_{3i}\}$. The alternative direction implicit method [19] for solving the linear system $Ax = b$ is in following form:

$$(H + r_1 I)u^{(k+1/2)} = b - (V - r_1 I)u^{(k)}, \quad (3.5)$$

$$(V + r_2 I)u^{(k+1)} = b - (H - r_2 I)u^{(k+1/2)}, \quad (3.6)$$

The ADI preconditioner is defined as $M = (H + r_1 I)(V + r_2 I)$ and $M_1 = (H + r_1 I)$ and $M_2 = (V + r_2 I)$ where Parameters r_1 and r_2 are acceleration parameters. Young and Varga [20,21] proved that the optimum value for r_1 and r_2 is $\sqrt{\alpha\beta}$ where $\alpha \le \mu_i, \nu_i \le \beta$ and μ_i, ν_i are eigen-values of matrices H and V respectively.

3.3. BLAGE Preconditioner

The block alternating group explicit (BLAGE) method [22,23] was originally introduced as analogue of the alternating group explicit (AGE) method [24]. The BLAGE uses fractional splitting technique that is applied in two half steps on linear systems with block tri-diagonal matrices of order $N^2 \times N^2$ and in the form

$$A=\begin{pmatrix} B_1 & C_1 & & & \\ A_2 & B_2 & C_2 & & \\ & \ddots & \ddots & \ddots & \\ & & A_{n-1} & B_{n-1} & C_{n-1} \\ & & & A_n & B_n \end{pmatrix}$$

where A_i, B_i and C_i are tri-diagonal matrices of order $N \times N$. The splitting of matrix ***A*** is sum of matrices G_1 and G_2 in which $A = G_1 + G_2$ where G_1 and G_2 are of the form

$$G_1=\begin{pmatrix} B_1' & & & & \\ & B_2' & C_2 & & \\ & A_3 & B_3' & & \\ & & & \ddots & \\ & & & B_{n-1}' & C_{n-1} \\ & & & A_n & B_n' \end{pmatrix}$$

and

$$G_2=\begin{pmatrix} B_1' & C_1 & & & \\ A_2 & B_2' & & & \\ & & \ddots & & \\ & & & B_{n-2}' & C_{n-2} \\ & & & A_{n-1} & B_{n-1}' \\ & & & & B_n' \end{pmatrix}$$

for odd values of n where $B_i' = \frac{1}{2}B_i$. The BLAGE preconditioner is as $M = (G_1 + \omega_1 I)(G_2 + \omega_2 I)$ that $M_1 = (G_1 + \omega_1 I)$ and $M_2 = (G_2 + \omega_2 I)$ where ω_1 and ω_2 are optimal iteration parameters. We have experimentally chosen the relaxation parameter $\omega_1 = \sqrt{\alpha_1\beta_2}$ and $\omega_2 = \sqrt{\alpha_2\beta_1}$ where $\alpha_1 = \lambda_{\min}(M_1)$, $\beta_1 = \lambda_{\max}(M_1)$ and $\alpha_2 = \lambda_{\min}(M_2)$, $\beta_2 = \lambda_{\max}(M_2)$ so that we will have the minimum condition number.

4. Numerical Illustrations

In this section, we present one numerical example to show the computational efficiency of the preconditioner which introduced in Section 3. Our initial guess is the zero vector and the iterations are stopped when the relative residual is less than 10^{-6}. We show the number of outer iterations and inner iterations GMRES (m) method with "ou" and "in" respectively in following tables. Also, we show the iteration number without using preconditioner by "no pre" and the coefficient matrix is order of $N^2 \times N^2$. The computations have been done on a P.C. with Corw 2 Pue 2.0 Ghz and 1024 MB RAM.

Test: We consider 2-D partial differential equation:

$$\alpha u_{xx} + \beta u_{yy} = u_x + u_y + r u_t - \exp(-t)\cos(x + y) \quad (4.1)$$

with Dirichlet boundary conditions on the unit square where

$$u(x, y, t) = \exp(-t)\cos(x)\sin(y). \quad (4.2)$$

where $\alpha = \beta = 5 \times 10^{-4}$. We apply the fourth-order approximation for discretization of Equation (4.1) **(Figure 1)**. We have shown the number of iteration for different preconditioned methods in **Tables 1-5** or different preconditioners. The convergence behavior of preconditioned Krylov subspace methods is given by **Figures 2-7**. Also, in **Figures 8-10** for we show the distribution of eigen-values SSOR, ADI and BLAGE preconditioners. In this test the condition number of problem is high and our problem is ill-conditioned. So, in regard of other preconditioner, results show the ADI preconditioner requires more iteration. It is seen that we obtain the optimal convergence with SSOR and BLAGE preconditioner and our time consumption is reduced.

Tabale 1. Number of iterations with GMRES.

h	no pre	Jacobi	SOR	SSOR	ADI	BLAGE
1/20	75	54	36	21	33	26
1/40	124	89	61	36	61	51
1/60	119	87	60	35	65	54
1/80	139	102	58	37	76	63
1/100	162	119	58	40	87	72

Tabale 2. Number of iterations with QMR.

h	no pre	Jacobi	SOR	SSOR	ADI	BLAGE
1/20	79	56	48	22	40	34
1/40	152	96	99	33	72	55
1/60	162	109	95	39	77	61
1/80	189	137	67	34	97	77
1/100	225	149	63	39	102	79

Tabale 3. Number of iterations with CGS.

H	no pre	Jacobi	SOR	SSOR	ADI	BLAGE
1/20	62	36	28	14	27	18
1/40	81	50	43	18	40	35
1/60	93	56	37	20	42	34
1/80	114	74	41	26	57	47
1/100	146	N	42	31	73	49

Tabale 4. Number of iterations with BiCG.

h	no pre	Jacobi	SOR	SSOR	ADI	BLAGE
1/20	85	57	52	22	41	34
1/40	152	99	97	36	72	55
1/60	162	108	86	39	77	67
1/80	190	137	67	34	95	73
1/100	223	131	67	39	99	87

Tabale 5. Number of iterations with BiCGSTAB.

h	no pre	Jacobi	SOR	SSOR	ADI	BLAGE
1/20	62	46	23	15	31	17
1/40	81	60	36	21	43	25
1/60	86	54	38	19	45	30
1/80	103	72	37	22	52	41
1/100	135	95	36	26	65	49

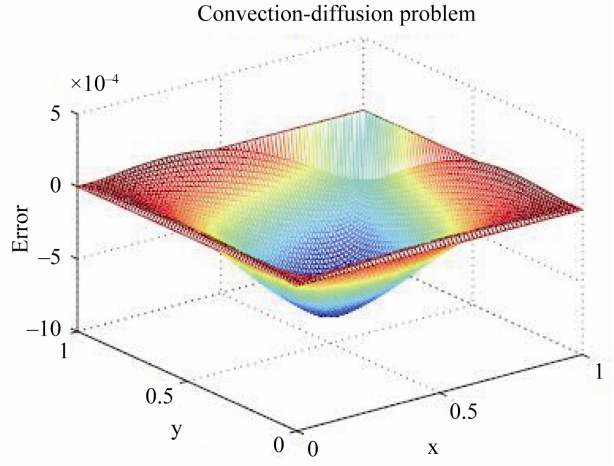

Figure 1. The 3D error of the compact fite diffence scheme with time $T = 10$.

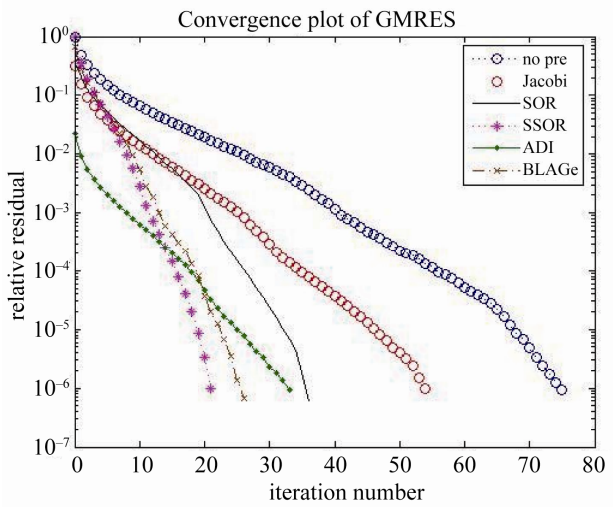

Figure 2. Convergence plot of GMRES.

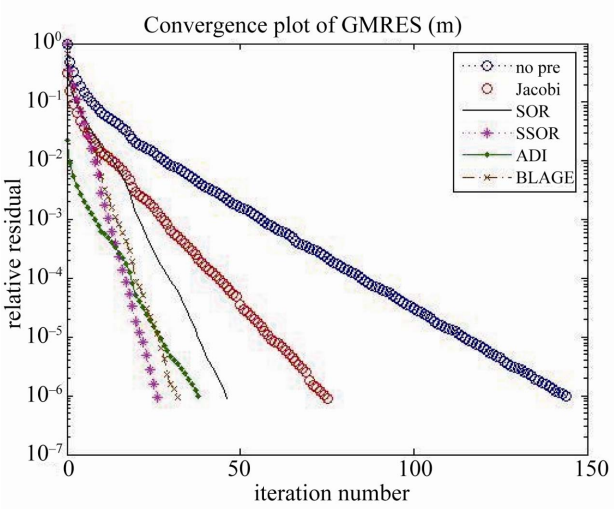

Figure 3. Convergence plot of GMRES (15).

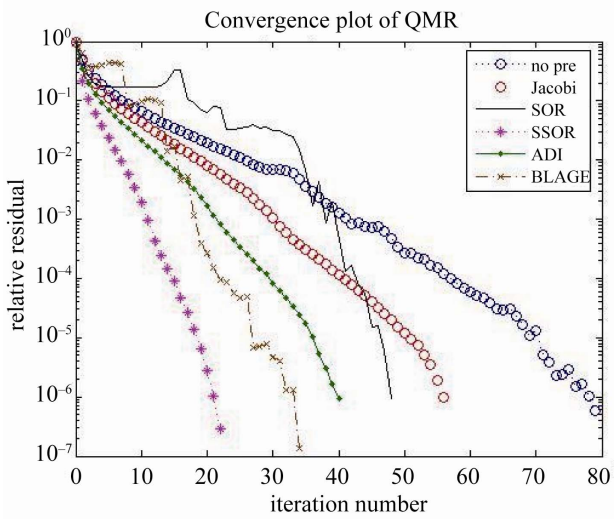

Figure 4. Convergence plot of QMR.

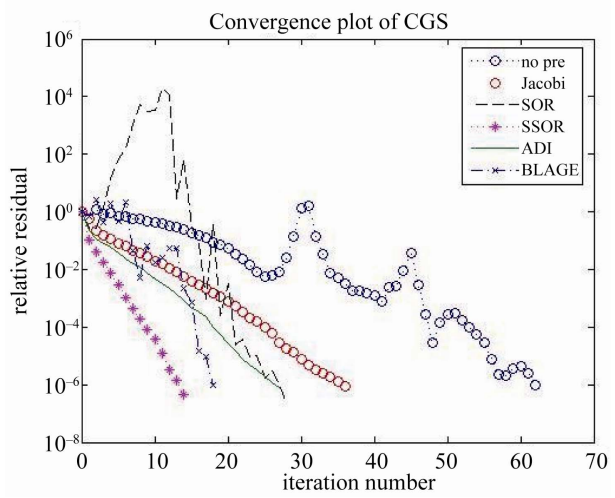

Figure 5. Convergence plot of CGS.

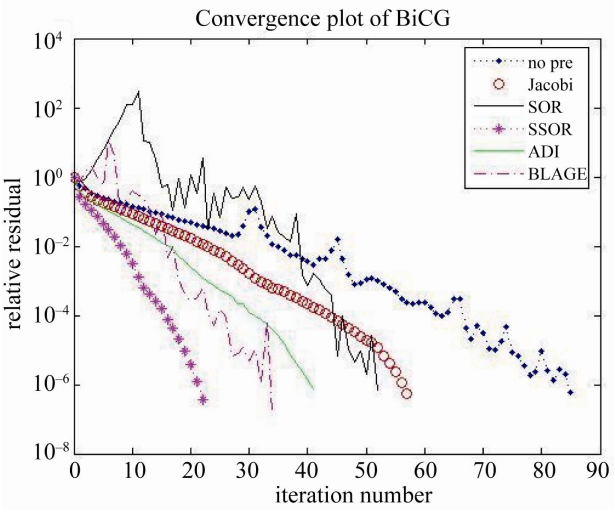

Figure 6. Convergence plot of BiCG.

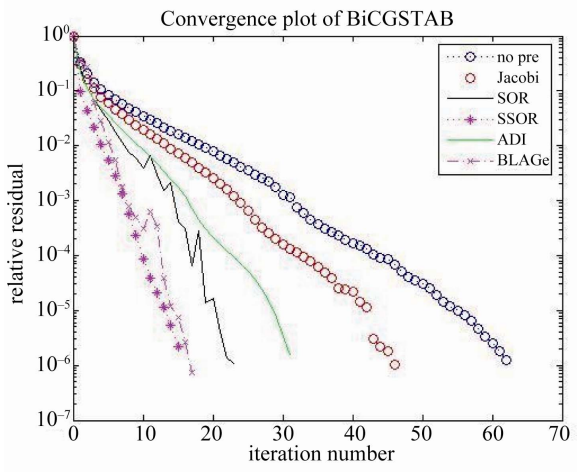

Figure 7. Convergence plot of BiCGSTAB.

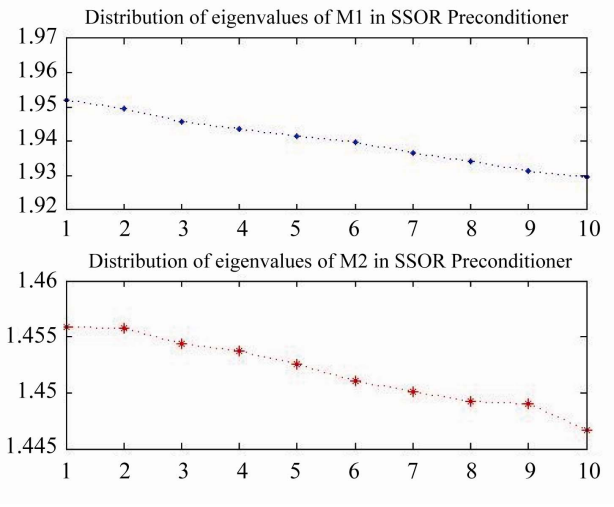

Figure 8. Distribution of eigen-values in SSOR preconditioner.

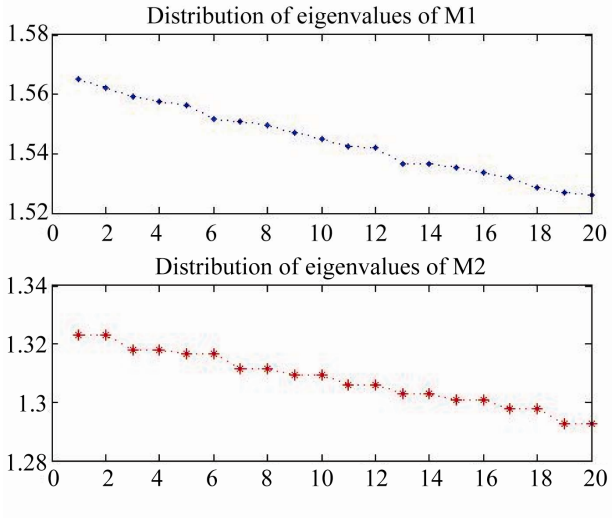

Figure 9. Distribution of eigen-values in ADI Preconditioner.

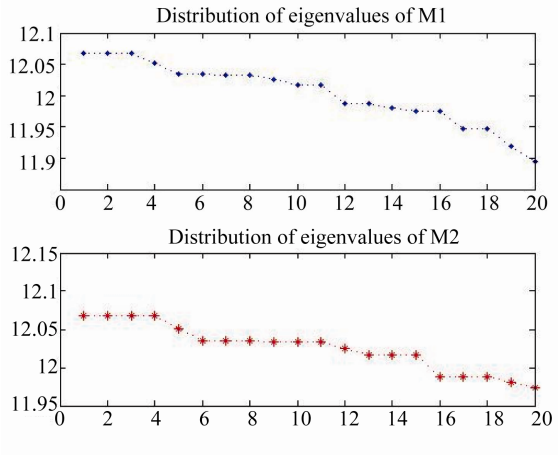

Figure 10. Distribution of eigen-values in BLAGE preconditioner.

5. Conclusions

A high-order compact scheme in combination preconditioner was applied successfully to Diffusion- Convection equation. We study comparison of different preconditioners in combination Krylov subspace methods. High-order approximation are designed by the need to produce more stable schemes which are efficient with respect to the operation number and that do not experience difficulties near boundaries. The numerical results which is given in the previous section demonstrate the good accuracy of this scheme and efficiency of preconditioned Krylov subspace methods. We got to this conclusion that the ADI preconditioner is effective for model problems rather than other. So we propose using ADI preconditioner in combination with Krylov subspace methods for solving non-symmetric systems because this preconditioner needs to less computing time and have the less iteration number than other. Also, we propose the BiCGSTAB method because of the need to less iteration number, simplicity in implementation, flat convergence and to save in comp tational time.

6. References

[1] L. C. Evans, "Partial Differential Equations," American Mathematical Society Providence, Rhode Island, 1999.

[2] A. Golbabai and M. M. Arabshahi, "A Numerical Method for Diffusion-Convection Equation Using High-Order Difference Schemes," *Computer Physics Communications*, Vol. 181, No. 7, 2010, pp. 1224-1230. doi:10.1016/j.cpc.2010.03.008

[3] A. Golbabai and M. M. Arabshahi, "On the Behavior of High-Order Compact Approximations in One Dimensional Sine-Gordon Equation," *Physica Scripta*, Vol. 83, No. 1, 2011, Article ID 015015. doi:10.1088/0031-8949/83/01/015015

[4] L. C. Evans, "Partial Differential Equations," American Mathematical Society Providence, Rhode Island, 1999.

[5] S. Sundar and B. K. Bhagavan, "CGS, Comparison of Krylov Subspace Methods with Preconditioning Techniques for Solving Boundary Value Problems," *Computers and Mathematics with Applications*, Vol. 38, No. 11-12, 1999, pp. 197-206. doi:10.1016/S0898-1221(99)00298-9

[6] A. M. Bruaset, "A Survey of Preconditioned Iterative Methods," Longman Scientific and Technical, UK, 1995.

[7] K. J. Hout and B. D. Welfert, "Unconditional Stability of Second-Order ADI Schemes Applied to Multi-Dimensional Diffusion Equations with Mixed Derivative Terms," *Applied Numerical Mathematics*, 2008, Article in Press.

[8] S. Ma and Y. Saad, "Block-ADI Preconditioners for Solving Sparse Non-Symmetric Linear Systems of Equations," *Numerical Linear Algebra*, 1993, pp. 165-178.

[9] M. Bhuruth and D. J. Evans, "Block Alternating Group Explicit Preconditioning (BLAGE) for a Class of Fourth-Order Difference Schemes," *International Journal of Computer Mathematics*, Vol. 63, No. 1-2, 1997, pp. 121-136. doi:10.1080/00207169708804555

[10] M. K. Jain, R. K. Jain and R. K. Mohanty, "Fourth-Order Finite Difference Method for 2-D Parabolic Partial Differential Equations with Non-Linear First-Derivative Terms," *Numerical Methods for Partial Differential Equations*, Vol. 8, No. 1, 1992, pp. 21-31. doi:10.1002/num.1690080102

[11] G. I. Shishkin and L. P. Shishkina, "A Higher Order Richardson Scheme for a Singularly Perturbed Semilinear Elliptic Convection-Diffusion Equation," *Computational Mathematics and Mathematical Physics*, Vol. 50, No. 3, 2010, pp. 437-456. doi:10.1134/S0965542510030061

[12] Y. Zhang, "Matrix Theory Basic Results and Techniques," Springer, Berlin, 1999.

[13] R. Barrett, *et al*., "Templates for the Solution of Linear Systems: Building Blocks for Iterative Methods," *Society for Industrial and Applied Mathematics* (*SIAM*), 1994, pp. xvii+118. doi:10.1137/1.9781611971538

[14] Y. Saad, "Iterative Methods for Sparse Linear Systems," Second Edition, PWS Publishing Company, Boston, 2000.

[15] H. A. Van der Vorst, "Iterative Krylov Subspace Methods for Large Linear Systems," Cambridge University Press, Cambridge, 2003. doi:10.1017/CBO9780511615115

[16] O. Axelsson, "Iterative Solution Methods," Cambridge University Press, New York, 1996.

[17] M. H. Koulaei and F. Toutounian, "On Computing of Block ILU Preconditioner for Block Tri-Diagonal Systems," *Journal of Computational and Applied Mathematics*, Vol. 202, No. 2, 2007, pp. 248-257. doi:10.1016/j.cam.2006.02.029

[18] R.C. Mittal and A.H. Al-Kurdi, "An Efficient Method for Constructing an ILU Preconditioner for Solving Large Sparse Non-Symmetric Linear Systems by the GMRES Method," *Computers and Mathematics with Applications*, Vol. 45, 2003, pp. 1757-1772.

doi:10.1016/S0898-1221(03)00154-8

[19] D. W. Peaceman and H. H. Rachford, "The Numerical Solution of Parabolic and Elliptic Differential Equations," *Journal of the Society for Industrial and Applied Mathematics*, Vol. 3, No. 1, 1955, pp. 28-41. doi:10.1137/0103003

[20] D. M. Young, "Iterative Solution of Large Linear Systems," Academic Press, New York, 1971.

[21] R. S. Varga, "Matrix Iterative Analysis," Prentice Hall, Englewood Cliffs, 1962.

[22] D. J. Evans and W. S. Yousif, "The Block Alternating Group Explicit Method (BLAGE) for the Solution of Elliptic Difference Equations," *International Journal of Computer Mathematics*, Vol. 22, No. 2, 1987, pp. 177-185. doi:10.1080/00207168708803590

[23] R. K. Mohanty, "Three-Step BLAGE Iterative Method for Two-Dimensional Elliptic Boundary Value Problems with Singularity," *International Journal of Computer Mathematics*, Vol. 84, No. 11, 2007, pp. 1613-1624. doi:10.1080/00207160600825205

[24] D. J. Evans and M. Sahimi, "The Alternating Group Explicit (AGE) Iterative Method to Solve Parabolic and Hyperbolic Partial Differential Equations," *Annual Review of Numerical Fluid Mechanics and Heat Transfer*, Vol. 11, 1989, pp. 283-390.

Applied Mathematics, **2011, 2, 1469-1478**
doi:10.4236/am.2011.212209 Published Online December 2011 (http://www.SciRP.org/journal/am)

The Analytical and Numerical Solutions of Differential Equations Describing of an Inclined Cable Subjected to External and Parametric Excitation Forces

Mohamed S. Abd Elkader[1,2]
[1]*Department of Mathematics and Statistics, Faculty of Science, Taif University, El-Taif, Kingdom of Saudi Arabia*
[2]*Department of Engineering Mathematics, Faculty of Electronic Engineering, Menoufia University, Menouf, Egypt*
E-mail: *moh_6_11@yahoo.com*
Received October 21, 2011; *revised November* 22, 2011; *accepted November* 30, 2011

Abstract

The analytical and numerical solutions of the response of an inclined cable subjected to external and parametric excitation forces is studied. The method of perturbation technique are applied to obtained the periodic response equation near the simultaneous principal parametric resonance in the presence of 2:1 internal resonance of the system. All different resonance cases are extracted. The effects of different parameters and worst resonance case on the vibrating system are investigated. The stability of the system are studied by using frequency response equations and phase-plane method. Variation of the parameters α_2, α_3, β_2, γ_2, η_2, γ_3, η_3, f_2 leads to multi-valued amplitudes and hence to jump phenomena. The simulation results are achieved using MATLAB 7.6 programs.

Keywords: Perturbation Method, Resonance, Chaotic Response, Stability

1. Introduction

Cable structures play an important role in many engineering fields, such as civil, ocean and electric engineering. Arafat and Nayfeh [1] studied the motion of shallow suspended cables with primary resonance excitation. The method of multiple scales is applied to study nonlinear response of this suspended cables and its stability and the dynamic solutions. Some interesting work on the nonlinear dynamics of cables to the harmonic excitations can be found in the review articles by Rega [2,3]. Nielsen and Kierkegaard [4] investigated simplified models of inclined cables under super and combinatorial harmonic excitation and gave analytical and purely numerical results. Zheng, Ko and Ni [5] considered the super-harmonics and internal resonance of a suspended cable with almost commensurable natural frequencies. Zhang and Tang [6] investigated the chaotic dynamics and global bifurcations of the suspended inclined cable under combined parametric and external excitations. Nayfeh *et al*. [7] investigated the nonlinear nonplanar responses of suspended cables to external excitations. The equations of motion governing such systems contain quadratic and cubic nonlinearities, which may result in 2:1 and 1:1 internal resonances. Chen and Xu [8] investigated the global bifurcations of the inclined cable subjected to a harmonic excitation leading to primary resonances with the external damping by using averaging method. Kamel and Hamed [9], studied the nonlinear behavior of an inclined cable subjected to harmonic excitation near the simultaneous primary and 1:1 internal resonance using multiple scale method. Abe [10] investigated the accuracy of nonlinear vibration analyses of a suspended cable, which possesses quadratic and cubic nonlinearities, with 1:1 internal resonance. The nonlinear dynamics of suspend cable structures have been studied with 2:1 internal resonances by the authors [11,12]. Experimental studies of this problem have been conducted by Alaggio and Rega [13] and Rega and Allagio [14], however explicit stability regions for the semi-trivial solution have not been calculated analytically. Here, we use a modal model to compute the instability boundary for a range of excitation frequencies close to the 2:1 resonance for an inclined cable, including nonlinear modal interaction. The out-of-plane

dynamic stability of inclined cables subjected to in-plane vertical support excitation is investigated by Gonzalez-Buelga *et al*. [15]. Perkins [16] examined the effect of one support motion on the three-dimensional nonlinear response. Using the Galerkin method, he constructed a two-degree-of-freedom model to analyze the 2:1 internal resonance. Lee and Perkins [17] extended the work to include second-order perturbations and multiple internal resonances. Still, the focus was on the 2:1 internal resonance, whereas the excitation was changed to a harmonically varying load per unit length acting in the static equilibrium plane. Lee and Perkins [18] also used a three-degree-of-freedom model to simulate non-linear response of suspended, inclined cables driven by planar excitation and determined the existence and stability of four classes of periodic solutions.

Eissa and Sayed [19-21] and Sayed [22], studied the effects of different active controllers on simple and spring pendulum at the primary resonance via negative velocity feedback or its square or cubic. Sayed and Hamed [23] studied the response of a two-degree-of-freedom system with quadratic coupling under parametric and harmonic excitations. The method of multiple scale perturbation technique is applied to solve the non-linear differential equations and obtain approximate solutions up to and including the second-order approximations. Sayed and Kamel [24,25] investigated the effects of different controllers on the vibrating system and the saturation control to reduce vibrations due to rotor blade flapping motion. The stability of the obtained numerical solution is investigated using both phase plane methods and frequency response equations. Amer and Sayed [26], studied the response of one-degree-of freedom, non-linear system under multi-parametric and external excitation forces simulating the vibration of the cantilever beam. Variation of some parameters leads to multi-valued amplitudes and hence to jump phenomena. Sayed *et al*. [27], investigated the non-linear dynamics of a two-degree-of freedom vibration system including quadratic and cubic non-linearities subjected to external and parametric excitation forces. The stability of the system is investigated using both frequency response curves and phase-plane trajectories. The effects of different parameters of the system are studied numerically.

This work deals with model having two-degree-of-freedom nonlinear system subjected to external and parametric excitation forces describes the vibrations of an inclined cable. The method of multiple scales perturbation is applied to obtain modulation response equations near the simultaneous principal parametric resonance in the presence of 2:1 internal resonance ($\Omega_2 \cong 2\omega_2$ and $\omega_1 \cong 2\omega_2$). The stability of the proposed analytic nonlinear solution near the above case is studied and the stability condition is determined. The effect of different parameters on the steady state response of the vibrating system is studied and discussed from the frequency response curves. The numerical solution and chaotic responses of the nonlinear system of an inclined cable for some different parameters are also studied. A comparison with previously published work is included**.**

2. Mathematical Analysis

Our attention is focused on an elastic-sag hanging at fixed supports and excited by harmonic and parametric distributed vertical forcing in plane. The two-degree-of-freedom describing the nonlinear dynamics of cable shown in **Figure 1**, can be written as:

$$\ddot{x} + 2c_1\dot{x} + \omega_1^2 x + \alpha_2 x^2 + \beta_2 y^2 + \gamma_2 x^3 + \eta_2 xy^2 = 0 \quad (1)$$

$$\begin{aligned} &\ddot{y} + 2c_2\dot{y} + \omega_2^2 y + \alpha_3 x y + \gamma_3 y^3 + \eta_3 x^2 y \\ &= f_1 \cos\Omega_1 t + y f_2 \cos\Omega_2 t \end{aligned} \quad (2)$$

where x and y denote in-plane and out-of-plane displacements, respectively, and dots denote derivatives with respect to the time t. The parameters c_1 and c_2 are the viscous damping coefficients, ω_1 and ω_2 are the natural frequencies associated with in-plane and out-of-plane modes Ω_1 and Ω_2 are the excitation frequencies, f_1 and f_2 are the excitation forces amplitude, $\alpha_2, \beta_2, \gamma_2$, $\eta_2, \alpha_3, \gamma_3$ and η_3 are the coefficients of nonlinear parameters. The linear viscous damping forces, the exciting forces and nonlinear parameters are assumed to be

$$\begin{aligned} &c_1 = \varepsilon^2\hat{c}_1, c_2 = \varepsilon^2\hat{c}_2, f_n = \varepsilon^2\hat{f}_n,\ \gamma_s = \varepsilon^2\hat{\gamma}_s,\ \hat{\eta}_s = \varepsilon^2\hat{\eta}_s, \\ &\hat{\alpha}_s = \varepsilon\hat{\alpha}_s,\ \beta_2 = \varepsilon\hat{\beta}_2 \\ &n = 1,2 \quad s = 2,3 \end{aligned}$$

where ε is a small perturbation parameter and $0 < \varepsilon \ll 1$. For the convenience of the analysis of Equations (1)-(2), the non-dimensional parameter ε is introduced. We can obtain

$$\begin{aligned} &\ddot{x} + 2\varepsilon^2\hat{c}_1\dot{x} + \omega_1^2 x + \varepsilon(\hat{\alpha}_2 x^2 + \hat{\beta}_2 y^2) \\ &+ \varepsilon^2(\hat{\gamma}_2 x^3 + \hat{\eta}_2 x y^2) = 0 \end{aligned} \quad (3)$$

$$\begin{aligned} &\ddot{y} + 2\varepsilon^2\hat{c}_2\dot{y} + \omega_2^2 y + \varepsilon\hat{\alpha}_3 x y + \varepsilon^2(\hat{\gamma}_3 y^3 + \hat{\eta}_3 x^2 y) \\ &= \varepsilon^2(\hat{f}_1 \cos\Omega_1 t + y\hat{f}_2 \cos\Omega_2 t) \end{aligned} \quad (4)$$

The parameters $\hat{\alpha}_2, \hat{\alpha}_3, \hat{\beta}_2$ are of the order of 1 and the parameters $\hat{c}_1, \hat{c}_2, \hat{\gamma}_2, \hat{\gamma}_3, \hat{\eta}_2, \hat{\eta}_3, \hat{f}_1, \hat{f}_2$ are of the order of 2. The approximate solution of Equations (3)-(4) can be obtained using the method of multiple scales [28]. Let

$$\begin{aligned} x(t;\varepsilon) &= x_0(T_0, T_1, T_2) + \varepsilon x_1(T_0, T_1, T_2) \\ &+ \varepsilon^2 x_2(T_0, T_1, T_2) \end{aligned} \quad (5)$$

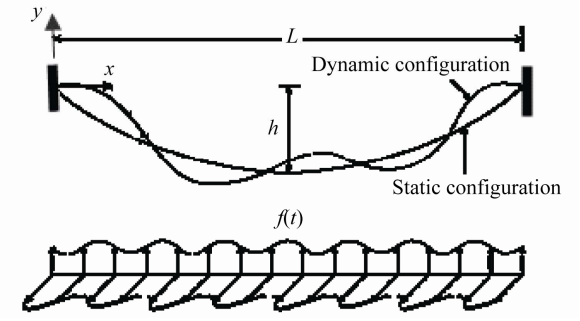

Figure 1. A schematic of inclined cable under combined excitations.

$$y(t;\varepsilon) = y_0(T_0,T_1,T_2) + \varepsilon\, y_1(T_0,T_1,T_2) + \varepsilon^2 y_2(T_0,T_1,T_2) \tag{6}$$

where, $T_n = \varepsilon^n t$ (n = 0, 1, 2) are the fast and slow time scales respectively. In terms of T_0, T_1 and T_2, the time derivatives transform according to

$$\frac{\mathrm{d}}{\mathrm{d}t} = D_0 + \varepsilon D_1 + \varepsilon^2 D_2$$
$$\frac{\mathrm{d}^2}{\mathrm{d}t^2} = D_0^2 + 2\varepsilon D_0 D_1 + \varepsilon^2 (D_1^2 + 2D_0 D_2) \tag{7}$$

where $D_n = \partial/\partial T_n$. Substituting Equations (5)-(6) and (7) into Equations (3)-(4) and equating the coefficients of similar powers of ε in both sides, we obtain the differential equations as follows:

Order (ε^0):

$$(D_0^2 + \omega_1^2)\, x_0 = 0 \tag{8}$$

$$(D_0^2 + \omega_2^2)\, y_0 = 0 \tag{9}$$

Order (ε^1):

$$(D_0^2 + \omega_1^2) x_1 = -2D_0 D_1 x_0 - \hat{\alpha}_2 x_0^2 - \hat{\beta}_2 y_0^2 \tag{10}$$

$$(D_0^2 + \omega_2^2) y_1 = -2D_0 D_1 y_0 - \hat{\alpha}_3 x_0 y_0 \tag{11}$$

Order (ε^2):

$$(D_0^2 + \omega_1^2) x_2 = -D_1^2 x_0 - 2D_0 D_1 x_1 - 2D_0 D_2 x_0 - 2\hat{c}_1 D_0 x_0 - 2\hat{\alpha}_2 x_0 x_1 - 2\hat{\beta}_2 y_0 y_1 - \hat{\gamma}_2 x_0^3 - \hat{\eta}_2 x_0 y_0^2 \tag{12}$$

$$(D_0^2 + \omega_2^2) y_2 = -D_1^2 y_0 - 2D_0 D_1 y_1 - 2D_0 D_2 y_0 - 2\hat{c}_2 D_0 y_0 - \hat{\alpha}_3 (x_0 y_1 + y_0 x_1) - \hat{\gamma}_3 y_0^3 - \hat{\eta}_3 y_0 x_0^2 + \hat{f}_1 \cos\Omega_1 T_0 + y_0 \hat{f}_2 \cos\Omega_2 T_0 \tag{13}$$

The solution of Equations (8)-(9) can be expressed in the complex form:

$$x_0 = A(T_1, T_2)\exp(i\omega_1 T_0) + cc \tag{14}$$

$$y_0 = B(T_1, T_2)\exp(i\omega_2 T_0) + cc \tag{15}$$

where cc denotes the complex conjugate of the preceding terms and A, B are complex functions in T_1 and T_2 which determined through the elimination of secular and small-divisor terms from the first and second-order of approximations.

In this case, we analyze the case where $\Omega_2 \cong 2\omega_2$ and $\omega_1 \cong 2\omega_2$. To describe quantitatively the nearness of the resonances, we introduce the detuning parameters σ_1 and σ_2 according to $\Omega_2 = 2\omega_2 + \varepsilon\hat{\sigma}_1$, $\omega_1 = 2\omega_2 + \varepsilon\hat{\sigma}_2$. Substituting Equations (14)-(15) into Equations (10)-(11) and eliminating the secular terms leads to the solvability conditions for the first-order expansion as:

$$2i\omega_1 D_1 A + \hat{\beta}_2 B^2 \exp(-i\hat{\sigma}_2 T_1) = 0 \tag{16}$$

$$2i\omega_2 D_1 B + \hat{\alpha}_3 A\bar{B}\exp(i\hat{\sigma}_2 T_1) = 0 \tag{17}$$

After eliminating the secular terms, the particular solutions of Equations (10)-(11) are given by:

$$x_1 = \frac{\hat{\alpha}_2}{3\omega_1^2} A^2 \exp(2i\omega_1 T_0) - \frac{\hat{\alpha}_2}{\omega_1^2} A\bar{A} - \frac{\hat{\beta}_2}{\omega_1^2} B\bar{B} + cc \tag{18}$$

$$y_1 = -\frac{\hat{\alpha}_3}{\left[\omega_2^2 - (\omega_1 + \omega_2)^2\right]} AB\exp\left(i(\omega_1 + \omega_2)T_0\right) + cc \tag{19}$$

Now substituting Equations (14)-(15) and Equations (18)-(19) into Equations (12)-(13), the following are obtained

$$(D_0^2 + \omega_1^2) x_2 = (-D_1^2 A - 2i\omega_1 \hat{c}_1 A - 2i\omega_1 D_2 A + \Gamma_1 AB\bar{B} + \Gamma_2 A^2\bar{A})\exp(i\omega_1 T_0) + NST + cc \tag{20}$$

$$(D_0^2 + \omega_2^2) y_2 = \left(-D_1^2 B - 2i\omega_2 \hat{c}_2 B - 2i\omega_2 D_2 B + \Gamma_3 A\bar{A}B + \Gamma_4 \bar{B}B^2\right)\exp(i\omega_2 T_0) + \frac{1}{2}\hat{f}_2 \bar{B}\exp(i(\Omega_2 - \omega_2)T_0) + NST + cc \tag{21}$$

where

$$\Gamma_1 = \left\{\frac{2\hat{\beta}_2\hat{\alpha}_3}{\omega_2^2 - (\omega_1+\omega_2)^2} + \frac{4\hat{\alpha}_2\hat{\beta}_2}{\omega_1^2} - 2\hat{\eta}_2\right\},$$

$$\Gamma_2 = \left\{\frac{10\hat{\alpha}_2^2}{3\omega_1^2} - 3\hat{\gamma}_2\right\},$$

$$\Gamma_3 = \left\{\frac{\hat{\alpha}_3^2}{\left[\omega_2^2 - (\omega_1+\omega_2)^2\right]} + \frac{2\hat{\alpha}_2\hat{\alpha}_3}{\omega_1^2} - 2\hat{\eta}_3\right\},$$

$$\Gamma_4 = \left\{\frac{2\hat{\beta}_2\hat{\alpha}_3}{\omega_1^2} - 3\hat{\gamma}_3\right\}$$

and NST stands for non-secular terms. Eliminating the

secular terms leads to the solvability conditions for the second-order expansion

$$2i\omega_1 D_2 A = -D_1^2 A - 2i\omega_1 \hat{c}_1 A + \Gamma_1 AB\overline{B} + \Gamma_2 A^2 \overline{A} \quad (22)$$

$$\begin{aligned} 2i\omega_2 D_2 B = &-D_1^2 B - 2i\omega_2 \hat{c}_2 B + \Gamma_3 A\overline{A}B \\ &+ \Gamma_4 \overline{B}B^2 + \frac{1}{2}\hat{f}_2 \overline{B}\exp(i\hat{\sigma}_1 T_1) \end{aligned} \quad (23)$$

Stability Analysis of Nonlinear Solutions

From Equation (7), multiplying both sides be $2i\omega_1$, $2i\omega_2$ we get

$$2i\omega_1 \frac{\mathrm{d}A}{\mathrm{d}t} = \varepsilon\, 2i\omega_1 D_1 A + \varepsilon^2\, 2i\omega_1 D_2 A \quad (24)$$

$$2i\omega_2 \frac{\mathrm{d}B}{\mathrm{d}t} = \varepsilon\, 2i\omega_2 D_1 B + \varepsilon^2\, 2i\omega_2 D_2 B \quad (25)$$

To analyze the solutions of Equations (16)-(17) and Equations (22)-(23), we express A and B in the polar form

$$A(T_1, T_2) = (a/2)e^{i\gamma_1}, B(T_1, T_2) = (b/2)e^{i\gamma_2} \quad (26)$$

where a, b and $\gamma_s\ (s = 1, 2)$ are the steady state amplitudes and phases of the motion respectively. Substituting Equations (26), (16)-(17) and Equations (22)-(23) into Equations (24)-(25) and equating the real and imaginary parts we obtain the following equations describing the modulation of the amplitudes and phases:

$$\dot{a} = -c_1 a + \left\{\frac{\beta_2}{4\omega_1} + \frac{\sigma_2\beta_2}{8\omega_1^2}\right\} b^2 \sin\theta_2 \quad (27)$$

$$\begin{aligned} a\dot{\gamma}_1 = &\left\{\frac{\beta_2}{4\omega_1} + \frac{\sigma_2\beta_2}{8\omega_1^2}\right\} b^2 \cos\theta_2 \\ &- \left\{\frac{\Gamma_5}{8\omega_1} + \frac{\beta_2\alpha_3}{16\omega_1^2\omega_2}\right\} ab^2 - \frac{\Gamma_6}{8\omega_1} a^3 \end{aligned} \quad (28)$$

$$\dot{b} = -c_2 b + \left\{\frac{\sigma_2\alpha_3}{8\omega_2^2} - \frac{\alpha_3}{4\omega_2}\right\} a\, b \sin\theta_2 + \frac{f_2}{4\omega_2} b \sin\theta_1 \quad (29)$$

$$\begin{aligned} b\dot{\gamma}_2 = &\left\{\frac{\alpha_3}{4\omega_2} - \frac{\sigma_2\alpha_3}{8\omega_2^2}\right\} a\, b \cos\theta_2 + \Gamma_9 a^2 b \\ &- \Gamma_{10} b^3 - \frac{f_2}{4\omega_2} b\cos\theta_1 \end{aligned} \quad (30)$$

where

$$\begin{aligned} &\Gamma_9 = \left\{\frac{\alpha_3^2}{32\omega_2^3} - \frac{\Gamma_7}{8\omega_2}\right\},\ \Gamma_{10} = \left\{\frac{\beta_2\alpha_3}{32\omega_1\omega_2^2} + \frac{\Gamma_8}{8\omega_2}\right\} \\ &\left[\Gamma_5, \Gamma_6, \Gamma_7, \Gamma_8\right] = \left[\varepsilon^2\Gamma_1, \varepsilon^2\Gamma_2, \varepsilon^2\Gamma_3, \varepsilon^2\Gamma_4\right] \\ &\text{and } \theta_1 = \hat{\sigma}_1 T_1 - 2\gamma_2, \theta_2 = \hat{\sigma}_2 T_1 + \gamma_1 - 2\gamma_2 \end{aligned} \quad (31)$$

Form the system of Equations (27)-(30) to have stationary solutions, the following conditions must be satisfied:

$$\dot{a} = \dot{b} = \dot{\theta}_1 = \dot{\theta}_2 = 0 \quad (32)$$

It follows from Equation (31) that

$$\dot{\gamma}_2 = \frac{1}{2}\sigma_1, \dot{\gamma}_1 = \sigma_1 - \sigma_2 \quad (33)$$

Hence, the steady state solutions of Equations (27)-(30) are given by

$$c_1 a - \left\{\frac{\beta_2}{4\omega_1} + \frac{\sigma_2\beta_2}{8\omega_1^2}\right\} b^2 \sin\theta_2 = 0 \quad (34)$$

$$\begin{aligned} a(\sigma_1 - \sigma_2) - &\left\{\frac{\beta_2}{4\omega_1} + \frac{\sigma_2\beta_2}{8\omega_1^2}\right\} b^2 \cos\theta_2 + \frac{\Gamma_6}{8\omega_1} a^3 \\ &+ \left\{\frac{\Gamma_5}{8\omega_1} + \frac{\beta_2\alpha_3}{16\omega_1^2\omega_2}\right\} ab^2 = 0 \end{aligned} \quad (35)$$

$$c_2 b - \left\{\frac{\sigma_2\alpha_3}{8\omega_2^2} - \frac{\alpha_3}{4\omega_2}\right\} a\, b \sin\theta_2 - \frac{f_2}{4\omega_2} b \sin\theta_1 = 0 \quad (36)$$

$$\begin{aligned} \frac{1}{2} b\sigma_1 + &\left\{\frac{\sigma_2\alpha_3}{8\omega_2^2} - \frac{\alpha_3}{4\omega_2}\right\} ab\cos\theta_2 - \Gamma_9 a^2 b \\ &+ \Gamma_{10} b^3 + \frac{f_2}{4\omega_2} b\cos\theta_1 = 0 \end{aligned} \quad (37)$$

Solving the resulting algebraic equations for the fixed points of the practical case where $a \neq 0$, $b \neq 0$, that is non-planar motions, we obtain the following frequency response equations

$$\begin{aligned} a^2(\sigma_1 - \sigma_2)^2 + &c_1^2 a^2 + K_1^2 a^2 b^4 + K_2^2 a^6 - K_3 b^4 \\ &+ 2(\sigma_1 - \sigma_2) K_1 a^2 b^2 + 2(\sigma_1 - \sigma_2) K_2 a^6 \\ &+ 2K_1 K_2 a^4 b^2 = 0 \end{aligned} \quad (38)$$

$$\begin{aligned} \frac{1}{4} b^2\sigma_1^2 + c_2^2 b^2 + \Gamma_9^2 a^4 b^2 + \Gamma_{10}^2 b^6 - \Gamma_9 \sigma_1 b^2 a^2 \\ + \Gamma_{10}\sigma_1 b^4 - 2\Gamma_9\Gamma_{10} a^2 b^4 - K_4 a^2 b^2 - \frac{f_2^2}{16\omega_2^2} b^2 \\ - \frac{K_4 f_2}{2\omega_2} ab^2 \cos(\theta_1 - \theta_2) = 0 \end{aligned} \quad (39)$$

where

$$K_1 = \left\{\frac{\Gamma_5}{8\omega_1} + \frac{\beta_2\alpha_3}{16\omega_1^2\omega_2}\right\}, K_2 = \frac{\Gamma_6}{8\omega_1},\ K_3 = \left\{\frac{\beta_2}{4\omega_1} + \frac{\sigma_2\beta_2}{8\omega_1^2}\right\}$$

and $K_4 = \left\{\frac{\sigma_2\alpha_3}{8\omega_2^2} - \frac{\alpha_3}{4\omega_2}\right\}$.

The stability of the obtained fixed points for the simul-

taneous primary, principal parametric and 2:1 internal resonance case is determined and studied as follows:
one lets

$$a = a_{10} + a_{11}, b = b_{10} + b_{11} \quad \text{and } \theta_s = \theta_{s0} + \theta_{s1} \tag{40}$$

where a_{10}, b_{10} and θ_{s0} are the solutions of Equations (34)-(37) and a_{11}, b_{11}, θ_{s1} are perturbations which are assumed to be small compared to a_{10}, b_{10} and θ_{s0}. Substituting Equation (40) into Equations (27)-(30), using Equations (34)-(37) and keeping only the linear terms in a_{11}, b_{11}, θ_{s1} we obtain:

$$\dot{a}_{11} = -c1a11 + \left\{K_3 b_{10}^2 \cos\theta_{20}\right\}\theta_{21} + \left\{2K_3 b_{10}\sin\theta_{20}\right\} b_{11} \tag{41}$$

$$\begin{aligned}\dot{\theta}_{21} &= \left\{\frac{(\sigma_2-\sigma_1)}{a_{10}} - \frac{K_1 b_{10}^2}{a_{10}} - \frac{3\Gamma_6 a_{10}}{8\omega_1} + K_4\cos\theta_{20} - 2\Gamma_9 a_{10}\right\} a_{11} \\ &+ \left\{-K_4\, a_{10}\sin\theta_{20} - \frac{K_3 b_{10}^2}{a_{10}}\sin\theta_{20}\right\}\theta_{21} \\ &+ \left\{\frac{\sigma_1}{2b_{10}} + \frac{2K_3 b_{10}}{a_{10}}\cos\theta_{20} - 2K_1 b_{10} + \frac{K_4 a_{10}}{b_{10}}\cos\theta_{20}\right. \\ &\quad \left. - \frac{\Gamma_6 a_{10}^2}{b_{10}} + 3\Gamma_{10} b_{10} + \frac{f_2}{4\omega_2}\cos\theta_{10}\right\} b_{11} \\ &- \left\{\frac{f_2}{2\omega_2}\sin\theta_{10}\right\}\theta_{11}\end{aligned} \tag{42}$$

$$\begin{aligned}\dot{b}_{11} &= \left\{K_4\, b_{10}\sin\theta_{20}\right\} a_{11} \\ &+ \left\{-c_2 + K_4\, a_{10}\sin\theta_{20} + \frac{f_2}{4\omega_2}\sin\theta_{10}\right\} b_{11} \\ &+ \left\{K_4\, a_{10} b_{10}\cos\theta_{20}\right\}\theta_{21} + \left\{\frac{f_2}{4\omega_2} b_{10}\cos\theta_{10}\right\}\theta_{11}\end{aligned} \tag{43}$$

$$\begin{aligned}\dot{\theta}_{11} &= \left\{K_4\cos\theta_{20} - 2\Gamma_9 a_{10}\right\} a_{11} - \left\{K_4\, a_{10}\sin\theta_{20}\right\}\theta_{21} \\ &+ \left\{\frac{\sigma_1}{2b_{10}} + \frac{K_4 a_{10}}{b_{10}}\cos\theta_{20} - \frac{\Gamma_9 a_{10}^2}{b_{10}} + 3\Gamma_{10} b_{10} + \frac{f_2}{4\omega_2}\cos\theta_{10}\right\} b_{11} \\ &- \left\{\frac{f_2}{2\omega_2}\sin\theta_{10}\right\}\theta_{11}\end{aligned} \tag{44}$$

The system of Equations (41)-(44) are first order autonomous ordinary differential equations and the stability of a particular fixed point with respect to an infinitesimal disturbance proportional to $\exp(\lambda t)$ is determined by eigenvalues of the Jacobian matrix of the right hand sides of Equations (41)-(44). The zeros of the characteristic equation are given by

$$\lambda^4 + L_1\lambda^3 + L_2\lambda^2 + L_3\lambda + L_4 = 0 \tag{45}$$

where, L_1, L_2, L_3 and L_4 are functions of the parameters ($a, b, \omega_1, \omega_2, c_1, c_2, \alpha_2, \alpha_3, \beta_2, \eta_2, \eta_3, \gamma_2, \gamma_3, f_2, \theta_1, \sigma_1, \sigma_2$). According to the Routh-Hurwitz criterion the necessary and sufficient conditions for all the roots of Equation (45) to possess negative real parts are:

$$L_1 > 0,\ L_1 L_2 - L_3 > 0,\ L_3\left(L_1 L_2 - L_3\right) - L_1^2 L_4 > 0, L_4 > 0 \tag{46}$$

The system is stable if the eigenvalues have negative real parts, otherwise is unstable. In the frequency response curves, solid/dotted lines denote stable/ unstable periodic responses, respectively.

3. Results and Discussion

The response of the two-degree-of-freedom nonlinear system under both parametric and external excitations is studied. The solution of this system is determined up to and including the second order approximation by applying the multiple time scale perturbation. The steady state solution and its stability are determined and representative numerical results are included. The stability zone and effects of the different parameters are discussed using frequency response curve. The stability of the numerical solution is studied also using the phase-plane method. Some of the resulting resonance cases are confirmed applying well-known numerical techniques. The effects of the some different parameters on the vibrating system behavior are investigated and discussed.

3.1. Numerical Solution

Figure 2 shows that the response of the inclined cable for the non-resonant at the practical values of the parameters c_1 = 0.0002, c_2 = 0.03, α_2 = 0.2, β_2 = 0.5, γ_2 = 0.3, η_2 = 0.5, α_3 = 0.03, η_3 = 0.05, γ_3 = 0.04, f_1 = 2, f_2 = 0.01, Ω_1 = 2.75, Ω_2 = 3.2, ω_1 = 1.2, ω_2 = 1.5. It can be seen from this figure that the steady state amplitude is about 0.005 with dynamic chaotic behavior for the in-plane mode and about 0.18 with multi-limit cycle for the out-of-plane mode. The amplitudes decreasing with increasing time and tend to steady state motion and have stable solution. The worst resonance case is also confirmed numerically as shown in **Figure 3**. From this figure, it can be notice that the maximum steady state amplitude of the in-plane mode is about 130 times that of basic case with multi-limit cycle, while the maximum amplitude of out-of-plane mode is about 4 times of the basic case with chaotic motion.

Effects of external and parametric excitation forces f_1 and f_2.

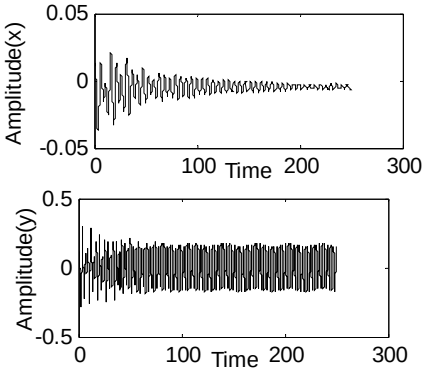

Figure 2. Non-resonance system behavior (basic case) $\Omega_1 \neq \omega_1 \neq \omega_2$.

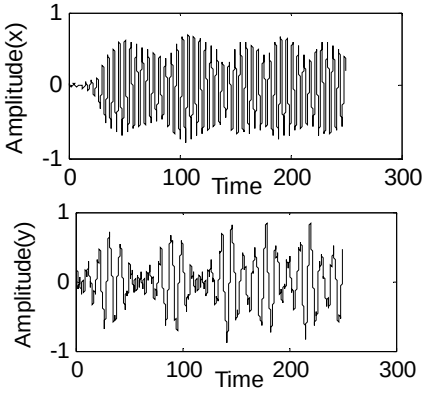

Figure 3. Simultaneous principal parametric resonance in the presence of 2:1 internal resonance ($\Omega_2 \cong 2\omega_2$ and $\omega_1 \cong 2\omega_2$).

For increasing the amplitude of the external or parametric excitation forces f_1 or f_2, we observe that the modes of vibration have increasing magnitudes and there exist chaotic dynamic motion as shown in **Figures 4** and **5**.

3.2. Frequency Response Curves

The frequency response Equations (38)-(39) are nonlinear algebraic equations in the amplitudes of the system a (in-plane mode) and b (out-of-plane mode). The stability of a fixed point solution is studied by examination of the eigenvalues of Equation (45). The numerical results of Equations (38) and (39) are plotted in **Figures 6-8**.

Figure 6, show the frequency response curves of the two modes of inclined cable against detuning parameter σ_1. From the geometry of the figures we observe that the amplitudes have two branches and these branches are bent to the right, the bending leads to multi-valued solutions and hence the effective nonlinearity is hardening type. In **Figure 6(a)**, there are two branches of nontrivial solution such that the left branch stable and the right branch lose stability as $\sigma_1 \leq 0.4$. **Figure 6(b)**, show that the steady state amplitudes are increasing for increasing

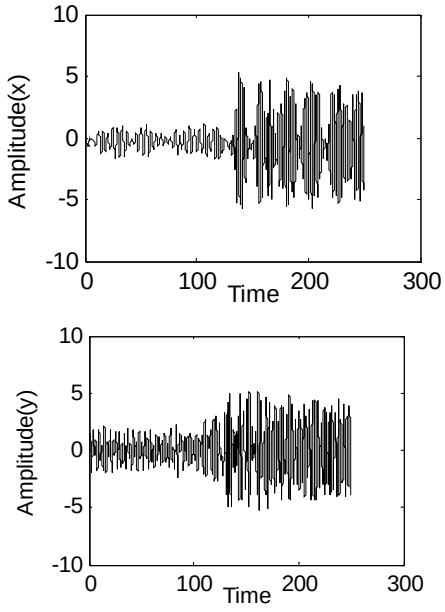

Figure 4. Effects of increasing value of external excitation force $f_1 = 5$.

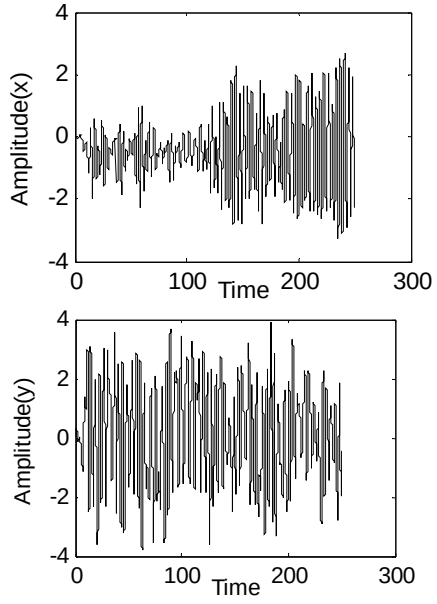

Figure 5. Effects of increasing value of parametric excitation force $f_2 = 3$.

parametric excitation force f_2. The region of instability for two modes is increasing for increasing f_2. For increasing nonlinear parameter β_2 (*i.e.* $\beta_2 = 1$) as shown in **Figure 6(c)**, we show that the regions of definition are decreasing and the two branches of the steady state amplitude curve are contracted and give one continuous curve which is stable and response amplitude of the in-plane mode is increased. **Figure 6(d)** show that the response amplitudes of the inclined cable are increasing for

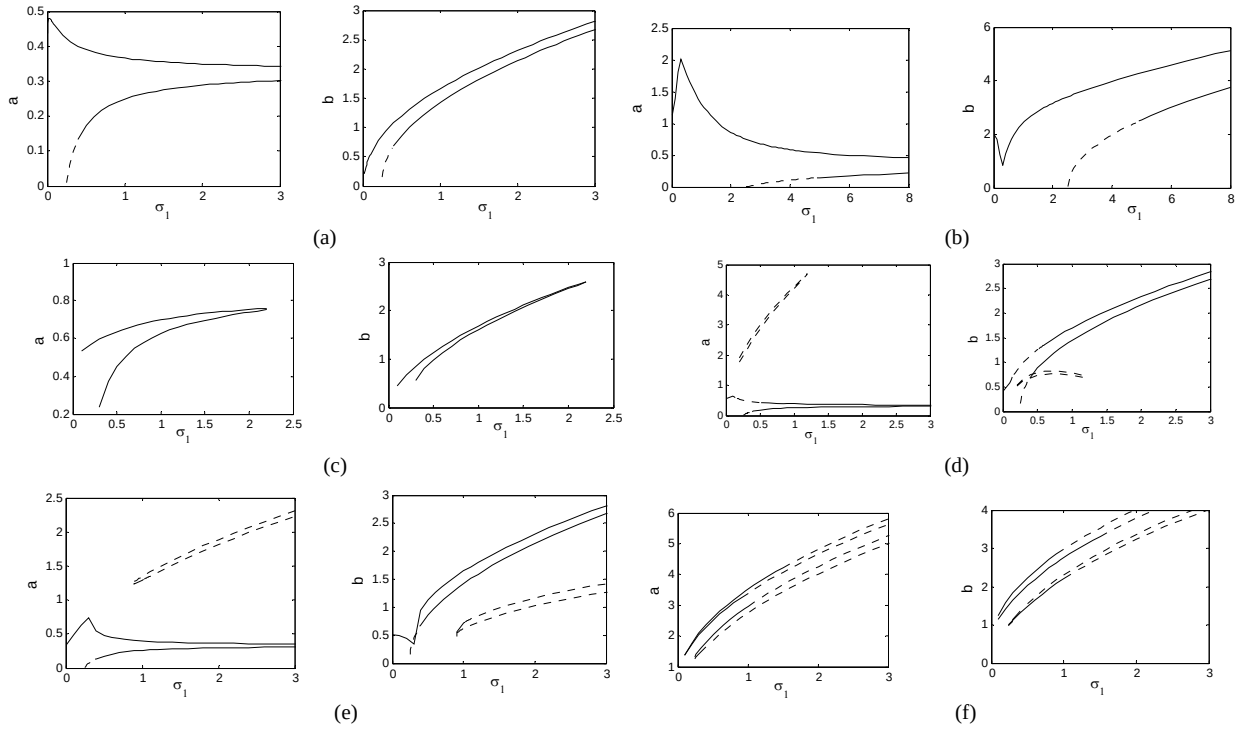

Figure 6. (a): Frequency response curves for amplitudes against σ_1; (b): Frequency response curve for increasing parametric excitation force $f_2 = 3.0$; (c): Frequency response curve for increasing nonlinear parameter $\beta_2 = 1.0$; (d): Frequency response curve for decreasing nonlinear parameter $\eta_3 = 0.1$; (e): Frequency response curve for increasing nonlinear parameter $\gamma_2 = 1.8$; (f): Frequency response curve for negative value of nonlinear parameter $\gamma_3 = -0.4$.

decreasing nonlinear parameter η_3 and the regions of multi-valued and instability of two modes are increasing. The regions of instability solutions are increasing for increasing nonlinear parameter γ_2 as shown in **Figure 6(e)**. **Figure 6(f)** shows that for negative value of nonlinear parameter γ_3 the response amplitudes are increasing and the stability solution are decreasing with increasing region of multi-valued.

Figure 7, represent the variation of the amplitudes of the inclined cable against the detuning parameter σ_2. In **Figure 7(a)**, we see that each mode of the inclined cable has one continuous curve and single valued solution and it is symmetric about the origin and it is noticed that the in-plane mode reaches maximum value at $\sigma_2 = 0$ and the out-of-plane mode reaches minimum value at the same value of σ_2. Also, it intersects in two points and these modes have stable and unstable solutions. From **Figure 7(b)**, we observe that for increasing parametric excitation force f_2 the symmetric branch moves up with increased magnitudes and the region of stability is increased. For increasing nonlinear parameter γ_3, we note that the amplitudes of the two modes of the inclined cable have decreasing magnitudes and increasing stable solutions, as shown in **Figure 7(c)**. The steady state amplitudes of the two modes are increasing for decreasing nonlinear parameter η_3 as shown in **Figure 7(d)**. Also, the region of stability solutions is increased. From **Figure 7(e)** we observe that the steady state amplitudes a and b of the two modes are increasing for decreasing value of nonlinear parameters α_3 respectively with increasing stable solutions. The stability solution is decreasing as the nonlinear parameter α_2 is increase and the curves are shifted to the right and has hardening phenomena and there exists jump phenomena, as shown in **Figure 7(f)**.

Figure 8 represent force-response curves for the nonlinear solution of the case of simultaneous principal parametric resonance in the presence of 2:1 internal resonances. In this figure the amplitudes of the inclined cable are plotted as a function of the parametric excitation force f_2. **Figure 8** shows that the response amplitudes of the inclined cable have a continuous curve and the curve has stable and unstable solutions.

4. Comparison with Published Work

In comparison with the previous work [8], we have the global bifurcation of this inclined cable leading to primary resonances and 1:1 internal resonance is investigated. A new global perturbation technique is employed to analyze Shilnikov type homoclinic orbits and chaotic dynamics in the inclined cable. Kamel and Hamed [9],

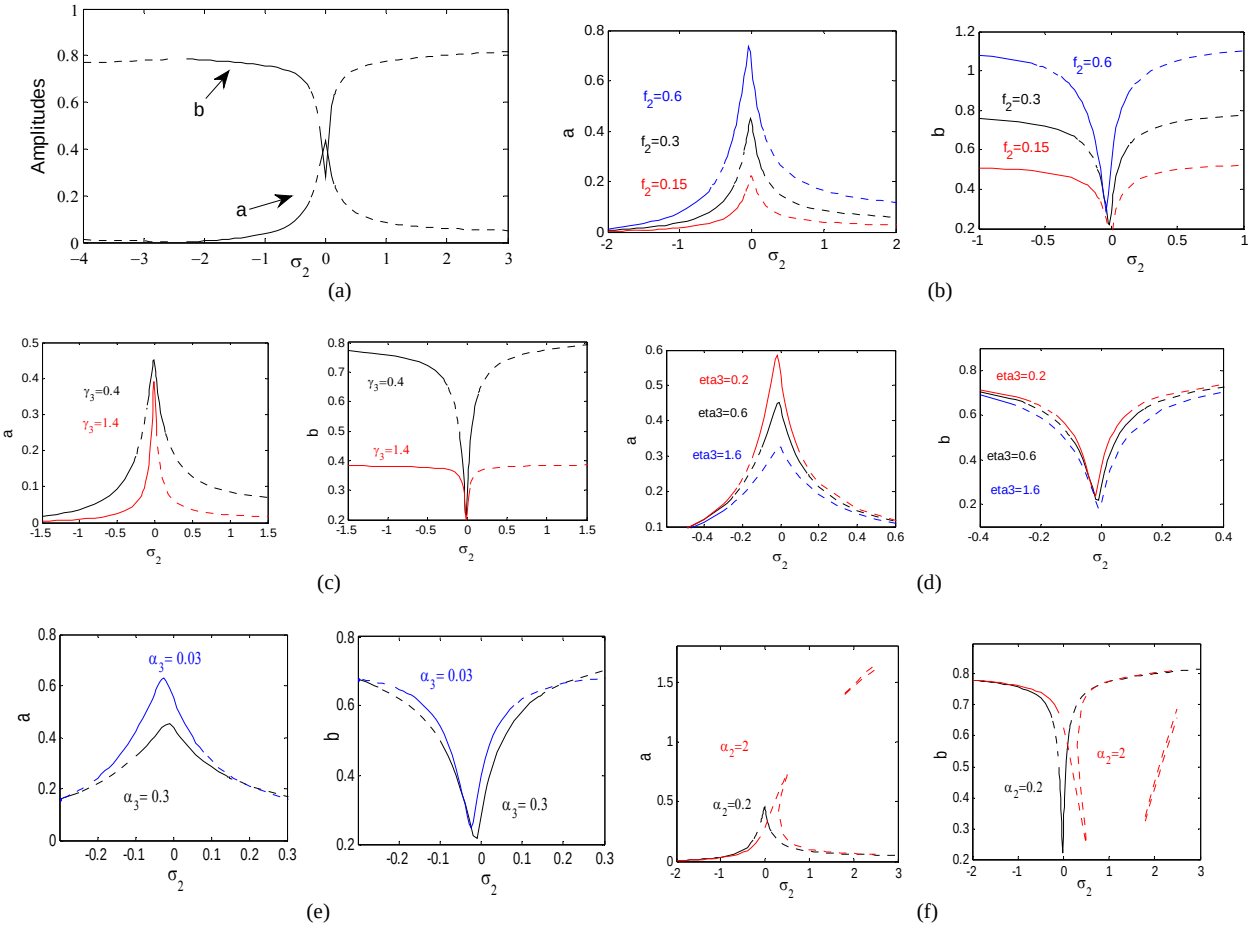

Figure 7. (a): Frequency response curves for simultaneous principal parametric resonance in the presence of 2:1 internal resonance $\Omega_2 \cong 2\omega_2$ and $\omega_1 \cong 2\omega_2$; (b): Frequency response curve for parametric excitation force f_2; (c): Frequency response curve for nonlinear parameter γ_3; (d): Frequency response curve for nonlinear parameter η_3; (e): Frequency response curve for nonlinear parameter α_3; (f): Frequency response curve for nonlinear parameter α_2.

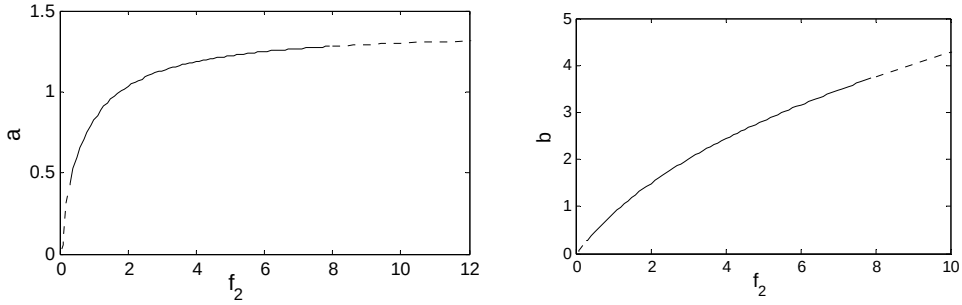

Figure 8. Force response curves for ($\Omega_2 \cong 2\omega_2$, $\omega_1 \cong 2\omega_2$).

studied the nonlinear behavior of an inclined cable subjected to harmonic excitation near the simultaneous primary and 1:1 internal resonance by using multiple scale method.

In this paper, periodic and chaotic response of a discretization two-degree-of-freedom model of a suspended inclined cable, containing a 2:1 internal resonance, subject to harmonic external and parametric excitation are obtained. The stable/unstable periodic solutions are determined using the method of multiple scale and are presented through frequency response plots. Chaotic responses are determined by numerical integration of the governing ordinary differential equations of motion. Variation of the parameters $\alpha_2, \alpha_3, \beta_2, \gamma_2, \eta_2, \gamma_3, \eta_3, f_2$ leads

to multi-valued amplitudes and hence to jump phenomena.

5. Conclusions

Cables are very efficient structural members and hence have been widely used in many long-span structures, including suspension, roofs and guyed towers. The nonlinear dynamic response of the nonlinear system subjected to external and parametric excitations is investigated. The method of multiple scales is applied to obtain the solution of the considered system up to second order approximation. The numerical solutions and chaotic response of this nonlinear system are investigated. The stability of the proposed analytic nonlinear solution is studied at worst resonance case which is the simultaneous principal parametric resonance in the presence of 2:1 internal resonances. The modulation equations of the amplitudes and phases are obtained and steady state solutions are determined. The effects of some nonlinear parameters on the steady state response of the vibrating cable leading to multi-valued solutions. From the analysis the following may be concluded.

1) For the resonance case $\Omega_2 \cong 2\omega_2, \omega_1 \cong 2\omega_2$ we note that the steady state amplitude is increased to about 130% compared to basic case with multi-limit cycle, and it is better to avoid this resonance case as working conditions for the system.

2) The steady state amplitude of the system are increasing for increasing external or parametric excitation force, and for large values of the system become unstable.

3) Variation of α_2, α_3, β_2, γ_2, η_2, γ_3, η_3, f_2 leads to multi-valued amplitudes and hence jump phenomena.

4) For increasing parametric excitation force f_2 or negative value of the nonlinear parameter γ_3 we observe that the steady state amplitudes of the two modes are increasing with increasing instability solutions.

5) Increasing of the nonlinear parameters η_3 or γ_3 can reduce the amplitude of the system and obtain the effect of reduction of the amplitude.

6) Variation of the parameter α_2 leads to multi-valued amplitudes and hence to jump phenomena.

7) For increasing parametric excitation force f_2 or decreasing nonlinear parameter α_3 we show that the steady state amplitudes of the two modes are increasing.

For increasing nonlinear parameter η_3 we note that the steady state amplitudes of the two modes are decreasing with decrease of the stability solutions.

6. References

[1] H. N. Arafat and A. H. Nayfeh, "Non-Linear Responses of Suspended Cables to Primary Resonance Excitations," *Journal of Sound and Vibration*, Vol. 266, No. 2, 2003, pp. 325-354. doi:10.1016/S0022-460X(02)01393-7

[2] G. Rega, "Non-Linear Vibrations of Suspended Cables; Part I: Modeling and Analysis," *Journal of Applied Mechanics Review*, Vol. 57, No. 6, 2004, pp. 443-478. doi:10.1115/1.1777224

[3] G. Rega, "Non-Linear Vibrations of Suspended Cables; Part II: Deterministic Phenomena," *Journal of Applied Mechanics Review*, Vol. 57, No. 6, 2004, pp. 479-514. doi:10.1115/1.1777225

[4] S. R. Nielsen and P. H. Kirkegaard, "Super and Combinatorial Harmonic Response of Flexible Inclined Cables with Small Sag," *Journal of Sound and Vibration*, Vol. 251, No. 1, 2002, pp. 79-102. doi:10.1006/jsvi.2001.3979

[5] G. Zheng, J. M. Ko and Y. O. Ni, "Super-Harmonic and Internal Resonances of a Suspended Cable with Nearly Commensurable Natural Frequencies," *Nonlinear Dynamics*, Vol. 30, No. 1, 2002, pp. 55-70. doi:10.1023/A:1020395922392

[6] W. Zhang and Y. Tang, "Global Dynamics of the Cable under Combined Parametrical and External Excitations," *International Journal of Non-Linear Mechanics*, Vol. 37, No. 3, 2002, pp. 505-526. doi:10.1016/S0020-7462(01)00026-9

[7] A. H. Nayfeh, H. Arafat, C. M. Chin and W. Lacarbonara, "Multimode Interactions in Suspended Cables," *Journal of Vibration and Control*, Vol. 8, No. 3, 2002, pp. 337-387. doi:10.1177/107754602023687

[8] H. Chen and Q. Xu, "Bifurcation and Chaos of an Inclined Cable," *Nonlinear Dynamics*, Vol. 57, No. 2-3, 2009, pp. 37-55. doi:10.1007/s11071-008-9418-3

[9] M. M. Kamel and Y. S. Hamed, "Non-Linear Analysis of an Inclined Cable under Harmonic Excitation," *Acta Mechanica*, Vol. 214, No. 3-4, 2010, pp. 315-325. doi:10.1007/s00707-010-0293-x

[10] A. Abe, "Validity and Accuracy of Solutions for Nonlinear Vibration Analyses of Suspended Cables with One-to-One Internal Resonance," *Nonlinear Analysis*: *Real World Applications*, Vol. 11, No. 4, 2010, pp. 2594-2602. doi:10.1016/j.nonrwa.2009.09.006

[11] N. Srinil, G. Rega and S. Chucheepsakul, "Two-yo-One Resonant Multi-Modal Dynamics of Horizontal/Inclined Cables. Part I: Theoretical Formulation and Model Validation," *Nonlinear Dynamics*, Vol. 48, No. 3, 2007, pp. 231-252. doi:10.1007/s11071-006-9086-0

[12] N. Srinil and G. Rega, "Two-To-One Resonant Multi-Modal Dynamics of Horizontal/Inclined Cables. Part II: Internal Resonance Activation Reduced-Order Models and Nonlinear Normal Modes," *Nonlinear Dynamics*, Vol. 48, No. 3, 2007, pp. 253-274. doi:10.1007/s11071-006-9087-z

[13] R. Alaggio and G. Rega, "Characterizing Bifurcations and Classes of Motion in the Transition to Chaos through 3D-Tori of a Continuous Experimental System in Solid Mechanics," *Physica D*, Vol. 137, No. 1, 2000, pp. 70-93. doi:10.1016/S0167-2789(99)00169-4

[14] G. Rega and R. Alaggio, "Spatio-Temporal Dimensional-

ity in the Overall Complex Dynamics of an Experimental Cable/Mass System," *International Journal of Solids and Structures*, Vol. 38, No. 10-13, 2001, pp. 2049-2068. doi:10.1016/S0020-7683(00)00152-9

[15] A. Gonzalez-Buelga, S. A. Neild, D. J. Wagg and J. H. G. Macdonald, "Modal Stability of Inclined Cables Subjected to Vertical Support Excitation," *Journal of Sound and Vibration*, Vol. 318, No. 3, 2008, pp. 565-579. doi:10.1016/j.jsv.2008.04.031

[16] N. C. Perkins, "Modal Interactions in the Non-Linear Response of Inclined Cables under Parametric/External Excitation," *International Journal of Non-linear Mechanics*, Vol. 27, No. 2, 1992, pp. 233-250. doi:10.1016/0020-7462(92)90083-J

[17] C. L. Lee and N. C. Perkins, "Nonlinear Oscillations of Suspended Cables Containing a Two-to-One Internal Resonance," *Nonlinear Dynamics*, Vol. 3, 1992, pp. 465-490.

[18] C. L. Lee and N. C. Perkins, "Three-Dimensional Oscillations of Suspended Cables Involving Simultaneous Internal Resonance," *Proceedings of ASME Winter Annual Meeting AMD*-14, 1992, pp. 59-67.

[19] M. Eissa and M. Sayed, "A Comparison between Passive and Active Control of Non-Linear Simple Pendulum Part-I," *Mathematical and Computational Applications*, Vol. 11, No. 2, 2006, pp. 137-149.

[20] M. Eissa and M. Sayed, "A Comparison between Passive and Active Control of Non-Linear Simple Pendulum Part-II," *Mathematical and Computational Applications*, Vol. 11, No. 2, 2006, pp. 151-162.

[21] M. Eissa and M. Sayed, "Vibration Reduction of a Three DOF Non-Linear Spring Pendulum," *Communication in Nonlinear Science and Numerical Simulation*, Vol. 13, No. 2, 2008, pp. 465-488. doi:10.1016/j.cnsns.2006.04.001

[22] M. Sayed, "Improving the Mathematical Solutions of Nonlinear Differential Equations Using Different Control Methods," Ph.D. Thesis, Menofia University, Egypt, November 2006.

[23] M. Sayed and Y. S. Hamed, "Stability and Response of a Nonlinear Coupled Pitch-Roll Ship Model under Parametric and Harmonic Excitations," *Nonlinear Dynamics*, Vol. 64, No. 3, 2011, pp. 207-220. doi:10.1007/s11071-010-9841-0

[24] M. Sayed and M. Kamel, "Stability Study and Control of Helicopter Blade Flapping Vibrations," *Applied Mathematical Modelling*, Vol. 35, No. 6, 2011, pp. 2820-2837. doi:10.1016/j.apm.2010.12.002

[25] M. Sayed and M. Kamel, "1:2 and 1:3 Internal Resonance Active Absorber for Non-Linear Vibrating System," *Applied Mathematical Modelling*, Vol. 36, No. 1, 2012, pp. 310-332. doi:10.1016/j.apm.2011.05.057

[26] Y. A. Amer and M. Sayed, "Stability at Principal Resonance of Multi-Parametrically and Externally Excited Mechanical System," *Advances in Theoretical and Applied Mechanics*, Vol. 4, No. 1, 2011, pp. 1-14.

[27] M. Sayed, Y. S. Hamed and Y. A. Amer, "Vibration Reduction and Stability of Non-Linear System Subjected to External and Parametric Excitation Forces under a Nonlinear Absorber," *International Journal of Contemporary Mathematical Sciences*, Vol. 6, No. 22, 2011, pp. 1051 - 1070.

[28] A. H. Nayfeh, "Non-Linear Interactions," Wiley/Inter-Science, New York, 2000.

Applied Mathematics, 2011, 2, 1479-1485
doi:10.4236/am.2011.212210 Published Online December 2011 (http://www.SciRP.org/journal/am)

Numerical Solution of Nonlinear Klein-Gordon Equation Using Lattice Boltzmann Method

Qiaojie Li[1], Zong Ji[2], Zhoushun Zheng[1], Hongjuan Liu[1]
[1]*School of Mathematical Science and Computing Technology*, *Central South University*, *Changsha*, *China*
[2]*Modern Service and Trade College*, *Yunnan University of Finance and Economics*, *Kunming*, *China*
E-mail: *qiaojie_li@foxmail.com*
Received October 24, 2011; *revised November* 24, 2011; *accepted December* 1, 2011

Abstract

In this paper, in order to extend the lattice Boltzmann method to deal with more nonlinear equations, a one-dimensional (1D) lattice Boltzmann scheme with an amending function for the nonlinear Klein-Gordon equation is proposed. With the Taylor and Chapman-Enskog expansion, the nonlinear Klein-Gordon equation is recovered correctly from the lattice Boltzmann equation. The method is applied on some test examples, and the numerical results have been compared with the analytical solutions or the numerical solutions reported in previous studies. The L_2, L_∞ and Root-Mean-Square (RMS) errors in the solutions show the efficiency of the method computationally.

Keywords: Lattice Boltzmann, Chapman-Enskog Expansion, Nonlinear Klein-Gordon Equation

1. Introduction

Nonlinear phenomena modeled by partial differential equation appear in many areas of scientific fields such as solid state physics, plasma physics, fluid dynamics, mathematical biology and chemical kinetics. The nonlinear Klein-Gordon equation has attracted much attention in studying solutions and condensed mater physics, in investigating the interaction of solitons in a collisionless plasma, the recurrence of initial states, and in examining the nonlinear wave equations [1,2]. In the last few decades, many powerful methods, such as the inverse scattering method, Baklund transformation, the auxiliary equation method [3,4], the Wadati trace method, Hirota bilinear forms, the tanh-sech method, the sine-cosine method, Jacobi elliptic functions, and the Riccati equation expansion method were used to investigate these types of equations (see [5] and references therein). A variety of finite difference scheme have been presented (see [6] and references therein) and the alternative approaches using spectral and pseudo-spectral methods have recently been presented [7,8]. To avoid the mesh generation, meshless techniques have attracted the attention of researchers in recent years. The radial basis function (RBF) as a truly meshless method was used to solve nonlinear Klein-Gordon equation in [9].

Recently, unlike convectional numerical methods which search for the macroscopic equation, the lattice Boltzmann method (LBM) has achieved much success in studying nonlinear equations and the evolution of complex systems [10,11]. By choosing appropriate collision or equilibrium distribution, the lattice Boltzmann model is able to recover the PDE of interest. This method is a new technique based on a mesoscopic kinetic equation for the particle distribution functions. Compared with the conventional numerical methods, the LBM provides many of the advantages, including geometrical flexibility, clear physical pictures, ease in incorporating complex boundary conditions, simplicity of programming and numerical efficiency. Recently, it has been developed to simulate linear and nonlinear PDE such as Laplace equation [12], Poisson equation [13,14], the shallow water equation [15], Burgers equation [16], Korteweg-de Vires equation [17], Wave equation [18,19], reaction-diffusion equation [20,21], convection-diffusion equation [22-24].

In this paper, the initial-value problem of the one-dimensional nonlinear Klein-Gordon equations is given by the following equation,

$$u_{tt} + \alpha u_{xx} + g(u) = f(x,t) \tag{1}$$

where $u = u(x,t)$ represents the wave displacement at position x and time t, α is a known constant and $g(u)$ is the nonlinear force.

The present work is motivated by the desire to extend

the lattice Boltzmann method to deal with evolution models characterized by nonlinear wave dispersion. By using Taylor expansion and the Chapman-Enskog expansion, the second-order nonlinear Klein-Gordon equation can be recovered from the present model correctly. The local equilibrium distribution function and the amending function are obtained. To make a comparison between numerical solutions and analytical ones, four Klein-Gordon equations with quadratic or cubic nonlinearity are considered. From the simulations, we find that the numerical results are in excellent agreement with the analytical solutions. This indicates that the present method is an efficient and flexible approach for practical application.

The organization of the paper as follows. In Section 2, the lattice Boltzmann model is described. Numerical examples are simulated in Section 3. Summary and conclusion are presented in Section 4.

2. The Lattice Boltzmann Model

The lattice Boltzmann model used on this study is the three-velocity lattice Bhatnagar-Gross-Krook (LBGK) model. The directions of the discrete velocity are defined as c_i $(i=0,1,2)$

$$[c_0,c_1,c_2]=[0,-c,c].$$

where c is a constant. The lattice Boltzmann equation with an amending function is given as follow

$$\begin{aligned} &f_i\left(x+c_i\Delta t,t+\Delta t\right)-f_i(x,t)\\ &=-\frac{1}{\tau}\left[f_i(x,t)-f_i^{eq}(x,t)\right]+\Delta t F_i(x,t)\end{aligned} \tag{2}$$

where $f_i(x,t)$ and $f_i^{eq}(x,t)$ are defined as the distribution and equilibrium distribution function, respectively. $F_i(x,t)$ is an amending function and τ is the dimensionless relaxation time. $\Delta x=c_i\Delta t$ and Δt are the lattice spacing and time step, respectively.

Unlike for the normal LBM, the first derivative of the macroscopic variable $u(x,t)$ meets the following conservation laws

$$\sum_i f_i(x,t)=\sum_i f_i^{eq}(x,t)=\frac{\partial u(x,t)}{\partial t} \tag{3}$$

Then, through choosing appropriate local equilibrium distributions, we can retrieve the corresponding macroscopic equation correctly.

Indeed, applying the Taylor expansion to left-hand side of Equation (2) and retaining terms up to $\mathcal{O}(\Delta t^3)$, we get

$$\begin{aligned} &\Delta t\left(c_i\frac{\partial}{\partial x}+\frac{\partial}{\partial t}\right)f_i+\frac{\Delta t^2}{2}\left(c_i\frac{\partial}{\partial x}+\frac{\partial}{\partial t}\right)^2 f_i\\ &+\mathcal{O}(\Delta t^3)=-\frac{1}{\tau}\left(f_i-f_i^{eq}\right)+\Delta t F_i\end{aligned} \tag{4}$$

The macroscopic equation can be recovered in the multi-scale analysis using a small expansion parameter ε which is proportional to the ration of the lattice spacing to the characteristic macroscopic length. To do this, the Chapman-Enskog expansion in time and space is applied:

$$\begin{aligned} &f_i=f_i^{eq}+\varepsilon f_i^{(1)}+\varepsilon^2 f_i^{(2)},\ F_i=\varepsilon^2 F_i^{(2)}\\ &\frac{\partial}{\partial t}=\varepsilon\frac{\partial}{\partial t_1}+\varepsilon^2\frac{\partial}{\partial t_2},\ \frac{\partial}{\partial x}=\varepsilon\frac{\partial}{\partial x_1}\end{aligned} \tag{5}$$

where $f_i^{(k)}$ and $F_i^{(2)}$ are the non-equilibrium distribution functions and non-equilibrium amending function, which satisfy the solvability conditions

$$\begin{aligned} &\sum_i f_i^{(k)}=0\ (k\geq 1)\\ &\sum_i F_i^{(2)}=F^{(2)}\end{aligned} \tag{6}$$

Substituting Equation (5) into (4), we have

$$\begin{aligned} &\left(\varepsilon c_i\frac{\partial}{\partial x_1}+\varepsilon\frac{\partial}{\partial t_1}+\varepsilon^2\frac{\partial}{\partial t_2}\right)\left(f_i^{eq}+\varepsilon f_i^{(1)}+\varepsilon^2 f_i^{(2)}\right)\\ &+\frac{\Delta t}{2}\left(\varepsilon c_i\frac{\partial}{\partial x_1}+\varepsilon\frac{\partial}{\partial t_1}+\varepsilon^2\frac{\partial}{\partial t_2}\right)^2\left(f_i^{eq}+\varepsilon f_i^{(1)}+\varepsilon^2 f_i^{(2)}\right)\\ &=-\frac{1}{\tau}\left(\varepsilon f_i^{(1)}+\varepsilon^2 f_i^{(2)}\right)+\varepsilon^2 F_i^{(2)}\end{aligned} \tag{7}$$

Comparing the two sides of Equation (7) and treating terms in order of ε and ε^2 gives

$$\mathcal{O}(\varepsilon):\ \left(c_i\frac{\partial}{\partial x_1}+\frac{\partial}{\partial t_1}\right)f_i^{eq}=-\frac{1}{\tau\Delta t}f_i^{(1)} \tag{8}$$

$$\begin{aligned} &\mathcal{O}(\varepsilon^2):\ \frac{\partial}{\partial t_2}f_i^{eq}+\left(c_i\frac{\partial}{\partial x_1}+\frac{\partial}{\partial t_1}\right)f_i^{(1)}\\ &+\frac{\Delta t}{2}\left(c_i\frac{\partial}{\partial x_1}+\frac{\partial}{\partial t_1}\right)^2 f_i^{eq}=-\frac{1}{\tau\Delta t}f_i^{(2)}+F_i^{(2)}\end{aligned} \tag{9}$$

Applying Equation (8) to the left side of Equation (9), we can rewrite Equation (9) as

$$\begin{aligned} &\frac{\partial}{\partial t_2}f_i^{eq}+\left(1-\frac{1}{2\tau}\right)\left(c_i\frac{\partial}{\partial x_1}+\frac{\partial}{\partial t_1}\right)f_i^{(1)}\\ &=-\frac{1}{\tau\Delta t}f_i^{(2)}+F_i^{(2)}\end{aligned} \tag{10}$$

In order to recover Equation (1), we must give appropriate local equilibrium distribution function. We choose f_i^{eq} such that,

$$\begin{aligned} &\sum_i f_i^{eq}=\frac{\partial u(x,t)}{\partial t}\\ &\sum_i c_i f_i^{eq}=0,\sum_i c_i c_i f_i^{eq}=c_s^2 u(x,t)\end{aligned} \tag{11}$$

where $c_s^2 = c^2/3$ is called the lattice Boltzmann sound speed. Equation (11) leads to three linear equations for $f_i^{eq}(x,t)$. Solving these equations determines the equilibrium distribution functions

$$\begin{aligned} f_0^{eq}(x,t) &= \frac{\partial u(x,t)}{\partial t} - \frac{u(x,t)}{3} \\ f_1^{eq}(x,t) &= \frac{u(x,t)}{6} \\ f_2^{eq}(x,t) &= \frac{u(x,t)}{6} \end{aligned} \tag{12}$$

Meanwhile, the amending function $F_i(x,t)$ is taken as

$$F_i(x,t) = \omega_i F(x,t) = \omega_i \left(f(x,t) - g(u) \right) \tag{13}$$

such that $\sum_i F_i(x,t) = F(x,t)$. For simplicity, only one case is given here

$$\begin{aligned} F_0(x,t) &= \frac{2}{3}\left(f(x,t) - g(u) \right) \\ F_1(x,t) &= \frac{1}{6}\left(f(x,t) - g(u) \right) \\ F_2(x,t) &= \frac{1}{6}\left(f(x,t) - g(u) \right) \end{aligned} \tag{14}$$

Summing Equation (8) and Equation (10) over *i*, and using Equation (6) and (11), we obtain

$$\frac{\partial}{\partial t_1}\left(\frac{\partial u}{\partial t} \right) = 0 \tag{15}$$

$$\frac{\partial}{\partial t_2}\left(\frac{\partial u}{\partial t} \right) + \left(1 - \frac{1}{2\tau} \right) \frac{\partial}{\partial x_1}\left(\sum_i c_i f_i^{(1)} \right) = F^{(2)} \tag{16}$$

Using Equation (8) and (11), we get

$$\begin{aligned} \sum_i c_i f_i^{(1)} &= -\tau \Delta t \sum_i c_i \left(c_i \frac{\partial}{\partial x_1} + \frac{\partial}{\partial t_1} \right) f_i^{eq} \\ &= -\tau \Delta t \sum_i \left[\frac{\partial}{\partial x_1}(c_i c_i f_i^{eq}) + \frac{\partial}{\partial t_1}(c_i f_i^{eq}) \right] \\ &= -\tau \Delta t \frac{\partial}{\partial x_1}(c_s^2 u) \end{aligned} \tag{17}$$

Then substituting Equation (17) into Equation (16), we have

$$\frac{\partial}{\partial t_2}\left(\frac{\partial u}{\partial t} \right) + c_s^2 \Delta t \left(\frac{1}{2} - \tau \right) \frac{\partial}{\partial x_1}\left(\frac{\partial u}{\partial x_1} \right) = F^{(2)} \tag{18}$$

When Equation $(15)\times\varepsilon + (18)\times\varepsilon^2$ is applied, the final nonlinear Klein-Gordon equation is recovered as

$$\frac{\partial^2 u}{\partial t^2} + \alpha \frac{\partial^2 u}{\partial x^2} = F(x,t) = f(x,t) - g(u) \tag{19}$$

where $\alpha = c_s^2 \Delta t \left(\frac{1}{2} - \tau \right)$

In the computational process, in order to obtain $u(x,t)$, we can apply backward difference to the item $\frac{\partial u(x,t)}{\partial t}$

$$\frac{\partial u(x,t)}{\partial t} = \frac{u(x,t) - u(x,t-\Delta t)}{\Delta t} \tag{20}$$

3. Numerical Simulation Results

In this section, we present the result of our LBM numerical experiments for the relevant equations. In comparison with the analytical solutions and results derived by existing literature, the efficiency of proposed model is validated. The distribution function $f_i(x,t)$ is initialized with $f_i^{eq}(x,t)$ for all nodes at $t = 0$. The macroscopic variable $u(x,t)$ is initialized by the initial condition and the non-equilibrium extrapolation scheme proposed by Guo [25] is used for boundary treatment. The following error norms are used to measure the accuracy

1) L_2-error

$$L_2 - error = \left(\sum_{i=1}^{n} e_i^2 \right)^{\frac{1}{2}}$$

2) L_∞-error

$$L_\infty - error = \text{Max } e_i, \quad 1 \le i \le n$$

3) The root mean square (RMS) error

$$RMS - error = \left(\sum_{i=1}^{n} \frac{e_i^2}{n} \right)^{\frac{1}{2}}$$

where $e_i = \left| u(x_i,t) - u^*(x_i,t) \right|$, $u(x_i,t)$ and $u^*(x_i,t)$ are the numerical solution and analytical one.

Example 1. The Klein-Gordon equation with quadratic nonlinearity in the interval $-1 \le x \le 1$

$$u_{tt} - u_{xx} = -x\cos t + x^2 \cos^2 t - u^2$$

The initial conditions are given by

$$u(x,0) = x, \; u_t(x,0) = 0$$

The exact solution is given in [9]

$$u(x,t) = x\cos t$$

We extract the boundary condition from the exact solution. In **Table 1**, the L_∞, L_2 and RMS errors are obtained for $t = 1,3,5,7,10$. The graph of analytical and LBM solution for $t = 1$ and $t = 10$ are given in **Figure 1** and the space-time graph of the LBM solution is given in **Figure 2**.

Example 2. Consider the nonlinear Klein-Gordon equation with quadratic nonlinearity in interval $0 \le x \le 1$.

Table 1. L_∞, L_2 and RMS errors with dx = 0.02 and dt = 2 × 10^{-5}.

t	errors		
	L_∞-error	L_2-error	RMS
1	1.9558e–03	1.1135e–03	1.1294e–04
3	1.3664e–03	7.6676e–03	7.6295e–04
5	1.5260e–03	8.5602e–03	8.5178e–04
7	1.6201e–03	9.5926e–03	9.5450e–04
10	1.0465e–03	6.9848e–03	6.9501e–04

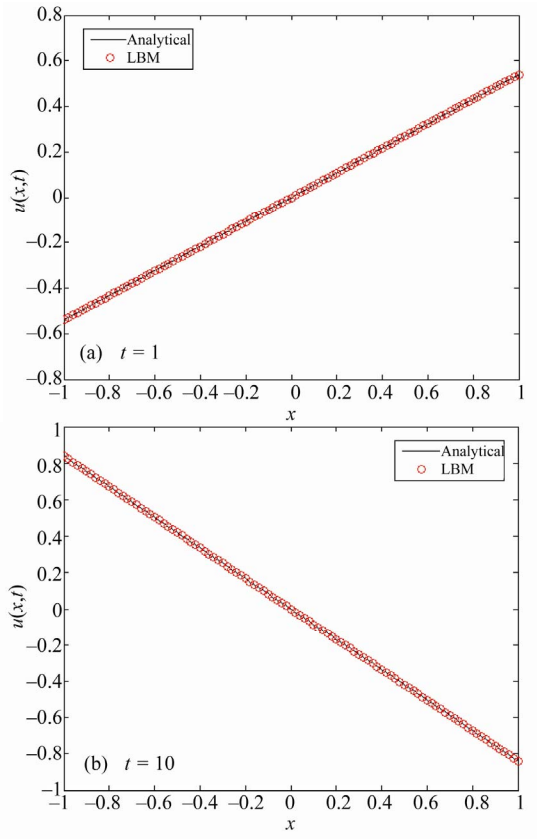

Figure 1. Analytical and LBM solutions with dx = 0.02 and dt = 2 × 10^{-5} for different time.

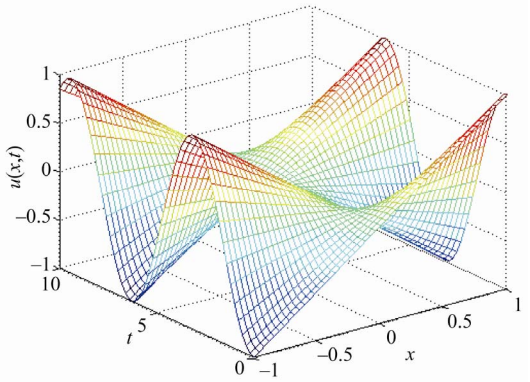

Figure 2. Space-time graph of the LBM solutions up to t = 10 with dx = 0.02 and dt = 2 × 10^{-5}.

$$u_{tt} - u_{xx} = 6xt\left(x^2 - t^2\right) + x^6t^6 - u^2$$

The initial conditions are given by

$$u(x,0) = 0,\ u_t(x,0) = 0$$

The exact solution is given in [9]

$$u(x,t) = x^3t^3$$

The Boundary condition is determined by the analytical solution. In **Table 2**, the L_∞, L_2 and RMS errors are obtained for $t = 1,2,3,4,5$. The graph of analytical and LBM solution for $t = 5$ and the space-time graph of the LBM solution are given in **Figure 3** and **Figure 4**, respectively.

Example 3. The nonlinear Klein-Gordon equation with cubic nonlinearity in interval $-1 \le x \le 1$.

$$u_{tt} + \alpha u_{xx} = -\beta u - \gamma u^3$$

We take $\alpha = -2.5, \beta = 1, \gamma = 1.5$ as the same in [9]. The initial conditions are given by

$$u(x,0) = B\tan(Kx),\ u_t(x,0) = BcK\sec^2(Kx)$$

The exact solution is

$$u(x,t) = B\tan\left(K\left(x + ct\right)\right)$$

where $B = \sqrt{\beta/\gamma}$ and $K = \sqrt{-\beta/2\left(\alpha + c^2\right)}$. In **Table 3**, the L_∞, L_2 and RMS errors are obtained for two values of c ($c = 0.5$ and $c = 0.05$) for $t = 1,2,3,4$. The graph of analytical and LBM solution for $t = 4$ and the space-time graph of the LBM solution for each value of c are given in **Figure 5** and **Figure 6**, respectively.

Example 4. We consider the nonlinear Klein-Gordon equation with the form [9].

$$u_{tt} - u_{xx} = -u - u^3;\ \ x \in [0,1.28]$$

with initial data

$$u(x,0) = A\left[1 + \cos\left(\frac{2\pi x}{1.28}\right)\right],\ u_t(x,0) = 0$$

The boundary conditions are given by

$$u_x(0,t) = 0, u_x(1.28,t) = 0$$

Table 2. L_∞, L_2 and RMS errors with dx = 0.01 and dt = 5 × 10^{-5}.

t	errors		
	L_∞-error	L_2-error	RMS
1	5.8742e–04	1.9270e–03	1.9174e–04
2	4.6618e–03	2.1643e–02	2.1535e–03
3	1.5139e–02	4.9465e–02	4.9219e–03
4	3.4225e–02	8.5102e–02	8.4679e–03
5	6.3219e–02	9.3035e–02	1.2970e–02

Table 3. L_∞, L_2 and RMS errors with dx = 0.01 and dt = 5 × 10^{-5}.

t	errors		
	L_∞-error	L_2-error	RMS
c = 0.5			
1	1.4189e–04	6.6508e–04	6.6171e–05
3	4.6601e–04	1.5438e–03	1.5362e–04
3	1.9445e–03	4.9588e–03	4.9342e–04
4	2.8219e–02	7.1870e–02	7.1513e–03
c = 0.05			
1	5.6970e–05	2.9718e–04	2.9570e–05
2	7.4878e–05	3.8699e–04	3.8507e–05
3	1.1972e–04	5.2203e–04	5.1944e–05
4	1.4008e–04	4.4143e–04	4.3924e–05

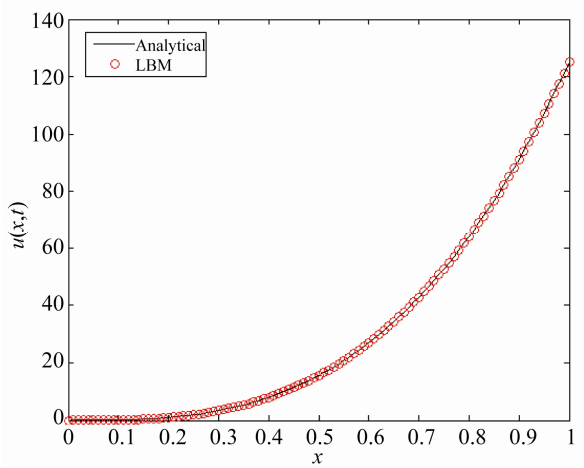

Figure 3. Analytical and LBM solutions at t = 5 with dx = 0.01 and dt = 5 × 10^{-5}.

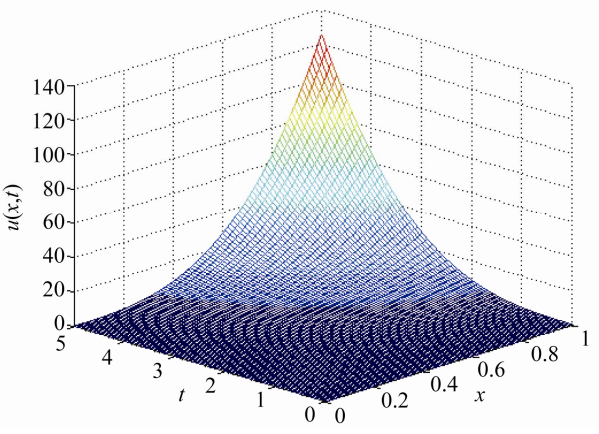

Figure 4. Space-time graph of the LBM solutions up to t = 5 with dx = 0.01 and dt = 5 × 10^{-5}.

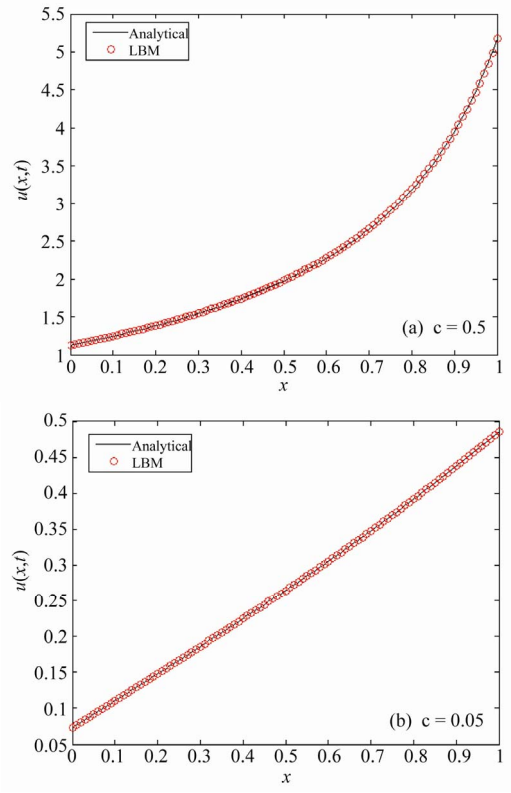

Figure 5. Analytical and LBM solutions at t = 4 with dx = 0.01 and dt = 5 × 10^{-5} for different c.

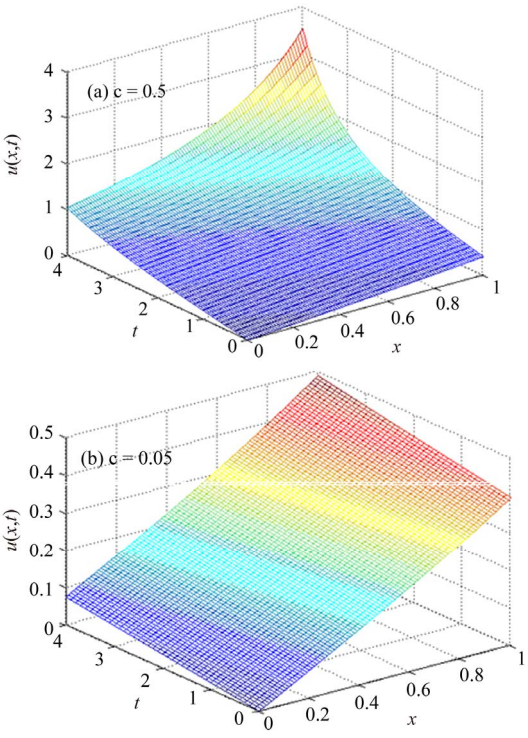

Figure 6. Space-time graph of the LBM solutions up to t = 4 with dx = 0.01 and dt = 5 × 10^{-5} for different c.

For the above problem due to the periodic boundary conditions, the continuous solutions remain always symmetric with respect to the center of the spatial interval. Authors of [26] also studied this problem and found undesirable characteristics in some of the numerical schemes, in particular a loss of spatial symmetry and the onset of instability for larger values of the parameter A (amplitude) in the initial condition of the equation. We solved the above problem using lattice Boltzmann method for several values of A. In **Figure 7**, we show the approximate solutions for $A = 1$ with $\Delta x = 0.0128$ and $\Delta t = 1.8286\times10^{-5}$. **Figure 8** presents the approximate solutions for $A = 100$ with $\Delta x = 0.0128$ and $\Delta t = 1.8286\times10^{-5}$. From **Figure 7** and **Figure 8**, we can find that the spatial symmetry is kept for different amplitude A. It indicates that the present lattice Boltzmann method is comparable with other numerical schemes.

4. Conclusions

In the current study, a new lattice Boltzmann model is proposed to solve 1D nonlinear Klein-Gordon equation. The efficiency and accuracy of the proposed model are validated through detail numerical simulation with quadratic and cubic nonlinearity. It can be found that the LBGK results are in excellent agreement with the analytical solution. It should be point out that in order to attain better accuracy the lattice Boltzmann model requires a relatively small time step Δt and the proper range is form 10^{-4} to 10^{-6}. Detailed stability analysis of present model is needed in further study.

5. Acknowledgements

This work was supported by the National Natural Science Foundation of China (50874123, 51174236) and National Basic Research Program of China (2011CB606306).

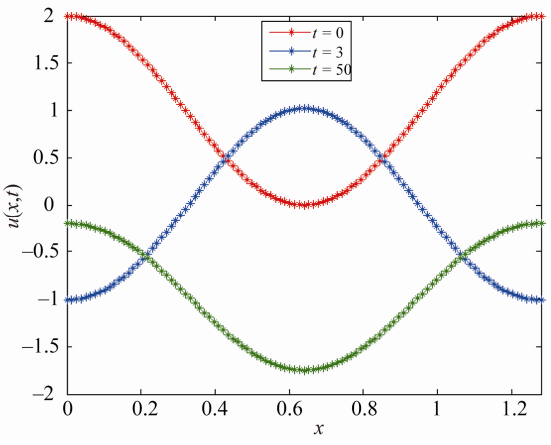

Figure 7. LBM solution at t = 0, 3, 50 with A = 1, dx = 0.0128 and dt = 1.8286 × 10^{-5}.

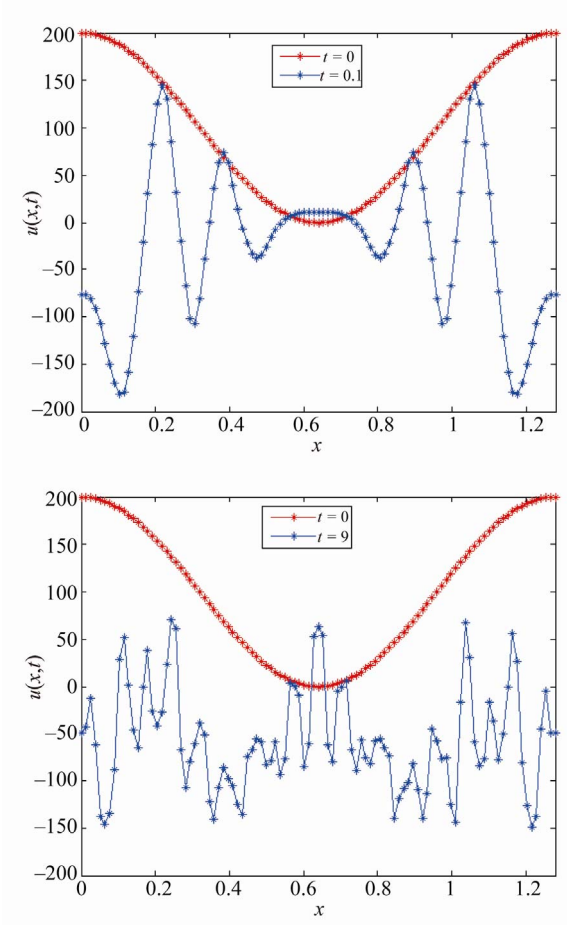

Figure 8. LBM solution with A = 100 at different time t.

6. References

[1] P. J. Caudrey, I. C. Eilbeck and J. D. Gibbon, "The Sine-Gordon Equation as a Model Classical Field Theory," *Nuovo Cimento*, Vol. 25, No. 2, 1975, pp. 497-511.

[2] R. K. Dodd, I. C. Eilbeck, J. D. Gibbon and H. C. Morris, "Solitons and Nonlinear Wave Equations," Academic, London, 1982.

[3] Sirendaoreji, "Auxiliary Equation Method and New Solutions of Klein-Gordon Equations," *Chaos, Solitons & Fractals*, Vol. 31, No. 4, 2007, pp. 943-950. doi:10.1016/j.chaos.2005.10.048

[4] Sirendaoreji, "A New Auxiliary Equation and Exact Travelling Wave Solutions of Nonlinear Equation," *Physics Letters A*, Vol. 356, No. 2, 2006, pp. 124-130. doi:10.1016/j.physleta.2006.03.034

[5] A. M. Wazwaz, "New Travelling Wave Solutions to the Boussinesq and Klein-Gordon Equations," *Communications in Nonlinear Science and Numerical Simulation*,

Vol. 13, No. 5, 2008, pp. 889-901. doi:10.1016/j.cnsns.2006.08.005

[6] M. A. Lynch, "Large Amplitude Instability in Finite Difference Approximates to the Klein-Gordon Equation," *Applied Numerical Mathematics*, Vol. 31, No. 2, 1999, pp. 173-182. doi:10.1016/S0168-9274(98)00128-7

[7] X. Li, B. Y. Guo and L. Vazquez, "A Legendre Spectral Method for Solving the Nonlinear Klein-Gordon Equation," *Mathematics Applied and Computation*, Vol. 15, No. 1, 1996, pp. 19-36.

[8] X. Li and B. Y. Guo, "A Legendre Spectral Method for Solving Nonlinear Klein-Gordon Equation," *Journal Computation of Mathematics*, Vol. 15, No. 2, 1997, pp. 105-126.

[9] M. Deghan and A. Shokri, "Numerical Solution of the Nonlinear Klein-Gordon Equation Using Radial Basis Functions," *Journal of Computational and Applied Mathematics*, Vol. 230, No. 2, 2009, pp. 400-410. doi:10.1016/j.cam.2008.12.011

[10] R. Benzi, S. Succi and M. Vergassola, "The Lattice Boltzmann Equation: Theory and Application," *Physics Reports*, Vol. 222, No. 3, 1992, pp. 145-197. doi:10.1016/0370-1573(92)90090-M

[11] S. Y. Chen and G. D. Doolen, "Lattice Boltzmann Method for Fluid Flows," *Annual Review of Fluid Mechanics*, Vol. 30, No. 1, 1997, pp. 329-364. doi:10.1146/annurev.fluid.30.1.329

[12] J. Y. Zhang, G. W. Yan and Y. F. Dong, "A New Lattice Boltzmann Model for the Laplace Equation," *Applied Mathematics and Computation*, Vol. 215, No. 2, 2009, pp. 539-547.doi:10.1016/j.amc.2009.05.047

[13] Z. H. Chai and B. C. Shi, "A Novel Lattice Boltzmann Model for the Poisson Equation," *Applied Mathematical Modelling*, Vol. 32, No. 10, 2008, pp. 2050-2058. doi:10.1016/j.apm.2007.06.033

[14] M. Hirabayashi, Y. Chen and H. Ohashi, "The Lattice BGK Model for the Poisson Equation," *JSME International Journal Series B*, Vol. 44, No. 1, 2001, pp. 45-52. doi:10.1299/jsmeb.44.45

[15] J. G. Zhou, "Lattice Boltzmann Method for Shallow Water Flows," Springer Verlag, New York, 2004.

[16] Z. Shen, G. Yuan and L. Shen, "Lattice Boltzmann Method for Burgers Equation," *Chinese Journal of Computational Physics*, Vol. 175, No. 1, 2000, pp. 172-177.

[17] J. Y. Zhang and G. W. Yan, "A Lattice Boltzmann Model for the Korteweg-de Vries Equation with Two Conservation Laws," *Computer Physics Communications*, Vol. 180, No. 7, 2009, pp. 1054-1062. doi:10.1016/j.cpc.2008.12.027

[18] G. W. Yan, "A Lattice Boltzmann Equation for Waves," *Journal of Computational Physics*, Vol. 161, No. 1, 2000, pp. 61-69. doi:10.1006/jcph.2000.6486

[19] J. Y. Zhang, G. W. Yan and X. Shi, "Lattice Boltzmann Model for Wave Propagation," *Physics Review E*, Vol. 80, 2009, Article ID 026706. doi:10.1103/PhysRevE.80.026706

[20] S. P. Dawson, S. Chen and G. D. Doolen, "Lattice Boltzmann Computations for Reaction-Diffusion Equation," *Journal of Chemical Physics*, Vol. 98, No. 2, 1993, pp. 1514-1523. doi:10.1063/1.464316

[21] X. Yu and B. C. Shi, "A Lattice Boltzmann Model for Reaction Dynamical Systems with Time Delay," *Applied Mathematics and Computation*, Vol. 181, No. 2, 2006, pp. 958-965. doi:10.1016/j.amc.2006.02.020

[22] S. R. Vander and M. Ernst, "Convection-Diffusion Lattice Boltzmann Scheme for Irregular Lattice," *Journal of Computational Physics*, Vol. 160, No. 2, 2000, pp. 766-782. doi:10.1006/jcph.2000.6491

[23] Z. L. Guo, B. C. Shi and N. C. Wang, "Fully Lagrangian and Lattice Boltzmann Method for the Advection-Diffusion Equation," *Journal of Scientific Computing*, Vol. 14, No. 3, 1999, pp. 291-300. doi:10.1023/A:1023273603637

[24] B. C. Shi and Z. L. Guo, "Lattice Boltzmann Model for Nonlinear Convection-Diffusion Equations," *Physics Review E*, Vol. 79, 2009, Article ID 016701. doi:10.1103/PhysRevE.79.016701

[25] Z. L. Guo, C. G. Zheng and B. C. Shi, "Non-Equilibrium Extrapolation Method for Velocity and Pressure Boundary Conditions in the Lattice Boltzmann Method," *Chinese Physics*, Vo. 11, No. 4, 2002, pp. 366-374. doi:10.1088/1009-1963/11/4/310

[26] S. Jiminez and L. Vazquez, "Analysis of Four Numerical Scheme for a Nonlinear Klein-Gordon Equation," *Applied Mathematics and Computation*, Vol. 35, No. 1, 1990, pp. 61-94. doi:10.1016/0096-3003(90)90091-G

Applied Mathematics, 2011, 2, 1486-1496
doi:10.4236/am.2011.212211 Published Online December 2011 (http://www.SciRP.org/journal/am)

Controllability of Neutral Impulsive Differential Inclusions with Non-Local Conditions

Dimplekumar N. Chalishajar[1], Falguni S. Acharya[2*]
[1]*Department of Mathematics and Computer Science, Virginia Military Institute (VMI), Lexington, USA*
[2]*Department of Applied Sciences Humanities, Institute of Technology and Management Universe, Vadodara, India*
*E-mail: *falguni 69@yahoo.co.in, dipu17370@yahoo.com, chalishajardn@vmi.edu*
Received July 14, 2011; *revised September* 27, 2011; *accepted October* 7, 2011

Abstract

In this short article, we have studied the controllability result for neutral impulsive differential inclusions with nonlocal conditions by using the fixed point theorem for condensing multi-valued map due to Martelli [1]. The system considered here follows the P.D.E involving spatial partial derivatives with α-norms.

Keywords: Controllability, Neutral Impulsive Differential Inclusions, Spatial Partial Derivative, Martelli Fixed Point Theorem

1. Introduction

In this paper we have discussed the controllability of nonlocal Cauchy problem for neutral impulsive differential inclusions of the form

$$\begin{cases} \dfrac{\mathrm{d}}{\mathrm{d}t}\left[x(t)-F\left(t,x\left(h_1(t)\right)\right)\right]\in Ax(t)+Bu(t)+G\left(t,x\left(h_2(t)\right)\right); \\ \qquad\qquad t\in J:=[0,b]; t\neq t_k \\ \Delta x|_{t=t_k}=I_k\left(x(t_k^-)\right); k=1,2,\cdots m;\ x(0)+g(x)=x_0\in X \end{cases} \tag{1}$$

where the linear operator $(-A)$ generates an analytic semigroup $\{T(t)\}_{t\geq 0}$; G is a multi-valued map and $\Delta x_{t=t_k}=x(t_k^+)-x(t_k^-)$, $x(t_k^+)=\lim_{h\to 0^+}x(t_k+h)$ and $x(t_k^-)=\lim_{h\to 0^+}x(t_k-h)$ represent the right and left limits of $x(t)$ at $t=t_k$ respectively, $x_0\in X$, $F: J\times X\to P(X)\backslash\phi$ is a multi-valued map [$P(X)$ is the family of all subsets of X] and $g\in C(J,X)$. Also the control function $u\in L^2(J,U)$, a Banach space of admissible control functions with U as a Banach space. B is a bounded linear operator from U to X and X is a separable Banach space with norm $\|\cdot\|$.
$I_k: X\to\overline{D(A)}$; $k=1,2,\cdots,m$ and $h_1,h_2\in C(J,J)$.

As a model we consider the following system of heat equations;

$$\begin{cases} \dfrac{\partial}{\partial t}\left[z(t,x)-F(t,z(\cos t,x)),\dfrac{\partial z}{\partial x}(\cos t,x)\right] \\ =\dfrac{\partial^2 z(t,x)}{\partial x^2}+u(t,x)+G\left(t,z(\cos t,x),\dfrac{\partial z}{\partial x}(\cos t,x)\right), \\ z(t,0)=z(t,\pi)=0; \\ z(t_k^+)-z(t_k^-)=I_k(z(t_k^-)), \\ t\neq t_k; k=1,2,\cdots,m \\ z(0,x)+g(z(t,x))=z_0(x), 0\leq x\leq\pi, t\in[0,1] \end{cases} \tag{2}$$

Since F and G involve spatial partial derivative, the results obtained by other authors cannot be applied to our system even if $g(.)=0$. This is the main motivation of this paper.

The existence and controllability of the following system is studied by Benchohra and Ntouyas [2]

$$\begin{cases} \dfrac{\mathrm{d}}{\mathrm{d}t}\left[x(t)-g(t,x_t)\right]\in Ax(t)+Bu(t)+F(t,x_t); \\ \qquad\qquad t\in J:=[0,b]; t\neq t_k \\ \Delta x|_{t=t_k}=I_k(x(t_k^-)); k=1,2,\cdots,m; x(t)=\phi(t), t\in(-\infty,0). \end{cases} \tag{3}$$

Here authors have proved exact controllability by using fixed point theorem for condensing multi-valued maps due to Martelli. In this paper, we have discussed controllability results with α-norms as in [3] with de-

viating arguments in terms involving spatial partial derivatives.

As indicated in [4], and reference therein, the nonlocal Cauchy problem $x(0)+g(x)=x_0$ can be applied in different fields with better effect than the classical initial condition $x(0)=x_0$. For example in [5], the author described the diffusion phenomenon of a small amount of gas in a transparent tube by using the formula

$$g(x)=\sum_{i=0}^{p} c_i x(t_i),$$

where $c_i, i=0,1,\cdots,p$ are given constants and $0<t_0,t_1,\cdots,t_p<b$. In this case the above equation allows the additional measurement at t_i, $i=0,1,\cdots,p$. In the past several years theorems about controllability of differential, integro-differential, fractional differential systems and inclusions with nonlocal conditions have been studied by Chalishajar and Acharya [6-9], Benchohra and Ntouyas [10,11], and Hernandez, Rabello and Henriquez [12] and the references therein. In [13], Chalishajar discussed exact controllability of third order nonlinear integro-differential dispersion system without compactness of semigroup.

Xianlong Fu and Yueju Cao [14], has discussed the existence of mild solution for neutral partial differential inclusions involving spatial partial derivative with α-norms in Banach space. However in their work authors impose some severe assumptions on the operator family generator by $(-A)$, *i.e.* $(-A):D(A)\subset X\to X$ is an infinitesimal generator of a compact analytic semigroup of a uniformly bounded linear operator $\{T(t)\}_{t\geq 0}$, which imply that underlying space X has finite dimension and so the example considered in [14], and subsequently in Section 4 is ordinary differential equation but not partial differential equation which shows lack of existence (exact controllability) in abstract (control) system (refer [15]). This fact and several other applications of neutral equation (inclusions) are the main motivation of this paper.

In Section 3 (followed by Preliminaries) of present paper we discuss the controllability of neutral impulsive differential inclusion with nonlocal condition with deviating arguments with α-norm, which is the generalization of [14], in a finite dimensional space. The example is given in Section 4 to support the theory. In Section 5 we study exact controllability of same system in infinite dimension space by dropping the compactness assumption of semigroup $\{T(t)\}_{t\geq 0}$. Here we generalized the result proved in Section 3.

2. Preliminaries

In this section, we shall introduce some basic definitions, notations and lemmas which are used throughout this paper.

Let $\left(X,\|\cdot\|\right)$ be a Banach space. $C(J,X)$ is the Banach space of continuous functions from J into X with the norm defined by

$$\|x\|_J := \sup\{\|x(t)\| : t\in J\}.$$

Let $B(X)$ be the Banach space of bounded linear operators from X into X with standard norm

$$\|N\|_{B(X)} := \sup\{\|N(x)\| : \|x\|=1\}.$$

A measurable function $x:J\to X$ is Bochner integrable if and only if $\|x\|$ is Lebesgue integrable. (For properties of the Bochner integral see [16]). Let $L^1(J,X)$ denotes the Banach space of Bochner integrable functions $x:J\to X$ with norm

$\|x\|_{L^1}=\int_0^b \|x(t)\|\,\mathrm{d}t$ for all $x\in L^1(J,X)$.

We use the notations $P(X)=\{Y\in 2^X : Y\neq\phi\}$,
$P_{cl}(X)=\{Y\in P(X): Y closed\}$,
$P_b(X)=\{Y\in P(X): Y bounded\}$,
$P_c(X)=\{Y\in P(X): Y convex\}$, and
$P_{cp}(X)=\{Y\in P(X): Y compact\}$.

A multi-valued map $G:X\to 2^X$ is convex (respectively closed) valued if $G(x)$ is convex (respectively closed) for all $x\in X$.

The map G is bounded on bounded sets if $G(B)=\cup_{x\in B}G(x)$ is bounded in X for any bounded set B of X. $\left(i.e.\ \sup_{x\in B}\left\{\sup\{\|x\| : x\in G(x)\}\right\}<\infty\right)$.

G is called upper semi-continuous (u.s.c.) on X if for each $x_0\in X$, the set $G(x_0)$ is a nonempty closed subset of X and if for each open set B of X containing $G(x_0)$, there exists an open neighborhood A of x_0 such that $G(A)\subseteq B$.

The map G is said to be completely continuous if $G(B)$ is relatively compact for every bounded subset $B\subseteq X$.

If the multi-valued map G is completely continuous with nonempty compact values, then G is u.s.c. if and only if G has a closed graph, That is, if $x_n\to x_0, y_n\to y_0$, where $y_n\in G(x_n)$ then $y_0\in G(x_0)$. G has a fixed point if there is $x\in X$ such that $x\in G(x)$.

A multi-valued map $G:J\to BCC(X)$ is said to be measurable, if for each $x\in X$, the distance function $Y:J\to R$ defined by

$$Y(t)=d\left(x,G(t)\right)=\inf\{\|x-z\| : z\in G(t)\}$$

is measurable.

An upper semi-continuous map $G:X\to 2^X$ is said to be condensing, if for any bounded subset $B\subseteq X$, with $\alpha(B)\neq 0$, we have $\alpha\left(G(B)\right)<\alpha(B)$, where α denotes the Kuratowski measure of non-compactness.

We remark that a completely continuous multi-valued map is the easiest example of a condensing map. For more details on multivalued maps see the books of Deimling [17].

Throughout this paper, $A: D(A) \subset X \to X$ will be the infinitesimal generator of a compact analytic semigroup of uniformly bounded linear operator $T(t)$. Let $0 \in \rho(A)$, then it is possible to define the fractional power A^{α}, *for* $0 \le \alpha \le 1$, as a closed linear operator on its domain $D(A^{\alpha})$. Furthermore, the subspace $D(A^{\alpha})$ is dense in X and the expression

$$\|x\|_{\alpha} = \|A^{\alpha}x\|;\ x \in D(A^{\alpha})$$

defines a norm on $D(A^{\alpha})$. Hereafter we denote by X_{α}, the Banach space $D(A^{\alpha})$ normed with $\|x\|_{\alpha}$. Then for each $0 < \alpha \le 1$, X_{α} is a Banach space, and $X_{\alpha} \rightarrowtail X_{\beta}$ *for* $0 < \beta < \alpha \le 1$ and the imbedding is compact whenever the resolvent operator of A is compact.

Semigroup $\{T(t)\}_{t\ge 0}$ satisfies the following properties:

a) there is a $M \ge 1$ such that

$$\|T(t)\| \le M \text{ for all } 0 \le t \le \alpha;$$

b) for any $0 < \alpha \le 1$, there exists a positive constant C_{α} such that

$$\|A^{\alpha}T(t)\| \le \frac{C_{\alpha}}{t^{\alpha}}; 0 < t \le \alpha$$

For more details about the above preliminaries, we refer to ([18,19]).

In order to define the solution of the system (1) we shall consider the space

$$\Omega = \{x : [0,b] \to X_{\alpha}; x_k \in C(J_k, X_{\alpha}); k = 0,1,\cdots,m$$
$$\text{and there exist } x(t_k^-) \text{ and } x(t_k^+); k = 0,1,\cdots,m$$
$$\text{with } x(t_k^-) = x(t_k), x(0) + g(x) = x_0\},$$

which is a Banach space with the norm

$$\|x\|_{\Omega} = max\left\{\|x_k\|_{J_k}; k = 0,1,\cdots,m\right\}$$

where x_k is the restriction of x to $J_k = (t_k, t_{k+1}], k = 0,1,\cdots,m$ and $\|x_k\|_{J_k} = sup_{s\in J_k}\|x_k(s)\|_{\alpha}$.

For the system (1) we assume that the following hypotheses are satisfied for some $\alpha \in (0,1)$:

(H1) Let $W: L^2(J,U) \to X_{\alpha}$ be the linear operator defined by

$$Wu = \int_0^b T(b-s)Bu(s)\mathrm{d}s$$

The $W: L^2(J,U)/kerW \to X_{\alpha}$ induces a bounded invertible operator $\tilde{W}^{-1}$ and there exists positive constant M_1 and M_2 such that and $\|B\| \le M_1$ and $\|\tilde{W}^{-1}\| \le M_2$.

(H2) i) there exists a constant $\beta \in (0,1)$ such that $F: [0,b] \times X_{\alpha} \to X_{\beta}$ is a continuous function, and $A^{\beta}F: [0,b] \times X_{\alpha} \to X_{\beta}$ satisfies the Lipschitz condition, that is, there exists a constant $L > 0$ such that

$$\|A^{\beta}F(t_1,x_1) - A^{\beta}F(t_2,x_2)\|_{\alpha} \le L\left(|t_1 - t_2| + \|x_1 - x_2\|_{\alpha}\right),$$

for any $0 \le t_1, t_2 \le b; x_1, x_2 \in X_{\alpha}$.

ii) Moreover, there exists a constant $L_1 > 0$ such that the inequality

$$\|A^{\beta}F(t,x)\|_{\alpha} \le L_1\left(\|x\|_{\alpha} + 1\right),$$

holds for any $x \in X_{\alpha}$.

(H3) The multi-valued map $G: J \times X_{\alpha} \to P_{c,cp}(X)$ satisfies the following conditions:

i) for each $t \in J$, the function $G(t,.): X_{\alpha} \to P_{c,cp}(X)$ is u.s.c. and for each $x \in X_{\alpha}$, the function $G(.,x): J \to P_{c,cp}(X)$ is measurable. Also for each fixed $y \in \Omega$ the set

$$S_{G,x} = \left\{v \in L^1(J,X) : v(t) \in G(t, x(h_2(t))) \text{ for a.e. } t \in J\right\}$$

is nonempty.

ii) for each positive number $l \in N$, there exists a positive function $w(l)$ dependent on l such that

$$\sup_{\|x\|\le l}\|G(t,x)\| \le w(l)$$

and $\liminf_{l\to\infty} \frac{w(l)}{l} = \gamma < \infty$ where

$\|G(t,x)\| = \sup\{\|v\| : v \in G(t,x)\}$, $\|x\|_{\alpha} = \sup_{0\le s\le\alpha}\|x(s)\|_{\alpha}$.

(H4) $h_i \in C(J,J), i = 1,2$. $g: \Omega \to X_{\alpha}$ is continuous and satisfies that

i) there exists positive constants L_2 and $L_{2'}$ such that

$$\|g(y)\|_{\alpha} \le L_2\|y\|_{\Omega} + L_2' \text{ for all } y \in \Omega.$$

ii) $A^{\alpha}g$ is completely continuous map.

(H5) $I_k \in C(X_{\alpha}, X_{\alpha}), k = 1,2,\cdots,m,$ are all bounded, that is, there exist constants $d_k, k = 1,2,\cdots,m,$ such that

$$\|I_k(x)\|_{\alpha} \le d_k, \text{ for each } x \in X_{\alpha}.$$

Now we define the mild solution for the system (1).

DEFINITION 2.1 *The system* (1) *is said to be nonlocally controllable on the interval* J *if for every* $x(0) + g(x) \in D(A)$ *and* $x_0, z_1 \in X$, *there exists a control* $u \in L^2\left(0,b : L^2\left(0,2\pi\right)\right) = L^2\left(J,U\right)$ *such that the corresponding solution* $x(\cdot)$ *of* (1) *satisfies*

i) $x(b) + g(x) = z_1$ with $x(0) + g(x) = x_0$;

ii) $\Delta x|_{t=t_k} = I_k(x(t_k^-));\ k = 1,2,\cdots,m;$

iii) there exists a function $v \in L^1(J,X)$ such that

$v(t) \in G(t, x(h_2(t)))$ a.e. on J and

$$\begin{aligned} x(t) &= T(t)\left[x_0 - g(x) - F(0, x(h_1(0)))\right] + F(t, x(h_1(t))) \\ &\quad + \int_0^t AT(t-s)F(s, x(h_1(s)))\mathrm{d}s + \int_0^t T(t-s)v(s)\mathrm{d}s \\ &\quad + \int_0^t T(t-s)(Bu)(s)\mathrm{d}s \\ &\quad + \sum_{0<t_k<t} T(t-t_k)I_k(x(t_k^-)); t \in J, v \in S_{G,x}. \end{aligned} \tag{2.1}$$

The following lemmas are crucial in the proof of our main theorem.

LEMMA 2.2 [20] *Let X be a Banach space. Let $G: J \times X \to P_{b,cl,c}(X)$ satisfies that*

i) For each $x \in X$, $(t,x) \mapsto G(t,x)$ is measurable with respect to t and for each $t \in J$, $(t,x) \to G(t,x)$ is u.s.c. with respect to x .

ii) For each fixed $x \in C(J,X)$, the set

$$S_{G,x} = \left\{v \in L^1(J,X) : v(t) \in G(t, x(h_2(t))), \text{for } a.e.\ t \in J\right\}$$

is nonempty.

Let Γ be a linear continuous mapping from $L^1(J,X)$ to $C(J,X)$ then the operator

$\Gamma OS_G : C(J,X) \to P_{cp,c}\left(C(J,X)\right)$,

$x \to \left(\Gamma OS_G\right)(x) := \Gamma\left(S_{G,x}\right)$ is a closed graph operator in $C(J,X) \times C(J,X)$.

LEMMA 2.3 [17] *Let Ω be a bounded and convex set in Banach space X. $F: \Omega \to 2^{\Omega} \setminus \phi$ be an upper semi-continuous and condensing multi-valued map. If for every $x \in \Omega$, $F(x)$ is closed and convex set in Ω, then F has a fixed point in Ω.*

3. Controllability Result

We are now able to state and prove our main controllability result.

THEOREM 3.1 *Let $x_0 \in X_\alpha$. If the hypotheses* (*H*1)-(*H*5) *are satisfied, then the system* (1) *is controllable provided*

$$L_0 := L\left[(M+1)M_0 + \frac{1}{\beta}C_1 - \beta\alpha^{\beta}\right] < 1 \tag{3.1}$$

$$\begin{aligned} &\left(M_0L_1 + L_2\right)M + M_0L_1 \\ &+ \frac{1}{\beta}C_1 - \beta\alpha^{\beta}L_1 + \frac{1}{(1-\alpha)}C_\alpha\alpha^{1-\alpha}\gamma < 1 \end{aligned} \tag{3.2}$$

and

$$\begin{aligned} M_3 &= \|z_1\|_\alpha + M_1\|x_0\|_\alpha + (M+1)(L_2l + L_2') \\ &\quad + (M+1)M_0L_1(l+1) + \frac{C_{1-\beta}}{\beta}L_1(l+1)b^{\beta} \\ &\quad + \frac{C_\alpha}{1-\alpha}w(l)b^{1-\alpha} + M\sum_{k=1}^{m} d_k, \end{aligned} \tag{3.3}$$

where, $M_0 = \left\|A^{-\beta}\right\|$.

Proof. Let $C := C(J, \overline{D(A)})$ denote the Banach space of continuous functions from J to $\overline{D(A)}$ normed by

$$\|x\|_C = sup\left\{|x(t)| : t \in J\right\}$$

Using hypothesis (H5) for an arbitrary function $x(.)$ and $z_1 \in \overline{D(A)}$ define the control

$$\begin{aligned} u_x(t) &= \tilde{W}^{-1}\left[z_1 - g(x) - T(b)\left[x_0 - g(x) - F(0, x(h_1(0)))\right]\right. \\ &\quad - F(b, x(h_1(b))) + \int_0^b AT(b-s)F(s, x(h_1(s)))\mathrm{d}s \\ &\quad \left. + \int_0^b T(b-s)v(s)\mathrm{d}s + \sum_{0<t_k<t} T(t-t_k)I_k(x(t_k^-))\right] \end{aligned}$$

Using the above control, define a multi-valued map $N: \Omega \to 2^{\Omega}$ by

$$\begin{aligned} N(x) = \Big\{ y \in \Omega : y(t) &= T(t)\left[x_0 - g(x) - F(0, x(h_1(0)))\right] \\ &\quad + F(t, x(h_1(t))) + \int_0^t AT(t-s)F(s, x(h_1(s)))\mathrm{d}s \\ &\quad + \int_0^t T(t-s)v(s)\mathrm{d}s + \int_0^t T(t-s)(Bu)(s)\mathrm{d}s \\ &\quad + \sum_{0<t_k<t} T(t-t_k)I_k(x(t_k^-)); t \in J, v \in S_{G,x} \Big\}. \end{aligned}$$

By assumption on F, g, I_k and the fact that $x_0 \in X_\alpha$, it is obvious that $y(t) \in X_\alpha$.

Clearly the fixed points of *N* are mild solutions to (1). We shall show that N satisfies the hypotheses of Lemma 2.3. The proof will be given in several steps. **Step 1:** There exists a positive number $l \in N$ such that $N(H_l) \subset H_l$, where

$H_l = \left\{x \in \Omega : \|x(t)\|_\alpha \le l, 0 \le t \le \alpha\right\}$.

For each positive number l, H_l is clearly a bounded closed convex set in Ω. We claim that there exists a positive integer l such that $N(H_l) \subset H_l$, where $N(H_l) = \cup_{x \in H_l} N(x)$. If it is not true, then for each positive integer l, there exist the functions $x_l(.) \in H_l$ and $y_l \in N(x_l)$, but $y_l(.) \notin H_l$, that is $\|y_l(t)\|_\alpha > l$ for some $t(l) \in [0,b]$, where $t(l)$ denotes t is dependent on l. However on the other hand we have,

$$\begin{aligned} l < \|y_l(t)\|_\alpha &= \Big\|T(t)\left[x_0 - g(x_l) - F(0, x_l(h_1(0)))\right] \\ &\quad + F(t, x_l(h_1(t))) + \int_0^t AT(t-s)F(s, x_l(h_1(s)))\mathrm{d}s \\ &\quad + \int_0^t T(t-s)v_l(s)\mathrm{d}s + \int_0^t T(t-s)(Bu_l)(s)\mathrm{d}s \\ &\quad + \sum_{0<t_k<t} T(t-t_k)I_k(x_l(t_k^-))\Big\|_\alpha, \text{ where } v_l \in S_{G,x_l} \end{aligned}$$

Hence,

$$
\begin{aligned}
l &< \left\| T(t)\left[x_0 - g(x_l) - A^{-\beta}A^{\beta}F(0, x_l(h_1(0)))\right]\right\|_{\alpha} \\
&+ \left\| A^{-\beta}A^{\beta}F(t, x_l(h_1(t)))\right\|_{\alpha} \\
&+ \left\| \int_0^t A^{1-\beta}T(t-s)A^{\beta}F(s, x_l(h_1(s)))\mathrm{d}s\right\|_{\alpha} \\
&+ \left\| \int_0^t T(t-s)v_l(s)\mathrm{d}s\right\|_{\alpha} + \left\| \int_0^t T(t-s)(Bu_l)(s)\mathrm{d}s\right\|_{\alpha} \\
&+ \sum_{0<t_k<t} \left\| T(t-t_k)\right\|_{\alpha} \left\| I_k(x_l(t_k^-))\right\|_{\alpha} \\
l &\le M\left[\left\| x_0\right\|_{\alpha} + L_2 l + L_2' + M_0 L_1(l+1)\right] + M_0 L_1(l+1) \\
&+ \int_0^t \frac{C_{1-\beta}}{(t-s)^{(1-\beta)}} L_1(l+1)\mathrm{d}s + \int_0^t \frac{C_{\alpha}}{(t-s)^{\alpha}} w_1(l)\mathrm{d}s \\
&+ \int_0^t \frac{C_{\alpha}}{(t-s)^{\alpha}} M_1 M_2 M_3 \mathrm{d}s + M\sum_{k=1}^{m} d_k
\end{aligned}
$$

Dividing on both sides by l and taking the lower limit as $l \to +\infty$ we get

$$(M_0 L_1 + L_2)M + M_0 L_1 + C_{1-\beta}\frac{b^{\beta}}{\beta}L_1 + C_{\alpha}\frac{b^{1-\alpha}}{1-\alpha}\gamma \ge 1.$$

This is a contradiction with Formula (2). Hence for some positive integer $N(H_l) \subseteq H_l$.

Step 2: $N(x)$ is convex for each $x \in \Omega$.

Indeed if $y_1, y_2 \in N(x)$ then there exists $v_1, v_2 \in S_{G,x}$ such that for each $t \in J$, we have

$$
\begin{aligned}
y_i(t) &= T(t)\left[x_0 - g(x) - F(0, x(h_1(0)))\right] \\
&+ F(t, x(h_1(t))) + \int_0^t AT(t-s)F(s, x(h_1(s)))\mathrm{d}s \\
&+ \int_0^t T(t-s)v_i(s)\mathrm{d}s + \int_0^t T(t-s)(Bu_i)(s)\mathrm{d}s \\
&+ \sum_{0<t_k<t} T(t-t_k)I_k(x(t_k^-)); i = 1, 2.
\end{aligned}
$$

Let $0 \le \lambda \le 1$. Then for each $t \in J$ we have

$$
\begin{aligned}
&\left[\lambda y_1 + (1-\lambda)y_2\right](t) = T(t)\left[x_0 - g(x) - F(0, x(h_1(0)))\right] \\
&+ F(t, x(h_1(t))) + \int_0^t AT(t-s)F(s, x(h_1(s)))\mathrm{d}s \\
&+ \int_0^t T(t-s)\left[\lambda v_1(s) + (1-\lambda)v_2(s)\right]\mathrm{d}s \\
&+ \int_0^t T(t-s)B\left[\lambda u_1(s) + (1-\lambda)u_2(s)\right]\mathrm{d}s \\
&+ \sum_{0<t_k<t} T(t-t_k)I_k(x(t_k^-))
\end{aligned}
$$

Since $S_{G,x}$ is convex because G has convex values, $\lambda y_1 + (1-\lambda)y_2 \in N(x)$.

Step 3: $N(x)$ is closed for each $x \in \Omega$.

Let $\{y_n\}_{n\ge 0} \in N(x)$ such that $y_n \to y$ in Ω. Then $y \in \Omega$ and there exists $v_n \in S_{G,x}$ such that for every $t \in J$,

$$
\begin{aligned}
y_n(t) &= T(t)\left[x_0 - g(x) - F(0, x(h_1(0)))\right] + F(t, x(h_1(t))) \\
&+ \int_0^t AT(t-s)F(s, x(h_1(s)))\mathrm{d}s \\
&+ \int_0^t T(t-s)v_n(s)\mathrm{d}s + \int_0^t T(t-s)(Bu)(s)\mathrm{d}s \\
&+ \sum_{0<t_k<t} T(t-t_k)I_k(x(t_k^-))
\end{aligned}
$$

Using the fact that G has compact values, we may pass to a subsequence if necessary to get that v_n conver-ges to $v \in L^1(J, X)$ and hence $v \in S_{G,x}$. Then for each $t \in J$,

$$
\begin{aligned}
&y_n(t) \to y(t) = T(t)\left[x_0 - g(x) - F(0, x(h_1(0)))\right] \\
&+ F(t, x(h_1(t))) + \int_0^t AT(t-s) \times F(s, x(h_1(s)))\mathrm{d}s \\
&+ \int_0^t T(t-s)v(s)\mathrm{d}s + \int_0^t T(t-s)(Bu)(s)\mathrm{d}s \\
&+ \sum_{0<t_k<t} T(t-t_k)I_k(x(t_k^-)); t \in J.
\end{aligned}
$$

Hence $y \in N(x)$.

Step 4: Next we show that the operator N is u.s.c and condensing.

For this purpose, we decompose N as $N = N_1 + N_2$, where the operators N_1, N_2 are defined on H_l respectively by

$$
\begin{aligned}
(N_1 x)(t) &= F(t, x(h_1)(t)) - T(t)F(0, x(h_1(0)) \\
&+ \int_0^t AT(t-s)F(s, x(h_1(s)))\mathrm{d}s \\
N_2 x &= \Big\{ y \in \Omega : y(t) = T(t)\left[x_0 - g(x) - F(0, x(h_1(0)))\right] \\
&+ F(t, x(h_1(t))) + \int_0^t AT(t-s)F(s, x(h_1(s)))\mathrm{d}s \\
&+ \int_0^t T(t-s)v(s)\mathrm{d}s + \int_0^t T(t-s)(Bu)(s)\mathrm{d}s \\
&+ \sum_{0<t_k<t} T(t-t_k)I_k(x(t_k^-)); v \in S_{G,x}\Big\}.
\end{aligned}
$$

We will verify that N_1 is a contraction while N_2 is a completely continuous operator.

To prove that N_1 is a contraction, we take $x_1, x_2 \in H_l$ arbitrarily. Then for each $t \in J$ and by condition (H2), we have that

$$
\begin{aligned}
&\left\| (N_1 x_1)(t) - (N_1 x_2)(t)\right\|_{\alpha} \\
&\le \left\| F(t, x_1(h_1(t))) - F(t, x_2(h_1(t)))\right\|_{\alpha} \\
&+ \left\| T(t)[F(0, x_1(h_1(0))) - F(0, x_2(h_1(0)))]\right\|_{\alpha} \\
&+ \left\| \int_0^t AT(t-s)\left[F(s, x_1(h_1(s))) - F(s, x_2(h_1(s)))\right]\mathrm{d}s\right\|_{\alpha} \\
&= \left\| A^{-\beta}\left[A^{\beta}F(t, x_1(h_1(t))) - A^{\beta}F(t, x_2(h_1(t)))\right]\right\|_{\alpha} \\
&+ \left\| T(t)A^{-\beta}\left[A^{\beta}F(0, x_1(h_1(0)) - A^{\beta}F(0, x_2(h_1(0)))\right]\right\|_{\alpha} \\
&+ \Big\| \int_0^t A^{1-\beta}T(t-s) \\
&\quad \cdot \left[A^{\beta}F(s, x_1(h_1(s))) - A^{\beta}F(s, x_2(h_1(s)))\right]\mathrm{d}s\Big\|_{\alpha} \\
&\le \left[(M+1)M_0 L + \int_0^t \frac{C_{1-\beta}}{(t-s)^{1-\beta}} L\mathrm{d}s\right] . \sup_{0\le s\le \alpha} \left\| x_1(s) - x_2(s)\right\|_{\alpha} \\
&\le L\left[(M+1)M_0 + \frac{1}{\beta}C_{1-\beta}\alpha^{\beta}\right] \sup_{0\le s\le \alpha} \left\| x_1(s) - x_2(s)\right\|_{\alpha} \\
&= L_0 \sup_{0\le s\le \alpha} \left\| x_1(s) - x_2(s)\right\|_{\alpha}
\end{aligned}
$$

Thus, $\|N_1x_1 - N_2x_2\|_\alpha \le L_0\|x_1 - x_2\|_\alpha$. Therefore by assumption $0 < L_0 < 1$, N_1 is a contraction.

Next we show that N_2 is u.s.c. and condensing.

i) $N_2(H_l)$ is clearly bounded.

ii) $N_2(H_l)$ is equi-continuous.

Let $\tau_1, \tau_2 \in J, \tau_1 < \tau_2$. Let $x \in H_l$ and $y \in N_2(x)$. Then there exists $v \in S_{G,x}$ such that for each $t \in J$, we have

$$y(t) = T(t)\big[x_0 - g(x)\big] + \int_0^t T(t-s)v(s)\mathrm{d}s + \int_0^t T(t-s)(Bu)(s)\mathrm{d}s + \sum_{0<t_k<t} T(t-t_k)I_k(x(t_k^-))$$

Then,

$$\begin{aligned}
&\|y(\tau_2) - y(\tau_1)\|_\alpha \\
&\le \|[T(\tau_2) - T(\tau_1)](x_0 - g(x))\|_\alpha \\
&+ \left\|\int_0^{\tau_1}[T(\tau_2 - s) - T(\tau_1 - s)]v(s)\mathrm{d}s\right\|_\alpha + \left\|\int_{\tau_1}^{\tau_2} T(\tau_2 - s)v(s)\mathrm{d}s\right\|_\alpha \\
&+ \left\|\int_0^{\tau_1}\big[T(\tau_2 - s) - T(\tau_1 - s)\big]B\tilde{W}^{-1}\right. \\
&\quad \cdot \big\{z_1 - g(x) - T(b)\big[x_0 - g(x) - F(0, x(h_1(0)))\big] \\
&\quad - F(b, x(h_1(b))) - \int_0^b AT(b-\eta)F(\eta, x(h_1(\eta)))\mathrm{d}\eta \\
&\quad \left. - \int_0^b T(b-\eta)v(\eta)\mathrm{d}\eta - \sum_{0\le t_k\le\tau_1} T(t-t_k)I_k(x(t_k^-))\big\}\mathrm{d}s\right\|_\alpha \\
&+ \left\|\int_{\tau_1}^{\tau_2} T(\tau_2 - s)B\tilde{W}^{-1}\right. \\
&\quad \cdot \big\{z_1 - g(x) - T(b)\big[x_0 - g(x) - F(0, x(h_1(0)))\big] \\
&\quad - F(b, x(h_1(b))) - \int_0^b AT(b-\eta)F(\eta, x(h_1(\eta)))d\eta \\
&\quad \left. - \int_0^b T(b-\eta)v(\eta)\mathrm{d}\eta + \sum_{\tau_1\le t_k\le\tau_2} T(t-t_k)I_k(x(t_k^-))\big\}\mathrm{d}s\right\|_\alpha
\end{aligned}$$

The right hand side tends to zero as $(\tau_2 - \tau_1) \to 0$, since $T(t)$ is strongly continuous and the compactness of $\{T(t)\}_{t\ge 0}$ implies the continuity in the uniform operator topology. Thus $N_2(.)$ is equi-continuous on H_l.

iii) $(N_2H_l)(t)$ is relatively compact for each $t \in J$, where $(N_2H_l)(t) = \{y(t) : y \in (N_2H_l)\}$.

Obviously, by condition $(H4)(ii), (N_2H_l)(t)$ is relatively compact in X_α for $t = 0$. Let $0 < t \le b$ be fixed and $0 < \varepsilon < t$. For $x \in H_l$ and $y \in N_2(x)$, there exists a function $v \in S_{G,x}$ such that

$$y(t) = T(t)[x_0 - g(x)] + \int_0^{t-\varepsilon} T(t-s)v(s)\mathrm{d}s + \int_{t-\varepsilon}^t T(t-s)v(s)\mathrm{d}s + \int_0^{t-\varepsilon} T(t-s)(Bu)(s)\mathrm{d}s + \int_{t-\varepsilon}^t T(t-s)(Bu)(s)\mathrm{d}s + \sum_{0<t_k<t} T(t-t_k)I_k(x(t_k^-))$$

Define,

$$y_\varepsilon(t) = T(t)\big[x_0 - g(x)\big] + \int_0^{t-\varepsilon} T(t-s)v(s)\mathrm{d}s + \int_0^{t-\varepsilon} T(t-s)(Bu)(s)\mathrm{d}s + \sum_{0<t_k<t} T(t-t_k)I_k(x(t_k^-))$$

$$y_\varepsilon(t) = T(t)\big[x_0 - g(x)\big] + T(\varepsilon)\int_0^{t-\varepsilon} T(t-\varepsilon-s)v(s)\mathrm{d}s + T(\varepsilon)\int_0^{t-\varepsilon} T(t-\varepsilon-s)(Bu)(s)\mathrm{d}s + \sum_{0<t_k<t} T(t-t_k)I_k(x(t_k^-))$$

Since $T(t)$ is compact, the set $Y_\varepsilon(t) = \{y_\varepsilon(t) : y \in N_2(H_l)\}$ is relatively compact in X_α for every $\varepsilon, 0 < \varepsilon < t$.

Moreover, for every $y \in N_2(H_l)$,

$$\begin{aligned}
&\|y(t) - y_\varepsilon(t)\|_\alpha \\
&= \left\|\int_{t-\varepsilon}^t T(t-s)v(s)\mathrm{d}s\right\|_\alpha + \left\|\int_{t-\varepsilon}^t T(t-s)(Bu)(s)\mathrm{d}s\right\|_\alpha \\
&\le M\int_{t-\varepsilon}^t w(l)\mathrm{d}s \\
&+ MM_1M_2\int_{t-\varepsilon}^t \Big\{\|z_1\|_\alpha + \|g(x)\|_\alpha \\
&\qquad + \|T(b)\|\big[\|x_0\| + \|g(x)\| + \|F(0, x(h_1(0)))\|\big] \\
&\qquad + \|F(b, x(h_1(b)))\| \\
&\qquad + \left\|\int_0^b AT(b-\eta)F(\eta, x(h_1(\eta)))\mathrm{d}\eta\right\| \\
&\qquad + \left\|\int_0^b T(b-\eta)v(\eta)\mathrm{d}\eta\right\| \\
&\qquad + \left\|\sum_{0<t_k<t} T(t-t_k)I_k(x(t_k^-))\right\|\Big\}\mathrm{d}s \\
&\le Mw(l)\varepsilon \\
&+ MM_1M_2\int_{t-\varepsilon}^t \Big\{\|z_1\|_\alpha + (L_2l + L_2') \\
&\qquad + M\big[\|x_0\| + (L_2l + L_2') + M_0L_1(l+1)\big] \\
&\qquad + M_0L_1(l+1) + \int_0^b \frac{C_{1-\beta}}{(b-\eta)^{(1-\beta)}}L_1(l+1)\mathrm{d}\eta \\
&\qquad + \int_0^b \frac{C_\alpha}{(b-\eta)^\alpha}w(l)\mathrm{d}\eta + M\sum_{k=1}^m d_k\Big\}\mathrm{d}s \\
&\le Mw(l)\varepsilon + MM_1M_2M_3\varepsilon \\
&\le M\varepsilon\big[w(l) + M_1M_2M_3\big]
\end{aligned}$$

Therefore, letting $\varepsilon \to 0$, we see that there are relatively compact sets arbitrarily close to the set $\{y(t) : y \in N_2(H_l)\}$. Hence the set $\{y(t) : y \in N_2(H_l)\}$ is relatively compact in X_α.

As a consequence of (i),(ii), (iii) and together with the Arzela-Ascoli theorem we can conclude that $N_2 : H_l \to 2^{H_l}$ is a completely continuous multi-valued map and, therefore, a condensing multi- valued map.

iv) N_2 has a closed graph.

From the above steps we can see, for every $x \in H_l$, $N_2(x)$ is relatively compact and closed set, which can be testified as in Step 3. Hence $N_2(x)$ is a compact set.

Let $x_n \to x_*$, $x_n \in H_l, y_n \in N_2(x_n)$ and $y_n \to y_*$. We must show that $y_* \in N_2(x_*); y_n \in N_2(x_n)$ means that there exists $v_n \in S_{G,x_n}$ such that , for each $t \in J$.

$$y_n(t) = T(t)\left[x_0 - g(x_n)\right] + \int_0^t T(t-s)v_n(s)\mathrm{d}s + \int_0^t T(t-s)(Bu_n)(s)\mathrm{d}s + \sum_{0<t_k<t} T(t-t_k)I_k(x_n(t_k^-))$$

where

$$u_{x_n}(t) = \tilde{W}^{-1}\left[z_1 - g(x_n) - T(b)\left[x_0 - g(x_n) - F(0, x(h_1(0)))\right] - F(b, x(h_1(b))) + \int_0^b AT(b-s)F(s, x(h_1(s)))\mathrm{d}s + \int_0^b T(b-s)v_n(s)\mathrm{d}s + \sum_{0<t_k<t} T(t-t_k)I_k(x_n(t_k^-))\right]$$

We must prove that there exists $v_* \in S_{G,x_*}$ such that

$$y_*(x) = T(t)\left[x_0 - g(x_*)\right] + \int_0^t T(t-s)v_*(s)\mathrm{d}s + \int_0^t T(t-s)(Bu_*)(s)\mathrm{d}s + \sum_{0<t_k<t} T(t-t_k)I_k(x_*(t_k^-))$$

where

$$u_{x_*}(t) = \tilde{W}^{-1}\left[z_1 - g(x_*) - T(b)\left[x_0 - g(x_*) - F(0, x(h_1(0)))\right] - F(b, x(h_1(b))) + \int_0^b AT(b-s)F(s, x(h_1(s)))\mathrm{d}s + \int_0^b T(b-s)v_*(s)\mathrm{d}s + \sum_{0<t_k<t} T(t-t_k)I_k(x_*(t_k^-))\right]$$

Clearly, since $I_k, k = 1, 2, \cdots, m$ and g are continuous we have that

$$\left\| \left(y_n(t) - T(t)\left[x_0 - g(x_n)\right] - \int_0^t T(t-s)(Bu_n)(s)\mathrm{d}s - \sum_{0<t_k<t} T(t-t_k)I_k(x_n(t_k^-)) \right) - \left(y_*(x) - T(t)\left[x_0 - g(x_*)\right] - \int_0^t T(t-s)(Bu_*)(s)\mathrm{d}s - \sum_{0<t_k<t} T(t-t_k)I_k(x_*(t_k^-)) \right) \right\|_\Omega \to 0, \text{ as } n \to \infty.$$

Consider the linear continuous operator

$$\Gamma : L^1(J, X) \to C(J, X), v \mapsto \Gamma(v)(t) = \int_0^t T(t-s)v(s)\mathrm{d}s.$$

From Lemma (H3) it follows that ΓOS_G is a closed graph operator.

Moreover, we obtain that

$$\left(y_n(t) - T(t)\left[x_0 - g(x_n)\right] - \int_0^t T(t-s)(Bu_n)(s)\mathrm{d}s - \sum_{0<t_k<t} T(t-t_k)I_k(x_n(t_k^-)) \right) \in \Gamma(S_{G,x_n}).$$

Since $x_n \to x_*$, it follows from (H3) that

$$y_*(t) - T(t)\left[x_0 - g(x_*)\right] \int_0^t T(t-s)(Bu_*)(s)\mathrm{d}s - \sum_{0<t_k<t} T(t-t_k)I_k(x_*(t_k^-)) \in \Gamma(S_{G,x_*})$$

that is, there must exist a $v_*(t) \in S_{G,x_*}$ such that

$$y_*(t) - T(t)\left[x_0 - g(x_*)\right] - \int_0^t T(t-s)(Bu_*)(s)\mathrm{d}s - \sum_{0<t_k<t} T(t-t_k)I_k(x_*(t_k^-)) = \Gamma(v_*(t)) = \int_0^t T(t-s)v_*(s)\mathrm{d}s.$$

Therefore, N_2 has a closed graph. Since N_2 is a completely continuous multi-valued map with compact value, N_2 is u.s.c. On the other hand N_1 is a contraction. Hence $N = N_1 + N_2$ is u.s.c. and condensing.

By Lemma 2.3, there exists a fixed point $x(.)$ for N on H_l. Therefore, the nonlocal Cauchy problem with impulsive effect (1) is controllable on J.

Particularly, if $G(t, x(h_2(t)))$ is a single-valued map, then the system (1) will become

$$\begin{cases} \dfrac{\mathrm{d}}{\mathrm{d}t}\left[x(t) - F\left(t, x\left(h_1(t)\right)\right)\right] = Ax(t) + Bu(t) + G\left(t, x\left(h_2(t)\right)\right); \\ \qquad t \in J := [0, b]; \\ \Delta x|_{t=t_k} = I_k(x(t_k^-)); k = 1, 2, \cdots, m;\ t \neq t_k; \\ \qquad x(0) + g(x) = x_0 \end{cases} \tag{4}$$

by using Sadovskii's fixed-point theorem for condensing map, we can analogously study the controllability of the system (4).

(H3)' The function $G : J \times X_\alpha \to X$ satisfies the following conditions:

i) for each $t \in J$, the function $G(t,.) : X_\alpha \to X$ is

continuous; and for each $x \in X_\alpha$, the function $G(.,x): J \to X$ is strongly measurable.

ii) for each positive number $l \in N$, there exists a positive function $w(l)$ dependent on l such that

$$sup\|G(t,x)\| \le w(l) \text{ and } \lim_{l\to\infty} \frac{w(l)}{l} = \gamma < \infty$$

where

$$\|x\|_\alpha = \sup_{0\le s\le\alpha} \|x(s)\|_\alpha .$$

THEOREM 3.2 *Let* $x_0 \in X_\alpha$. *If the hypotheses* $(H1),(H2),(H3)',(H4)$ and $(H5)$ *are satisfied, then the system* (4) *is controllable on* J *provided* (1), (2) *and* (1) *hold.*

Proof The mild solution of the system (4) is given by

$$\begin{aligned} x(t) &= T(t)\left[x_0 - g(x) - F(0, x(h_1(0)))\right] \\ &\quad + F(t, x(h_1(t))) + \int_0^t AT(t-s)F(s, x(h_1(s)))ds \\ &\quad + \int_0^t T(t-s)G(s, x(h_2(s)))ds + \int_0^t T(t-s)(Bu)(s)ds \\ &\quad + \sum_{0<t_k<t} T(t-t_k)I_k(x(t_k^-)); t \in J. \end{aligned}$$

We define the operator $N: \Omega \to \Omega$ by

$$\begin{aligned} (Nx)(t) &= T(t)\left[x_0 - g(x) - F(0, x(h_1(0)))\right] \\ &\quad + F(t, x(h_1(t))) + \int_0^t AT(t-s)F(s, x(h_1(s)))ds \\ &\quad + \int_0^t T(t-s)G(s, x(h_2(s)))ds + \int_0^t T(t-s)(Bu)(s)ds \\ &\quad + \sum_{0<t_k<t} T(t-t_k)I_k(x(t_k^-)) \end{aligned}$$

Then we can decompose N as $N = N_1 + N_2$, where

$$\begin{aligned} (N_1x)(t) &= F(t, x(h_1)(t)) - T(t)F(0, x(h_1(0)) \\ &\quad + \int_0^t AT(t-s)F(s, x(h_1(s)))ds \end{aligned}$$

and

$$\begin{aligned} (N_2x)(t) &= T(t)\left[x_0 - g(x)\right] + \int_0^t T(t-s)G(s, x(h_2(s)))ds \\ &\quad + \int_0^t T(t-s)(Bu)(s)ds \end{aligned}$$

and verify that N_1 is a contraction while N_2 is a compact operator, thus Sadovskii's fixed-point theorem can be applied to the operator N and hence N has atleast a fixed point on Ω, which shows that system (4) is controllable on the interval J. The desired proof is similar to Step 4 of Theorem 3.1.

4. Example

As an application of Theorem 3.2, we study the following impulsive partial function differential system with nonlocal condition

$$\begin{cases} \dfrac{\partial}{\partial t}\left[z(t,x) - \int_0^\pi b(t,y,x)\left[z(\sin t, y) + \dfrac{\partial z}{\partial y}(\sin t, y)\right] dy\right] \\ = \dfrac{\partial^2 z(t,x)}{\partial x^2} + u(t,y) + h\left(t, z(\sin t, x), \dfrac{\partial z}{\partial x}(\sin t, x)\right), \\ \qquad 0 \le t \le 1, 0 \le x \le \pi, t \ne t_k, k = 1,2,\cdots,m; \\ z(t,0) = z(t,\pi) = 0;\ z(t_k^+) - z(t_k^-) = I_k(z(t_k)), \\ \qquad k = 1,2,\cdots,m \\ z(0,x) + \sum_{i=0}^{p} \int_0^\pi k_i(y,x) z(s_i, y) dy = z_0(x), 0 \le x \le \pi \end{cases} \tag{4.1}$$

where p is a positive integer, $0 < s_0 < s_1 < \cdots < s_p < 1$, and $0 < t_1 < t_2 < \cdots t_m < \cdots < 1; z_0(x) \in X = L^2([0,\pi])$. A is defined by $A\omega = \omega''$ with the domain

$$\begin{aligned} D(A) = H_0^2([0,\pi]) = \{\omega(.) \in X : \omega, \\ \omega' \text{ are absolutely continuous}, \\ \omega'' \in X, \omega(0) = \omega(\pi) = 0\} \end{aligned}$$

Then A generates a strongly continuous semigroup $T(.)$ which is compact, analytic and self-adjoint.

a') Also A has a discrete spectrum representation

$$A\omega = \sum_{n=1}^{\infty} (-n^2) < \omega, \omega_n > \omega_n, \omega \in D(A), n \in N;$$

where $\omega_n(x) = \sqrt{\dfrac{2}{\pi}} sin(nx); n = 1,2,\cdots$ is the orthogonal set of eigenvector of A. The eigenvalues are $-n^2, n \in N$.

b') The operator $A^{\frac{1}{2}}$ is given by

$$A^{\frac{1}{2}}\omega = \sum_{n=0}^{\infty} n < \omega, \omega_n > \omega_n$$

on the space $D(A^{\frac{1}{2}}) = \left\{\omega(.) \in X : \sum_{n=1}^{\infty} n < \omega, \omega_n > \omega_n \in X\right\}$.

The control operator $B: L^2(J,X) \to X$ is defined by $(Bu)(t)(y) = u(t,y); y \in (0,\pi)$ which satisfies condition (H5). Here B is an identity operator and the control function $u(.)$ is given in $L^2([0,\pi],U)$.

We assume that the following conditions hold:

i) The function b is measurable and

$$\sup_{0\le t\le 1} \int_0^\pi \int_0^\pi b^2(t,y,x) dy dx < \infty.$$

ii) The function $\dfrac{\partial^2 b(t,y,x)}{\partial x^2}$ is measurable, $b(t,y,0) = b(t,y,\pi) = 0$, and

$$N_1 = \sup_{0\le t\le 1} \left[\int_0^\pi \int_0^\pi \left(\frac{\partial^2 b(t,y,x)}{\partial x^2} \right)^2 dy dx \right]^{\frac{1}{2}} < \infty.$$

iii) For the function $h:[0,1]\times R\times R\to R$ the following three conditions are satisfied:

1) For each $t\in[0,1], h(t,.,.)$ is continuous.

2) For each $z\in X_{\frac{1}{2}}, h(.,z,z')$ is measurable.

3) There is a positive number c_1 such that

$$\|g(t,z,z')\|\le c_1\|z\|,$$

for all $(t,z)\in[0,1]\times X_{\frac{1}{2}}$.

iv) $I_k\in C\left(X_{\frac{1}{2}},X_{\frac{1}{2}}\right), k=1,\cdots,$ and there exist constants $d_k, k=1,\cdots,m,$ such that

$$\|I_k(z)\|_{\frac{1}{2}}\le d_k, z\in X_{\frac{1}{2}}.$$

Here we choose $\alpha=\beta=\frac{1}{2}$. According to paper [21], we know that, if $z\in X_{\frac{1}{2}}$, then z is absolutely continuous , $z'\in X,$ and $z(0)=z(\pi)=0$. In view of this result, for $(t,z)\in[0,1]\times X_{\frac{1}{2}}, \omega\in\Omega$ (Ω is defined as in Section 3), we can define respectively that

$$F(t,z)(x)=\int_0^\pi b(t,y,x)\left[z(y)+z'(y)\right]\mathrm{d}y.$$

$$G(t,z)(x)=h(t,z(x),z'(x)),$$

and

$$g(\omega(t))=\sum_{i=0}^{p}K_i\omega_1(s_i),\omega\in\Omega,$$

where $K_i:X_{\frac{1}{2}}\to X_{\frac{1}{2}}$ is completely continuous [16] such that $K_i(z)(x)=\int_0^\pi k_i(y,x)z(y)\mathrm{d}y$ and $G:[0,1]\times X_{\frac{1}{2}}\to X$ It is easy to see that

$F:[0,1]\times X_{\frac{1}{2}}\to X_{\frac{1}{2}}, A^{\frac{1}{2}}F:[0,1]\times X_{\frac{1}{2}}\to X_{\frac{1}{2}}\cdots$ In fact, for each $t\in[0,1],$ we have

$$\left\langle F(t,z),\omega_n\right\rangle$$
$$=\frac{1}{n}\sqrt{\frac{2}{\pi}}\left\langle\int_0^\pi\frac{\partial b(t,y,x)}{\partial x}\left[z(y)+z'(y)\right]\mathrm{d}y,\cos(nx)\right\rangle,$$

also,

$$\left\langle F(t,z),\omega_n\right\rangle$$
$$=\frac{-1}{n^2}\sqrt{\frac{2}{\pi}}\left\langle\int_0^\pi\frac{\partial^2 b(t,y,x)}{\partial x^2}\left[z(y)+z'(y)\right]\mathrm{d}y,\sin(nx)\right\rangle.$$

This shows that F and $A^{\frac{1}{2}}F$ both take values in $X_{\frac{1}{2}}$ in terms of properties (a') and (b'), and therefore the function g. Since, for any $x_1,x_2\in X_{\frac{1}{2}}$,

$$\|x_2-x_1\|^2=\sum_{n=0}^{\infty}\langle x_2-x_1,z_n\rangle^2\le\sum_{n=0}^{\infty}n^2\langle x_2-x_1,z_n\rangle^2$$
$$\le\|x_2-x_1\|_{\frac{1}{2}}^2.$$

This inequality alongwith condition (ii) says that (H2) is satisfied. Also G satisfies $(H3)'$ and g satisfies (H4). By (i), $F(t,z)$ is a bounded linear operator on X. Thus $(H1),(H2),(H3)',(H4),(H5)$ are satisfied and the system (1) is controllable on [0,1].

5. Exact Controllability in Infinite Dimensional Space

It has been observed that the example in ([2-11,22]) cannot be recovered as special case of the abstract result. If the semigroup is compact then the assumption (H1) in Section 2 is valid only in finite dimensional space so the applications are restricted to ordinary differential control system but not to partial differential equations (refer [15]). We have tried to overcome to this problem in Section 3 for the inclusion (1). Here we present another way of exact controllability result of the system (4) in infinite dimension space.

LEMMA 5.1 *Let* $\mathcal{PC}([0,\tau]),X_\alpha)$ *be a space formed by normalized piecewise continuous function* $([0,\tau],X_\alpha)$. *Let* $\mathcal{B}\subseteq\mathcal{PC}$ *such tha* $\tilde{\mathcal{B}}_k=\left\{\tilde{V}_k:V\in\mathcal{B}\right\}$; *where*

$$\tilde{V}_k(t)=\begin{cases}V(t);\ t\in\left(t_k,t_{k+1}\right]\\ V(t_k^+);\ t=t_k\end{cases}$$

The set $\mathcal{B}\subseteq\mathcal{PC}$ is relatively compact if and only if each set $\tilde{\mathcal{B}}_k$ is relatively compact in the space $C([t_k,t_{k+1}];X_\alpha)$.

THEOREM 5.2 *Assume that the function F and G verify the assumptions* $(H1)$ *and* $(H2)'$ *respectively and suppose that the following conditions are fulfilled:*

a1) For every $r>0$ and all $\varepsilon>0$ there are compact sets $U^i_{\varepsilon,r}\subseteq X_\alpha, i=1,2,$ such that $T(\varepsilon)A^\beta F(s,\xi)\in U^1_{\varepsilon,r}$ and $T(\varepsilon)G(s,\xi)\in U^2_{\varepsilon,r}$ for every $F(\xi):J\times\mathcal{B}_r(0,\Omega)$.

b1) Conditions $(H3)$ and $(H4)$ are satisfied. Then there exists a mild solution of the system (3.4).

Proof Consider the system (3.4). As a main portion of the theorem, we prove that N is completely continuous operator.

The mild solution given in Theorem (3.2) can be splitted up into following four parts:

$$N^{(1)}(t) = T(t)\left[x(0) - g(x) - F(0, x(h_1(0)))\right] + F(t, x(h_1(t)))$$

$$N^{(2)}(t) = \int_0^t AT(t-s)F(s, x(h_1(s)))\mathrm{d}s$$

$$N^{(3)}(t)z = \int_0^t T(t-s)G(s, x(h_2(s)))\mathrm{d}s + \int_0^t T(t-s)Bu(s)\mathrm{d}s$$

$$N^{(4)}(t) = \sum_{0\le t_k \le t} T(t-t_k)I_k(x(t_k^-)), \text{for each } t \in J.$$

Obviously each $N^{(i)}$ is continuous. To prove that N is compact operator we will show separately that $N^{(i)}(\mathcal{B}_r(0,\Omega))$ is relatively compact in Ω for every $x \in \mathcal{B}_r = \mathcal{B}_r(0,\Omega)$.

Step 1: Let $N^{(1)}(\mathcal{B}_r)$ is relatively compact in Ω.

Let $V = N^{(1)}(\mathcal{B}_r)$. Let $T(.)$ is uniformly bounded on $[0,b]$ and continuous for the norm of the operator in $(0,b]$, we can observe that the sets

$\tilde{V}_k \subseteq -T(t)F(0, x(h_1(0))) + A^{-\beta}U^1_{\varepsilon,r}$; it follows that $\tilde{V}_k$ is relatively compact for every $t \in [t_k, t_{k+1}], k = 0,1,2,\cdots,m.$

Step 2: Let $N^{(2)}(\mathcal{B}_r)$ is relatively compact in Ω.

We first show that $N^2(\mathcal{B}_r(t))$ is relatively compact for each $t \in J$. For $t = 0$ it is trivial. Assume that $0 < 2\varepsilon < t \le b$ and let $U^1_{\varepsilon,r}$ be the compact set introduced in the hypothesis $(a1)$. Since $A^{\beta}T(.)$ is strongly continuous on $[\varepsilon, b]$, it follows that $U_\varepsilon = \left\{A^{1-\beta}T(s)x : s \in [\varepsilon, b], x \in U^1_{\varepsilon,r}\right\}$ is relatively compact in X_α.

Now using mean value theorem for Bochner integral, we can write

$$N^{(2)}x(t) = \int_0^{t-2\varepsilon} A^{1-\beta}T(t-s-\varepsilon)T(\varepsilon)A^{\beta}F(s, x(h_1(s)))\mathrm{d}s + \int_{t-2\varepsilon}^t A^{1-\beta}T(t-s)A^{\beta}F(s, x(h_1(s)))\mathrm{d}s$$

$$\in (t-2\varepsilon)\overline{co(U_\varepsilon)} + (\mathcal{B}_{r^*})(0, X_\alpha)$$

for each $x \in (\mathcal{B}_r)$, where $co(U_\varepsilon)$ denotes convex hull of U_ε and

$$r^* = 2^{\beta}C_{1-\beta}\left\{L_1\left(\|x\|_\alpha + 1\right)\right\}\frac{\varepsilon^{\beta}}{\beta}.$$

Thus $N^2(\mathcal{B}_r)(t)$ is relatively compact in X_α.

Next we show that $N^{(2)}(\mathcal{B}_r)$ is equi-continuous.

Let $0 \le t_0 < t \le b$. Then

$$N^{(2)}x(t) - N^{(1)}x(t) = -\int_0^t AT(t-s)F(s, x(h_1(s)))\mathrm{d}s + \int_0^{t_0} AT(t_0-s)F(s, x(h_1(s)))\mathrm{d}s$$

$$= (I - T(t-t_0))N^{(2)}x(t_0) - \int_{t_0}^t AT(t-s)F(s, x(h_1(s)))\mathrm{d}s$$

Since the elements $N^{(2)}x(t_0)$; for $x \in \mathcal{B}_r$; are included in a compact set, it follows that the first term on right hand side converges uniformly to zero as $t \to t_0$. Similarly it follows from $(b1)$ that the function $AT(t-s)F(s, x(h_1(s))), x \in \mathcal{B}_r$ are equi-integrable, which imply that the second term on right hand side also converges uniformly to zero as $t \to t_0$.

This show that $N^{(2)}(\mathcal{B}_r)$ is equi-continuous from the right at t_0. Similarly it can be prove that $N^2(\mathcal{B}_r)$ is equi-continuous from the left at $t_0 > 0$. Thus $N^{(2)}(\mathcal{B}_r)$ is equi-continuous and hence $N^{(2)}(\mathcal{B}_r)$ is relatively compact in Ω.

Step 3: By using same argument as in Step 2 we can prove that the set $N^{(3)}(\mathcal{B}_r)$. is relatively compact in Ω.

Step 4: The relatively compactness of $N^{(4)}(\mathcal{B}_r)$. is consequence of assumption (H4) and Lemma 5.1 Hence the proof.

Remark Throughout Section 5 we have used compactness assumption of Theorem 5.2 (a1) and growth condition (H2) (ii) and (H5). If the maps F and $I_k, k = 1,2,\cdots,m$ satisfy some Lipschitz conditions (H2) (i) and (H5) instead of compactness in (a1) then also we can prove controllability result.

6. References

[1] M. Martelli, "A Rothe's Type Theorem for Noncompact Acyclic-Valued Map," *Bollettino dell'Unione Matematica Italiana*, Vol. 2, 1975, pp. 70-76.

[2] M. Benchohra and S. K. Ntouyas, "Existence Results for Nondensely Defined Impulsive Semilinear Functional Differential Inclusion with Infinite Delay," *Journal of Fixed Point Theory and Applications*, Vol. 2, No. 1, 2007, pp. 11-51.

[3] C. C. Travis and G. F. Webb, "Existence, Stability and Compactnes with α-Norm for Partial Functional Differential Equations," *Transaction of American Mathematical Society*, Vol. 240, 1978, pp. 129-143.

[4] L. Byszewski, "Theorems about the Existence and Uniqueness of a Semilinear Evolution Nonlocal Cauchy Problem," *Journal of Mathematical Analysis and Applications*, Vol. 162, 1991, pp. 496-505.

[5] K. Deng, "Exponential Decay of Solutions of Semilinear Paprabolic Equations with Nonlocal Initial Conditions," *Journal Mathematical Analysis and Applications*, Vol. 179, 1993, pp. 630-637. doi:10.1006/jmaa.1993.1373

[6] D. N. Chalishajar, "Controllability of Second Order Semilinear Neutral Functional Differential Inclusions with Non-Local Conditions in Banach Spaces," *Nonlinear Functional Analysis and Applications*, Vol. 14, No. 1, 2009, pp. 1-15.

[7] D. N. Chalishajar and F. S. Acharya, "Controllability of Semilinear Impulsive Partial Neutral Functional Differential Equations with Infinite Delay," *Proceeding of Fourth International Conference on Neural, Parallel Scientific and Computations*, Atlanta, 2010, pp. 83-89.

[8] D. N. Chalishajar and F. S. Acharya, "Controllability of Second Order Semi-linear Neutral Impulsive Differential Inclusions on Unbounded Domain with Infinite Delay in Banach Spaces," *Bulletin of Korean Mathematical Society*, Vol. 48, No. 4, 2011, pp. 813-838.

[9] D. N. Chalishajar, R. K. George, A. K. Nandakumaran and F. S. Acharya, "Trajectory Controllability of Nonlinear Integro-Differential System," *Journal of Franklin Institute*, Vol. 347, 2010, pp. 1065-1075.

[10] M. Benchohra and S. K. Ntouyas, "Existence and Controllability Results for Nonlinear Differential Inclusions with Nonlocal Conditions in Banach Spaces," *Journal of Applied Analysis*, Vol. 1, No. 8, 2002, pp. 45-52.

[11] M. Benchohra and S. K. Ntouyas, "On Second Order Impulsive Functional Differential Equations in Banach Spaces," *Journal of Applied Mathematics and Stochastic Analysis*, Vol. 15, 2002, pp. 45-52. doi:10.1155/S1048953302000059

[12] E. Hernandez, M. Rabello and H. R. Henriquez, "Existence of Solutions for Impulsive Partial Neutral Functional Differential Equations," *Journal of Mathematical Analysis and Applications*, Vol. 31, 2007, pp. 1135-1158. doi:10.1016/j.jmaa.2006.09.043

[13] D. N. Chalishajar, "Controllability of Nonlinear Integro-Differential Third Order Dispersion System," *Journal Mathematical Analysis and Applications*, Vol. 348, 2008, pp. 480-486. doi:10.1016/j.jmaa.2008.07.047

[14] X. L. Fu and Y. J. Cao, "Existence for Neutral Impulsive Differential Inclusions with Nonlocal Conditions," *Nonlinear Analysis—TMA*, Vol. 68, 2008, pp. 3707-3718.

[15] R. Triggani, "A Note on Lack of Exact Controllability for Mild Solution in Banach Spaces," *SIAM*, *Journal of Control and Optimization*, Vol. 18, No. 1, 1980, pp. 98-99.

[16] K. Yosida, "Functional Analysis," 6th Edition, Springer-Verlag; Berlin, 1980.

[17] K. Deimling, "Multivalued Differential Equations," De Gruyter, Berlin, 1992. doi:10.1515/9783110874228

[18] L. Byszewski, "Existence of Solutions of Semilinear Functional-Differential Evolution Nonlocal Problem," *Nonlinear Analysis*, Vol. 34, 1998, pp. 65-72. doi:10.1016/S0362-546X(97)00693-7

[19] A. Pazy, "Semigroups of Linear Operators and Applications to Partial Differential Equations," Springer-Verlag, New York, 1983. doi:10.1007/978-1-4612-5561-1

[20] H. Themies, "Integrated Semigroup and Integral Solutions to Abstract Cauchy Problems," *Journal Mathematical Analysis and Applications*, Vol. 152, 1990, pp. 416-447. doi:10.1016/0022-247X(90)90074-P

[21] C. C. Travis and G. F. Webb, "Partial Functional Differential Equations with Deviating Arguments in Time Variable," *Journal of Mathematical Analysis and Applications*, Vol. 56, 1976, pp. 397-409. doi:10.1016/0022-247X(76)90052-4

[22] Y. K. Chang and D. N. Chalishajar, "Controllability of Mixed Volterra-Fredholm-Type Integro-Differential Inclusions in Banach Spaces," *Journal of Franklin Institute*, Vol. 345, 2008, pp. 449-507. doi:10.1016/j.jfranklin.2008.02.002

Applied Mathematics, **2011, 2, 1497-1506**
doi:10.4236/am.2011.212212 Published Online December 2011 (http://www.SciRP.org/journal/am)

Precision of a Parabolic Optimum Calculated from Noisy Biological Data, and Implications for Quantitative Optimization of Biventricular Pacemakers (Cardiac Resynchronization Therapy)

Darrel P. Francis
International Centre for Circulatory Health, *National Heart and Lung Institute*, *Imperial College London*, *London*, *United Kingdom*
E-mail: *d.francis@imperial.ac.uk*
Received August 26, 2011; *revised November* 9, 2011; *accepted November* 17, 2011

Abstract

In patients with heart failure and disordered intracardiac conduction of activation, doctors implant a biventricular pacemaker ("cardiac resynchronization therapy", CRT) to allow adjustment of the relative timings of activation of parts of the heart. The process of selecting the pacemaker timings that maximize cardiac function is called "optimization". Although optimization—more than any other clinical assessment—needs to be precise, it is not yet conventional to report the standard error of the optimum alongside its value in clinical practice, nor even in research, because no method is available to calculate precision from one optimization dataset. Moreover, as long as the determinants of precision remain unknown, they will remain unconsidered, preventing candidate haemodynamic variables from being screened for suitability for use in optimization. This manuscript derives algebraically a clinically-applicable method to calculate the precision of the optimum value of x arising from fitting noisy biological measurements of y (such as blood flow or pressure) obtained at a series of known values of x (such as atrioventricular or interventricular delay) to a quadratic curve. A formula for uncertainty in the optimum value of x is obtained, in terms of the amount of scatter (irreproducibility) of y, the intensity of its curvature with respect to x, the width of the range and number of values of x tested, the number of replicate measurements made at each value of x, and the position of the optimum within the tested range. The ratio of scatter to curvature is found to be the overwhelming practical determinant of precision of the optimum. The new formulae have three uses. First, they are a basic science for anyone desiring time-efficient, reliable optimization protocols. Second, asking for the precision of every reported optimum may expose optimization methods whose precision is unacceptable. Third, evaluating precision quantitatively will help clinicians decide whether an apparent change in optimum between successive visits is real and not just noise.

Keywords: Cardiac, Pacemaker, Parabolic, Haemodynamics

1. Introduction

ὁ δὲ ἀνεξέταστος βίος οὐ βιωτὸς ἀνθρώπῳ
Plato, *Apology of Socrates*, 38a

Every year, ~100,000 cardiac resynchronization pacemakers are being implanted into patients with heart failure, because they deliver substantial symptomatic and survival benefits [1-3] by altering intracardiac timings. After implantation, the process of determining which timings to programme is described as "optimization" [4-6]. Responses of physiological variables to changes in pacemaker settings fit well to a parabola in the vicinity of the optimum [6,7]. Curve-fitting to calculate a clinical optimum has the advantage of permitting interpolation to settings which were not directly tested, and also avoids the problem that simply "picking the highest" leads to illusory optima, illusory increments in physiology from optimization, and illusory changes in optimum over time [8].

In clinical practice physiological measurements con-

tain noise which can sometimes be substantial in comparison to the underlying signal, and which prevents the true underlying optimum being identified precisely even with curve fitting (**Figure 1**). The impact of such noise can be reduced by averaging multiple measurements, but this consumes resources such as time in a clinical environment or battery power if the measurements are conducted by the implanted device. It is therefore important to be able to calculate the precision of an optimum so that resource usage can be planned to be appropriate to achieve the clinically-required precision.

As well as needing to know how many replicates are required, doctors planning an optimization protocol also need guidance regarding what range of settings to cover during testing, and how coarsely or finely. Widening the range or making finer-grained measurements (*i.e.* at more closely-spaced intervals) increase the cost of the optimization process, and so are only justified if there is a clinically-valuable increase in precision of the optimum.

Finally, doctors caring for patients from day to day need to know the uncertainty of the optimum obtained this clinical optimization process. Without this knowledge, it is impossible to interpret apparent differences in optimum within an individual patient between one assessment method and another, or over time [8,9] or after an operation or a heart attack.

This paper derives a simple formula for the uncertainty of the parabolically-defined optimal setting of a pacemaker, and presents practical implications for protocol design and for medical practice.

2. Description of Method

2.1. Physiological Measurements with Noise

The pacemaker setting may be adjusted over a wide range of values. Within individual patients, clinical information provides *a priori* a constrained range which contains all biologically plausible locations of the optimum for that patient. During the optimization procedure, the clinician acquires a series of pairs of values of the pacemaker setting and the corresponding physiological measurement. The first value, the pacemaker setting, has negligible uncertainty because it is programmed digitally. However the second value, the measured physiological variable, is not perfectly reproducible and therefore has an element of uncertainty.

Some choices of physiological variable, such as blood pressure, permit automatic acquisition, while others, such as Doppler velocity-time integral, typically require human involvement for each measurement. In practice the protocol is often to make more than one replicate measurement at each setting, and then to summarize the data

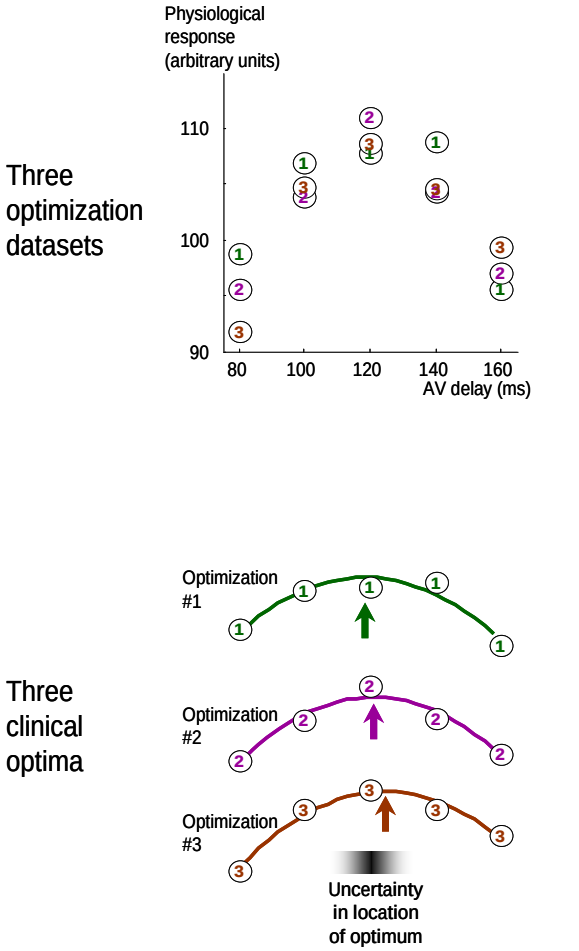

Figure 1. Sketch showing how noise in the measured data creates uncertainty in the optimum. Note: If there is enough time to conduct many optimizations, they can be analyzed separately to provide separate estimates of the optimum, so the uncertainty in the optimum can be observed. The upper panel sketches 3 optimization datasets in one simulated patient. All 3 datasets are plotted on the same graph and labeled "1" to "3". The lower panel shows the 3 individual interpolated optima obtained by curve fitting with a parabola. This paper provides a method of calculating the uncertainty in a clinically-obtained optimum, without having to conduct several independent optimizations.

for each setting by the mean of the raw measurements at that setting.

Let the optimization protocol try S different values x_i of the pacemaker setting, evenly spaced at intervals of Δx. Let the averaged physiological measurements representing each setting be denoted y_i, each of which is the mean of R replicate raw measurements. The observed data y_i during clinical testing are composed of an underlying value $y_{und,i}$ and an error component ε_R.

$$y_i = y_{und,i} + \varepsilon_R$$

Let us consider the error component to be independent

of $y_{und,i}$ and normally distributed, with its standard deviation for a single raw measurement being σ_{ε_1} and, by the central limit theorem, the standard deviation for the error ε_R of the average of R replicates being $\sigma_{\varepsilon_R} = \sigma_{\varepsilon_1} / \sqrt{R}$.

2.2. The Optimization Process

The best-fit parabola, $Ax_i^2 + Bx_i + C$, to the observed data is defined by the standard least-squares method, to minimize the squared deviation between the observations y_i and the parabola. The clinical optimum from that fitted parabola is $-B/2A$, which will differ from the true optimum Opt_{True} by an amount whose standard deviation can be calculated as follows. The best-fit parabola is defined by having A, B and C values that minimize the squared error $F = \sum\left(Ax_i^2 + Bx_i + C - y_i\right)^2$.

This is achieved by setting all the partial derivatives of F with respect to A, B and C to zero:

$$\partial F/\partial A = 2\sum\left[\left(Ax_i^2 + Bx_i + C - y_i\right)x_i^2\right] = 0$$

$$\partial F/\partial B = 2\sum\left[\left(Ax_i^2 + Bx_i + C - y_i\right)x_i\right] = 0$$

$$\partial F/\partial C = 2\sum\left[\left(Ax_i^2 + Bx_i + C - y_i\right)\right] = 0$$

Therefore

$$A\sum x_i^4 + B\sum x_i^3 + C\sum x_i^2 = \sum x_i^2 y_i$$

$$A\sum x_i^3 + B\sum x_i^2 + C\sum x_i = \sum x_i y_i$$

$$A\sum x_i^2 + B\sum x_i + C\sum 1 = \sum y_i$$

These can be solved for A, B and C as follows:

$$A = \frac{S\sum x_i^2 y_i - \sum x_i^2 \sum y_i}{S\sum x_i^4 - \left(\sum x_i^2\right)^2}$$

$$B = \frac{\sum x_i y_i}{\sum x_i^2},\ C = \frac{\sum x_i^4 \sum y_i - \sum x_i^2 \sum x_i^2 y_i}{S\sum x_i^4 - \left(\sum x_i^2\right)^2}$$

3. Results

3.1. The Clinical Optimum

The clinician will choose as optimal the pacemaker setting which corresponds to the middle of the fitted parabola, *i.e.* $\hat{x}_{opt} = \frac{-B}{2A}$. In terms of the clinical data x_i and y_i, this clinical optimum is

$$\hat{x}_{opt} = \frac{\left(\sum x_i^2\right)^2 - S\sum x_i^4}{2S\sum x_i^2 \sum x_i^2 y_i - 2\sum x_i^2 \sum y_i}.$$

For simplicity, and without loss of generality, a coordinate system for x can be chosen that makes 0 the centre of the range of settings tested during optimization. This symmetrical arrangement of x_i values provides the following convenient identities:

$$\sum x_i = 0, \sum x_i^2 = \Delta x^2 S\left(S-1\right)\left(S+1\right)/12,$$

$$\sum x_i^3 = 0, \sum x_i^4 = \Delta x^4 S\left(S-1\right)\left(3S^2-7\right)\left(S+1\right)/240$$

Applying these substitutions permits the clinical optimum to be described as follows:

$$\hat{x}_{opt} = \frac{2\left(S^2-4\right)\Delta x^2 \sum x_i y_i}{5\left(S^2-1\right)\Delta x^2 \sum y_i - 60\sum x_i^2 y_i}. \quad (1)$$

If y_i is augmented by any constant k, the numerator is unchanged because $\sum x_i\left(y_i + k\right) = \sum x_i y_i + k\sum x_i = \sum x_i y_i$. The denominator is also unchanged because it is augmented by $5\left(S^2-1\right)\Delta x^2 \sum k - 60k\sum x_i^2$ which is

$$5kS\left(S^2-1\right)\Delta x^2 - \frac{60k\Delta x^2 S\left(S^2-1\right)}{12} = 0.$$

Therefore without loss of generality the observed values y_i may be defined in terms of the underlying quadratic curvature coefficient A_{und}, the true optimum x_{opt}, and the noise component ε_R as follows:

$$y_i = A_{und}\left(x_i - x_{opt}\right)^2 + \varepsilon_{R,i}$$

$$\sum y_i = \sum A_{und}\left(x_i - x_{opt}\right)^2 + \varepsilon_{R,i}$$

$$= A_{und}\left[\sum x_i^2 - 2x_{opt}\sum x_i + S\cdot x_{opt}^2\right] + \sum \varepsilon_{R,i}$$

$$= A_{und}\Delta x^2 \frac{S\left(S^2-1\right)}{12} + A_{und}\cdot S\cdot x_{opt}^2 + \sum \varepsilon_{R,i}$$

$$\sum x_i y_i = \sum x_i\left[A_{und}\left(x_i - x_{opt}\right)^2 + \varepsilon_{R,i}\right]$$

$$= A_{und}\left[\sum x_i^3 - 2x_{opt}\sum x_i^2 + x_{opt}^2\sum x_i\right] + \sum x_i \varepsilon_{R,i}$$

$$= -x_{opt}A_{und}\Delta x^2 \frac{S\left(S^2-1\right)}{6} + \sum x_i \varepsilon_{R,i}$$

$$\sum x_i^2 y_i = \sum x_i^2\left[A_{und}\left(x_i - x_{opt}\right)^2 + \varepsilon_{R,i}\right]$$

$$= A_{und}\left[\sum x_i^4 - 2x_{opt}\sum x_i^3 + x_{opt}^2\sum x_i^2\right] + \sum x_i^2 \varepsilon_{R,i}$$

$$= A_{und}\left[\Delta x^4 \frac{S\left(S^2-1\right)\left(3S^2-7\right)}{240} + x_{opt}^2\Delta x^2 \frac{S\left(S^2-1\right)}{12}\right]$$

$$+\sum x_i^2 \varepsilon_{R,i}$$

3.2. Expression for the Clinical Optimum

Applying these within Equation (1) gives:

$$\hat{x}_{opt} = \frac{2\left(S^2-4\right)\Delta x^2\left[-x_{opt}A_{und}\Delta x^2\dfrac{S\left(S^2-1\right)}{6}+\sum x_i\varepsilon_{R,i}\right]}{5\left(S^2-1\right)\Delta x^2\left[A_{und}\Delta x^2\dfrac{S\left(S^2-1\right)}{12}+A_{und}Sx_{opt}^2+\sum\varepsilon_{R,i}\right]-60\left(A_{und}\left[\Delta x^4\dfrac{S\left(S^2-1\right)\left(3S^2-7\right)}{240}+x_{opt}^2\Delta x^2\dfrac{S\left(S^2-1\right)}{12}\right]+\sum x_i^2\varepsilon_{R,i}\right)}$$

$$= \frac{2\left(S^2-4\right)\Delta x^2\left[-2x_{opt}A_{und}\Delta x^2\dfrac{S\left(S^2-1\right)}{12}+\sum x_i\varepsilon_{R,i}\right]}{5\left(S^2-1\right)\Delta x^2\left[A_{und}\Delta x^2\dfrac{S\left(S^2-1\right)}{12}+\sum\varepsilon_{R,i}\right]-60A_{und}\Delta x^4\dfrac{S\left(S^2-1\right)\left(3S^2-7\right)}{240}-60\sum x_i^2\varepsilon_{R,i}}$$

$$= \frac{-A_{und}x_{opt}\Delta x^4\dfrac{S\left(S^2-1\right)\left(S^2-4\right)}{3}+2\left(S^2-4\right)\Delta x^2\sum x_i\varepsilon_{R,i}}{\Delta x^4\dfrac{5\left(S^2-1\right)S\left(S^2-1\right)}{12}-\Delta x^4\dfrac{S\left(S^2-1\right)\left(3S^2-7\right)}{4}+\dfrac{5\left(S^2-1\right)\Delta x^2}{A_{und}}\sum\varepsilon_{R,i}-\dfrac{60}{A_{und}}\sum x_i^2\varepsilon_{R,i}}$$

$$\hat{x}_{opt} = \frac{-x_{opt}\Delta x^4\dfrac{S\left(S^2-1\right)\left(S^2-4\right)}{3}+\dfrac{2\left(S^2-4\right)\Delta x^2}{A_{und}}\sum x_i\varepsilon_{R,i}}{-\Delta x^4\dfrac{S\left(S^2-1\right)\left(S^2-4\right)}{3}+\dfrac{5\left(S^2-1\right)\Delta x^2}{A_{und}}\sum\varepsilon_{R,i}-\dfrac{60}{A_{und}}\sum x_i^2\varepsilon_{R,i}}$$

$$= \frac{x_{opt}-\dfrac{6}{A_{und}\Delta x^2S\left(S^2-1\right)}\sum x_i\varepsilon_{R,i}}{1-\dfrac{15}{A_{und}\Delta x^2S\left(S^2-4\right)}\sum\varepsilon_{R,i}-\dfrac{180}{A_{und}\Delta x^4S\left(S^2-1\right)\left(S^2-4\right)}\sum x_i^2\varepsilon_{R,i}}$$

3.3. Imprecision of the Clinical Optimum

It can be seen from this that the clinically observed optimum $\hat{x}_{opt}$ differs from the underlying optimum x_{opt} because of two types of error, which affect the numerator and denominator respectively. The component in the numerator is a simple additive error. The impact of the denominator error, however, scales with x_{opt}.

In clinical situations where the errors are large in comparison with the degree of curvature that is manifested, the entire denominator of this formula falls near (or beyond) zero and behavior of the expression becomes strongly nonlinear. In such a situation there is almost no useful information about the underlying optimum available from the acquired data. Clinically this can be considered likely whenever the information content (or intraclass correlation coefficient) is low [8].

In most situations of well-designed optimization protocols, however, the error is not large compared with the curvature of the signal, which makes it possible to provide a closed-form expression for the imprecision of the optimum.

To do this, the variance of the numerator is first shown to be

$$Var\left[\frac{6}{A_{und}\Delta x^2S\left(S^2-1\right)}\sum x_i\varepsilon_{R,i}\right] = \left(\frac{6}{A_{und}\Delta x^2S\left(S^2-1\right)}\sigma_{\varepsilon_R}\right)^2\sum_{i=-\frac{S-1}{2}}^{\frac{S-1}{2}}i^2 = \frac{3}{{A_{und}}^2\Delta x^2S\left(S^2-1\right)}\sigma_{\varepsilon_R}^2$$

Likewise the variance of the denominator is

$$Var\left[-\frac{15}{A_{und}\Delta x^2S\left(S^2-4\right)}\sum\varepsilon_{R,i}+\frac{180}{A_{und}\Delta x^4S\left(S^2-1\right)\left(S^2-4\right)}\sum x_i^2\varepsilon_{R,i}\right]$$

$$= Var\left[-\frac{15\sum\left(S^2-1+12i^2\right)\varepsilon_{R,i}}{A_{und}\Delta x^2S\left(S^2-1\right)\left(S^2-4\right)}+\right] = \frac{180}{A_{und}^2\Delta x^4S\left(S^2-1\right)\left(S^2-4\right)}\sigma_{\varepsilon_R}^2$$

By the binomial expansion, $1/(1-z) = 1 + z + z^2 + z^3 \cdots$ which can be approximated with $1 + z$ as long as the magnitude of z is well below 1. Thus as long as we can make the following assumption:

$$A_{und}^2 \Delta x^4 S\left(S^2-1\right)\left(S^2-4\right) \gg 180\sigma_{\varepsilon_R}^2 \qquad (2),$$

and as long as the numerator and denominator errors are not large, a linear approximation can be used for the variance of $\hat{x}_{opt}$ as follows:

$$\begin{aligned} Var\left(\hat{x}_{opt}\right) &\approx \frac{3}{A_{und}^2 \Delta x^2 S\left(S^2-1\right)}\sigma_{\varepsilon_R}^2 \\ &\quad + x_{opt}^2 \cdot \frac{180}{A_{und}^2 \Delta x^4 S\left(S^2-1\right)\left(S^2-4\right)}\sigma_{\varepsilon_R}^2 \\ &= \frac{\sigma_{\varepsilon_R}^2}{A_{und}^2 \Delta x^2} \frac{3\left(S^2-4\right)+180x_{opt}^2}{S\left(S^2-1\right)\left(S^2-4\right)} \end{aligned}$$

The standard error of the clinical optimum, being the square root of this, is therefore

$$SE\left(\hat{x}_{opt}\right) \approx \frac{\sigma_{\varepsilon_R}}{A_{und}\Delta x} \frac{\sqrt{3}\sqrt{1+\frac{60}{S^2-4}\left(\frac{x_{opt}}{\Delta x}\right)^2}}{\sqrt{S\left(S^2-1\right)}}.$$

3.4. Contributory Factors to Imprecision of the Clinical Optimum

In general the optimization protocol may have multiple replicates, *i.e.* $R \geq 1$, in order to reduce the effect of noise. $\sigma_{\varepsilon_R} = \sigma_{\varepsilon_1}/\sqrt{R}$ so that in terms of the fundamental biological characteristics, the standard error of the clinical optimum is

$$\begin{aligned} &SE\left(\hat{x}_{opt}\right) \\ &\approx \frac{\sqrt{3}}{\sqrt{R\cdot S}} \cdot \frac{1}{\Delta x\sqrt{\left(S^2-1\right)}} \cdot \frac{\sigma_{\varepsilon_1}}{A_{und}} \cdot \sqrt{1+\frac{60}{S^2-4}\left(\frac{x_{opt}}{\Delta x}\right)^2} \end{aligned} \qquad (3)$$

This formulation highlights the 4 contributory factors to imprecision of the optimum clearly. First, the imprecision of the clinical optimum falls with the square root of $R \cdot S$, the number of individual physiological measurements made. Since making additional measurements either consumes scarce time in a clinical environment, or battery power if conducted automatically by the pacemaker, having knowledge of this tradeoff between number of measurements and imprecision may be helpful.

Second, by observing that the second term is almost the reciprocal of the width of the range of settings tested, $(S-1)\Delta x$, it can be seen that the wider the range tested, the more precise the optimum. In practice this is limited by loss of fit to the parabola for settings far from the optimum. However, within the range over which behaviour is parabolic, this analysis suggests it is desirable to cover a wide range rather than to focus exclusively on the very close vicinity of the optimum.

Third, biology sets an lower limit on $\frac{\sigma_{\varepsilon_1}}{A_{und}}$. While measurement error can be reduced by choosing measurement techniques with smaller instrument noise, eventually almost all the variability between replicates is genuine biological variation between heart beats, which places a lower boundary on σ_{ε_1}. Meanwhile A_{und} is a manifestation of dependence of physiology upon changes in pacemaker setting, and is determined by the patient's own biological characteristics. For ideal measurement modalities, where the equipment contributes no noise, all the variability is biological, and may well be similar across different modalities. For example, measures of pressure and flow, although fundamentally different and having distinct units, may change proportionally with the same constant of proportionality in response to both signal (change in pacemaker setting) and noise (spontaneous biological variability). Thus $\frac{\sigma_{\varepsilon_1}}{A_{und}}$ may have a biologically-imposed lower limit within an individual patient which cannot be improved upon by the clinician.

The final term can be neglected if the optimum is very close to the centre of the tested range, *i.e.* $\left|x_{opt}\right| \ll \frac{S-1}{2}\Delta x$. However, it rises as $\left|x_{opt}\right|$ rises. For rapid interpretation by non-mathematicians it may be useful to develop a dimensionless variable E, representing how far the true optimum is away from the centre of the tested range, running from 0 when $x_{opt} = 0$, to 1 when $\left|x_{opt}\right| = \frac{S-1}{2}\Delta x$.

Reworking Equation (3) to use this, and introducing $W = (S-1)\Delta x$, the width of the range of settings tested, gives:

$$SE\left(\hat{x}_{opt}\right) \approx \frac{\sqrt{3}}{\sqrt{R\cdot S}} \cdot \frac{1}{W} \frac{S-1}{\sqrt{S^2-1}} \cdot \frac{\sigma_{\varepsilon_1}}{A_{und}} \cdot \sqrt{1+15\frac{(S-1)^2}{S^2-4}E^2} \qquad (4)$$

This formula is only valid when the condition described above in (2) is satisfied. That condition, the bare minimum number of raw measurements needed before the standard error of the optimum can be validly estimated, can be approximated in this simplified way:

$$R\cdot S \gg 180\left(\frac{\sigma_{\varepsilon_1}}{W^2 A_{und}}\right)^2 \qquad (5)$$

If $R \cdot S$ exceeds the above formula by (for example) more than 5-fold, the uncertainty of the optimum is identified reliably using Equation (4). If $R \cdot S$ exceeds by only a small margin, Equation (4) will underestimate the observed scatter between repeat optimizations. Finally, if $R \cdot S$ does not even exceed the right hand side, the dataset is so poor in information content that it should be discarded, and the protocol redesigned.

In practice the doctor does not know the underlying values of σ_{ε_1} and A_{und} but instead assesses them from clinical measurements: $\hat{\sigma}_{\varepsilon_1}$ and $\hat{A}$ respectively.

Figure 2 summarizes all the relevant variables in a format convenient for visual appreciation. It shows the steps necessary to gauge the uncertainty of the optimum.

The expressions can be applied to any unit of "pacemaker setting", and any unit of "physiological response". Typically pacemaker settings (atrioventricular and interventricular delay) are expressed in either milliseconds or seconds. Physiological response may be based on flow, for which suitable units might be true flow rates (e.g. ml/min, L/min) or expressed per beat (ml/beat), or as a peak instantaneous flow rate, or as an average velocity (cm/min or m/min) or peak velocity, or velocity-time integral (cm/beat). Alternatively physiological response may be pressure (e.g. mmHg) as a systolic, mean, or pulse pressure, or a value derived from pressure such as intraventricular peak first derivative of pressure (dp/dt_{max}). In principle uncalibrated physiological response variables and even those of unknown physical unit may be used, as long as it is reasonable to believe they vary approximately linearly with cardiac performance.

Any physical units may be used to express scatter σ_{ε_1} and width W but, once they are decided, the units that must be used to express curvature A_{und} are [scatter]/[width]^2.

3.5. Simplified Expression for Rapid Appreciation

In practice the number of settings tested is usually fairly large, e.g. S ≥ 6, and $|E|$ does not exceed 1. Thus to explain the implications of the formula to a non-mathematician protocol designer, it may be sufficient to use the following simplified approximation. First check that $R \cdot S \gg 180\left(\frac{\hat{\sigma}_{\varepsilon_1}}{W^2 \hat{A}}\right)^2$, otherwise redesign the experiment, with more replicates or with a variable which has a smaller $\hat{\sigma}_{\varepsilon_1} / \hat{A}$ ratio. Second:

$$SE\left(\hat{x}_{opt}\right) \sim \frac{\sqrt{3}}{W\sqrt{R \cdot S}} \cdot \frac{\sigma_{\varepsilon_1}}{A_{und}} \sqrt{1+15E^2} \qquad (6)$$

The left factor contains 3 variables known precisely from the experimental design. The right factor contains 3 variables that must be estimated from observations in the patient.

3.6. Examples of Application to Existing Protocols

3.6.1. Example 1. Atrioventricular Delay Optimization

In a published study [10] of clinical optimization in 15 patients, there were S = 6 atrioventricular delay settings tested, and R = 6 replicate measurements. The width of the spectrum of settings covered was W = 0.200 − 0.040 s = 0.160 s. The observed scatter between individual replicate measurements was $\hat{\sigma}_{\varepsilon_1}$ = 3.9 mmHg. The observed curvature was $\hat{A}$ = 1194 mmHg·s^{-2}. With these observed data, $180\left(\frac{\hat{\sigma}_{\varepsilon_1}}{W^2 \hat{A}}\right)^2$ was 2.9, which $R \cdot S$ comfortably exceeded.

For an optimum lying near the middle of the tested range, $E \approx 0$, so $SE\left(\hat{x}_{opt}\right) \approx \frac{\sqrt{3}}{\sqrt{6 \times 6}} \cdot \frac{1}{0.200} \cdot \frac{5}{\sqrt{35}} \cdot \frac{3.9}{1194} \approx 0.005$ s. For optima half-way to the edge of the tested spectrum, $SE\left(\hat{x}_{opt}\right)$ is almost double, at 0.010 s. For optima at the edge of the tested spectrum, $SE\left(\hat{x}_{opt}\right)$ is almost 4-fold higher than at the middle of the range, *i.e.* ≈ 0.019 s.

Pacemakers only permit quantized values to be programmed, for example in steps of 0.010 s. For optima lying near the centre of the tested range in that study, the optimization procedure can be seen to be sufficient to identify the optimum for clinical purposes. However, for optima at the edge of the tested range, the protocol would need to be adjusted to maintain that level of optimization precision. The most generically effective step to achieve this would be to conduct more replicate measurements.

3.6.2. Example 2. Interventricular Delay Optimization

In the same study, [10] optimization of interventricular delay was also examined. There were again S = 6 settings tested, and R = 6 replicate measurements. The width of the spectrum of settings covered was W = 0.120 s. Observed measurement scatter $\hat{\sigma}_{\varepsilon_1}$ = 3.9 mmHg. Curvature was measured to be A_{und} = 67 mmHg·s^{-2}. The bare minimum number of measurements needed $180\left(\frac{\hat{\sigma}_{\varepsilon_1}}{W^2 \hat{A}}\right)^2$ is ~2900, which $R \cdot S$ falls far below. This signals that application of Equation (4) will likely substantially underestimate the true standard error of the optimum.

Despite therefore being only a crude lower estimate,

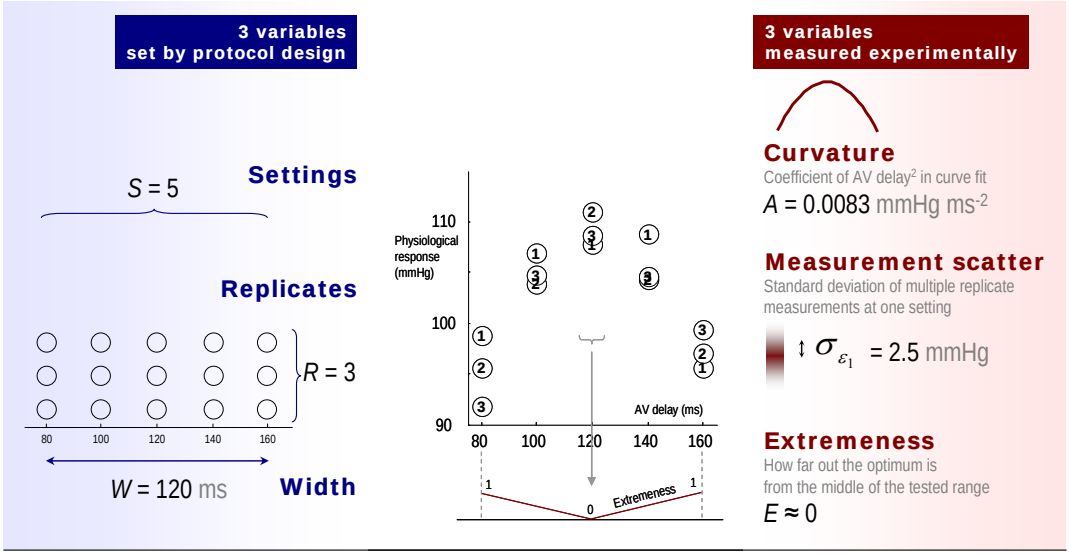

Step 1. **To exclude grossly inadequate optimizations**, check that In this case, 15 >> 0.08, which is very satisfactory.

$$R \cdot S >> 180\left(\frac{\hat{\sigma}_{\varepsilon_1}}{W^2 \hat{A}}\right)^2$$

Step 2. **Calculate standard error of optimum**

$$SE\left(\hat{x}_{opt}\right) \approx \frac{\sqrt{3}}{\sqrt{R \cdot S}} \cdot \frac{1}{W} \frac{S-1}{\sqrt{S^2-1}} \cdot \frac{\hat{\sigma}_{\varepsilon_1}}{\hat{A}} \cdot \sqrt{1+15\frac{(S-1)^2}{S^2-4}E^2} \approx 0.9 \text{ ms}$$

Figure 2. Illustration of the 6 variables that affect precision of the optimum. Note: Three are set by the design of the protocol and are therefore under the control of the clinician (within reason) and three are measured experimentally and depend on biology and on the physiological variable chosen for monitoring. Step 1 highlights the necessity for performing enough replicate measurements before attempting to calculate a standard error.

for an optimum lying in the middle of the tested range, Equation (4) provides $SE\left(\hat{x}_{opt}\right)$ > ~0.118 s. For optima at the edge of the tested spectrum, $SE\left(\hat{x}_{opt}\right)$ is 4-fold higher, *i.e.* > ~0.422 ms. These lower limits on the standard error are so large that the 95% confidence intervals (±1.96 standard errors) dwarf the entire spectrum of clinically plausible settings.

This analysis shows that interventricular delay optimization conducted in this way in such patients is unreliable. Interventricular delay optimization protocols recommending a few (or even just one) measurement at each setting will never work. Biological variability has an ineradicable lower limit which can only be overcome by repetitions so numerous as to be unrealistic for manual methods such as echocardiography, and challenging even for automatable haemodynamic approaches.

The curious silence of the world literature on the elementary question of blinded test-retest reproducibility of interventricular delay optimization is a dog that didn't bark [11].

3.7. Examples of Application in Protocol Design

A doctor designing an optimization protocol can use this formula to ensure that the protocol delivers a clinically-satisfactory degree of precision. Suppose the protocol needs to deliver optimization within ±0.010 s on 95% of occasions, *i.e.* $SE\left(\hat{x}_{opt}\right)$ needs to be 0.005 s. Rewriting Equation (4), we see that the number of replicate measurements required is:

$$R \approx 3\frac{(S-1)^2}{S^3-S}\left(\frac{1}{W \cdot SE\left(\hat{x}_{opt}\right)} \cdot \frac{\sigma_{\varepsilon_1}}{A_{und}}\right)^2 \cdot \left(1+15\frac{(S-1)^2}{S^2-4}E^2\right) \quad (7).$$

A simplified form of the relationship, for easy appreciation by non-mathematicians, is shown below:

$$R \sim \frac{3}{S}\left(\frac{1}{W \cdot SE\left(\hat{x}_{opt}\right)} \cdot \frac{\sigma_{\varepsilon_1}}{A_{und}}\right)^2 \cdot \left(1+15E^2\right)$$

Three of the variables are handled easily. The protocol designer can choose how many settings to test (S, e.g. 6), and the width covered (W, e.g. 0.160 s) and can arrange from physiological knowledge that the optimum will lie in the middle 50% of the spectrum of tested settings, *i.e.* $E < 1/2$.

The value of $\hat{\sigma}_{\varepsilon_1} / \hat{A}$ must be assessed experimentally

for each proposed optimization variable. This requires only a few minutes per subject.

Table 1 shows how this ratio, and other variables, affect the number of replicates needed, *R*, to achieve the desired optimization precision.

Although mathematically the tested range *W*, the required precision $SE\left(\hat{x}_{opt}\right)$, and the scatter-to-curvature ratio $\hat{\sigma}_{\varepsilon_1} \big/ \hat{A}$ each have the same impact on the number of replicates required, in clinical practice $\hat{\sigma}_{\varepsilon_1} \big/ \hat{A}$ has by far the greatest range of possible values, and the design process should therefore focus on ensuring that this is small, if the optimization protocol is to be practical.

The many haemodynamic variables that are affected by AV delay appear to be initially change proportionally [12] which suggests that A_{und} may be approximately the same proportion of the baseline value of each variable. The protocol designer desiring small $\hat{\sigma}_{\varepsilon_1} \big/ \hat{A}$ should therefore favour the variable whose scatter $\hat{\sigma}_{\varepsilon_1}$ is the smallest proportion of its baseline value.

4. Limitations

Although it is convenient to describe optimization responses with a parabola, the true underlying shape may

Table 1. Impact of physiology (scatter, curvature and extremeness) and protocol design (number of tested settings, width of spectrum) on the number of replicates needed for optimization of a desired level of precision.

Distribution of tested settings and physiological characteristics							Number of replicates per setting needed to achieve this
Number of tested settings	Width of spectrum	Desired precision	Extremeness	Scatter	Curvature	Scatter/ Curvature ratio	
S	W	$SE\left(\hat{x}_{opt}\right)$	E	$\hat{\sigma}_{\varepsilon_1}$	$\hat{A}$	$\hat{\sigma}_{\varepsilon_1} \big/ \hat{A}$	R
	s	s		mmHg	mmHg·s^{-2}	s^2	
6	0.16	0.010	0.5	3.9	1194	0.00327	**6**
6	0.16	0.005	0.5	3	**30**	0.1	**21,929**
6	0.16	0.005	0.5	3	**100**	0.03	**1974**
6	0.16	0.005	0.5	3	**300**	0.01	**219**
6	0.16	0.005	0.5	3	**1000**	0.003	**20**
6	0.16	0.005	0.5	3	**3000**	0.001	**2**
6	0.16	0.005	0.5	**1**	1000	0.001	**2**
6	0.16	0.005	0.5	**3**	1000	0.003	**20**
6	0.16	0.005	0.5	**10**	1000	0.01	**219**
6	0.16	0.005	0.5	**30**	1000	0.03	**1974**
6	0.16	0.005	**0**	3	1000	0.003	**5**
6	0.16	0.005	**0.25**	3	1000	0.003	**9**
6	0.16	0.005	**0.5**	3	1000	0.003	**20**
6	0.16	0.005	**0.75**	3	1000	0.003	**38**
6	0.16	0.005	**1**	3	1000	0.003	**64**
6	0.16	**0.002**	0.5	3	1000	0.003	**123**
6	0.16	**0.005**	0.5	3	1000	0.003	**20**
6	0.16	**0.010**	0.5	3	1000	0.003	**5**
6	0.16	**0.020**	0.5	3	1000	0.003	**1**
6	**0.08**	0.005	0.5	3	1000	0.003	**79**
6	**0.12**	0.005	0.5	3	1000	0.003	**35**
6	**0.16**	0.005	0.5	3	1000	0.003	**20**
6	**0.20**	0.005	0.5	3	1000	0.003	**13**
4	0.16	0.005	0.5	3	1000	0.003	**24**
6	0.16	0.005	0.5	3	1000	0.003	**20**
8	0.16	0.005	0.5	3	1000	0.003	**17**
10	0.16	0.005	0.5	3	1000	0.003	**14**
12	0.16	0.005	0.5	3	1000	0.003	**13**

In practice the number of tested settings, width of spectrum, desired precision, and extremeness, all have a limited range of realistic values (as shown). In contrast, curvature and scatter have a wide range of possible values and, although rarely formally quantified in research reports, have enormous impact on the precision of the optimization process. This table can be used for physiological response measures that have any measurement unit (not only mmHg) since it is the relative size of scatter versus curvature, rather than their absolute values, that is important. For example, if "mmHg" was replaced by "% of value at reference setting", the table could without any other alteration be used for any variable such as echo-Doppler velocity-time integral, uncalibrated pressure signal, bioimpedance-derived stroke volume, or any marker of pulsatility in the peripheral circulation.

be more complex. For example, where intrinsic (or even just fusion) conduction becomes active as AV delay is lengthened, the data points may deviate upwards from the parabolic trend, and so fitting to a parabola may bias the fitted AV delay optimum toward higher values. Nevertheless, the principles in this manuscript would still hold true. Moreover, in the close vicinity of the optimum, which is relevant to precise optimization, curvature may be closer to parabolic.

Merely applying formulae will not make optima more precise. Only selecting a physiological variable of suitably low $\hat{\sigma}_{\varepsilon_1} / \hat{A}$ ratio, and taking time to conduct enough measurements (shown in Equation (7)), can improve precision. Lack of interest in scatter and curvature in a doctor conducting optimization is as uninspiring as lack of interest in wings and engines in an aircraft pilot.

5. Conclusions

The practical implications may be summarized from inspection of each factor in Equation (6) in turn. To obtain precise clinical optima:

- most importantly, either commit enough resources to obtain enough measurements, or do not embark on optimization;
- cover a wide range of pacemaker settings while remaining within the parabolic region of the response curve;
- choose a physiological variable with as narrow a random variability (in relation to its sensitivity to pacemaker setting change) as possible; and
- if possible, design the spectrum of settings tested so that the true optimum will lie near its middle rather than at an extreme.

Clinicians treating patients and scientists designing and conducting studies have not had simple, quick methods to establish the uncertainty in planned or actual optimization procedures. As a result, patients may be undergoing apparent optimization procedures that are in fact worsening the programming of their pacemaker. Moreover without methods for recognizing unreliable optimizations, clinicians finding the optimum appearing to change every 1 or 2 years may feel compelled to carry out worthless optimization procedures more frequently, [8] which wastes clinical resources and may be harmful to patients.

The results in this paper permit easy quantification of uncertainty of the optimum of a cardiac resynchronization therapy pacemaker. They help patients gain the best physiological benefit, help doctors design protocols that deliver efficient and reliable optimization, and assist in distinguishing genuine change in patient physiology over time, versus random noise.

An unexamined optimization is not worth doing.

6. Acknowledgements

The author is supported by a Senior Research Fellowship (FS/10/038) from the British Heart Foundation.

7. References

[1] W. T. Abraham, W. G. Fisher and A. L. Smith, "Cardiac Resynchronization in Chronic Heart Failure," *New England Journal of Medicine*, Vol. 346, 2002, pp. 1845-1853. doi:10.1056/NEJMoa013168

[2] A. Kyriacou, P. A. Pabari, and D. P. Francis, "Cardiac Resynchronization Therapy Is Certainly Cardiac Therapy, But How Much Resynchronization and How Much Atrioventricular Delay Optimization?" *Heart Failure Reviews*, 2011, Article in Press. doi:10.1007/s10741-011-9271-1

[3] J. G. Cleland, J. C. Daubert, E. Erdmann, N. Freemantle, D. Gras, L. Kappenberger and L. Tavazzi, "Cardiac Resynchronization-Heart Failure (CARE-HF) Study Investigators. The Effect of Cardiac Resynchronization on Morbidity and Mortality in Heart Failure," *New England Journal of Medicine*, Vol. 352, No. 15, 2005, pp. 1539-1549. doi:10.1056/NEJMoa050496

[4] A. Auricchio, C. Stellbrink, S. Sack, M. Block, J. Vogt, P. Bakker, C. Huth, F. Schöndube, U. Wolfhard, D. Böcker, O. Krahnefeld and H. Kirkels, "Pacing Therapies In Congestive Heart Failure (PATH-CHF) Study Group. Long-Term Clinical Effect of Hemodynamically Optimized Cardiac Resynchronization Therapy in Patients With Heart Failure and Ven-Tricular Conduction Delay," *Journal of the American College of Cardiology*, Vol. 39, No. 12, 2002, pp. 2026-2033. doi:10.1016/S0735-1097(02)01895-8

[5] M. D. Bogaard, P. A. Doevendans, G. E. Leenders, P. Loh, R. N. Hauer, H. van Wessel and M. Meine, "Can Optimization of Pacing Settings Compensate for a Non-Optimal Left Ventricular Pacing Site?" *Europace*, Vol. 12, No. 9, 2010, pp. 1262-1269. doi:10.1093/europace/euq167

[6] I. E. van Geldorp, T. Delhaas, B. Hermans, K. Vernooy, B. Broers, J. Klimusina, F. Regoli, F. F. Faletra, T. Moccetti, B. Gerritse, R. Cornelussen, J. Settels, H. J. Crijns, A. Auricchio and F. W. Prinzen, "Comparison of a Non-Invasive Arterial Pulse Contour Technique and Echo Doppler Aorta Velocity-Time Integral on Stroke Volume Changes in Optimization of Cardiac Resynchronization Therapy," *Europace*, Vol. 13, No. 1, 2011, pp. 87-95. doi:10.1093/europace/euq348

[7] Z. I. Whinnett, J. E. Davies, G. Nott, K. Willson, C. H. Manisty, N. S. Peters, P. Kanagaratnam, D. W. Davies, A. D. Hughes, J. Mayet and D. P. Francis, "Efficiency, Reproducibility and Agreement of Five Different Hemodynamic Measures for Optimization of Cardiac Resynchronization Therapy," *International Journal of Cardiology*, Vol. 129, No. 2, 2008, pp. 216-226.

doi:10.1016/j.ijcard.2007.08.004

[8] P. A. Pabari, K. Willson, B. Stegemann, I. E. van Geldorp, A. Kyriacou, M. Moraldo, J. Mayet, A. D. Hughes and D. P. Francis, "When Is an Optimization Not an Optimization? Evaluation of Clinical Impli-Cations of Information Content (Signal-to-Noise Ratio) in Optimization of Cardiac Resynchronization Therapy, and How to Measure and Maximize It," *Heart Failure Reviews*, Vol. 16, No. 3, 2011, pp. 277-290. doi:10.1007/s10741-010-9203-5

[9] W. T. Abraham, D. Gras, C. M. Yu, L. Guzzo and M. S. Gupta, "Rationale and Design of A Randomized Clinical Trial to Assess the Safety and Efficacy of Frequent Optimization of Cardiac Resynchronization Therapy: The Frequent Optimization Study Using the Quickopt Method (FREEDOM) Trial," *American Heart Journal*, Vol. 159, No. 6, 2010, pp. 944-948. doi:10.1016/j.ahj.2010.02.034

[10] Z. I. Whinnett, J. E. R. Davies, K. Willson, C. H. Manisty, A. C. Chow, R. A. Foale, D. W. Davies, A. D. Hughes, J. Mayet and D. P. Francis, "Haemodynamic Effects of Changes in AV and VV Delay in Cardiac Resynchronization Therapy Show a Consistent Pattern: Analysis of Shape, Magnitude and Relative Importance of AV and VV Delay," *Heart*, Vol. 92, 2006, pp. 1628-1634. doi:10.1136/hrt.2005.080721

[11] A. C. Doyle, "The Curious Incident of the Dog in the Night-Time," *Strand Magazine*, Vol. 4, No. 4, 1892, pp. 645-660. http://www.archive.org/download/StrandMagazine24/Strand24_text.pdf

[12] C. H. Manisty, A. Al-Hussaini, B. Unsworth, R. Baruah, P. A. Pabari, J. Mayet, A. D. Hughes, Z. I. Whinnett and D. P. Francis, "The Acute Effects of Changes to AV Delay on Blood Pressure and Stroke Volume: Potential Implications for Design of Pacemaker Optimization Protocols," *Circulation*: *Arrhythmia and Electrophysiology*, Article in Press.

Applied Mathematics, **2011, 2, 1507-1514**
doi:10.4236/am.2011.212213 Published Online December 2011 (http://www.SciRP.org/journal/am)

Pattern Formation in Tri-Trophic Ratio-Dependent Food Chain Model

Dawit Melese, Sunita Gakkhar
Department of Mathematics, Indian Institute of Technology Roorkee, Roorkee, India
E-mail: *mahifikir@gmail.com, sungkfma@iitr.ernet.in*
Received October 27, 2011; *revised November* 26, 2011; *accepted December* 5, 2011

Abstract

In this paper, a spatial tri-trophic food chain model with ratio-dependent Michaelis-Menten type functional response under homogeneous Neumann boundary conditions is studied. Conditions for Hopf and Turing bifurcation are derived. Sufficient conditions for the emergence of spatial patterns are obtained. The results of numerical simulations reveal the formation of labyrinth patterns and the coexistence of spotted and stripe-like patterns.

Keywords: Reaction-Diffusion Equations, Hopf Bifurcation, Turing Instability, Turing Pattern, Food Chain

1. Introduction

Food chains in the environment are very important systems in ecological science, applied mathematics, economic and engineering science [1]. They have been applied to management in Aquatic ecosystem for problems like water quality and lake management [2]. Modeling of food chain dynamics has challenges in the fields of both theoretical ecology and applied mathematics. Tri-trophic food chain models have been studied in both spatially homogeneous [1-4] and spatially inhomogeneous environments [5-10] for the last two decades. Those models exhibit rich and complex dynamics and nonlinear mathematical behavior, including varying numbers and stability of equilibrium states, limit cycles, patterns and chaos.

It is well known that in real life, the resources are not uniformly distributed in the habitat. The biological species move (diffuse) from place to place in search of food in their habitat and hence interact with each other and with the environment. This movement (diffusiveness) of species has an impact on their trophic interactions. Consequently, spatial patterns evolve.

One can easily observe patterns in both aquatic and terrestrial populations [10]. A number of recent contributions have begun to suggest that it is critical to begin to fully consider the implications of spatial flows on the dynamics of ecological communities [7]. In the literatures [11,12], the spatial component of ecological interactions (trophic-interactions) is identified as an important factor in shaping ecological communities. However, there is lack of recognition about the role of spatial considerations in food chain dynamics [7]. In addition to this, ignorance of spatial scales of food chains limits our ability to predict how trophic interactions will vary in different contexts, across space and time [2]. The dynamics and stability of the interacting species in relation to spatial phenomena such as pattern formation has recently become a focus of intensive research in theoretical ecology [13], chemical and biological systems [14]. The spatial patterns modify the temporal dynamics at a range of spatial scales, whose effects must be incorporated in temporal ecological models that do not represent space explicitly. In recent decades, stationary patterns induced by diffusion have been studied extensively, and lots of important phenomena have been observed.

Spatial patterns of interacting species are ubiquitous in nature and may occur due to stochastic process, environmental fluctuations or variability, or deterministic process, growth and movement of interacting species. The deterministic process is intrinsic to the interacting species and results in population-driven and self-organized spatial patterns. The formation of population-driven spatial patterns was first pointed out by Alan Turing. Turing, one of the key scientist of the 20^{th} century, mathematically showed that a system of coupled reaction-diffusion equations can give rise to spatial concentration patterns of a fixed characteristic length from an arbitrary initial configuration due to diffusion—driven instability or Turing instability [15].

Reaction-Diffusion systems are capable of qualitatively imitating many biological patterns such as the stripes of a zebra, tiger and snakes or spots of a cheetah and

even more irregular patterns such as those on leopards and giraffes, the patterns on exotic fish, butterflies or beetles through Turing instability.

Pattern formation for two species model [11-14,16-19] based on coupled reaction diffusion equations has been intensively investigated. The necessary and sufficient condition for Turing instability, which leads to the formation of spatial patterns, has been derived [9,16,17,20] and very interesting patterns are also obtained from the numerical simulation results [9,21,22].

For three species case, the authors [2,23] used a three species interacting discrete model to study the formation of pattern. In the literatures [9,10,24], the authors have considered a food chain model with diffusion and investigate the persistence of the system, the stability of the positive steady state solution of the system.

In this paper, the formation of patterns in a tri-trophic food chain model with ratio-dependent Michaelis-Menten type functional response and diffusion has been investigated.

The organization of the paper is as follows: In Section 2 the mathematical model is given. Section 3 is devoted to the stability and bifurcation analysis of the system. Section 4 presents the results of numerical simulations. Section 5 is devoted to some conclusions.

2. The Mathematical Model

Let $U(X,Y,T)$, $V(X,Y,T)$ and $W(X,Y,T)$ denote the densities of the prey, intermediate predator and top predator respectively at time T and position (X,Y) in the habitat $\Omega \subseteq \mathbb{R}_+^2$. The prey is assumed to grow logistically. The intermediate predator, *V*, and the top predator, *W*, follow the ratio-dependent Michaelis-Menten type functional response. Thus the mathematical model governing the spatiotemporal dynamics of the three interacting species prey-predator community can be described by the following system of reaction-diffusion equations.

$$\begin{cases} \dfrac{\partial U}{\partial T} - D_1\left(\dfrac{\partial^2 U}{\partial X^2} + \dfrac{\partial^2 U}{\partial Y^2}\right) = r\left(1-\dfrac{U}{K}\right)U - \dfrac{B_1 UV}{U+\beta_1 V}, \\ \qquad\qquad (X,Y)\in\Omega, \\ \dfrac{\partial V}{\partial T} - D_2\left(\dfrac{\partial^2 V}{\partial X^2} + \dfrac{\partial^2 V}{\partial Y^2}\right) = \dfrac{B_2 UV}{U+\beta_1 V} - \dfrac{B_3 VW}{V+\beta_2 W} - B_4 V, \\ \qquad\qquad (X,Y)\in\Omega, \\ \dfrac{\partial W}{\partial T} - D_3\left(\dfrac{\partial^2 W}{\partial X^2} + \dfrac{\partial^2 W}{\partial Y^2}\right) = \dfrac{B_5 VW}{V+\beta_2 W} - B_6 W, (X,Y)\in\Omega, \\ \dfrac{\partial U}{\partial \nu} = \dfrac{\partial V}{\partial \nu} = \dfrac{\partial W}{\partial \nu} = 0, \qquad (X,Y)\in\partial\Omega, \\ U(X,Y,0) = U_0(X,Y) \ge 0, V(X,Y,0) = V_0(X,Y) \ge 0, \\ W(X,Y,0) = W_0(X,Y) \ge 0, \qquad (X,Y)\in\Omega. \end{cases} \tag{1}$$

The reaction parameters are assumed to be positive constants and have the usual biological meaning. The positive constants D_1, D_2 and D_3 are the diffusion coefficients of U, V and W respectively. ν is the outward unit normal vector to the smooth boundary $\partial\Omega$. The initial population densities $U_0(X,Y)$, $V_0(X,Y)$ and $W_0(X,Y)$ are assumed to be positive and continuous functions.

Introduce the following non-dimensional variables and parameters so as to reduce the number of parameters of the system (2.1):

$$u = \frac{U}{K},\ v = \frac{\beta_1 V}{K},\ w = \frac{\beta_1\beta_2 W}{K},\ t = rT,$$
$$x = X\sqrt{\frac{r}{D_2}},\ y = Y\sqrt{\frac{r}{D_2}},\ d_1 = \frac{D_1}{D_2},\ d_3 = \frac{D_3}{D_2},$$
$$c_1 = \frac{B_1}{r\beta_1},\ c_3 = \frac{B_3}{r\beta_2},\ c_i = \frac{B_i}{r}(i = 2,4,5,6).$$

The spatio-temporal system (2.1) is transformed to the following system of equations in non-dimensional variables:

$$\begin{cases} \dfrac{\partial u}{\partial t} - d_1\left(\dfrac{\partial^2 u}{\partial x^2} + \dfrac{\partial^2 u}{\partial y^2}\right) = (1-u)u - \dfrac{c_1 uv}{u+v}, (x,y)\in\Omega, \\ \dfrac{\partial v}{\partial t} - \left(\dfrac{\partial^2 v}{\partial x^2} + \dfrac{\partial^2 v}{\partial y^2}\right) = \dfrac{c_2 uv}{u+v} - \dfrac{c_3 vw}{v+w} - c_4 v, (x,y)\in\Omega, \\ \dfrac{\partial w}{\partial t} - d_3\left(\dfrac{\partial^2 w}{\partial x^2} + \dfrac{\partial^2 w}{\partial y^2}\right) = \dfrac{c_5 vw}{v+w} - c_6 w, (x,y)\in\Omega, \\ \dfrac{\partial u}{\partial \nu} = \dfrac{\partial v}{\partial \nu} = \dfrac{\partial w}{\partial \nu} = 0, \qquad (x,y)\in\partial\Omega, \\ u(x,y,0) = u_0(x,y) \ge 0, v(x,y,0) = v_0(x,y) \ge 0, \\ w(x,y,0) = w_0(x,y) \ge 0, \qquad (x,y)\in\Omega. \end{cases} \tag{2}$$

3. Stability and Bifurcation Analysis

The spatio-temporal system (2) has at most three spatially homogeneous non-negative steady states:

1) predators free steady state: $E_0 = (1,0,0)$

2) top predator free steady state: $E_1 = (u',v',0)$

$$u' = 1 - c_1\left(1 - \frac{c_4}{c_2}\right), v' = \left(-1 + \frac{c_2}{c_4}\right)u',$$

3) coexistence of the three species: $E = (\tilde{u},\tilde{v},\tilde{w})$;

$$\tilde{u} = c_1\left(-1 + \frac{1}{A}\right) + 1, \tilde{v} = (A-1)\tilde{u},$$
$$\tilde{w} = \left(-1 + \frac{c_5}{c_6}\right)\tilde{v}, A = \frac{c_2 c_5}{c_3(c_5 - c_6) + c_4 c_5}.$$

The equilibrium point E lies in the first octant if and

only if

$$c_5 > c_6, A > 1, 0 < c_1 < \frac{A}{A-1} \tag{3}$$

From biological point of view the stability of the non-trivial steady state E which ensures the coexistence of the three species is of interest.

To perform linear stability analysis, the spatio-temporal system (2) is linearized at the spatially homogeneous steady state E for small space and time dependent fluctuations. For this, set

$$u(x,y,t) = \tilde{u} + \bar{u}(x,y,t); |\bar{u}(x,y,t)| \ll \tilde{u},$$
$$v(x,y,t) = \tilde{v} + \bar{v}(x,y,t); |\bar{v}(x,y,t)| \ll \tilde{v},$$
$$w(x,y,t) = \tilde{w} + \bar{w}(x,y,t); |\bar{w}(x,y,t)| \ll \tilde{w}.$$

Let us assume solutions of the form

$$\begin{pmatrix} \bar{u}(x,y,t) \\ \bar{v}(x,y,t) \\ \bar{w}(x,y,t) \end{pmatrix} = \begin{pmatrix} \alpha_0 \\ \alpha_1 \\ \alpha_2 \end{pmatrix} e^{\lambda t} \cos(k_x x)\cos(k_y y),$$

where λ is the growth rate of perturbation in time t, $\alpha_i (i = 0,1,2)$ represent the amplitudes, k_x and k_y are the wave number of the solutions. The corresponding linearized system has the characteristic equation

$$|J - k^2 D - \lambda I| = 0. \tag{4}$$

Here $D = diag(d_1, 1, d_3)$, $k^2 = k_x^2 + k_y^2$ and $J = (a_{ij})_{3x3}$ is the community matrix of the system (2). The elements are obtained as

$$a_{11} = -1 + c_1\left(1 - \frac{1}{A^2}\right), a_{12} = -\frac{c_1}{A^2}, a_{13} = 0,$$
$$a_{21} = \frac{(-1+A)^2 c_2}{A^2}, a_{22} = \left(\frac{c_2}{A^2} - c_4 - c_3\left(1 - \frac{c_6}{c_5}\right)^2\right),$$
$$a_{23} = -\frac{c_3 c_6^2}{c_5^2}, a_{31} = 0, a_{32} = c_5\left(1 - \frac{c_6}{c_5}\right)^2, a_{33} = c_6\left(-1 + \frac{c_6}{c_5}\right).$$

The characteristic equation corresponding to E is

$$\lambda^3 + b_2(k^2)\lambda^2 + b_1(k^2)\lambda + b_0(k^2) = 0, \tag{5}$$

with

$$b_2(k^2) = -(a_{11} + a_{22} + a_{33} - k^2(d_1 + 1 + d_3)),$$

$$b_1(k^2) = a_{11}a_{33} + a_{11}a_{22} + a_{22}a_{33} - a_{32}a_{23} - a_{21}a_{12} - k^2\left((d_1 + d_3)a_{22} + (1 + d_3)a_{11} + (d_1 + 1)a_{33}\right), + k^4(d_1 + d_3 + d_1 d_3)$$

$$b_0(k^2) = -a_{11}a_{33}a_{22} + a_{11}a_{32}a_{23} + a_{12}a_{21}a_{33} + k^2\left((-a_{21}a_{12} + a_{11}a_{22})d_3 + (a_{22}a_{33} - a_{32}a_{23})d_1 + a_{11}a_{33}\right) - k^4(d_1 a_{33} + a_{22}d_3 d_1 + a_{11}d_3) + k^6 d_1 d_3.$$

The reaction-diffusion systems have led to the characterization of two basic types of symmetry-breaking bifurcations—Hopf and Turing bifurcation, responsible for the emergence of spatio-temporal patterns. See, for details, references [15,16,23,24].

According to Routh-Hurwitz criteria $\mathrm{Re}(\lambda(k)) < 0$ if and only if

$$b_0(k^2) > 0, b_2(k^2) > 0, b_1(k^2)b_2(k^2) - b_0(k^2) > 0 \tag{6}$$

Contradiction of any one of the above conditions implies the existence of an eigenvalue with positive real part, hence, instability. Turing instability (or diffusion driven instability) occurs if the homogeneous steady state E is stable in the absence of diffusion $(k^2 = 0)$ but driven unstable by diffusion $(k^2 > 0)$. Thus we need two conditions which must hold simultaneously. First, the spatially uniform steady state must be stable to small perturbation, that is, all $\lambda(k^2)$ in Equation (5) have $\mathrm{Re}(\lambda(k^2 = 0)) < 0$, and second, only patterns of a certain spatial extent, that is, patterns within a definite range of wave length k, can begin to grow, with $\mathrm{Re}(\lambda(k^2 \neq 0)) > 0$.

It is clear that the homogeneous steady state E is locally asymptotically stable if and only if $b_0(0) > 0$, $b_2(0) > 0$ and $b_1(0)b_2(0) - b_0(0) > 0$. But it will be driven unstable by diffusion if any of the conditions in Equation (3.4) fail to hold. However, it can be easily seen that diffusion driven instability cannot occur by contradicting $b_2(k^2) > 0$. Hence, we have to look for conditions which reverse the sign of the other two conditions in Equation (3.4). The expressions for $b_0(k^2)$ and $b_1(k^2)b_2(k^2) - b_0(k^2)$ are both cubic functions of k^2 of the form:

$$F(k^2) = F_3 k^6 + F_2 k^4 + F_1 k^2 + F_0; F_3 > 0, F_0 > 0. \tag{7}$$

The coefficients $F_i (i = 0,1,2,3)$ are given in **Table 1**.

For $F(k^2)$ to be negative for some positive real number $k^2 (\neq 0)$, the minimum must be negative. This minimum occurs at

$$k^2 = k_c^2 = \frac{-F_2 + \sqrt{F_2^2 - 3F_1F_3}}{3F_3}. \tag{8}$$

Now k_c^2 is real and positive if

$$F_1 < 0 \text{ or} \left(F_2 < 0 \text{ and } F_2^2 > 3F_1F_3\right) \tag{9}$$

Hence,

Table 1. Values of $F_i(i = 0, 1, 2, 3)$ of the coefficients $b_0(k^2)$ and $b_1(k^2)$ $b_2(k^2) - b_0(k^2)$ which are used to determine conditions for Turing instability.

	b_0	$b_1b_2 - b_0$
F_3	d_1d_3	$(1+d_1)(1+d_3)(d_1+d_3)$
F_2	$d_1a_{33} + d_3a_{11} + d_1d_3a_{22}$	$-(1+d_3)(1+2d_1+d_3)a_{11}$ $-(d_1+d_3)(2+d_1+d_3)a_{22}$ $-(1+d_1)(1+d_1+2d_3)a_{33}$
F_1	$d_1(a_{22}a_{33} - a_{23}a_{32}) + a_{11}a_{33}$ $+d_3(a_{11}a_{22} - a_{12}a_{21})$	$(1+d_1)(a_{33}^2 - a_{12}a_{21}) + (d_1+d_3)a_{22}^2$ $+(1+d_3)(a_{11}^2 - a_{23}a_{32})$ $+2(1+d_1d_3)(a_{22}a_{33} + a_{11}a_{22} + a_{11}a_{33})$
F_0	$b_0(0)$	$b_1(0)b_2(0) - b_0(0)$

$$F_{\min} = F\left(k_c^2\right) = \frac{2F_2^3 - 9F_1F_2F_3 - 2\left(F_2^2 - 3F_1F_3\right)^{3/2} + 27F_3^2F_0}{27F_3^2} \quad (10)$$

Thus,

$$F\left(k_c^2\right) < 0 \text{ if } 2F_2^3 - 9F_1F_2F_3 - 2\left(F_2^2 - 3F_1F_3\right)^{3/2} + 27F_3^2F_0 < 0 \quad (11)$$

The conditions given in Equations (9) and (11) are sufficient for the occurrence of Turing instability.

At bifurcation, when $F_{\min} = 0$, we require

$$2F_2^3 - 9F_1F_2F_3 - 2\left(F_2^2 - 3F_1F_3\right)^{3/2} + 27F_3^2F_0 = 0 \quad (12)$$

The above discussion is summarized in the following theorem.

Theorem 3.1: The spatio-temporal system (2) will undergo Turing instability at the homogeneous steady state E provided the following two conditions are satisfied:

1) $F_1 < 0$ or $\left(F_2 < 0 \text{ and } F_2^2 > 3F_1F_3\right)$

2) $2F_2^3 - 9F_1F_2F_3 - 2\left(F_2^2 - 3F_1F_3\right)^{3/2} + 27F_3^2F_0 < 0$

Proof: The proof directly follows from the above discussion.

Based on the linear stability analysis of system (2), a two-parameter bifurcation diagram with respect to parameters c_1 and d_1 is obtained for the parametric choice

$$c_2 = 0.9, c_3 = 0.4, c_4 = 0.1, c_5 = 0.3, c_6 = 0.15, d_3 = 10. \quad (13)$$

For this parametric choice, the Hopf bifurcation point is computed as $c_1 = 1.26882$ and the expression for the Turing bifurcation curve is obtained by solving Equation (3.10) for c_1, as a function of d_1. The Hopf line and the Turing bifurcation curve, which are shown in the bifurcation diagram **Figure 1**, separate the parametric space

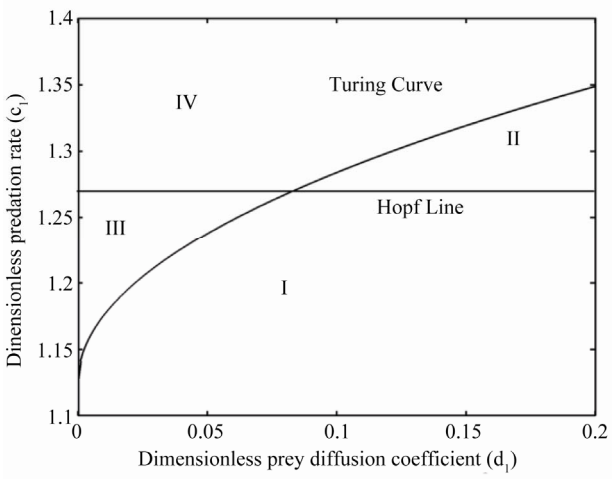

Figure 1. Two parameter bifurcation diagram for the system (2) with parameters (13).

in to four distinct domains. In domain I, located below both of the lines, the steady state is the only stable solution of the system. Domain II and III are the regions of pure Hopf and pure Turing instabilities respectively, while domain IV, which is located above both the curves, is the region of both Hopf and Turing instabilities.

For Turing instability to occur, at least one of the coefficients of the dispersion relation must be negative for some range of k^2. From **Figure 2** it is clear that the coefficient $b_0\left(k^2\right)$ is negative in the range $0 < k^2 < 6$.

4. Spatio-Temporal Pattern Formation

It is well known that it is not always possible to obtain the analytical solutions of coupled system of nonlinear PDE. Hence, one has to use numerical simulations to solve them. The spatio-temporal system (2) is solved numerically in two-dimensional space using a finite difference approximation for the spatial derivatives and an explicit Euler method for the time integration [11]. In order to avoid numerical artifacts the values of the time and space steps have been chosen sufficiently small. This method finally results to a sparse, banded linear system of algebraic equations. The linear system obtained is then solved by using GMRES algorithm [11].

For the numerical simulations, the initial distributions of the species are considered as small spatial perturbation of the uniform equilibrium point.

All the numerical simulations employ the zero-flux (Neumann) boundary conditions in a square habitat of size 50 × 50. Iterations are performed for different step sizes in time and space until the solution seems to be invariant. The time step size of $\Delta t = 0.01$ and space step size $\Delta x = \Delta y = 0.25$ are chosen. In this section, extensive numerical simulations of the spatially extended

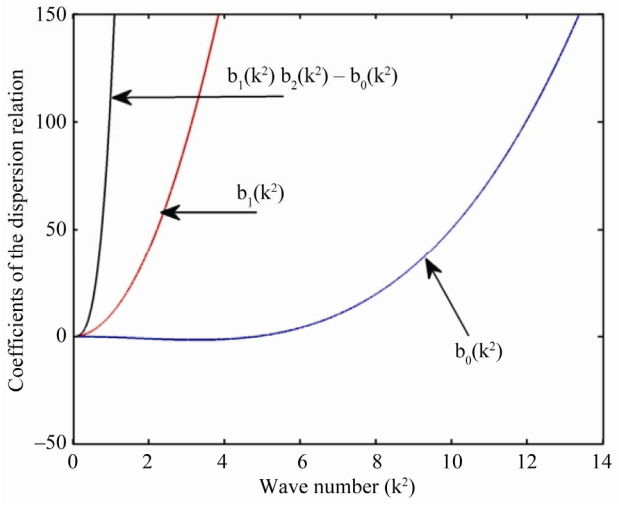

Figure 2. Coefficient of the dispersion relation (5) of the system (2) for parameters (13), c_1 = 1.24, d_1 = 0.01.

system (2) in two-dimensional space are performed and the qualitative results are analyzed. The following system parameters are chosen as fixed based on the stability and bifurcation analysis carried out in Section 3, whereas the control parameter c_1 is varied in the simulation experiments:

$$c_2 = 0.9, c_3 = 0.4, c_4 = 0.1, c_5 = 0.3, c_6 = 0.15, \quad d_1 = 0.01, d_3 = 10. \tag{14}$$

From the analysis and phase-transition bifurcation diagram of **Figure 1**, it is observed that the system dynamics is determined by the values of c_1 and d_1. For different sets of parameters, the feature of the spatial patterns become essentially different if c_1 exceeds the Hopf bifurcation threshold c_{1Hopf} and Turing bifurcation threshold $c_{1Turing}$, which depends on d_1, respectively. For the choice of parameters given in (14), Turing bifurcation threshold and Hopf bifurcation threshold are computed as $c_{1Turing} = 1.1753$ and $c_{1Hopf} = 1.26882$ respectively.

For $c_1 = 1.35$, which is greater than both the Turing bifurcation threshold and the Hopf bifurcation threshold, the system parameters lie in domain IV of the bifurcation diagram of **Figure 1**.

In two species spatial models, the patterns of the prey and the predator are of the same type. As a result, the analysis of pattern formation can be restricted to one of the species only [17-19]. However, different behavior is observed for the three species system. Accordingly the **Figures 3-5** are drawn for prey, intermediate predator and top predator respectively for $c_1 = 1.35$. In each of these figures, slide **(a)** corresponds to the initial distribution in the habitat. The time evolution of the patterns at 50000, 200000 and 500000 iterations are shown in slides **(b)**, **(c)** and **(d)**, respectively. The coexistence of spotted pattern, ring-shaped and the stripe like patterns are observed for the three species.

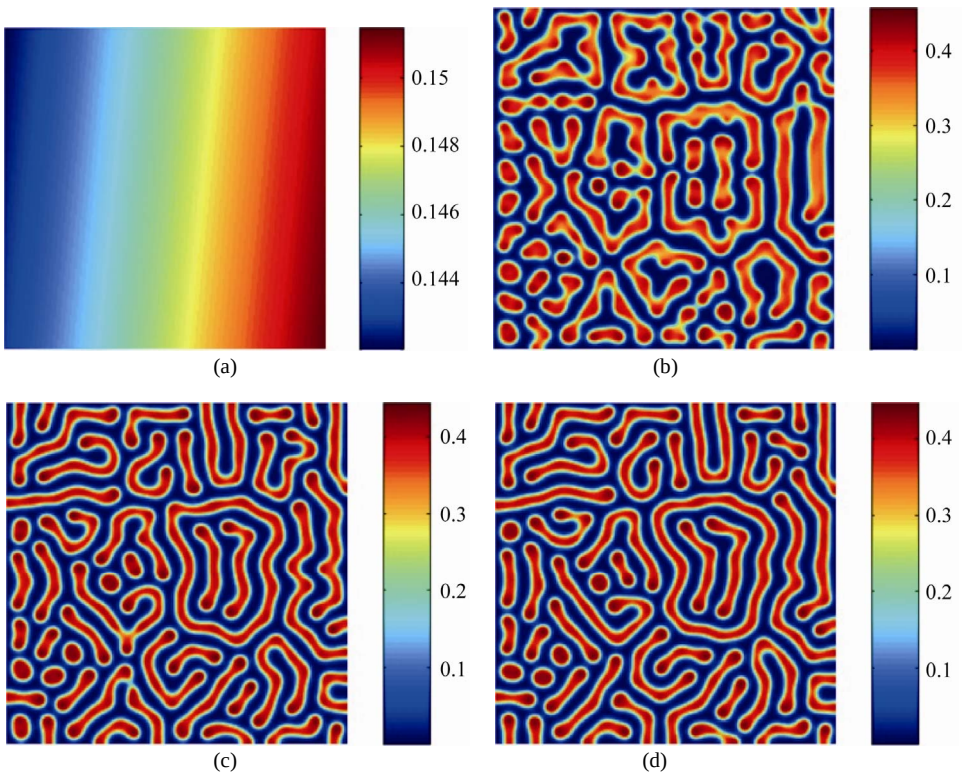

Figure 3. Patterns of the prey for c_1 = 1.35 at different time steps (iterations) (a) 0; (b) 50,000; (c) 200,000; (d) 500,000.

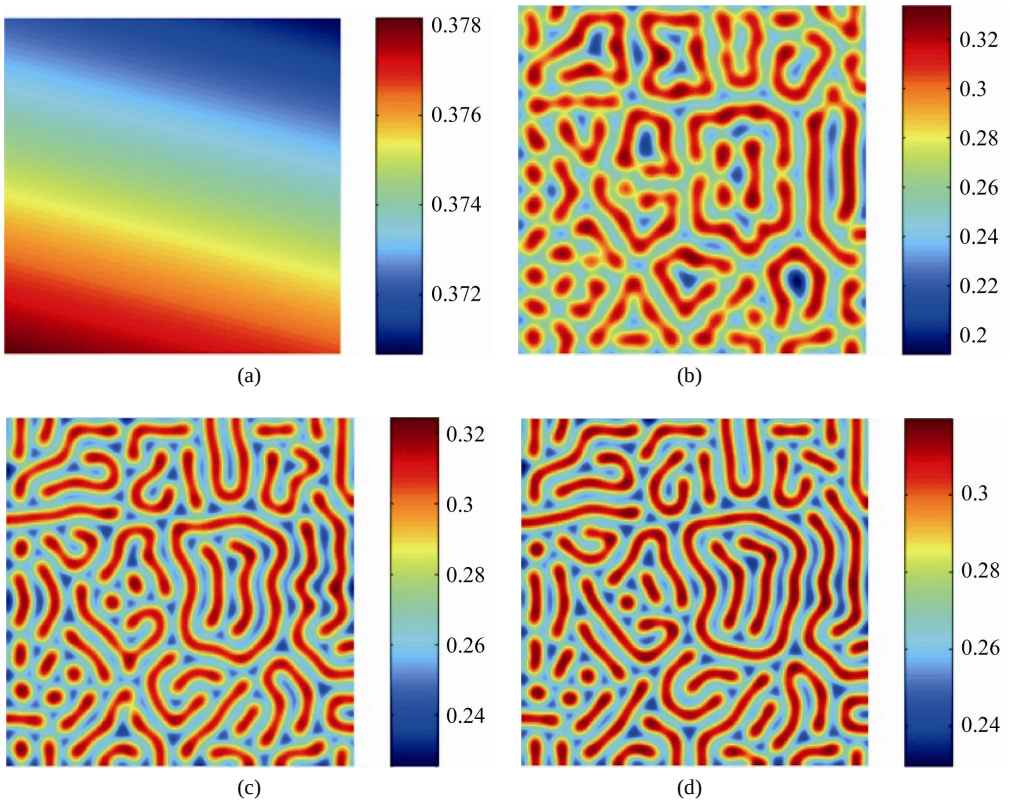

Figure 4. Patterns of the intermediate predator for c_1 = 1.35 at different time steps (iterations) (a) 0; (b) 50,000; (c) 200,000; (d) 500,000.

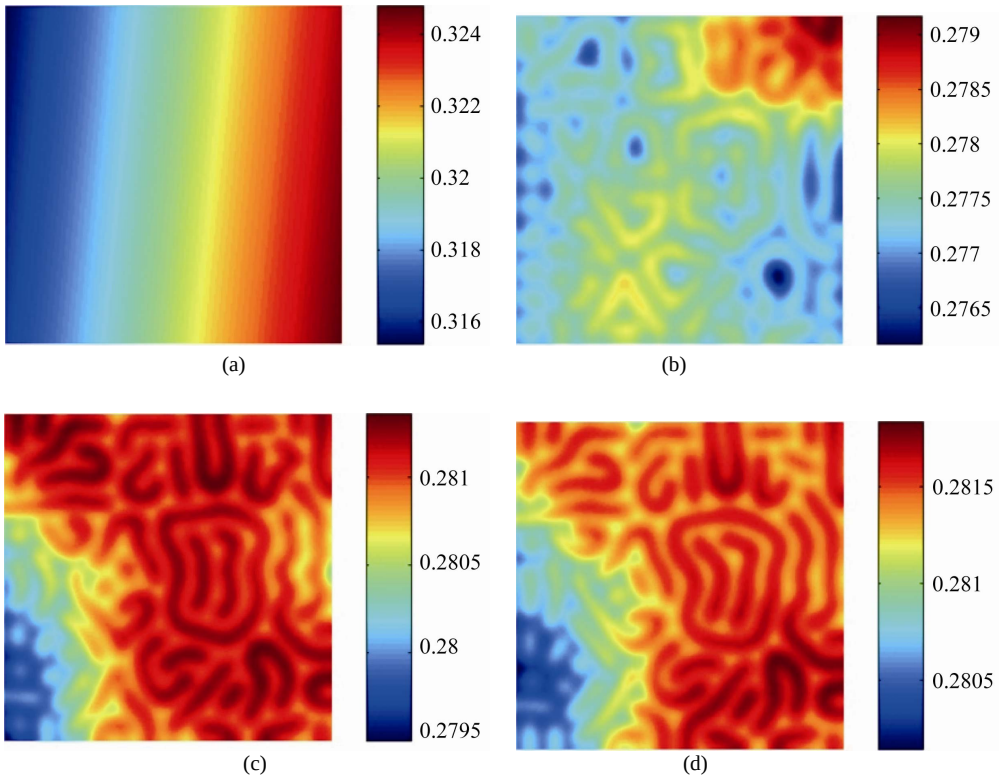

Figure 5. Patterns of the top predator for c_1 = 1.35 at different time steps (iterations) (a) 0; (b) 50,000; (c) 200,000; (d) 500,000.

In **Figure 3**, one can see that the small spatial perturbations to the homogeneous steady state of the spatio-temporal system (2) leads to the formation of spots and stripes of high prey density on a blue background of low prey density (c.f. **Figure 3(b)**). However, at later time some of the spots merge together to form stripes. This results in an increase in the number of stripes and a decrease in the number of spots. Ring-shaped pattern is also formed (c.f. **Figures 3(c)** and **(d)**).

The patterns of the intermediate predator shown in **Figure 4** is structurally similar with that of the patterns of the prey shown in **Figure 3**. But, the background color is not spatially uniform and varying temporally. In particular, the background density is decreasing with time.

The basic skeleton of the pattern of the top predator (c.f. **Figure 5**) is similar with that of the patterns of the prey and intermediate predator. However the background density and the density in the patterns keep changing spatially as well as temporally. Patches of different densities are also visible.

Figure 6 shows the steady state patterns of the three species for $c_1 = 1.24$. In this case, the control parameter c_1 is greater than the Turing bifurcation threshold $c_{1Turing}$ but less than the Hopf bifurcation threshold c_{1Hopf}. That is, the parametric space is domain III of the bifurcation diagram of **Figure 1**. This means that the system has pure Turing instability and Turing patterns are expected for this choice. The numerical simulation results show that the small spatial perturbations given to the homogeneous steady state lead to the formation of the stationary labyrinth like patterns. The density gradient of the prey is greater than that of the intermediate predator and of the top predator. There is a sharp contrast between two consecutive ribbons in the case of prey. The contrast becomes progressively lower for intermediate predator to top predator.

5. Conclusions

In this paper, we have presented a theoretical analysis of evolutionary processes that involves organisms' distribution and trophic interaction in spatially extended environment with self diffusion. The numerical simulations were consistent with the theoretical findings that there are a range of parameters in $c_1 - d_1$ plane where the different spatial patterns emerge. When the parameters are located in region III of **Figure 1**, pure Turing instability occurs and labyrinth like patterns emerge. Whereas when the parameters are in region IV, both Turing and Hopf instability occur and ring, stripe-like and spotted patterns coexist.

In this study, the results show that the ratio-dependent tri-trophic model with Michaelis–Menten type functional response and diffusion represents rich spatial dynamics, such as labyrinth pattern, coexistence of ring-shaped pattern, spotted pattern and stripe-like pattern, which will

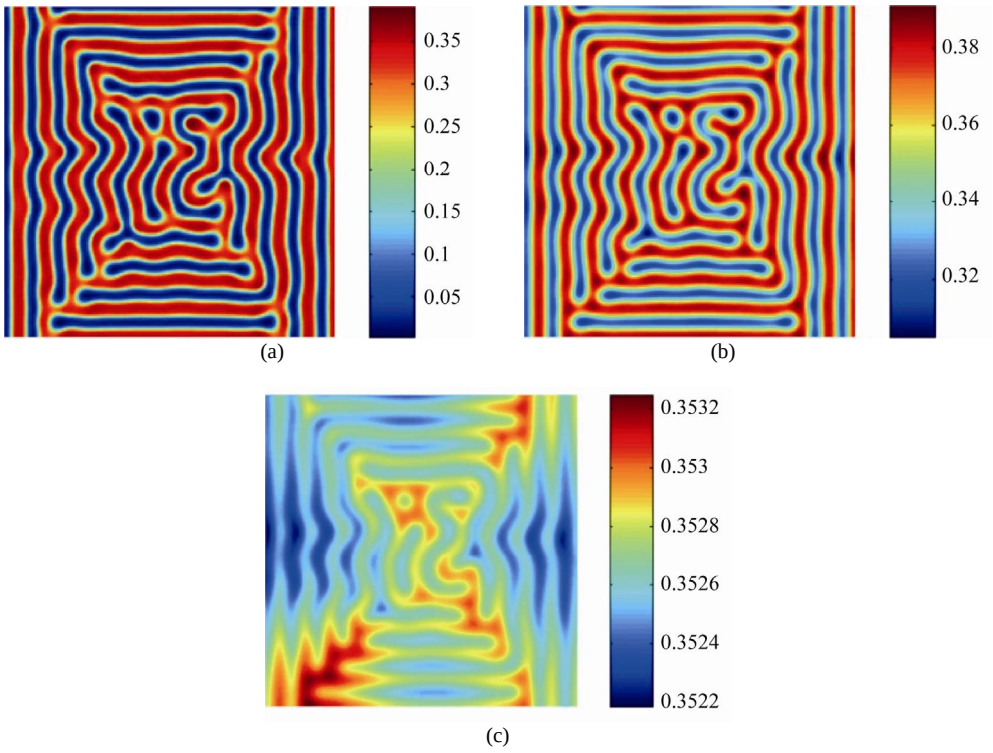

Figure 6. Steady state patterns of the prey (a), intermediate predator (b) and top predator (c) for c_1 = 1.24.

be useful for studying the dynamic complexity of ecosystems or physical systems.

6. References

[1] A. Al-Khedhairi, "The Chaos and Control of Food Chain Model Using Nonlinear Feedback," *Applied Mathematical Sciences*, Vol. 3, No. 12, 2009, pp. 591-604.

[2] N. J. Gotelli and A. M. Ellison, "Food-Web Models Predict Species Abundances in Response to Habitat Change," *PLoS Biology*, Vol. 4, No. 10, 2006, pp. 1869-1873. doi:10.1371/journal.pbio.0040324

[3] S. Gakkhar and R. K. Naji, "Chaos in Three Species Ratio Dependent Food Chain," *Chaos, Solitons and Fractals*, Vol. 14, No. 5, 2002, pp. 771-778. doi:10.1016/S0960-0779(02)00038-3

[4] S. B. Hsu, T. W. Hwang and Y. Kuang, "A Ratio-Dependent Food Chain Model and Its Applications to Biological Control," *Mathematical Biosciences*, Vol. 181, No. 1, 2003, pp. 55-83. doi:10.1016/S0025-5564(02)00127-X

[5] K. A. J. White and C. A. Gilligan, "Spatial Heterogeneity in Three-Species, Plant-Parasite-Hyperparasite, Systems," *Philosophical Transactions of Royal Society B*, Vol. 353, No. 1368, 1998, pp. 543-557. doi:10.1098/rstb.1998.0226

[6] C. Neuhauser and S. W. Pacala, "An Explicitly Spatial Version of Lotka-Voltera Model with Inter-Specific Competition," *The Annals of Applied Probability*, Vol. 9, No. 4, 1999, pp. 1226-1259. doi:10.1214/aoap/1029962871

[7] K. S. McCann, J. B. Rasmussen and J. Umbanhowar, "The Dynamics of Spatially Coupled Food Webs," *Ecology Letters*, Vol. 8, No. 5, 2005, pp. 513-523. doi:10.1111/j.1461-0248.2005.00742.x

[8] S. H. Lee, H. K. Pak, H. S. Wi, T. S. Chon and T. Matsumoto, "Growth Dynamics of Domain Pattern in a Three-Trophic Population Model," *Physica A*, Vol. 334, No. 1-2, 2004, pp. 233-242. doi:10.1016/j.physa.2003.11.017

[9] D. O. Maionchi, S. F. dos Reis and M. A. M. de Aguiar, "Chaos and Pattern Formation in a Spatial Tritrophic Food Chain," *Ecological Modelling*, Vol. 191, No. 2, 2006, pp. 291-303. doi:10.1016/j.ecolmodel.2005.04.028

[10] M. Wang, "Stationary Patterns for a Prey-Predator Model with Prey-Dependent and Ratio-Dependent Functional Responses and Diffusion," *Physica D*, Vol. 196, No. 1-2, 2004, pp. 172-192. doi:10.1016/j.physd.2004.05.007

[11] M. R. Garvie, "Finite-Difference Schemes for Reaction-Diffusion Equations Modeling Predator-Prey Interactions in MATLAB," *Bulletin of Mathematical Biology*, Vol. 69, No. 3, 2007, pp. 931-956. doi:10.1007/s11538-006-9062-3

[12] A. B. Medvinsky, S. V. Petrovskii, I. A. Tikhonov, H. Malchow and B. L. Li, "Spatiotemporal Complexity of Plankton and Fish Dynamics," *SIAM Review*, Vol. 44, No. 3, 2002, pp. 311-370. doi:10.1137/S0036144502404442

[13] S. V. Petrovskii, B. L. Li and H. Malchow, "Transition to Spatiotemporal Chaos Can Resolve the Paradox of Enrichment," *Ecological Complexity*, Vol. 1, No. 1, 2004, pp. 37-47. doi:10.1016/j.ecocom.2003.10.001

[14] H. Shen and Z. Jin, "Two Dimensional Pattern Formation of Prey-Predator System," *Eighth ACIS International Conference on Software Engineering, Artificial Intelligence, Networking, and Parallel/Distributed Computing*, Qingdao, 30 July - 1 August 2007, pp. 343-346. doi:10.1109/SNPD.2007.215

[15] A. M. Turing, "The Chemical Basis of Morphogenesis," *Philosophical Transactions of Royal Society B*, Vol. 237, No. 641, 1952, pp. 37-72. doi:10.1098/rstb.1952.0012

[16] M. Banerjee and S.V. Petrovskii, "Self-Organized Spatial Patterns and Chaos in a Ratio-Dependent Predator Prey System," *Theoretical Ecology*, Vol. 4, No. 1, 2011, pp. 37-53. doi:10.1007/s12080-010-0073-1

[17] W. Wang, L. Zhang, Y. Xue and Z. Jin, "Spatiotemporal Pattern Formation of Beddington-DeAngelis-Type Predator-Prey Model," arXiv: 0801.0797v1 [q-bio.PE], January 2008.

[18] L. Zhang, W. Wang and Y. Xue, "Spatiotemporal Complexity of a Predator-Prey System with Constant Harvest Rate," *Chaos Solitons Fractals*, Vol. 41, No. 1, 2009, pp. 38-46. doi:10.1016/j.chaos.2007.11.009

[19] W. Wang, Q. X. Liu and Z. Jin, "Spatiotemporal Complexity of a Ratio-Dependent Predator-Prey System," *Physical Review E*, Vol. 75, No. 5, 2007, Article ID 051913. doi:10.1103/PhysRevE.75.051913

[20] J. D. Murray, "Mathematical Biology II: Spatial Models and Biomedical Applications," Springer, Berlin, 2003.

[21] G. Sun, Z. Jin, Q. X. Liu and L. Li, "Pattern Formation in a Spatial S-I model with Nonlinear Incidence Rates," *Journal of Statistical Mechanics*: *Theory and Experiment*, Vol. 2007, 2007, P11011. doi:10.1088/1742-5468/2007/11/P11011

[22] H. Malchow, "Spatio-Temporal Pattern Formation in Coupled Models of Plankton Dynamics and Fish School Motion," *Nonlinear Analysis*: *Real World Applications*, Vol. 1, No. 1, 2000, pp. 53-67. doi:10.1016/S0362-546X(99)00393-4

[23] S. B. L. Araújo and M. A. M. de Aguiar, "Pattern Formation, Outbreaks, and Synchronization in Food Chains with Two and Three Species," *Physical Review E*, Vol. 75, No. 6, 2007, Article ID 061908. doi:10.1103/PhysRevE.75.061908

[24] W. Ko and I. Ahn, "Analysis of Ratio-Dependent Food Chain Model," *Journal of Mathematical Analysis Applications*, Vol. 335, No. 1, 2007, pp. 498-523. doi:10.1016/j.jmaa.2007.01.089

Applied Mathematics, **2011, 2, 1515-1521**
doi:10.4236/am.2011.212214 Published Online December 2011 (http://www.SciRP.org/journal/am)

Scientific Research

On Solutions of Generalized Bacterial Chemotaxis Model in a Semi-Solid Medium

Ahmed M. A. El-Sayed[1], Saad Z. Rida[2], Anas A. M. Arafa[2]
[1]*Department of Mathematics, Faculty of Science, Alexandria University, Alexandria, Egypt*
[2]*Department of Mathematics, Faculty of Science, South Valley University, Qena, Egypt*
E-mail: {*amasayed*5, *szagloul*, *anaszi*2}*@yahoo.com*
Received July 4, 2011; *revised October* 22, 2011; *accepted October* 31, 2011

Abstract

In this paper, the Adomian's decomposition method has been developed to yield approximate solution of bacterial chemotaxis model of fractional order in a semi-solid medium. The fractional derivatives are described in the Caputo sense. The method introduces a promising tool for solving many linear and nonlinear fractional differential equations.

Keywords: Decomposition Method, Bacterial Chemotaxis, Semi-Solid Medium, Fractional Calculus

1. Introduction and Preliminaries

This paper deals with numerical solutions of bacterial chemotaxis model of fractional order in a semi-solid medium. We are primarily interested in describing the behaviour of the generalized biological mechanisms that govern the bacterial pattern formation processes in the experiments of Budrene and Berg [1] for populations of E. coli. The model for the semi-solid medium experiment with E. coli is considered. The key players in this paper seem to be the bacteria, the chemoattractant (aspartate) and the stimulant (succinate) so the three variables is considered: the cell density u, the chemoattractant concentration v, and the stimulant concentration w. The bacteria diffuse, move chemotactically up gradients of the chemoattractant, proliferate and become non-motile. The non-motile cells can be thought of as dead, for the purpose of the model. The chemoattractant diffuses, and is produced and ingested by the bacteria while the stimulant diffuses and is consumed by the bacteria. The model consisting of three conservation equations is:

Rate of change of cell density, u	=	Diffusion of u	+	Chemotaxis of u to v	+	Proliferation (growth and death) of u
Rate of change of chemoattratant concentration, v	=	Diffusion of v	+	Production of v by u	–	Uptake of v by u
Rate of change of stimulant concentration, w	=	Diffusion of w	–	Uptake of w by u		

In recent years, fractional calculus starts to attract much more attention of physicists and mathematicians. It was found that various; especially interdisciplinary applications can be elegantly modeled with the help of the fractional derivatives. Other authors have demonstrated applications of fractional derivatives in the areas of electrochemical processes [2,3], dielectric polarization [4], colored noise [5], viscoelastic materials [6-9] and chaos [10]. Mainardi [11] and Rossikhin and Shitikova [12] presented survey of the application of fractional derivatives, in general to solid mechanics, and in particular to modeling of viscoelastic damping. Magin [13-15] presented a three part critical review of applications of fractional calculus in bioengineering. Applications of fractional derivatives in other fields and related mathematical tools and techniques could be found in [16-18]. Rida *et al.* presented a new solutions of some bio-mathematical models of fractional order [19-24].

In this paper, we implemented the Adomian's decomposition method (ADM) [25,26] to the generalized bacterial pattern formation models in a semi-solid medium:

$$\begin{aligned}
\frac{\partial^\alpha u}{\partial t^\alpha} &= D_u \nabla^2 u - \nabla \cdot \left(\frac{k_1 u}{(k_2+v)^2} \nabla v \right) + k_3 u \left(\frac{k_4 w^2}{k_9 + w^2} - u \right), \\
\frac{\partial^\alpha v}{\partial t^\alpha} &= D_v \nabla^2 v + k_5 w \frac{u^2}{k_6 + u^2} - k_7 uv \qquad (1.1) \\
\frac{\partial^\alpha w}{\partial t^\alpha} &= D_w \nabla^2 w + k_8 u \frac{w^2}{k_9 + w^2}
\end{aligned}$$

where $0 < \alpha \le 1, u, v$ and w are the cell density, the concentration of the chemoattractant and of the stimulant respectively. There are three diffusion coefficients, three initial values $(u, v, w \text{ at } t = 0)$ and nine parameters k in the model.

Subject to initial conditions:

$$u(\mathrm{X},0) = u_0(\mathrm{X}),\ v(\mathrm{X},0) = v_0(\mathrm{X}) \text{ and } w(\mathrm{X},0) = w_0(\mathrm{X})$$

where u, v and w are the cell density, the concentration of the chemoattractant and of the stimulant respectively. There are three diffusion coefficients, three initial values $(u, v, w$ at $t = 0)$ and nine parameters k in the model.

The fractional systems of Equations (1.1) are obtained by replacing the first time derivative term by a fractional derivative of order $\alpha > 0$. The Derivatives are understood in the Caputo sense. The general response expression contains a parameter describing the order of the fractional derivative that can be varied to obtain various responses.

In the case of $\alpha \to 1$, the fractional system equations reduce to the standard system of partial differential equations. The Adomian's decomposition method will be applied for computing solutions to the systems of fractional partial differential equations considered in this paper. This method has been used to obtain approximate solutions of a large class of linear or nonlinear differential equations. It is also quite straightforward to write computer codes in any symbolic languages. The method provides solutions in the form of power series with easily computed terms. It has many advantages over the classical techniques mainly; it provides efficient numerical solutions with high accuracy, minimal calculations.

The reason of using fractional order differential equations (FOD) is that FOD are naturally related to systems with memory which exists in most biological systems. Also they are closely related to fractals which are abundant in biological systems. The results derived of the fractional system (1.1) are of a more general nature. Respectively, solutions to the fractional reaction-diffusion equations spread at a faster rate than the classical diffusion equation, and may exhibit asymmetry. However, the fundamental solutions of these equations still exhibit useful scaling properties that make them attractive for applications.

Cherruault [27] proposed a new definition of the method and he then insisted that it would become possible to prove the convergence of the decomposition method. Cherruault and Adomian [28] proposed a new convergence series. A new approach of the decomposition method was obtained in a more natural way than was given in the classical presentation [29]. Recently, the application of the method is extended for fractional differential equations [30-33].

There are several approaches to the generalization of the notion of differentiation to fractional orders e.g. Riemann-Liouville, GruÖnwald-Letnikow, Caputo and Generalized Functions approach [34]. Riemann-Liouville fractional derivative is mostly used by mathematicians but this approach is not suitable for real world physical problems since it requires the definition of fractional order initial conditions, which have no physically meaningful explanation yet. Caputo introduced an alternative definition, which has the advantage of defining integer order initial conditions for fractional order differential equations [34]. Unlike the Riemann-Liouville approach, which derives its definition from repeated integration, the GruÖnwald-Letnikow formulation approaches the problem from the derivative side. This approach is mostly used in numerical algorithms.

2. Fractional Calculus

Here, we mention the basic definitions of the Caputo fractional-order integration and differentiation, which are used in the up coming paper and play the most important role in the theory of differential and integral equation of fractional order.

The main advantages of Caputo's approach are the initial conditions for fractional differential equations with Caputo derivatives take on the same form as for integer order differential equations.

Definition 2.1 The fractional derivative of $f(x)$ in the Caputo sense is defined as [34]:

$$\begin{aligned} D^{\alpha} f(x) &= I^{m-\alpha} D^{m} f(x) \\ &= \frac{1}{\Gamma(m-\alpha)} \int_0^x (x-t)^{m-\alpha+1} f^{(m)}(t)\mathrm{d}t \end{aligned}$$

for $m-1 < \alpha \le m,\ m \in N,\ x > 0$.

For the Caputo derivative we have $D^{\alpha} C = 0$, C is constant

$$D^{\alpha} t^{n} = \begin{cases} 0, & (n \le \alpha - 1) \\ \dfrac{\Gamma(n+1)}{\Gamma(n-\alpha+1)} t^{n-\alpha}, & (n > \alpha - 1) \end{cases}$$

Definition 2.2 For m to be the smallest integer that exceeds α, the Caputo fractional derivatives of order $\alpha > 0$ is defined as [34]:

$$D^{\alpha} u(x,t) = \frac{\partial^{\alpha} u(x,t)}{\partial t^{\alpha}}$$

$$= \begin{cases} \dfrac{1}{\Gamma(m-\alpha)} \displaystyle\int_0^t (t-\tau)^{m-\alpha+1} \frac{\partial^{m} u(x,\tau)}{\partial \tau^{m}} \mathrm{d}\tau, & \text{for } m-1<\alpha<m \\ \dfrac{\partial^{m} u(x,t)}{\partial t^{m}}, & \text{for } \alpha = m \in N \end{cases}$$

3. Analysis of the Method

To give the approximate solution of nonlinear fractional-order differential equations by means of the ADM, we write the systems in the form

$$\begin{aligned} D^{\alpha_1}u_1(\mathrm{X},t) &= N_1(u_1,u_2,\cdots,u_m)+f_1(\mathrm{X},t)\\ D^{\alpha_2}u_2(\mathrm{X},t) &= N_2(u_1,u_2,\cdots,u_m)+f_2(\mathrm{X},t)\\ &\vdots\\ D^{\alpha_m}u_m(\mathrm{X},t) &= N_m(u_1,u_2,\cdots,u_m)+f_m(\mathrm{X},t) \end{aligned} \tag{3.1}$$

where $D^{\alpha_i}(i=1,2,\cdots,m)$ are the fractional operators, and $N_1,N_2,\cdots N_m$ are nonlinear operators.

Applying the inverse operators $I^{\alpha_1},I^{\alpha_2},\cdots,I^{\alpha_M}$ to the systems (3.1)

$$\begin{aligned} u_1(\mathrm{X},t) &= I^{\alpha_1}\left(N_1(u_1,u_2,\cdots,u_m)+f_1(\mathrm{X},t)\right)\\ u_2(\mathrm{X},t) &= I^{\alpha_2}\left(N_2(u_1,u_2,\cdots,u_m)+f_2(\mathrm{X},t)\right)\\ &\vdots\\ u_m(\mathrm{X},t) &= I^{\alpha_M}\left(N_m(u_1,u_2,\cdots,u_m)+f_m(\mathrm{X},t)\right) \end{aligned} \tag{3.2}$$

Subject to the initial conditions

$$u_i(\mathrm{X},0)=g_i(\mathrm{X}),\ (i=1,2,\cdots,m) \tag{3.3}$$

The Adomian decomposition method suggests that the linear terms $u_i(\mathrm{X},t)$ are decomposed by an infinite series of components

$$u_i(\mathrm{X},t)=\sum_{n=0}^{\infty}u_{i,n}(\mathrm{X},t),\ (i=1,2,\cdots,m) \tag{3.4}$$

and the nonlinear operators are defined by the infinite series of the so called Adomian polynomials

$$N_i=\sum_{n=0}^{\infty}A_{i,n} \tag{3.5}$$

where $u_{i,n}(\mathrm{X},t)$; $n\geq 0$ are the components of $u_i(\mathrm{X},t)$, that will be elegantly determined, and $A_{i,n}$; $n\geq 0$ are Adomian's polynomials that can be generated for all forms of non linearity [35]. Substituting (3.4) and (3.5) into (3.2) gives

$$\begin{aligned} \sum_{n=0}^{\infty}u_{1,n}(\mathrm{X},t) &= g_1(\mathrm{X})+I^{\alpha_1}\left(\sum_{n=0}^{\infty}A_{1,n}+f_1(\mathrm{X},t)\right)\\ \sum_{n=0}^{\infty}u_{2,n}(\mathrm{X},t) &= g_2(\mathrm{X})+I^{\alpha_2}\left(\sum_{n=0}^{\infty}A_{2,n}+f_2(\mathrm{X},t)\right)\\ &\vdots\\ \sum_{n=0}^{\infty}u_{m,n}(\mathrm{X},t) &= g_m(\mathrm{X})+I^{\alpha_m}\left(\sum_{m=0}^{\infty}A_{m,n}+f_m(\mathrm{X},t)\right) \end{aligned} \tag{3.6}$$

Following adomian analysis, the nonlinear system (3.1) is transformed into a set of recursive relations given by

$$\begin{aligned} u_{i,0}(\mathrm{X},t) &= g_i(\mathrm{X})\\ u_{i,n+1}(\mathrm{X},t) &= I^{\alpha}\left(A_{i,n}+f_i(\mathrm{X},t)\right)\quad n\geq 0, \end{aligned} \tag{3.7}$$

where $(i=1,2,\cdots,m)$.

It is an essential feature of the decomposition method that the zeroth components $u_{i,0}(\mathrm{X},t)$ are defined always by all terms that arise from initial data and from integrating the inhomogeneous terms. The remaining pairs $(u_{i,n},n\geq 1)$ can be easily determined in a parallel manner. Additional pairs for the decomposition series normally account for higher accuracy. Have been determined the components of $u_i(\mathrm{X},t)$, the solutions of the system follow immediately in the form of a power series expansion upon using (3.4). The series obtained can be summed up in many cases to give a closed form solution for concrete problems, the n term approximants can be used for numerical purposes. Comparing the scheme presented above with existing techniques such as characteristics method and Riemann invariants, it is clear that the decomposition method introduces a fundamental qualitative difference in approach, because no assumptions are made. The approach is straightforward and the rapid convergence is guaranteed. To give a clear overview of the content of this work, several illustrative examples have been selected to demonstrate the efficiency of the method.

4. Applications and Numerical Results

In order to illustrate the advantages and the accuracy of the ADM, we consider time-fractional chemotaxis model of bacteria colonies in a semi-solid medium (1.1) in one dimensional in the form:

$$\begin{aligned} D^{\alpha}u &= D_uL_{xx}u\\ &\quad -L_x\left(\frac{k_1u}{(k_2+v)^2}L_xv\right)+k_3u\left(\frac{k_4w^2}{k_9+w^2}-u\right)\\ D^{\alpha}v &= D_vL_{xx}v+k_5w\frac{u^2}{k_6+u^2}\\ D^{\alpha}w &= D_wL_{xx}w+k_8u\frac{w^2}{k_9+w^2} \end{aligned} \tag{4.2}$$

Subject to the initial conditions

$$\begin{aligned} u(x,0) &= n_0\\ v(x,0) &= \lambda e^{-\mu x^2}\\ w(x,0) &= s_0 \end{aligned}$$

where n_0,λ,μ,s_0 are constants.

Operating with I^{α} in both sides of system (4.2) we find

$$
\begin{aligned}
&u(x,t)=u(x,0)\\
&\quad+I^{\alpha}\left(D_u L_{xx}u-L_x\left(\frac{k_1 u}{(k_2+v)^2}L_x v\right)+k_3 u\left(\frac{k_4 w^2}{k_9+w^2}-u\right)\right)\\
&v(x,t)=v(x,0)+I^{\alpha}\left(D_v L_{xx}v+k_5 w\frac{u^2}{k_6+u^2}\right)\\
&w(x,t)=w(x,0)+I^{\alpha}\left(D_w L_{xx}w+k_8 u\frac{w^2}{k_9+w^2}\right)
\end{aligned}
\tag{4.3}
$$

The ADM assumes a series solution for $u(x,t), v(x,t)$ and $w(x,t)$ given by:

$$
\begin{aligned}
u(x,t)&=\sum_{n=0}^{\infty}u_n(x,t)\\
v(x,t)&=\sum_{n=0}^{\infty}v_n(x,t)\\
w(x,t)&=\sum_{n=0}^{\infty}w_n(x,t)
\end{aligned}
\tag{4.4}
$$

Substituting the decomposition series (4.4) into (4.3) yields

$$
\begin{aligned}
&\sum_{n=0}^{\infty}u_n(x,t)=u(x,0)\\
&+I^{\alpha}\left(D_u L_{xx}\sum_{n=0}^{\infty}u_n(x,t)-k_1 L_x\sum_{n=0}^{\infty}A_n+k_3k_4\sum_{n=0}^{\infty}B_n-k_3\sum_{n=0}^{\infty}C_n\right)\\
&\sum_{n=0}^{\infty}v_n(x,t)=v(x,0)+I^{\alpha}\left(D_v L_{xx}\sum_{n=0}^{\infty}v_n(x,t)+k_5\sum_{n=0}^{\infty}D_n\right)\\
&\sum_{n=0}^{\infty}w_n(x,t)=w(x,0)+I^{\alpha}\left(D_w L_{xx}\sum_{n=0}^{\infty}w_n(x,t)+k_8\sum_{n=0}^{\infty}B_n\right)
\end{aligned}
$$

Identifying the zeros components, $u_0(x,t), v_0(x,t)$ and $w_0(x,t)$ by $u_0(x,0), v_0(x,0)$ and $w_0(x,0)$ the remaining components where $n\geq 0$ can be determined by using recurrence relation:

$$
\begin{aligned}
&u_0(x,t)=u_0(x,0)\\
&u_{n+1}(x,t)=I^{\alpha}(D_u L_{xx}u_n-k_1 L_x A_n+k_3k_4B_n-k_3C_n),\quad n\geq 0
\end{aligned}
\tag{4.5}
$$

$$
\begin{aligned}
&v_0(x,t)=v_0(x,0)\\
&v_{n+1}(x,t)=I^{\alpha}(D_v L_{xx}v_n+k_5D_n),\qquad n\geq 0
\end{aligned}
\tag{4.6}
$$

$$
\begin{aligned}
&w_0(x,t)=w_0(x,0)\\
&w_{n+1}(x,t)=I^{\alpha}(D_w L_{xx}w_n+k_8B_n),\ n\geq 0
\end{aligned}
\tag{4.7}
$$

where A_n, B_n, C_n, and D_n are the Adomian's polynomials calculated for all forms of nonlinearity according to specific algorithms constructed by Adomian as:

$$
\begin{aligned}
A_0&=\frac{k_1u_0v_{0x}}{(k_2+v)^2}=u_0\frac{\partial}{\partial x}\frac{v_0}{k_2+v_0},\\
A_1&=u_1\frac{\partial}{\partial x}\frac{v_0}{k_2+v_0}+k_2u_0v_1\frac{\partial}{\partial x}\frac{1}{(k_2+v_0)^2}
\end{aligned}
\tag{4.8}
$$

$$
\begin{aligned}
B_0&=\frac{u_0w_0^2}{k_9+w_0^2}\\
B_1&=\frac{u_1w_0^2}{k_9+w_0^2}+\frac{2k_9u_0w_0w_1}{(k_9+w_0^2)}
\end{aligned}
\tag{4.9}
$$

$$
\begin{aligned}
C_0&=u_0^2\\
C_1&=2u_0u_1
\end{aligned}
\tag{4.10}
$$

and

$$
\begin{aligned}
D_0&=\frac{w_0u_0^2}{k_6+u_0^2}\\
D_1&=\frac{w_1u_0^2}{k_6+u_0^2}+\frac{2k_6w_0u_0u_1}{(k_6+u_0^2)}
\end{aligned}
\tag{4.11}
$$

Using Equations (4.5)-(4.11), we can calculate some of the terms of the decomposition series (4.4) as:

$$
\begin{aligned}
u_0(x,t)&=f(x)\\
u_1(x,t)&=f_1(x)\frac{t^{\alpha}}{\Gamma(\alpha+1)}\\
u_2(x,t)&=f_2(x)\frac{t^{2\alpha}}{\Gamma(2\alpha+1)}\\
v_0(x,t)&=g(x)\\
v_1(x,t)&=g_1(x)\frac{t^{\alpha}}{\Gamma(\alpha+1)}\\
v_2(x,t)&=g_2(x)\frac{t^{2\alpha}}{\Gamma(2\alpha+1)}
\end{aligned}
$$

and

$$
\begin{aligned}
w_0(x,t)&=h(x)\\
w_1(x,t)&=h_1(x)\frac{t^{\alpha}}{\Gamma(\alpha+1)}\\
w_2(x,t)&=h_2(x)\frac{t^{2\alpha}}{\Gamma(2\alpha+1)}
\end{aligned}
$$

where:

$$
\begin{aligned}
f(x)&=n_0\\
f_1(x)&=D_uf^{(2)}-k_1f\frac{\partial}{\partial x}\frac{g}{k_2+g}+k_3k_4\frac{fh^2}{k_9+h^2}-k_3f^2\\
f_2(x)&=D_uf_1^{(2)}-k_1\left(f_1\frac{\partial}{\partial x}\frac{g}{k_2+g}+k_2fg_1\frac{\partial}{\partial x}\frac{g}{(k_2+g)^2}\right),\\
&\quad+k_3k_4\left(\frac{f_1h^2}{k_9+h^2}+\frac{2k_9fhh_1}{(k_9+h^2)^2}\right)-2k_3f\,f_1
\end{aligned}
$$

$$g(x) = \lambda e^{-\mu x^2}$$

$$g_1(x) = D_v g^{(2)} + k_5 \frac{h f^2}{k_6 + f^2}$$

$$g_2(x) = D_v g_1^{(2)} + k_5 \left(\frac{h_1 f^2}{k_6 + f^2} + \frac{2k_6 h f f_1}{(k_6 + f^2)^2} \right)$$

and

$$h(x) = s_0$$

$$h_1(x) = D_w h^{(2)} + k_8 \frac{f h^2}{k_9 + h^2}$$

$$h_2(x) = D_w h_1^{(2)} + k_8 \left(\frac{f_1 h^2}{k_9 + h^2} + \frac{2k_9 f h h_1}{(k_9 + h^2)^2} \right)$$

and so on, substituting $u_0, u_1, u_2, \cdots, v_0, v_1, v_2, \cdots$ and $w_0, w_1, w_2, \cdots$ into (4.4) gives the solution $u(x,t)$, $v(x,t)$ and $w(x,t)$ in a series form by:

$$\begin{aligned} u(x,t) &= u_0 + u_1 + u_2 + \cdots \\ v(x,t) &= v_0 + v_1 + v_2 + \cdots \\ w(x,t) &= w_0 + w_1 + w_2 + \cdots \end{aligned} \tag{4.12}$$

See **Figure 1** and **Table 1**.

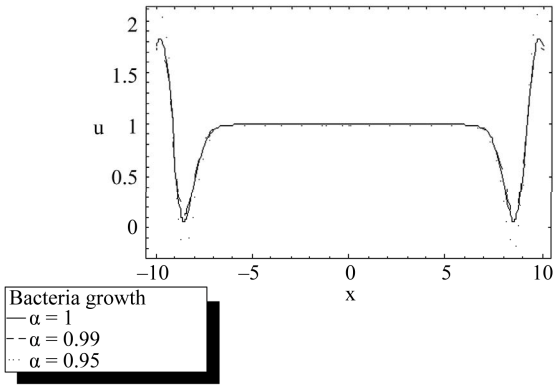

Figure 1. The Numerical results *u*(*x*,*t*).

Table 1. Density of the active bacteria in a semi-solid medium.

x	$\alpha = 1$	$\alpha = 0.99$	$\alpha = 0.95$
–10	1.7620E+00	1.7078E+00	1.9998E+00
–8	4.3328E–01	4.7356E–01	2.5642E–01
–6	9.9630E–01	9.9656E–01	9.9515E–01
–4	9.9997E–01	9.9997E–01	9.9995E–01
–2	1.0000E+00	1.0000E+00	1.0000E+00
0	1.0000E+00	1.0000E+00	1.0000E+00
2	1.0000E+00	1.0000E+00	1.0000E+00
4	9.9997E–01	9.9997E–01	9.9995E–01
6	9.9630E–01	9.9656E–01	9.9515E–01
8	4.3328E–01	4.7356E–01	2.5642E–01
10	1.7620E+00	1.7078E+00	1.9998E+00

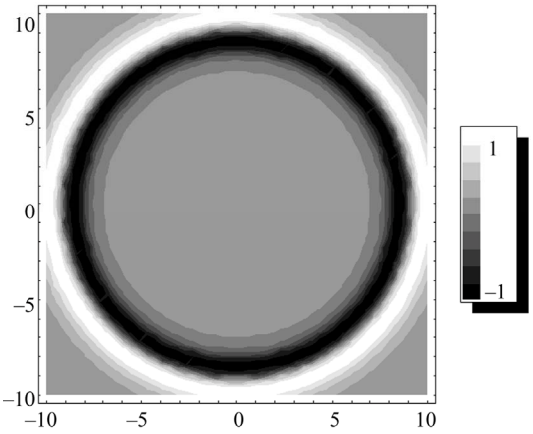

Figure 2. The movement of bacteria cells *u*(*x*,y,*t*) at $\alpha = 1$, white color corresponds to high cell density.

5. Conclusions

In this paper, the decomposition method was implemented to describe the evolution of the bacterial chemotaxis model in a semi-solid medium. The results shows that the solution continuously depends on the time-fractional derivative see **Figure 1**. In other words, we solve the model in two dimensional forms. **Figure 2** is time evolution of the bacteria density $u(x,y,t)$ at, $\alpha \to 1$ which the light regions represent high density of bacteria. In **Figure 2**, Bacteria patterns obtained in semi-solid medium begin with a very low density bacterial lawn spreading out from the initial inoculums. But high density ring of bacteria appears at some radius less than the radius of the lawn, which is very similar to the experimental results (Budrene and Berg (1991)). Finally, it may be concluded that the decomposition method does not change the problem into a convenient one for use of linear theory. It therefore provides more realistic solutions. It provides series solutions which generally converge very rapidly in real physical problems. Respectively, the recent appearance of fractional differential equations as models in some fields of applied mathematics makes it necessary to investigate methods of solution for such equations (analytical and numerical) and we hope that this work is a step in this direction.

6. References

[1] E. O. Budrene and H. C. Berg, "Complex Patterns Formed by Motile Cells of Escherichia Coli," *Nature*, Vol. 349, 1991, pp. 630-633. doi:10.1038/349630a0

[2] M. Ichise, Y. Nagayanagi and T. Kojima, "An Analog Simulation of Non-Integer Order Transfer Functions for Analysis of Electrode Processes," *Journal of Electronically Chemistry Interfacial Electrochemical*, Vol. 33, No. 2, 1971, pp. 253-265.

[3] H. H. Sun, B. Onaral and Y. Tsao, "Application of Positive Reality Principle to Metal Electrode Linear Polarization Phenomena," *IEEE Transactions on Biomedical Engineering*, Vol. 31, No. 10, 1984, pp. 664-674. doi:10.1109/TBME.1984.325317

[4] H. H. Sun, A. A. Abdelwahab and B. Onaral, "Linear Approximation of Transfer Function with a Pole of Fractional Order," *IEEE Transactions on Automatic Control*, Vol. 29, No. 5, 1984, pp. 441-444. doi:10.1109/TAC.1984.1103551

[5] B. Mandelbrot, "Some Noises with 1/f Spectrum, a Bridge between Direct Current and White Noise," *IEEE Transactions on Information Theory*, Vol. 13, No. 2, 1967, pp. 289-298. doi:10.1109/TIT.1967.1053992

[6] R. L. Bagley and R. A. Calico, "Fractional Order State Equations for the Control of Viscoelastic Structures," *Journal of Guidance Control Dynamics*, Vol. 14, No. 2, 1991, pp. 304-311. doi:10.2514/3.20641

[7] R. C. Koeller, "Application of fractional calculus to the theory of viscoelasticity," *Journal of Applied Mechanics*, Vol. 51, No. 2, 1984, pp. 299-307. doi:10.1115/1.3167616

[8] R. C. Koeller, "Polynomial Operators. Stieltjes Convolution and Fractional Calculus in Hereditary Mechanics," *Acta Mechanics*, Vol. 58, No. 3-4, 1986, pp. 251-264. doi:10.1007/BF01176603

[9] S. B. Skaar, A. N. Michel and R. K. Miller, "Stability of Viscoelastic Control Systems," *IEEE Transactions on Automatic Control*, Vol. 33, No. 4, 1988, pp. 348-357. doi:10.1109/9.192189

[10] T. T. Hartley, C. F. Lorenzo and H. K. Qammar, "Chaos in a Fractional Order Chua System," *IEEE Transactions on Circuits Systems*, Vol. 42, No. 8, 1995, pp. 485-490. doi:10.1109/81.404062

[11] F. Mainardi, "Fractional Calculus: Some Basic Problem in Continuum and Statistical Mechanics," In: A. Carpinteri and F. Mainardi, Eds., *Fractals and Fractional Calculus in Continuum Mechanics*, Springer, Wein, New York, 1997, pp. 291-348.

[12] Y. A. Rossikhin and M. V. Shitikova, "Applications of Fractional Calculus to Dynamic Problems of Linear and Nonlinear Hereditary Mechanics of Solids," *Applied Mechanics Reviews*, Vol. 50, No. 1, 1997, pp. 15-67. doi:10.1115/1.3101682

[13] R. L. Magin, "Fractional Calculus in Bioengineering," *Critical Reviews in Biomedical Engineering*, Vol. 32, No. 1, 2004, pp. 1-104.

[14] R. L. Magin, "Fractional Calculus in Bioengineering: Part 2," *Critical Reviews in Biomedical Engineering*, Vol. 32, No. 2, 2004, pp. 105-193.

[15] R. L. Magin, "Fractional Calculus in Bioengineering: Part 3," *Critical Reviews in Biomedical Engineering*, Vol. 32, No. 3-4, 2004, pp. 194-377.

[16] K. B. Oldham, "The Fractional Calculus," Academic Press, New York, 1974.

[17] S. G. Samko, A. A. Kilbas and O. I. Marichev, "Fractional Integrals and Derivatives-Theory and Applications," Gordon and Breach Science Publishers, Longhorne, 1993.

[18] I. Podlubny, "Fractional Differential Equations," Academic Press, New York, 1999.

[19] S. Z. Rida, A. M. A. El-Sayed and A. A. M. Arafa, "Effect of Bacterial Memory Dependent Growth by Using Fractional Derivatives Reaction-Diffusion Chemotactic Model," *Journal of Statistical Physics*, Vol. 140, No. 4, 2010, pp. 797-811. doi:10.1007/s10955-010-0007-8

[20] A. M. A. El-Sayed, S. Z. Rida and A. A. M. Arafa, "On the Solutions of the Generalized Reaction-Diffusion Model for Bacteria Growth," *Acta Applicandae Mathematicae*, Vol. 110, No. 3, 2010, pp. 1501-1511. doi:10.1007/s10440-009-9523-4

[21] S. Z. Rida, A. M. A. El-Sayed and A. A. M. Arafa, "On the Solutions of Time-Fractional Reaction-Diffusion Equations," *Communication in Nonlinear Science & Numerical Simulation*, Vol. 15, 2010, pp. 3847-3854.

[22] S. Z. Rida, A. M. A. El-Sayed and A. A. M. Arafa, "A Fractional Model for Bacterial Chemoattractant in a Liquid Medium," *Nonlinear Science Letter A*, Vol. 1, No. 4, 2010, pp. 415-420.

[23] A. M. A. El-Sayed, S. Z. Rida and A. A. M. Arafa, "Exact Solutions of the Fractional-Order Biological Population Model," *Communication in Theoretical Physics*, Vol. 52, No.6, 2009, pp. 992-996. doi:10.1088/0253-6102/52/6/04

[24] A. M. A. El-Sayed, S. Z. Rida and A. A. M. Arafa, "On the Solutions of Time-Fractional Bacterial Chemotaxis in a Diffusion Gradient Chamber," *International journal of Nonlinear Science*, Vol. 7, No. 4, 2009, pp. 485-492.

[25] G. Adomian, "Solving Frontier Problems of Physics: The Decomposition Method," Kluwer, Academic, Dordrecht, 1994.

[26] G. A domain, "A Review of the Decomposition Method in Applied Mathematics," *Mathematical Analysis and Applications*, Vol. 135, 1988, pp. 501-544.

[27] Y. Cherruault, "Convergence of Adomian's Method," *Kybernetes*, Vol. 18, No. 2, 1989, pp. 31-38. doi:10.1108/eb005812

[28] Y. Cherruault and G. Adomian, "Decomposition Methods: A New Proof of Convergence," *Mathematical and Computer Modelling*, Vol. 18, No. 2, 1993, pp. 103-106. doi:10.1016/0895-7177(93)90233-O

[29] N. Nagarhasta, B. Some, K. Abbaoui and Y. Cherruault, "New Numerical Study of Adomian Method Applied to a Diffusion Model," *Kybernetes*, Vol. 31, No. 1, 2002, pp. 61-75. doi:10.1108/03684920210413764

[30] S. Momani, "Non-Perturbative Analytical Solutions of the Space- and Time-Fractional Burgers Equations," *Chaos, Solitons & Fractals*, Vol. 28, No. 4, 2006, pp. 930-937. doi:10.1016/j.chaos.2005.09.002

[31] S. Momani and Z. Odibat, "Analytical Solution of a Time-Fractional Navier-Stokes Equation by Adomian Decomposition Method," *Applied Mathematics and Computation*, Vol. 177, No. 2, 2006, pp. 488-494. doi:10.1016/j.amc.2005.11.025

[32] S. Momani and Z. Odibat, "Numerical Comparison of Methods for Solving Linear Differential Equations of Fractional Order," *Chaos, Solitons & Fractals*, Vol. 31, No. 5, 2007, pp. 1248-1255. doi:10.1016/j.chaos.2005.10.068

[33] Z. Odibat and S. Momani, "Approximate Solutions for Boundary Value Problems of Time-Fractional Wave Equation," *Applied Mathematics and Computation*, Vol. 181, No. 1, 2006, pp. 767-774. doi:10.1016/j.amc.2006.02.004

[34] I. Podlubny and A. M. A. El-Sayed, "On Two Definition of Fractional Calculus," Solvak Academy of Science-Institute of Experimental Physics, UEF-03-96 ISPN 80-7099-252-2, 1996.

[35] A. Wazwaz, "A New Algorithm for Calculating Adomian Polynomials for Nonlinear Operators," *Applied Mathematics and Computation,* Vol. 111, No. 1, 2000, pp. 53-69. doi:10.1016/S0096-3003(99)00063-6

Note: Parameters Taken as:

$n_0 = 1,\ \lambda = 0.01,\ \mu = 0.1,$

$k_1 = 3.9(10)^{-9},\ k_2 = 5(10)^{-6},\ k_3 = 1.62(10)^{-8},$

$k_5 = k_6 = k_7 = k_8 = 1,\ k_9 = 4(10)^{-6},\ s_0 = 1 - 3(10)^{-3},$

$D_u = 2 - 4(10)^{-6},\ D_v = 8.9(10)^{-6},\ D_w = 9(10)^{-6},\ t = 100$

Applied Mathematics, 2011, 2, 1522-1524
doi:10.4236/am.2011.212215 Published Online December 2011 (http://www.SciRP.org/journal/am)

Special Lattice of Rough Algebras

Yonghong Liu
School of Automation, Wuhan University of Technology, Wuhan, China
E-mail: *hylinin@163.com*
Received October 14, 2011; *revised November* 16, 2011; *accepted November* 24, 2011

Abstract

This paper deals with the study of the special lattices of rough algebras. We discussed the basic properties such as the rough distributive lattice; the rough modular lattice and the rough semi-modular lattice etc., some results of lattice are generalized in this paper. The modular lattice of rough algebraic structure can provide academic base and proofs to analyze the coverage question and the reduction question in information system.

Keywords: Lattice, Rough Distributive Lattice, Rough Modular Lattice, Rough Semi-Modular Lattice

1. Introduction

It is generally known that the order and the partial order set theory were widely applied in the discrete mathematics and fuzzy mathematics. In algebraic theories about the notion of lattice as both profound and sweeping.

The rough set was introduced by Pawlak in 1982 [1]. The lattice to characterize rough set is an important task [2-6]. Actually, we can use a lattice model to represent different information flow policies and play an important role in Boolean algebra. Obviously, the coverage problem and the reductions problem are two problems of the cores in information system of lattice relation, which boosts the development of lattice theory. We give several special lattices of rough algebras that we discuss in this article; for instance, we prove that a lattice is necessary and sufficient condition of the rough semi-modular lattice.

We will now describe a lattice definition and then we introduce rough approximation spaces. The main contents are as the following:

Definition 1.1. [7] Let L is a set. Define the meet $(\wedge)$ and join $(\vee)$ operations by

$$x \wedge y = \mathrm{glb}(x, y),$$
$$x \vee y = \mathrm{lub}(x, y).$$

The following properties hold for all elements $x, y, z \in L$.

1) commutative laws:

$$x \wedge y = y \wedge x \text{ and } x \vee y = y \vee x.$$

2) associative laws:

$$(x \wedge y) \wedge z = x \wedge (y \wedge z) \text{ and}$$
$$(x \vee y) \vee z = x \vee (y \vee z).$$

3) absorption laws:

$$x \wedge (x \vee y) = x \text{ and } x \vee (x \wedge y) = x.$$

4) idempotent laws:

$$x \wedge x = x \text{ and } x \vee x = x.$$

A lattice is an algebra structure $\langle L, \vee, \wedge \rangle$ that has two binary composition $\wedge$ and $\vee$, it satisfies the above-mentioned condition 1), 2), 3) and 4).

Definition 1.2. [7] Let L is a lattice, if for any $x, y, z \in L$.

$$1)\ x \wedge (y \vee z) = (x \wedge y) \vee (x \wedge z), \text{or}$$
$$2) x \vee (y \wedge z) = (x \vee y) \wedge (x \vee z).$$

Therefore, L is called a distributive lattice.

Definition 1.3. [7] A distributive lattice is called a modular lattice.

Theorem 1.1. [7] Let L is modular lattice, then L is called a semi-modular lattice.

Definition 1.4. [8] Assume that U is a finite and non-empty set with the universe, $R \subseteq U \times U$ denote a binary relation on U. Let (U, R) is an approximation spaces. Define $\mathbb{R} = \left\{ (\underline{R}, \overline{R}) \middle| R \subseteq U \right\}$ is a rough approximation spaces. $\underline{R}$ and $\overline{R}$ are referred to as the lower and upper approximation operators respectively.

Theorem 1.2. [8] Let (U, R) be an approximation spaces. Then algebra $\langle \mathbb{R}, \vee, \wedge \rangle$ is a complete distributive lattice.

2. Main Results

Definition 2.1. Let (U, R) be an approximation spaces. For all $x, y \in R$. If $\underline{R}(x) = \underline{R}(y)$, then the rough x and y

are called lower rough equal. The notation $x \simeq y$ denotes that x and y are lower rough equal. If $\overline{R}(x) = \overline{R}(y)$, then the rough x and y are called upper rough equal. The notation $x \simeq y$ denotes that x and y are upper rough equal. If $x \simeq y$ and $x \simeq y$, then the rough x and y are called rough equal. The notation $x \approx y$ denotes that x and y are rough equal.

Definition 2.2. Let $\vee x_t, \wedge x_t \in \mathbb{R}$, and S be a unary operation. We use the notation

$$\underset{t\in T}{\vee} x_t \approx \underset{t\in T}{\vee} \underline{x}_t \vee S(\underset{t\in T}{\vee} \overline{x}_t),$$

$$\underset{t\in T}{\wedge} x_t \approx \underset{t\in T}{\wedge} \underline{x}_t \vee S(\underset{t\in T}{\wedge} \overline{x}_t).$$

The definition represents that the rough union and rough intersection (where T is an index set).

Definition 2.3. Let algebra $\langle \mathbb{R}, \vee, \wedge \rangle$ be a rough lattice, if for any $x, y, z \in R,$ satisfying

$$x \preceq y \Rightarrow x \vee (z \wedge y) \approx (x \vee z) \wedge y,$$

Therefore, R is a rough modular lattice.

Theorem 2.1. The rough distributive lattice $\langle \mathbb{R}, \vee, \wedge \rangle$ is rough modular lattice.

Proof. Suppose that R is a rough distributive lattice, if for any $x, y, z \in R,\ x \preceq y$, then

$$\begin{aligned}
&x \vee (z \wedge y) \approx (\underline{x} \vee (\underline{y} \wedge \underline{z})) \vee S(\overline{x} \vee (\overline{y} \wedge \overline{z})) \\
&\approx ((\underline{x} \vee \underline{y}) \wedge (\underline{x} \vee \underline{z})) \vee S((\overline{x} \vee \overline{y}) \wedge (\overline{x} \vee \overline{z})) \\
&\approx (\underline{x \vee y} \wedge \underline{x \vee z}) \vee S(\overline{x \vee y} \wedge \overline{x \vee z}) \\
&\approx (\underline{x \vee y \wedge x \vee z}) \vee S(\overline{x \vee y \wedge x \vee z}) \\
&\approx (x \vee y) \wedge (x \vee z) \\
&\approx (x \vee z) \wedge y.
\end{aligned}$$

Hence the $\langle \mathbb{R}, \vee, \wedge \rangle$ is rough modular lattice.

Theorem 2.2. The rough modular lattice $\langle \mathbb{R}, \vee, \wedge \rangle$ is rough distributive lattice, if and only if for any $x, y, z \in R,$ the following formulas hold:

$$\begin{aligned}
&(x \wedge y) \vee (y \wedge z) \vee (z \wedge x) \\
&\approx (x \vee y) \wedge (y \vee z) \wedge (z \vee x).
\end{aligned}$$

Proof. Necessity:

If for any $x, y, z \in R,$ then

$$\begin{aligned}
&(x \wedge y) \vee (y \wedge z) \vee (z \wedge x) \\
&\approx (((x \wedge y) \vee y) \wedge ((x \vee y) \vee z)) \vee (z \wedge x) \\
&\qquad \text{(distributive laws)} \\
&\approx (y \wedge (x \vee z) \wedge (y \vee z)) \vee (z \wedge x) \\
&\qquad \text{(absorption laws and distributive laws)} \\
&\approx (y \vee z) \wedge (y \vee x) \wedge (x \vee z \vee z) \wedge (x \vee z \vee x) \\
&\quad \wedge (\mathrm{y} \vee \mathrm{z} \vee \mathrm{z}) \wedge (\mathrm{y} \vee \mathrm{z} \vee \mathrm{x}) \\
&\qquad \text{(distributive laws)} \\
&\approx (y \vee z) \wedge (x \vee y) \wedge (z \vee x) \wedge (x \vee y \vee z) \\
&\qquad \text{(idempotent laws and commutative laws)} \\
&\approx (x \vee y) \wedge (y \vee z) \wedge (z \vee x).
\end{aligned}$$

Sufficiency:

If for any $x, y, z \in R,$ then

$$\begin{aligned}
x \wedge (y \vee z) &\approx x \wedge (x \vee z) \wedge (y \vee z) \\
&\approx x \wedge (x \vee y) \wedge (x \vee z) \wedge (y \vee z) \\
&\approx \mathrm{x} \wedge ((\mathrm{x} \vee \mathrm{y}) \wedge (\mathrm{y} \vee \mathrm{z}) \wedge (\mathrm{z} \vee \mathrm{x})) \\
&\approx x \wedge ((x \wedge y) \vee (y \wedge z) \vee (z \wedge x)) \\
&\approx ((x \wedge y) \vee (y \wedge z) \vee (z \wedge x))) \wedge x
\end{aligned}$$

Because $x \wedge y \preceq x,$ and since the rough modular laws. We see that

$$\begin{aligned}
&((x \wedge y) \vee ((y \wedge z) \vee (z \vee x))) \wedge x \\
&\approx (x \wedge y) \vee (((y \wedge z) \vee (z \wedge x)) \wedge x).
\end{aligned}$$

Because $z \wedge x \preceq x,$ and since the rough modular laws. It follows that

$$(x \wedge y) \vee (z \wedge x) \vee (y \wedge z \wedge x) \approx (x \vee y) \vee (x \wedge z).$$

We conclude that

$$x \wedge (y \vee z) \approx (x \vee y) \vee (x \wedge z).$$

Show that $\langle \mathbb{R}, \vee, \wedge \rangle$ is the rough distributive lattice.

Theorem 2.3. A necessary and sufficient condition that rough lattice R is a rough modular lattice, for any $x, y \in R,\ x \preceq y$ and $z \in R,$ we have

$$x \vee z \approx y \vee z, x \wedge z \approx y \wedge z, \text{ then } x \approx y.$$

Proof. Necessity:

$$\begin{aligned}
x &\approx x \vee (x \wedge z) \\
&\approx x \vee (y \wedge z) \\
&\approx x \vee (z \wedge y) \\
&\approx (x \vee z) \wedge y \\
&\approx (y \vee z) \wedge y \approx y.
\end{aligned}$$

Sufficiency:

Let $x \preceq y$. To show that z, we thus have

$$x \vee (z \wedge y) \approx (x \vee z) \wedge y.$$

We shall prove that the two laws:

1) $(x \vee (z \wedge y)) \wedge z \approx ((x \vee z) \wedge y) \wedge z,$

2) $(x \vee (z \wedge y)) \vee z \approx ((x \vee z) \wedge y) \vee z.$

To prove 1). In fact,

$$\begin{aligned}
&((x \vee z) \wedge y) \wedge z \approx ((x \vee z) \wedge z) \wedge y \approx z \wedge y, \\
&(x \vee (z \wedge y)) \wedge z \\
&\preceq (y \vee (z \wedge y)) \wedge z \approx y \wedge z \approx z \wedge y, \text{ and} \\
&y \wedge z \approx z \wedge y \approx (y \wedge z) \wedge z \preceq (x \vee (z \wedge y)) \wedge z,
\end{aligned}$$

thus

$$((x \vee z) \wedge y) \wedge z \approx z \wedge y.$$

For part 2),

$$(x \vee (z \wedge y)) \vee z \approx x \vee ((z \wedge y) \vee z) \approx x \vee z.$$

and

$$((x \vee z) \wedge y) \vee z \preceq (x \vee z) \vee z \approx x \vee z.$$

Since $x \preceq y$, we conclude that $x \wedge y \approx x$, then

$$x \vee z \approx (x \wedge y) \vee z \preceq ((x \vee z) \wedge y) \vee z,$$

thus

$$((x \vee z) \wedge y) \vee z \approx x \vee z,$$

which proves 2).

Definition 2.4. The R is called a rough semi-modular lattice denotes that $\overline{x}$ is coverage of $\overline{x} \wedge \underline{y}$, and $\underline{y}$ is also coverage of $\overline{x} \wedge \underline{y}$, then $\overline{x} \vee \underline{y}$ is coverage of $\overline{x}$ and it is also coverage of $\underline{y}$.

Theorem 2.4. If R is a rough modular lattice, then R is a rough semi-modular lattice.

Proof. Let $\overline{x}$ be coverage of $\overline{x} \wedge \underline{y}$ and let $\underline{y}$ is also coverage of $\overline{x} \wedge \underline{y}$, if for every $f \in R$, and

$$\overline{x} \preceq f < \overline{x} \vee \underline{y},$$

which proves that $f \approx \overline{x}$, whence $\overline{x} \vee \underline{y}$ is coverage of $\overline{x}$. In fact,

$$\overline{x} \preceq f < \overline{x} \vee \underline{y},$$

we have

$$\overline{x} \wedge \underline{y} \preceq f \wedge \underline{y} \preceq (\overline{x} \vee \underline{y}) \wedge \underline{y} \approx \underline{y},$$

but $f \wedge \underline{y} \not\approx \underline{y}$, if not, $\overline{x} \preceq f$ and $\underline{y} \preceq f$. This leads to the contradiction $\overline{x} \vee \underline{y} \preceq f$. We see that $\underline{y}$ is coverage of $\overline{x} \wedge \underline{y}$, so that

$$\overline{x} \wedge \underline{y} \approx f \wedge \underline{y},$$

thus

$$f \approx f \wedge (\underline{y} \vee \overline{x}) \approx (f \vee \underline{y}) \vee \overline{x} \approx (\overline{x} \wedge \underline{y}) \vee \overline{x} \approx \overline{x}.$$

Similarly, $\overline{x} \vee \underline{y}$ is coverage of $\underline{y}$.

Theorem 2.5. Assume that rough semi-modular lattice $R_1, R_2, \cdots, R_n$. Then the Cartesian product $R \approx R_1 \times R_2 \times \cdots \times R_n$ is a rough semi-modular lattice.

Proof. Let $\overline{x} \approx (\overline{x}_1, \overline{x}_2, \cdots, \overline{x}_n)$ and $\underline{y} \approx (\underline{y}_1, \underline{y}_2, \cdots, \underline{y}_n) \in R$, $R \approx R_1 \times R_2 \times \cdots \times R_n$, and let $\overline{x}$, $\underline{y}$ are coverage of $\overline{x} \wedge \underline{y} \approx (z_1, z_2, \cdots, z_n)$, if there exists i, then $\overline{x}_i$ is coverage of z_i, and let $k \not\approx i$, we have $z_k \approx \overline{x}_k$. If there exists j, then $\underline{y}_j$ is coverage of z_j, and let $k \not\approx j$, we have $z_k \approx \underline{y}_k$. If $i \not\approx j$, then $\overline{x} \vee \underline{y} \approx (t_1, t_2, \cdots, t_n)$, where $t_i \approx \overline{x}_i$, $t_j \approx \underline{y}_j$, $t_k \approx z_k$ $(k \not\approx i, j)$.

Here, $\overline{x} \vee \underline{y}$ is coverage of $\overline{x}$, it is also coverage of y. If $i \approx j$, then $\overline{x} \vee \underline{y} \approx (u_1, u_2, \cdots, u_n)$, where $u_i \approx \overline{x}_i \vee \underline{y}_i$, $u_k \approx z_k$ $(k \not\approx i)$.

Because R_i be a rough semi-modular lattice, hence u_i is coverage of $\overline{x}_i$, and it is also coverage of $\underline{y}_i$. Therefore, $\overline{x} \vee \underline{y}$ is not only coverage of $\overline{x}$, but also coverage of $\underline{y}$.

Corollary 2.1. Let (U, R) be an approximation spaces. Suppose that X is a nonempty set, $X \subseteq U$, and R be a set of equivalent relation, then R is a rough semi-modular lattice based on the inclusion relation.

3. References

[1] Z. Pawlak, "Rough Sets," *International Journal of Computer and Information Sciences*, Vol. 11, No. 5, 1982, pp. 341-356. doi:10.1007/BF01001956

[2] M. Novotny and Z. Pawlak, "Characterization of Rough Top Equalities and Rough Bottom Equalities," *Bulletin of the Polish Academy of Sciences. Mathematics*, Vol. 33, No. 1-2, 1985, pp. 91-97.

[3] D. Dubois and H. Prade, "Rough Fuzzy Sets and Fuzzy Rough Sets," *International Journal of General Systems*, Vol. 17, No. 2-3, 1990, pp. 191-209. doi:10.1080/03081079008935107

[4] Y. H. Liu, "Lattice to Characterizing Rough Set," *Pattern Recognition and Artificial Intelligence*, Vol. 16, No. 2, 2003, pp. 174-177.

[5] W. Q. Liu and C. X. Wu, "The Approximation Operator on F-Lattice," *Acta Mathematical Seneca*, Vol. 46, No. 6, 2003, pp. 1163-1170.

[6] G. L. Liu, "The Lattice Properties of Rough Set Quotient Spaces," *Computer Engineering & Science*, Vol. 26, No. 12, 2004, pp. 82-90.

[7] D. C. Sheng, "Abstract Algebra," Science Press, Beijing, 2001, pp. 114-127.

[8] W. X. Zhang, W. Z. Wu, J. Y. Liang and D. Y. Li, "Rough Sets: Theory and Methods," Science Press, Beijing, 2001, pp. 72-77.

Applied Mathematics, 2011, 2, 1525-1530
doi:10.4236/am.2011.212216 Published Online December 2011 (http://www.SciRP.org/journal/am)

On Signed Product Cordial Labeling

Jayapal Baskar Babujee, Shobana Loganathan
Department of Mathematics, Anna University, Chennai, India
E-mail: {*baskarbabujee*, *shobana_2210*}*@yahoo.com*
Received September 19, 2011; *revised October* 25, 2011; *accepted November* 3, 2011

Abstract

A new concept of labeling called the signed product cordial labeling is introduced and investigated for path graph, cycle graphs, star-$K_{1,n}$, Bistar-$B_{n,n}$, $P_n^+, n \geq 3$ and $C_n^+, n \geq 3$. Some general results on signed product cordial labeling are studied.

Keywords: Graph, Labeling, Function, Cordial Labeling

1. Introduction

If the vertices of the graph are assigned values subject to certain conditions then it is known as graph labeling. Most of the graph labeling problems have the following three common characteristics: a set of numbers for assignment of vertex labels, a rule that assigns a label to each edge and some condition(s) that these labels must satisfy.

Cordial labelings were introduced by Cahit [1] who called a graph G cordial if there is a vertex labeling $f : V(G) \to \{0,1\}$ such that the induced labeling $f^* : E(G) \to \{0,1\}$, defined by $f^*(xy) = |f(x) - f(y)|$, for all edges $xy \in E(G)$ and with the following inequalities holding: $|v_f(0) - v_f(1)| \leq 1$ and $|e_f(0) - e_f(1)| \leq 1$, where $v_f(i)$ (respectively $e_f(i)$) is the number of vertices (respectively, edges) labeled with i. Sundaram and Somasundaram [2] introduced the notion of product cordial labelings. A product cordial labeling of a graph G with vertex set V is a function f from V to $\{0,1\}$ such that if each edge uv is assigned the label $f(u)f(v)$, the number of vertices labeled with 0 and the number of vertices labeled with 1 differ by at most 1, and the number of edges labeled with 0 and the number of edges labeled with 1 differ by at most 1. A graph with a product cordial labeling is called a product cordial graph.

For detail survey on graph labeling one can refer Gallian [3]. Let $G = (V, E)$ be a graph. As given in [4] a mapping $f : V(G) \to \{0,1\}$ is called binary vertex labeling of G and $f(v)$ is called the label of the vertex v of G under f. For an edge $e = uv$, the induced edge labeling $f^* : E(G) \to \{0,1\}$ is given by $f^*(e) = |f(u) - f(v)|$. Let $v_f(0)$, $v_f(1)$ be the number of vertices of G having labels 0 and 1 respectively under f and let $e_f(0)$, $e_f(1)$ be the number of edges having labels 0 and 1 respectively under f^*. A binary vertex labeling of a graph G is called a cordial labeling if $|v_f(0) - v_f(1)| \leq 1$ and $|e_f(0) - e_f(1)| \leq 1$.

In Section 2, we introduce the definition of signed product cordial labeling and work for few fundamental graphs. In Section 3 we prove that P_n^+, C_n^+ and bistar graph $B_{n,n}$ are signed product cordial. Finally in Section 4, we prove the existence of signed product cordial labeling for some general graphs.

2. Signed Product Cordial Labeling

We now introduce the definition of signed product cordial labeling.

Definition 2.1: A vertex labeling of graph G $f : V(G) \to \{-1,1\}$ with induced edge labeling $f^* : E(G) \to \{-1,1\}$ defined by $f^*(uv) = f(u)f(v)$ is called a signed product cordial labeling if $|v_f(-1) - v_f(1)| \leq 1$ and $|e_f(-1) - e_{f^*}(1)| \leq 1$, where $v_f(-1)$ is the number of vertices labeled with –1, $v_f(1)$ is the number of vertices labeled with 1, $e_{f^*}(-1)$ is the number of edges labeled with –1 and $e_{f^*}(1)$ is the number of edges labeled with 1. A graph G is signed product cordial if it admits signed product cordial labeling.

Theorem 2.2: *The Path graph P_n, $n \geq 2$ admits signed product cordial labeling.*

***Proof*:** Let $V = \{v_1, v_2, ..., v_n\}$ be the vertex set and $E = \{v_i v_{i+1}; 1 \leq i \leq n-1\}$ be the edge set of the path graph

P_n. To define vertex labeling $f:V(G)\to\{-1,1\}$ the following cases are to be considered.

Case 1: when $n\equiv 0,1,3 \pmod 4$
for $1\le i\le n$

$$f(v_i)=\begin{cases}1\,; i\equiv 1,2 \bmod 4\\ -1; i\equiv 0,3 \bmod 4\end{cases}$$

Case 2: when $n\equiv 2 \pmod 4$
for $1\le i\le n-2$

$$f(v_i)=\begin{cases}1\,; i\equiv 1,2 \bmod 4\\ -1; i\equiv 0,3 \bmod 4\end{cases}$$

and

$$f(v_{n-1})=1,\ f(v_n)=-1$$

The induced edge labeling f^* is given by

$$f^*(v_iv_{i+1})=f(v_i)f(v_{i+1})$$
$$=\begin{cases}1 & f(v_i)\text{ and }f(v_{i+1})\text{ have same sign}\\ -1 & f(v_i)\text{ and }f(v_{i+1})\text{ have different sign}\end{cases}$$

with respect to the above labeling pattern we give the proof as follows,

i) When $n\equiv 0 \mod 4$

The total number of vertices labeled with –1's are given by $v_f(-1)=n/2$ and the total number of vertices labeled with 1's are given by $v_f(1)=n/2$. Therefore the total difference between the vertices labeled with –1's and 1's is $\left|v_f(-1)-v_f(1)\right|=0$. The total number of edges labeled with –1's are given by $e_{f^*}(-1)=(n/2)-1$ and the total number of edges labeled with 1's are given by $e_{f^*}(1)=(n/2)$. Therefore the total difference between the edges labeled with –1's and 1's is

$\left|e_{f^*}(-1)-e_{f^*}(1)\right|=|-1|=1$, differ by one.

$$v_f(-1)=v_f(1)=n/2$$
$$e_{f^*}(-1)+1=e_{f^*}(1)=n/2$$

ii) When $n\equiv 2 \mod 4$

The total number of vertices labeled with –1's are given by $v_f(-1)=n/2$ and the total number of vertices labeled with 1's are given by $v_f(1)=n/2$. Therefore the total difference between the vertices labeled with –1's and 1's is $\left|v_f(-1)-v_f(1)\right|=0$. The total number of edges labeled with –1's are given by $e_{f^*}(-1)=(n/2)$ and the total number of edges labeled with 1's are given by $e_{f^*}(1)=(n/2)-1$. Therefore the total difference between the edges labeled with –1's and 1's is

$\left|e_{f^*}(-1)-e_{f^*}(1)\right|=1$, differ by one.

$$v_f(-1)=v_f(1)=n/2$$
$$e_{f^*}(-1)=e_{f^*}(1)+1=n/2$$

iii) When n is odd

The total number of vertices labeled with –1's are given by $v_f(-1)=(n-1)/2$ and the total number of vertices labeled with 1's are given by $v_f(1)=(n+1)/2$. Therefore the total difference between the vertices labeled with –1's and 1's is $\left|v_f(-1)-v_f(1)\right|=|-1|=1$. The total number of edges labeled with –1's are given by $e_{f^*}(-1)=(n-1)/2$ and the total number of edges labeled with 1's are given by $e_{f^*}(1)=(n-1)/2$. Therefore the total difference between the edges labeled with –1's and 1's is $\left|e_{f^*}(-1)-e_{f^*}(1)\right|=0$, differ by zero.

$$v_f(-1)+1=v_f(1)=(n+1)/2$$
$$e_{f^*}(-1)=e_{f^*}(1)=(n-1)/2$$

Thus in each cases we have $\left|v_f(-1)-v_f(1)\right|\le 1$ and $\left|e_{f^*}(-1)-e_{f^*}(1)\right|\le 1$. Hence the path graph P_n, $n\ge 2$ admits signed product cordial labeling.

Theorem 2.3: *The Cycle graph C_n, $n\ge 3$ admits signed product cordial labeling except when* $n\equiv 2 \bmod 4$.

***Proof*:** Let $V=\{v_1,v_2,\cdots,v_n\}$ be the vertex set and $E=\{v_iv_{i+1};1\le i\le n-1\}\cup\{v_1v_n\}$ be the edge set of the cycle graph C_n. To define vertex labeling $f:V(G)\to\{-1,1\}$ the following case is to be considered.

When $n\equiv 0,1,3 \pmod 4$
for $1\le i\le n$,

$$f(v_i)=\begin{cases}1\,; i\equiv 1,2 \bmod 4\\ -1; i\equiv 0,3 \bmod 4\end{cases}$$

The edge labeling is given by

$$f^*(v_iv_{i+1})=f(v_i)f(v_{i+1})$$
$$=\begin{cases}1 & f(v_i)\text{ and }f(v_{i+1})\text{ have same sign}\\ -1 & f(v_i)\text{ and }f(v_{i+1})\text{ have different sign}\end{cases}$$

In view of the above labeling pattern we have, **Table 1**.

Table 1. Vertex and edge conditions of a cycle graph.

n	$v_f(-1)$	$v_f(1)$	$\left\|v_f(-1)-v_f(1)\right\|$
$n\equiv 0 \bmod 4$	$n/2$	$n/2$	0
$n\equiv 1 \bmod 4$	$(n-1)/2$	$(n+1)/2$	1
$n\equiv 3 \bmod 4$	$(n-1)/2$	$(n+1)/2$	1

n	$e_{f^*}(-1)$	$e_{f^*}(1)$	$\left\|e_{f^*}(-1)-e_{f^*}(1)\right\|$
$n\equiv 0 \bmod 4$	$n/2$	$n/2$	0
$n\equiv 1 \bmod 4$	$(n-1)/2$	$(n+1)/2$	1
$n\equiv 3 \bmod 4$	$(n+1)/2$	$(n-1)/2$	1

Hence the cycle graph $C_n; n \neq 2 \mod 4$ admits signed product cordial labeling.

Theorem 2.4: *The star graph $K_{1,n}, n \geq 2$ admits signed product cordial labeling.*

***Proof*:** The star graph $K_{1,n}$ is a tree obtained by adding *n* pendent edge to the center vertex. Let $V = \{v_1, v_2, \cdots, v_n, v_{n+1}\}$ be the vertex set and the edge set is given by $E = \{v_1 v_i; 2 \leq i \leq n+1\}$. To define vertex labeling for $f : V(G) \to \{-1,1\}$ is given by
for $1 \leq i \leq n+1$

$$f(v_i) = \begin{cases} 1; i \equiv 1 \mod 2 \\ -1; i \equiv 0 \mod 2 \end{cases}$$

When *n* is even and odd, the edge labeling is given by

$$f^*(v_1 v_{2i}) = -1$$
$$f^*(v_1 v_{2i+1}) = 1; 1 \leq i \leq n/2$$

and

$$f^*(v_1 v_{2i}) = -1; 1 \leq i \leq (n+1)/2$$
$$f^*(v_1 v_{2i+1}) = 1; 1 \leq i \leq ((n+1)/2) - 1$$

respectively.

In view of the above labeling pattern we have, **Table 2**.

Hence the star graph $K_{1,n}$ admits signed product cordial labeling.

3. Signed Product Cordial Labeling for Special Graphs

In this section we prove the signed product cordial labeling for the graphs P_n^+, C_n^+ and the bistar graph $B_{n,n}$.

Theorem 3.1: *The Path graph $P_n^+, n \geq 3$ admits signed product cordial labeling.*

***Proof*:** Let $v_1, v_2, v_3 \cdots v_n$ and $u_1, u_2, u_3 \cdots u_n$ be the vertex sets of the path graph P_n^+ and the edge set is given by

$$E_1 = \{v_i v_{i+1}; 1 \leq i \leq n-1\}, E_2 = \{v_i u_i; 1 \leq i \leq n\}$$

The graph P_n^+ has $2n$ vertices and $2n-1$ edges. To define vertex labeling $f : V(G) \to \{-1,1\}$ the following cases are to be considered.

Table 2. Vertex and edge conditions of a star graph.

n	$v_f(-1)$	$v_f(1)$	$\lvert v_f(-1) - v_f(1) \rvert$
$n \equiv 0 \mod 2$	$(n-1)/2$	$(n+1)/2$	1
$n \equiv 1 \mod 2$	$(n+1)/2$	$(n+1)/2$	0

n	$e_{f^*}(-1)$	$e_{f^*}(1)$	$\lvert e_{f^*}(-1) - e_{f^*}(1) \rvert$
$n \equiv 0 \mod 2$	$n/2$	$n/2$	0
$n \equiv 1 \mod 2$	$(n-1)/2$	$(n-3)/2$	1

Case 1: when *n* is even
for $1 \leq i \leq n$

$$f(v_i) = \begin{cases} 1; i \equiv 1, 2 \mod 4 \\ -1; i \equiv 0, 3 \mod 4 \end{cases}$$

$$f(u_i) = \begin{cases} 1; i \equiv 1 \mod 2 \\ -1; i \equiv 0 \mod 2 \end{cases}$$

The edge labeling are defined as follows
for $1 \leq i \leq n-1$

$$f^*(v_i v_{i+1}) = f(v_i) f(v_{i+1}) = \begin{cases} 1 & \text{if } f(v_i) \text{ and } f(v_{i+1}) \text{ have same sign} \\ -1 & \text{if } f(v_i) \text{ and } f(v_{i+1}) \text{ have different sign} \end{cases}$$

for $1 \leq i \leq n$

$$f^*(v_i u_i) = f(v_i) f(u_i) = \begin{cases} 1 & \text{if } f(v_i) \text{ and } f(v_{i+1}) \text{ have same sign} \\ -1 & \text{if } f(v_i) \text{ and } f(v_{i+1}) \text{ have different sign} \end{cases}$$

Case 2: When *n* is odd
The vertex labeling is given by
for $1 \leq i \leq n-2$

$$f(v_i) = \begin{cases} 1; i \equiv 1, 2 \mod 4 \\ -1; i \equiv 0, 3 \mod 4 \end{cases}$$

$$f(v_{n-1}) = 1 ; f(v_n) = -1$$

for $1 \leq i \leq n-1$

$$f(u_i) = \begin{cases} 1; i \equiv 1 \mod 2 \\ -1; i \equiv 0 \mod 2 \end{cases}$$

$$f(u_n) = -1$$

The edge labeling are defined as follows
for $1 \leq i \leq n-1$

$$f^*(v_i v_{i+1}) = f(v_i) f(v_{i+1}) = \begin{cases} 1 & \text{if } f(v_i) \text{ and } f(v_{i+1}) \text{ have same sign} \\ -1 & \text{if } f(v_i) \text{ and } f(v_{i+1}) \text{ have different sign} \end{cases}$$

for $1 \leq i \leq n$

$$f^*(v_i u_i) = f(v_i) f(u_i) = \begin{cases} 1 & \text{if } f(v_i) \text{ and } f(v_{i+1}) \text{ have same sign} \\ -1 & \text{if } f(v_i) \text{ and } f(v_{i+1}) \text{ have different sign} \end{cases}$$

In view of the above labeling pattern we have, **Table 3**.

Hence the graph $P_n^+, n \geq 3$ admits signed product cordial labeling.

Theorem 3.2: *The graph $C_n^+, n \geq 3$ admits signed product cordial labeling except for $n \equiv 2 \mod 4$.*

Table 3. Vertex and edge conditions of the graph $P_n^+, n \geq 3$.

n	$v_f(-1)$	$v_f(1)$	$\lvert v_f(-1) - v_f(1)\rvert$
$n \equiv 0 \bmod 2$	n	n	0
$n \equiv 1 \bmod 4$	n	n	0
$n \equiv 3 \bmod 4$	n	n	0

n	$e_{f^*}(-1)$	$e_{f^*}(1)$	$\lvert e_{f^*}(-1) - e_{f^*}(1)\rvert$
$n \equiv 0 \bmod 2$	$n-1$	n	1
$n \equiv 1 \bmod 4$	n	$n-1$	1
$n \equiv 3 \bmod 4$	$n-1$	n	1

***Proof*:** Let $v_1, v_2, v_3 \cdots v_n$ and $u_1, u_2, u_3 \cdots u_n$ be the vertex sets of the graph $C_n^+, n \geq 3$ with $2n$ vertices and $2n$ edges. The edge set is given by

$$E_1 = \{v_i v_{i+1}; 1 \leq i \leq n-1\} \cup \{v_1 v_n\}$$
$$E_2 = \{v_i u_i; 1 \leq i \leq n\}$$

The vertex labeling is defined by
for $1 \leq i \leq n$

$$f(v_i) = \begin{cases} 1; i \equiv 1, 2 \bmod 4 \\ -1; i \equiv 0, 3 \bmod 4 \end{cases}$$

$$f(u_i) = \begin{cases} -1; i \equiv 1 \bmod 2 \\ 1; i \equiv 0 \bmod 2 \end{cases}$$

The edge labeling is given by
for $1 \leq i \leq n$

$$f^*(v_i v_{i+1}) = f(v_i) f(v_{i+1})$$
$$= \begin{cases} 1 & \text{if } f(v_i) \text{ and } f(v_{i+1}) \text{ have same sign} \\ -1 & \text{if } f(v_i) \text{ and } f(v_{i+1}) \text{ have different sign} \end{cases}$$

$$f^*(v_1 v_n) = \begin{cases} 1 & \text{if } f(v_i) \text{ and } f(v_{i+1}) \text{ have same sign} \\ -1 & \text{if } f(v_i) \text{ and } f(v_{i+1}) \text{ have different sign} \end{cases}$$

$$f^*(v_i u_i) = \begin{cases} 1 & f(v_i) \text{ and } f(v_{i+1}) \text{ have same sign} \\ -1 & f(v_i) \text{ and } f(v_{i+1}) \text{ have different sign} \end{cases}$$

In view of the above labeling pattern we have, the total number of vertices labeled with –1's are given by $v_f(-1) = n$ and the total number of vertices labeled with 1's are given by $v_f(1) = n$. Therefore the total difference between the vertices labeled with –1's and 1's is $\lvert v_f(-1) - v_f(1)\rvert = 0$. The total number of edges labeled with –1's are given by $e_{f^*}(-1) = n$ and the total number of edges labeled with 1's are given by $e_{f^*}(1) = n$. Therefore the total difference between the edges labeled with –1's and 1's is $\lvert e_{f^*}(-1) - e_{f^*}(1)\rvert = 0$, differ by zero.

$$v_f(-1) = v_f(1) = n$$
$$e_{f^*}(-1) = e_{f^*}(1) = n$$

Hence the cycle graph $C_n^+, n \geq 3$ admits signed product cordial labeling.

Theorem 3.3: *The graph $B_{n,n}, n \geq 2$ admits signed product cordial labeling.*

Proof: The graph $B_{n,n}, n \geq 2$ is a bistar obtained from two disjoint copies of $K_{1,n}$ by joining the centre vertices by an edge. It has $2n + 2$ vertices and $2n + 1$ edges. Let $v_1, v_2, v_3, \cdots, v_{2n+2}$ be the vertices of the bistar graph. The edge set is defined as

$$E_1 = \{v_1 v_{2i+1}; 1 \leq i \leq n\},$$
$$E_2 = \{v_2 v_{2i}; 2 \leq i \leq n+1\}$$

We now define vertex labeling $f : V(G) \to \{-1, 1\}$ as

$$f(v_i) = \begin{cases} 1; i \equiv 1 \bmod 2; & 1 \leq i \leq 2n \\ -1; i \equiv 0 \bmod 2; & 3 \leq i \leq 2n+2 \end{cases}$$
$$f(v_2) = 1$$
$$f(v_{2n+1}) = -1$$

The edge labeling is given by

$$f(v_2 v_{2i}) = -1; 2 \leq i \leq n+1$$
$$f(v_1 v_{2n+1}) = -1$$
$$f(v_1 v_{2i+1}) = 1; 1 \leq i \leq n-1$$

The total number of vertices labeled with –1's are given by $v_f(-1) = n+1$ and the total number of vertices labeled with 1's are given by $v_f(1) = n+1$. Therefore the total difference between the vertices labeled with –1's and 1's is $\lvert v_f(-1) - v_f(1)\rvert = 0$. The total number of edges labeled with –1's are given by $e_{f^*}(-1) = n$ and the total number of edges labeled with 1's are given by $e_{f^*}(1) = n+1$. Therefore the total difference between the edges labeled with –1's and 1's is $\lvert e_{f^*}(-1) - e_{f^*}(1)\rvert = 1$, differ by one. In view of the above labeling pattern we have,

$$v_f(-1) = v_f(1) - 1 = n+1$$
$$e_{f^*}(-1) = e_{f^*}(1) + 1 = n+1$$

From the above labeling pattern we have $\lvert v_f(-1) - v_f(1)\rvert \leq 1$ and $\lvert e_{f^*}(-1) - e_{f^*}(1)\rvert \leq 1$. Hence the bistar graph $B_{n,n}, n \geq 2$, admits signed product cordial labeling.

Example 3.4: Figure 1 illustrates the signed product cordial labeling for Bistar $B_{5,5}$. Among the eleven edges five edges receive the label +1 and six edges receive the label –1.

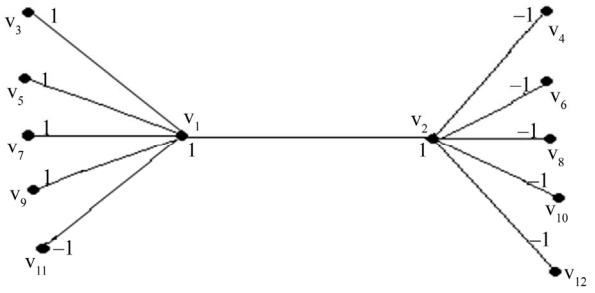

Figure 1. Signed product cordial labeling of Bistar $B_{5,5}$.

4. General Results on Signed Product Cordial Labeling

In this section we prove the Signed product cordial labeling for the some general graphs.

Definition 4.1: The tree $T@mK_1$ is obtained by attaching m copies of K_1 to any one of the vertices in T.

Theorem 4.2: *If a tree T admits signed product cordial labeling with n vertices then* $T@mK_1$ (*m even*) *is also a signed product cordial tree*.

***Proof*:** Let us assume that a tree T admits signed product cordial labeling. The mapping $f:V\to\{-1,1\}$ satisfies the condition of signed product cordial labeling.

Let $T'=T@mK_1=(V',E')$ where $V'=V\cup\{u_1,u_2,\cdots,u_n\}$ and $E'=E\cup\{vu_1,vu_2,\cdots,vu_n\}$. The vertex labeling for T', $g:V'\cup\{-1,1\}$ is defined as $g(v)=f(v)\,\forall\, v\in V$.

Let $\{u_1,u_2,\cdots,u_m\}$ be the m vertices joined to the vertex v of the tree T. The vertex labeling of $\{u_1,u_2,\cdots,u_m\}$ is given by $g(u_i)=(-1)^i; 1\le i\le m$. If $f(v)=1$, then the sign of $g(vu_1),g(vu_2),\cdots,g(vu_m)$ will be the sign of $g(u_1),g(u_2),\cdots,g(u_m)$ respectively and if $f(v)=-1$ then the sign of $g(vu_1),g(vu_2),\cdots,g(vu_m)$ will be the sign of $-g(u_1),-g(u_2),\cdots,-g(u_m)$. In both the cases the new m edges $\{vu_1,vu_2,\cdots,vu_m\}$ contributes equal number of edges labeled with –1's and 1's. Therefore in a tree $T@mK_1$, the difference between the total number of vertices labeled with –1's and 1's and the difference between the total number of edges labeled with –1's and 1's differs by utmost one.

Example 4.3: Figure 2 illustrates the signed product cordial labeling for $T@4K_1$ where T is an arbitrary tree having signed product cordial labeling.

Corollary 4.4: If a connected graph G has signed product cordial labeling then the graph $G@mK_1$ where m is even admits signed product cordial labeling.

Definition 4.5: The tree $T\hat{0}P_n$ is obtained by superimposing a pendant vertex of P_n with any of the selected vertex in T.

Theorem 4.6: *If a tree T as signed product cordial labeling then* $T\hat{0}P_n$ *where m is odd admits signed product cordial labeling*.

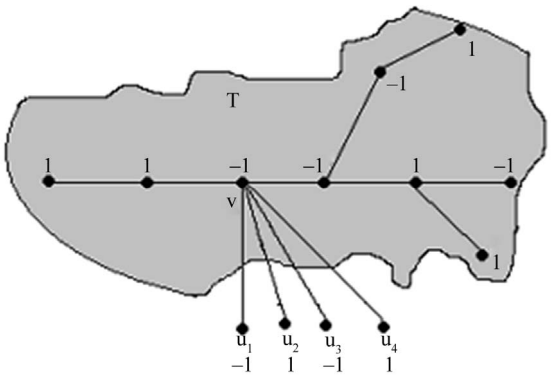

Figure 2. Signed product cordial labeling of $T@4K_1$.

***Proof*:** Let $T=(V,E)$ be a connected graph with vertex set V and edge set E then the tree $T\hat{0}P_n=(V',E')$ where $V'=V\cup\{u_1,u_2,\cdots,u_n\}$ and $E'=E\cup\{u_iu_{i+1};1\le i\le n-1\}$. Let v be a vertex in T. we superimpose a pendant vertex with a selected vertex v in T only if they preserves the same sign.

Case 1: If $f(v)=f(u_1)=1$, then the vertex labeling for the path graph follows from theorem 2.2

Case 2: If $f(v)=f(u_1)=-1$, then the vertex labeling is given by

Sub Case 2.1: when $n\equiv 0,1,3 \pmod 4$ for $1\le i\le n$

$$f(v_i)=1;\ i\equiv 0,3 \bmod 4$$
$$=-1;\ i\equiv 1,2 \bmod 4$$

Sub Case 2.2: when $n\equiv 2 \pmod 4$ for $1\le i\le n-2$

$$f(v_i)=1;\ i\equiv 0,3 \bmod 4$$
$$=-1;\ i\equiv 1,2 \bmod 4$$

and

$$f(v_{n-1})=-1,\ f(v_n)=1$$

As we superimpose the pendant vertex of P_n with any one of the vertex in T provided they preserve the same sign then the path graph contributes equal number of vertices and edges labeled with –1's and 1's. Hence the tree $T\hat{0}P_n$ admits signed product cordial labeling.

Corollary 4.7: *If a connected graph G has signed product cordial labeling then the graph* $T\hat{0}P_n$ *where n is odd admits signed product cordial labeling.*

Theorem 4.8: *If a connected graph G has a signed product cordial labeling with n vertices* ($n\equiv 0 \bmod 4$) *then* G^+ *admits signed product cordial.*

Proof: Let $G=(V,E)$ be a connected graph with vertex set $V=\{u_1,u_2,\cdots,u_n\}$. Since G has a signed product cordial labeling there exists $f:V\to\{-1,1\}$ such that $|v_f(-1)-v_f(1)|\le 1$ and $|e_{f^*}(-1)-e_{f^*}(1)|\le 1$.

As $n \equiv 0 \bmod 4$, $\left|v_f(-1) - v_f(1)\right| = 0$. Let $V = \{V_1 \cup V_2\}$ where $V_1 = \{u_i : i \equiv 1 \bmod 2\}$ and $V_2 = \{u_i : i \equiv 0 \bmod 2\}$. For our convenience let us assume that f maps all the vertices of V_1 to 1 and all the vertices of V_2 to -1. The graph $G^+ = (V', E')$ is obtained by attaching the pendant vertices $\{u_1', u_2', \cdots, u_n'\}$ to each of the vertices $\{u_1, u_2, \cdots, u_n\}$ in G. Let the vertex set and edge set of G^+ be defined as $V' = \{u_i, u_i' : 1 \le i \le n\}$ and $E' = E \cup \{u_i u_i'; 1 \le i \le n\}$.

The vertex labeling for the graph G^+, $g : V' \to \{-1, 1\}$ is defined as follows for, $1 \le i \le n$

$$g(u_i) = f(u_i)$$

$g(u_i')$

$$= \begin{cases} -1 \text{ when } i \equiv 0 \bmod 2 \text{ and } f(u_i) = -1 \text{ if } i \equiv 0 \bmod 4 \\ 1 \text{ when } i \equiv 1 \bmod 2 \text{ and } f(u_i) = 1 \text{ if } i \equiv 1 \bmod 4 \\ -1 \text{ when } i \equiv 0 \bmod 2 \text{ and } f(u_i) = 1 \text{ if } i \equiv 2 \bmod 4 \\ 1 \text{ when } i \equiv 1 \bmod 2 \text{ and } f(u_i) = -1 \text{ if } i \equiv 3 \bmod 4 \end{cases}$$

The induced edge labels $g^*(uv) = f(uv) \ \forall \ uv \in E$. All the newly added edges $g^*(u_i u_i')$ will share equally the labels -1 and 1 as per our construction above. Hence $\left|v_g(-1) - v_g(1)\right| = 0$ and $\left|e_{g^*}(-1) - e_{g^*}(1)\right| = 0$. Only by this labeling pattern the graph G^+ admits signed product labeling where n is a multiple of 4.

5. Acknowledgements

The referee is gratefully acknowledged for their suggestions that improved the manuscript.

6. References

[1] I. Cahit, "Cordial Graphs: A Weaker Version of Graceful and Harmonious Graphs," *Ars Combinatoria*, Vol. 23, 1987, pp. 201-207.

[2] M. Sundaram, R. Ponraj and S. Somasundram, "Total Product Cordial Labeling of Graphs," *Bulletin of Pure and Applied Sciences*: *Section E. Mathematics and Statistics*, Vol. 25, 2006, pp. 199-203.

[3] J. A. Gallian, "A Dynamic Survey of Graph Labeling," *Electronic Journal of Combinatorics*, Vol. 17, No. DS6, 2010, pp. 1-246.

[4] S. K. Vaidya, N. A. Dani, K. K. Kanani and P. L. Vihol, "Cordial and 3-Equitable Labeling for Some Star Related Graphs," *International Mathematical Forum*, Vol. 4, No. 31, 2009, pp. 1543-1553.

Applied Mathematics, **2011, 2, 1531-1534**
doi:10.4236/am.2011.212217 Published Online December 2011 (http://www.SciRP.org/journal/am)

Cryptographic PRNG Based on Combination of LFSR and Chaotic Logistic Map

Hamed Rahimov, Majid Babaei, Mohsen Farhadi
Department of Computer Engineering, Shahrood University of Technology, Shahrood, Iran
E-mail: *hrahimov@shahroodut.ac.ir*, *babaee@comp.tus.ac.ir*, *mfarhadi@shahroodut.ac.ir*
Received September 6, 2011; *revised October* 21, 2011; *accepted October* 30, 2011

Abstract

The random sequence generated by linear feedback shift register can't meet the demand of unpredictability for secure paradigms. A combination logistic chaotic equation improves the linear property of LFSR and constructs a novel random sequence generator with longer period and complex architecture. We present the detailed result of the statistical testing on generated bit sequences, done by very strict tests of randomness: the NIST suite tests, to detect the specific characteristic expected of truly random sequences. The results of NIST's statistical tests show that our proposed method for generating random numbers has more efficient performance.

Keywords: Random Bit Generator, Combination, Chaotic, Logistic Equations, LFSR, NIST Suite Tests

1. Introduction

With perfect method of cryptographic algorithm based on generating high performance of random numbers, the need for random numbers of high quality is growing [1, 2]. Random numbers are also used for key generation in symmetric. For example, in the Smart cards, the main problem is the security which improves by using reliable random number generators (RNGs) [3].

One of the most reliable methods that work as RNG in cryptographic algorithms is Linear Feedback Shift Register (LFSR) [4-6] in stream cipher usage and is appropriate to low power or high speed application [5]. Since LFSRs are linear systems. They lead to responsible easy cryptanalysis tools. The short period of LFSR's outputs is the negative point of using this system as a reliable method in cryptographic algorithms.

LFSR is a shift registered the inputs of which are based on linear function of its previous states. It uses two linear operators Exclusive-OR ($\oplus$) [6]. The LFSR is initializing by the random string that is called the seed and since the operation of register is deterministic, the result's string which is produced by the LFSR is completely determined (*i.e*. the current bit determined by its previous states) [4,7]. If the LFSR has the n bits the biggest number for internal state is 2^n so to gain the longest period of this method (*i.e*. 2^{n-1}), LFSR with length n needs to find n exponent primitive polynomial [4,7]. The architecture is shown in **Figure 1**.

However, the production of n exponent primitive polynomials becomes more difficult with the increment of n. Generally, through 2^{n-1} factorization, we can make sure that an n exponent polynomial is a primitive polynomial. Furthermore, the items of n exponent primitive polynomial are more complex to make a breakthrough. If the exponent of primitive polynomial is bigger, LFSR will be longer.

Reese defined a genetic algorithm for optimization problem. That parent population was generated by random number generator, pseudo random number generator, quasi random number generator [7]. Finally she ranked these generators with comparing precisions generated answers by GA and showed the genetic algorithm is a criterion to realize what initial population is more uniformity [8]. Also chaotic random number generator (CRNGs) was compared to other RNGs with this method [9]. In this Paper we used another famous test method: NIST suite test that is a statistical package comprising of 15 tests.

2. Chaotic Logistic Equation

The simple modified mathematical from of the logistic equation is given as:

$$f(x_n) = x_{n+1} = r \cdot x_n \cdot (1 - x_n) \quad (1)$$

where x_n is the state variable, which lies in the interval

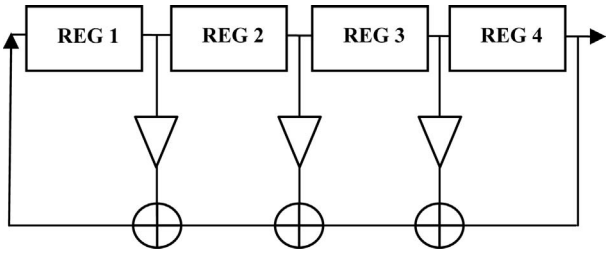

Figure 1. Linear Feedback Shift Register.

$[0\cdots1]$ and r is system parameter which can have any value between $[1\cdots4]$.

In **Figure 2**, we have displayed the Lyapunov exponent which is the quantities measure of chaos as a function of system parameter r. A positive Lyapunov exponent (for example at r = 3.99) indicates chaotic behavior.

This paper proposes a random bit generator, which is based on chaotic LFSR; the chaotic system starting from random independent initial conditions $x_0, y_0 \in (0,1)$ and $x_0 \neq y_0$.

Based on this theorem, in the next section we describe the new random number generator which can be used in the cryptology algorithms.

3. Proposed RNG

In this section, we describe the proposed method for generating random numbers, so based on previous sections in our method; in the first iteration it generated two random numbers (e.g. 0.9917 and 0.2375) with logistic chaotic equations. Then it defines a function with Equation (2):

$$G(n) = \sum_{n=0}^{M} (x_n + y_n) \mod 1 \qquad (2)$$

where $G:[0\cdots1]\to[0\cdots1]$ so $G(n)$ is the decimal parts of these numbers and $M \in \mathbb{N}$.

L.Y. Deng *et al*. have proved that combination generator should improve upon the uniformity as well as the independence over individual generators [10]. Knowing that for any real number x, $x \bmod 1 = x - [x]$, where $[x]$ is the generated integer $\leq x$.

In the next level of the proposed method, we define a function $f(x)$ which can compare x value with a threshold, the best threshold for interval $[0\cdots1]$ is 0.5. So according to **Figure 3**, if x is the larger than 0.5 number 1 *XOR* with LFSR output, else number 0 *XOR* with LFSR output. Linear correlation in LFSR outputs decreases with this technique. According to the NIST suite test the number of binary sequences at least should be 2000 which the length of each sequence is 10^6 bits so there is no experimental way to generate a valid sequence with the efficient period based on LFSR method. Our proposed RNG method prepares the external bit of

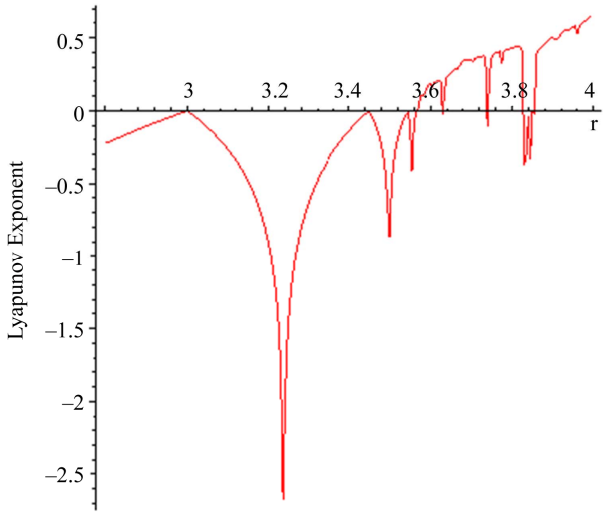

Figure 2. Plot of the lyapunov exponent versus *r* for logistic equation.

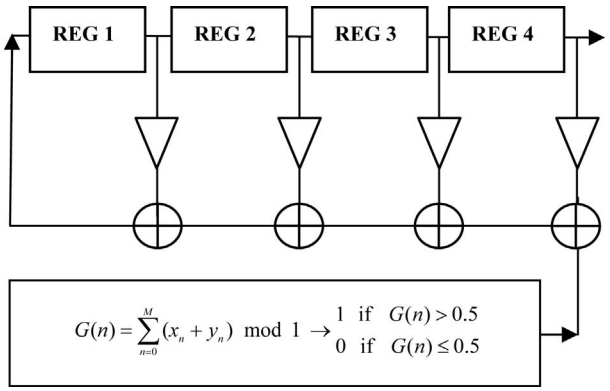

Figure 3. Chaotic liner feedback shift register diagram.

the chaotic logistic map that changes the system condition and generates the sequence of bits with no period.

4. Test Results

In the last part of our paper before conclusion, we will refer to the NIST suite test in the **Tables 1-4**; the first column in these tables is the test's names; the second column is the P-value that is in the interval $[0\cdots1]$, the test has the better condition (*i.e.* it's more reliable) when it's P-value tend to 1; and the third column shows the pass rate of these tests (*i.e.* how proportion of the sequences that tested by this method, pass the test). Considering these facts, we have 15 tests in **Table 1** that describe the general condition of the sequences which is produced by our proposed method and the other Tables show the proposed method condition with more detail. That is, non-overlapping templates in **Table 2**, the purpose of this test is to detect the number of occurrences of specific string. Random excursions test is shown in

Table 1. NIST suite tests table.

Test	P-Value	Pass Rate
Frequency	0.757790	0.9900
Block-Frequency	0.742917	0.9915
CuSums-forward	0.953553	0.9895
CuSums-backward	0.912069	0.9885
Rans	0.302657	0.9950
Long run	0.471146	0.9860
Rank	0.363593	0.9920
FFT	0.000159	0.9950
Overlapping templates	0.422638	0.9885
Universal	0.349676	0.9905
Approximate entropy	0.669359	0.9915
Serial 1	0.301194	0.9910
Serial 2	0.406499	0.9945
Linear complexity	0.125200	0.9920

Table 2. Non-overlapping templates.

Test	P-value	Pass Rate
Template = 000000001	0.069863	0.9895
Template = 000100111	0.292519	0.9895
Template = 001010011	0.028529	0.9935
Template = 010001011	0.342451	0.9880
Template = 011101111	0.515118	0.9910
Template = 101101000	0.845490	0.9935
Template = 110100100	0.786830	0.9900
Template = 111100000	0.892036	0.9885

Table 3. Random excursions test.

Test	P-value	Pass rate
X = –4	0.381162	0.9902
X = –3	0.379765	0.9878
X = –2	0.863888	0.9869
X = –1	0.464167	0.9918
X = +1	0.426003	0.9878
X = +2	0.700827	0.9894
X = +3	0.757015	0.9869
X = +4	0.899722	0.9878

Table 4. Random excursions variant test.

Test	P-value	Pass rate
X = –9	0.891536	0.9918
X = –8	0.510380	0.9918
X = –7	0.677158	0.9927
X = –6	0.710898	0.9927
X = –5	0.933972	0.9910
X = –4	0.651625	0.9869
X = –3	0.231937	0.9853
X = –2	0.113023	0.9927
X = –1	0.465727	0.9902
X = +1	0.518531	0.9910
X = +2	0.396742	0.9894
X = +3	0.908694	0.9878
X = +4	0.602174	0.9927
X = +5	0.651625	0.9886
X = +6	0.200238	0.9861
X = +7	0.445638	0.9869
X = +8	0.658445	0.9878
X = +9	0.326496	0.9878

Table 3; this test shows is the number of cycles having exactly K visits in a cumulative sum random walk. **Table 4** describes random excursions variant test, the focus of this test is the total number of times that the particular state is visited [11].

5. Conclusions

We have proposed a design of a pseudo random bit generator (PRBG) based on combination chaotic logistic equations and LFSR method. That chaotic system iterated independently starting from independent initial conditions. The pseudo random bit sequence is obtained by combining the outputs of both the chaotic logistic equations with LFSR method. We have also tested rigorously the generated sequences using the NIST suite tests. The results of statistical testing are encouraging and show that the proposed PRBG has perfect cryptographic properties and hence can be used in the design of new stream ciphers.

6. References

[1] R. C. Fairfield, R. L. Mortenson and K. B. Coulthart, "An LSI Random Number Generator (RNG)," *Advances in Cryptography*: *Proceeding of Cryptography* 84, Vol. 196, 1984, pp. 203-230.

[2] S. Callegari, R. Rovatti and G. Setti, "Embeddable ADC-Based True Random Number Generator for Cryptogra-

phic Applications Exploiting Nonlinear Signal Processing and Chaos," *Signal Processing IEEE Transactions*, Vol. 53, No. 2, 2005, pp. 793-805. doi:10.1109/TSP.2004.839924

[3] K. Tsoi, K. Leung and P. Leong, "Compact FPGA-Based True and Pseudo Random Number Generators," *Proceedings of IEEE Symposium on Field-Programmable Custom Computing Machines* (*FCCM*), 9-11 April 2003, pp. 51-61.

[4] H. Zhang, Y. Wang, B. Wang and X. Wu, "Evolutionary Random Sequence Generators Based on LFSR," *Wuhan University Journal of Natural Sciences*, Vol. 12, No. 1, 2007, pp. 75-78.

[5] T. Stojanovski, J. Pil and L. Kocarev, "Chaos-Based Random Number Generators. Part II: Practical Realization," *IEEE Transactions on Circuits and Systems I*: *Fundamental Theory and Applications*, Vol. 48, No. 3, 2001, pp. 382-385. doi:10.1109/81.915396

[6] M. Sharaf, H. A. K. Mansour and H. H. Zayed, "A Complex Linear Feedback Shift Register Design for the A5 Key Stream Generator," *Proceedings of the Twenty-Second National Radio Science Conference* (*NRSC* 2005), Cairo, 15-17 March 2005, pp. 395-402. doi:10.1109/NRSC.2005.194024

[7] L. C. Reese, W. M. Isenhower and S.-T. Wang. "Analysis and Design of Shallow and Deep Foundations," John Wiley & Sons, New York, 2006.

[8] L. Y. Deng and Y. C. Chu, "Combining Random Number Generators," *Proceedings of the* 23*rd Conference on Winter Simulation*, 1991, pp. 1043-1046.

[9] A. Reese, "Random Number Generators in Genetic Algorithms for Unconstrained and Constrained Optimization," *Nonlinear Analysis*, Vol. 71, 2009, pp. 679-692. doi:10.1016/j.na.2008.11.084

[10] M. Babaei and M. Ramyar, "Improved Performance of LFSR's System with Discrete Chaotic Iterations," *Word Applied Science Journal* (*ISI*), Vol. 13, No. 7, 2011, pp. 1720-1725.

[11] NIST Special Publication 800-22, Statistical Test Suite for Random and Pseudo Random Number Generators for Cryptographic Applications, Available at http://www.nist.gov

Applied Mathematics, **2011, 2, 1535-1538**
doi:10.4236/am.2011.212218 Published Online December 2011 (http://www.SciRP.org/journal/am)

Scientific Research

An Efficient Combinatorial-Probabilistic Dual-Fusion Modification of Bernstein's Polynomial Approximation Operator

Shanaz Ansari Wahid
Department of Mathematics & Statistics, *Faculty of Science & Agriculture*,
St. Augustine Campus of the University of the West Indies, *Debe*, *Trinidad & Tobago*
E-mail: *Shanaz.Wahid@sta.uwi.edu*, *shanazw@hotmail.com*
Received March 29, 2011; *revised November* 14, 2011; *accepted November* 22, 2011

Abstract

The celebrated Weierstrass Approximation Theorem (1885) heralded intermittent interest in polynomial approximation, which continues unabated even as of today. The great Russian mathematician Bernstein, in 1912, not only provided an interesting proof of the Weierstrass' theorem, but also displayed a sequence of the polynomials which approximate the given function $f(x) \in C[0,1]$. An efficient "Combinatorial-Probabilistic Dual-Fusion" version of the modification of Bernstein's Polynomial Operator is proposed. The potential of the aforesaid improvement is tried to be brought forth and illustrated through an empirical study, for which the function is assumed to be known in the sense of simulation.

Keywords: Approximation, Bernstein Operator, Dual-Fusion, Simulated Empirical Study

1. Introduction

The problem of approximation arises in many contexts of "Numerical Analyses and Computing" [1-4]. Weirstrass [5] proved his celebrated approximation theorem: "…If, $f \in C[a,b]$, then for every $\delta > 0$, $\exists$ a polynomial "p" such that "$\|f - p\| < \delta$". In other words, result established the existence of an algebraic polynomial in concerned variable capable of approximating the unknown function in that variable, as closely as we please!

This result was a big beginning of the Mathematicians' interest in "Polynomial Approximation" [4,6-8] of an unknown function using its values generated, experimentally or otherwise, at certain equidistant knots in the impugned interval of the relevant variable. The Great Russian mathematician Bernstein proved the Weirstrass theorem in a style, which was very thought-provoking and curious in many ways. He first noted a simple though a very significant feature of this theorem, namely that if it holds for $C[0,1]$, it does hold for $C[a,b]$ also vice-versa. In fact, $C[0,1]$ and $C[a,b]$ are essentially identical, for all practical purposes, inasmuch as they are linearly "isometric" as normed spaces, order isomorphic as lattices, and isomorphic as algebras (rings) [9].

Also, the most important contribution in the Bernstein's proof of the Weirstrass' theorem consisted in the fact that Bernstein actually displayed a sequence of polynomials that approximate a given function $f \in C[0,1]$.

If, $f(x)$ is any bounded function on $C[0,1]$, the sequence of "Bernstein Polynomials" [6] for $f(x)$ is defined by:

$$\left(\mathrm{Bn}(f)\right)(x) = \sum_{k=0}^{k=n} \binom{n}{k} x^k \cdot (1-x)^{(n-k)} \cdot f(k/n) \quad (1)$$

$x \in \mathrm{C}[0,1]$, Say $E[f(x)]$

The aim of this paper is to propose a more efficient polynomial approximation operator exploiting the "combinatorial structure" of the "Bernstein's Polynomial Approximation operator", and the fact that the unknown function might, without any loss of the generality, be assumed to be $f \in C\left[0, \frac{1}{2}\right]$, as in [10-14].

2. The Proposition of the Variant of the Bernstein Polynomial Approximator

In context of the aforementioned sequence of "Bernstein Polynomials" for $f(x)$, a significant observation which must be taken note of is that the use is made of the values

of the unknown function "$f(x)$" at the equidistant-knots "$\frac{k}{n}; k = 0(1)n$", assumed to be knowable through the experiment (s) in the relevant scientific field of investigation or known otherwise.

In any approximating polynomial operator use is made of the "Knots" and of the corresponding "Weights".

In our proposition of a variant of the "Bernstein's Polynomial" we propose to systematically introduce new corresponding weights, without essentially changing the location of the "equi-distant" "knots", except for the fact that the impugned interval is $C\left[0,\frac{1}{2}\right]$, rather than $C[0,1]$, thanks to "isometric" spaces noted earlier. We propose a variant of the "Bernstein Polynomial" which is having a better combinatorial structure in favor of the interval for $f \in C\left[0,\frac{1}{2}\right]$, and that is the main strategy for making it better than the original/usual "Bernstein's Polynomial"! We consider the following PRIMAL variant of the Bernstein's Polynomial:

Say,

$$\mathrm{B}^{\mathrm{P}}(f;x)[n] = \sum_{k=0}^{k=n}\binom{n}{k}.(0.67+x)^{k} \cdot (0.33-x)^{(n-k)} \cdot f\left(k/(2*n)\right)$$

3. The Combinatorial-Probability & Dual-Fusion Variant for Bernstein's Polynomial

The original interval $C[0,1]$ isometric to the impugned interval $C\left[0,\frac{1}{2}\right]$ could be thought of in terms of its two parts, namely "$0.33-x$" and "$0.67+x$" for $x \in C[0,1]$ with "k" and "$n-k$" "knots" sitting in each, respectively. The expected number of points sitting these two parts. Respectively, would be $n^{(0.33-x)}$ and $n^{(0.67+x)}$. The "combinatorial probability" of description would be: binomial

$$\left(n*(0.33-x), k\right)\text{binomial}\left(n*(0.67+x), n-k\right)/\text{binomial}(n,n)$$

$$\equiv \text{binomialn}\left((0.33-x), n-k\right)\text{binomialn}\left((0.67+x), n-k\right)$$

Hence the PRIMAL-Variant of the "Bernstein's Polynomial" in (2.1) comes off to be as below.

Say,

$$\mathrm{BV}^{\mathrm{P}}(f;x)[n] = \sum_{k=0}^{k=n}\text{binomial}\ \left(n*(0.33-x), k\right) * \text{binomial}\ \left(n*(0.67+x), n-k\right).f\left(k/(2*n)\right)$$

The correspondingly DUAL (-Weights) variant of Bernstein Polynomial would be:

Say,

$$\mathrm{BV}^{\mathrm{P}}(f;x)[n] = \sum_{k=0}^{k=n}\text{binomial}\ \left(n*(0.33+x), k\right) * \text{binomial}\ \left(n*(0.67-x), n-k\right)f\left(k/(2*n)\right)$$

We define the "PRIMAL-DUAL-Fusion-Weights" variant of the Bernstein Polynomial as

Follows: Say,

$$\mathrm{PDFBV}(f;x)[n] = \left[\mathrm{BV}^{\mathrm{P}}(f;x) + \mathrm{BV}^{\mathrm{D}}(f;x)\right]/2$$

To make comprehensive the combinatorial systematicness of PRIMAL-DUAL Fusion variant of Bernstein polynomial say $\mathrm{PDFBV}(f;x)[n]$, we note that it will work for an approximation polynomial focusing interval $[(1/3-x)/2, (1/3+x)/2]$ around "0.33", which will $\sim [0,1/3]$ for $x = 1/3$.

Impugned interval will be wider, the greater the value of "$x < 1/3$"! For example, in the approximating polynomial in "x" for values of $x \in [0,1/3]$; interval will be symmetrically, centered on "0.165", e.g. $\sim [0.035, 0.295]$ for $x = 0.26$.

To balance the "Pull", systematically, the weights "(1/2)" and "(1/2)" are assigned to the relevant weights in $\mathrm{B}^{\mathrm{P}}(f;x)[n]$ & $\mathrm{B}^{\mathrm{D}}(f;x)[n]$. These weights are also, respectively, "DUAL" to each-other, again!

The aforesaid (PRIMAL-DUAL Fusion) variant of the Bernstein Polynomial, namely, $\mathrm{PDFBV}(f;x)[n]$ will, apparently induce a "(Systematic)Bias" in the approximating "Polynomial", which is amenable more systematically than that in the original "Bernstein's Polynomial".

Similar to what was noted in Sahai (2004) [10], in the absence of any conclusive analytical study [The derivable "Upper" bounds on the error of approximation (as noted in the paper by Sahai (2004) [8]) are not of much use. In fact, a smaller/lower "Upper Bound" does not guarantee a better approximation and the extent of the resultant "GAIN" is unavailable, too! Hence, we go for an empirical simulation study to illustrate the potential "GAIN" through our PRIMAL-DUAL Fusion variant of the Bernstein Polynomial, namely, $\mathrm{PDFBV}(f;x)[n]$.

4. The Empirical Simulation Study

To illustrate gain in efficiency by using our proposed "Dual-Fusion" variant of Bernstein Polynomial Approximation, we have carried an empirical study. We have taken example-cases of n = 3, 6, and 9 (*i.e.* n + 1 = 4, 7, and 10 knots) in the empirical study.

To numerically illustrate the relative gain in efficiency in using "Dual-Fusion" variant of Bernstein Polynomial

proposed vis-à-vis the original (Primal) Bernstein's polynomial operator in each example case of *n*-value.

Essentially, the empirical study is a simulation one wherein we would assume that approximated function, namely "$f(x)$", is known to us.

We have confined to illustrations of relative gain in efficiency by Iterative Improvement for the following four illustrative-functions:

$$f(x)=\exp(x);\ \ln(2+x);\ \sin(2+x),\ \text{and}\ 10^{x}.$$

To illustrate the POTENTIAL of improvement with our proposed Dual-Fusion Operator $\mathrm{PDFBV}(f;x)[n]'$, we have TWO numerical values of quantities ~ two percentage relative errors (PREs) corresponding to original (Primal) Bernstein's Operator $\mathrm{B}^{\mathrm{P}}(f;x)[n]$: Say; $\mathrm{PRE\_PFB}(f;x)[n]$ verses that of the proposed Dual-Fusion Operator *i.e.*; $\mathrm{PRE\_PDFBV}(f;x)[n]$. We calculated Percentage Relative Gains (PRGs) in using our "Dual-Fusion" variant of Bernstein Polynomial in place of Original "Primal" variant of Bernstein Polynomial $\mathrm{PRG\_UPDFB}(f;x)[n]$. These quantities are defined: $\mathrm{PRE\_PFB}(f;x)[n]=100$.

$$\left[\left\{\int_{0}^{0.33}\text{abs.}\left(\mathrm{PFB}\ (f;x)[n]-f\ (x)\right)\mathrm{d}x\right\}\Big/\int_{0}^{0.33}f(x)\ \mathrm{d}x\right]$$

$$\&\mathrm{PRE\_PDFBV}(f;x)[n]=100.$$

$$\left[\left\{\int_{0}^{0.33}\text{abs.}\left(\mathrm{PDFBV}\ (f;x)[n]-f\ (x)\right)\mathrm{d}x\right\}\Big/\int_{0}^{0.33}f(x)\ \mathrm{d}x\right]$$

.

Hence, $\mathrm{PRG\_\ PDFBV}(f;x)[n]=100$.

$$\left[\left\{\mathrm{PRE\_PFB}(f;x)[n]-\mathrm{PRE\_PDFBV}(f;x)[n]\right\}\Big/\mathrm{PRE\_PFB}(f;x)[n]\right]$$

PREs for Original-Primal/Variant Primal-Dual Bernstein polynomial respectively for each of example # of approximation Knots/Intervals.

PRGs by using Proposed Dual-Fusion Polynomials with the *n* intervals in $[0,1/2]$ over using the Original Primal-Bernstein Polynomial for approximation of function, "$f(x)$" are tabulated in APPENDIX in **Tables 1-4**.

5. Conclusions

For all the FOUR illustrative functions, namely $f(x)=\exp 9x;\ \ln(2+x);\ \sin(2+x)$, and 10^{x}, the PRGs are above 99.9% for $n=3$, 6, and 9. It is very significant to note that the PRGs are (almost) 100% for $n=6$ for all example-functions, *i.e.* for only SEVEN "Knots"!

6. References

[1] W. Cheney and D. Kincaid, "Numerical Mathematics and Computing," Brooks/Cole Publishing Company, Belmont, 1994.

[2] P. J. Heartley, A. Wynn-Evans, "A Structured Introduction to Numerical Mathematics," Stanley Thornes, Belmont, 1979.

[3] B. F. Polybon, "Applied Numerical Analysis," PWS-Kent, Boston, 1992.

[4] A. Sheilds, "Polynomial Approximation," *The Math Intelligencer*, Vol. 9, No. 3, 1987, pp. 5-7.

[5] K. Weierstrass, "Uber die analytische Darstellbarkeit sogenannter willkurlicher Functionen einer reellen Veranderlichen Sitzungsberichteder," *Koniglich Preussischen Akademie der Wissenschcaften zu Berlin*, 1885, pp. 633-639 & pp. 789-805.

[6] N. L. Carothers, "A Short Course on Approximation Theory," Bowling Green State University, Bowling Green, OH, 1998.

[7] E. R. Hedrick, "The Significance of Weirstrass Theorem," *The American Mathematical Monthly*, Vol. 20, 1927, pp. 211-213. doi:10.2307/2974105

[8] G. G. Lorentz, "Approximation of Functions," Chelsea, New York, 1986.

[9] N. L. Carothers, "Real Analysis," Cambridge University Press, Cambridge, 2000.

[10] A. Sahai, "An Iterative Algorithm for Improved Approximation by Bernstein's Operator Using Statistical Perspective," *Applied Mathematics and Computation*, Vol. 149, No. 2, 2004, pp. 327-335. doi:10.1016/S0096-3003(03)00081-X

[11] A. Sahai and G. Prasad, "Sharp Estimates of Approximation by Some Positive Linear Operators," *Bulletin of the Australian Mathematical Society*, Vol. 29, No. 1, 1984, pp. 13-18. doi:10.1017/S0004972700021225

[12] A. Sahai and S. Verma, "Efficient Quadrature Operator Using Dual-Perspectives-Fusion Probabilistic Weights," *International Journal of Engineering and Technology*, Vol. 1, No. 1, 2009, pp. 1-8.

[13] S. A. Wahid, A. Sahai and M. R. Acharya, "A Computerizable Iterative-Algorithmic Quadrature Operator Using an Efficient Two-Phase Modification of Bernstein Polynomial," *International Journal of Engineering and Technology*, Vol. 1, No. 3, 2009, pp. 104-108.

[14] A. Sahai, S. A. Wahid and A. Sinha, "A Positive Linear Operator Using Probabilistic Approach," *Journal of Applied Science*, Vol. 6, No. 12, 2006, pp. 2662-2665.

APPENDIX

Table 1. (Iterative) algorithmic (In %) relative (absolute) efficiency/gain for $f(x) = \exp(x)$.

Items ↓	$n \to 3$	6	9
PRE_PFB $(f; x)[n]$	7.7098	7.97506	8.0614
PRE_PDFBV $(f; x)[n]$	0.0004	0.00000	0.0000
PRG_PDFBV $(f; x)[n]$	99.994	100.000	99.999

Table 2. (Iterative) algorithmic (In %) relative (absolute) efficiency/gain for $f(x) = \ln(2 + x)$.

Items ↓	$n \to 3$	6	9
PRE_PFB $(f; x)[n]$	5.0970	5.0217	4.9961
PRE_PDFBV $(f; x)[n]$	0.0001	0.0000	0.0000
PRG_PDFBV $(f; x)[n]$	99.996	100.00	99.999

Table 3. (Iterative) algorithmic (In %) relative (absolute) efficiency/gain for $f(x) = \sin(2 + x)$.

Items ↓	$n \to 3$	6	9
PRE_PFB $(f; x)[n]$	5.0404	5.3105	5.4020
PRE_PDFBV $(f; x)[n]$	0.0004	0.0000	0.0000
PRG_PDFBV $(f; x)[n]$	99.991	99.999	99.999

Table 4. (Iterative) algorithmic (In %) relative (absolute) efficiency/gain for $f(x) = 10^x$.

Items ↓	$n \to 3$	6	9
PRE_PFB $(f; x)[n]$	16.112	17.498	17.935
PRE_PDFBV $(f; x)[n]$	0.0120	0.0000	0.0000
PRG_PDFBV $(f; x)[n]$	99.925	99.999	99.999

Applied Mathematics, 2011, 2, 1539-1545
doi:10.4236/am.2011.212219 Published Online December 2011 (http://www.SciRP.org/journal/am)

Minimax Multivariate Control Chart Using a Polynomial Function

Johnson Ademola Adewara[1], Kayode Samuel Adekeye[2], Osebekwin Ebenezer Asiribo[3], Samuel Babatope Adejuyigbe[4]

[1]*Distance Learning Institute, University of Lagos, Akoka, Nigeria*
[2]*Department of Mathematical Sciences, Redeemer's University, Redemption City, Nigeria*
[3]*Department of Statistics, University of Agriculture, Abeokuta, Nigeria*
[4]*Department of Mechanical Engineering, University of Agriculture, Abeokuta, Nigeria*
E-mail: *adewaraja@yahoo.com*, *samadek_2017@yahoo.co.uk*, *asiribo@yahoo.com*
Received September 15, 2011; *revised November* 4, 2011; *accepted November* 12, 2011

Abstract

Minimax control chart uses the joint probability distribution of the maximum and minimum standardized sample means to obtain the control limits for monitoring purpose. However, the derivation of the joint probability distribution needed to obtain the minimax control limits is complex. In this paper the multivariate normal distribution is integrated numerically using Simpson's one third rule to obtain a non-linear polynomial (NLP) function. This NLP function is then substituted and solved numerically using Newton Raphson method to obtain the control limits for the minimax control chart. The approach helps to overcome the problem of obtaining the joint probability distribution needed for estimating the control limits of both the maximum and the minimum statistic for monitoring multivariate process.

Keywords: Minimax, Non-Linear Polynomial, Process, Maximum and Minimum

1. Introduction

Multivariate statistical process control (MSPC) is particularly important in the industries where data are collected on more than one variable. In practice, most of the quality characteristics to be controlled and monitored are not independent. The reason is that most of the variables involved are interconnected, that is, they are correlated. Hence, to monitor these interconnected or correlated variables is not simple but rather complex, especially for manufacturing processes. The use of multiple univariate control charts does not deliver a useful solution in this situation. The problems are that, the overall probability of signaling a false "out-of-control" situation is not controlled and more seriously the correlation among the variables are ignored.

In recent years, multivariate statistical process control (MSPC) procedures have enjoyed wide application in industry. This has resulted from expanded capability to monitor the key variables of a process with sensor and measurement technology, and the widespread availability of computers and statistical software programs that incorporate multivariate SPC capability.

Simultaneously, there have been many new technical developments that have made multivariate SPC more useful. For example, many authors have investigated methods of monitoring multivariate continuous data. [1] developed the multivariate T^2 statistic for quality control purposes. Multivariate generalizations of the CUSUM procedure have been studied by [2] and [3] developed and investigated multivariate exponentially weighted moving averages to identify quality problems. The use of multivariate exponentially weighted moving averages in monitoring multivariate data have been enhanced by [4]. Monitoring principal components of multivariate data has been studied by [5]. [6] discussed multivariate minimax control chart and he used the joint probability distribution function of the minimum and maximum standardized sample means to derive the control limits to make decision if the process is in or out of control. However, the derivation of the joint probability distribution needed to obtain the minimax control limits as discussed by [6] is complex. In this paper we propose a Non-Linear Polynomial function (NLP) approach to multivariate minimax control chart to monitor continuous data as an alternative approach to the use of joint probability for both the ma-

ximum ($Z_{[p]}$) and minimum ($Z_{[1]}$) limits used by [6]. The minimax control limits derived by [6] is modified and the multivariate normal distribution is integrated numerically using Simpson's one third rule to obtain a nonlinear polynomial (NLP) function. This NLP function is then substituted and solved numerically using Newton Raphson method to obtain the control limits for the minimax control chart.

2. Non Linear Polynomial Function

Polynomials are popular in curve and surface representations and many critical problems arising in Computer Aided Geometric Design such as surface integration, are reduced to finding the zero set of a system of nonlinear polynomial equations

$$f(x) = 0 \tag{2.1}$$

where $f = (f_1, f_2 \cdots f_n)$ and each f_i is a polynomial of independent variables $\underline{X} = (X_1, X_2, \cdots X_l)$. Several root-finding algorithms for multivariate polynomial systems (2.1) have been used in practice. Newton type methods, which are classified as *local* solution techniques, have been applied to many problems since they are quadratically convergent and produce accurate results. They, however, require good initial approximations of the roots of the systems, and fail to provide full assurance that all roots have been found. These limitations can be overcome by *global* solution technique, which can be categorized into three different types as proposed by [7]. The different types are algebraic and hybrid methods, homotropy methods, and subdivision methods. Among these techniques, the subdivision methods have been widely used in practice because of their performance and efficiency. The Interval Projected Polyhedral (IPP) algorithm proposed by [7] and [8] is one example, and it has been successfully applied to various problems. One particular interest is locating zeros of a univariate application of polynomial [9].

It is a critical problem in diverse fields such as control theory and many literature has been devoted to it (see e.g. [10]).

Most of the root finding algorithms, however, experience difficulties in dealing with roots with high multiplicity such as performance deterioration and lack of robustness in numerical computation. For example, the IPP algorithm, which belongs to the subdivision class of methods, slows down drastically and suffers from proliferation of boxes that are assumed to enclose roots. Moreover, since a root with high multiplicity is unstable with respect to small perturbation, round-off errors during floating point arithmetic may change the topological aspect in such a way that a cluster of roots could be formed around the root.

Solving univariate polynomials with multiple roots is an important but difficult task. [9] collated nine methods to bound multiple roots of polynomials and compared them rigorously. He also proposed a new hybrid algorithm which gives numerically nearly optimal bounds for multiple roots of univariate polynomials. Even though these methods work well in most cases, it is not easy for a user to control the size of the bound of a root in general. [11] used the Sturm sequences to compute all roots of a univariate polynomial, but his approach relies on the division of polynomials to compute Sturm sequences. So, it is not numerically robust unless exact arithmetic or symbolic computation is used.

This paper focuses on the particular case where the functions $f, i\ \varepsilon \{1, \cdots, Q\}$ in $\begin{cases} x_1 = f_1(s_1, \cdots, s_N) \\ \vdots \ = \quad \vdots \\ x_Q = f_Q(s_1, \cdots, s_N) \end{cases}$ are polynomials.

Thus, we write $X = f(s)$ where f is a nonlinear function $f : C^N \to C^Q$ and $f_1 \cdots f_Q$ constitute the component of *f*. The source separation problem consists of recovering the sources $s_1 \cdots s_N$ from the observation $x_1, \cdots, x_Q$ for all i, $f_i\ \varepsilon\ C(s)$, where $C(s)$ stands for the set of polynomials in variables $s_1, \cdots, s_N$ and with coefficients in *C*. This restriction is partly justified by the difficulty to tackle the nonlinear case because of its generality. In addition, polynomials constitute an important class of nonlinear models which may represent acceptable approximations of certain nonlinearities.

Finally, an important reason to deal with this model is the following:

Consider the case where the multidimensional source vector belongs to a finite set $s\ \varepsilon\ \mathrm{A} = \left\{a^{(1)}, \cdots, a^{(na)}\right\}$. Although seemingly restrictive, this situation is highly interesting since it occurs in digital communications, where the emitted source sequences belong to a finite alphabet depending on the modulation used.

An important observation is that if $s\ \varepsilon\ \mathrm{A}$ and A is finite, all instantaneous mixtures of the sources can be expressed as polynomial mixtures. This follows immediately from the fact that any function on a finite set can be interpolated by a polynomial in a way similar to Lagrange polynomial interpolation [12]. It follows that polynomial mixtures constitute the general model of nonlinear mixtures in the case of sources belonging to a finite alphabet.

The Model

$$\begin{cases} x_1 = f_1(s_1, \cdots, s_N) \\ \vdots \ = \quad \vdots \\ x_Q = f_Q(s_1, \cdots, s_N) \end{cases} \tag{2.2}$$

is a polynomial, and in order to be able to resort to alge-

braic techniques, we will restrict the separator to the class of polynomial functions in $x_1, \cdots, x_Q$, that is, $\forall_i,\ g_i\ \varepsilon\ C[x]$.

2.1. Simpson One Third Rule

The *Simpson's* 1/3rd rule is a numerical method for finding the integral $\int_a^b f(x)\mathrm{d}x$ within some finite limits *a* and *b*. *Simpson's* 1/3rd rule approximates $f(x)$ with a polynomial of degree two *p*(*x*), *i.e.*, a parabola between the two limits *a* and *b*, and then finds the integral of that bounded parabola, and is used to represent the approximate integral $\int_a^b f(x)\mathrm{d}x$. The integral of the approximated function is the area under the parabola bounded by the points *a* and *b* by the positive side of the *x* axis. The quadratic function has three points common to the function *f*(*x*), as follows: The end points of the approximate quadratic function *p*(*x*) is the same as the function *f*(*x*) at points *a* and *b*. *p*(*x*) takes the same value of the function *f*(*x*) at point $m = (a+b)/2$.

Thus three points are fixed each in equal interval $a > m > b$ and a parabola is drawn through these three points *f*(*a*), *f*(*m*), *f*(*b*). The area under the parabola through these points bounded by *a* and *b* with the positive side of the X axis is found and used as the approximated integral value. The iterative formula below can be used to find the integral of a function *f*(*x*) using *Simpson's* 1/3*rd* rule.

$$I_{SI} = \frac{h}{3}\left[f(x_0) + f(x_1) + f(x_2)\right] \tag{2.3}$$

2.2. Newton Raphson Method

The Newton-Raphson method is based on the principle that if the initial guess of the root of $f(x) = 0$ is at x_i, then if one draws the tangent to the curve at $f(x_i)$, the point (x_{i+1}) where the tangent crosses the *x*-axis is an improved estimate of the root.

Using the definition of the slope of a function, at $x = x_i$

$$f'(x) = \tan\theta = \frac{f(x) - 0}{x_i - x_{i+1}} \tag{2.4}$$

Form Equation (2.4) we have

$$x_{i+1} = x_i - \frac{f(x_i)}{f'(x_i)} \tag{2.5}$$

Equation (2.4) is called the Newton-Raphson formula for solving nonlinear equations of the form $f(x) = 0$. So starting with an initial guess, x_i, one can find the next guess, x_{i+1} by using Equation (2.5). One can repeat this process until one finds the root within a desirable tolerance.

Algorithm

The steps of the Newton-Raphson method to find the root of an equation $f'(x) = 0$ are:

Step 1. Evaluate $f'(x)$ symbolically

Step 2. Use an initial guess of the root, *i* x_i, to estimate the new value of the root, x_{i+1} as $x_{i+1} = x_i - \dfrac{f(x_i)}{f'(x_i)}$

Step 3. Find the absolute relative approximate error $|\varepsilon_\alpha|$ as

$$|\varepsilon_\alpha| = \left|\frac{x_{i+1} - x_i}{x_{i+1}}\right| * 100$$

Step 4. Compare the absolute relative approximate error with the pre-specified relative error tolerance, ε_s, If $|\varepsilon_\alpha| > \varepsilon_\alpha$, then go to Step 2, or else stop the algorithm. Also, check if the number of iterations has exceeded the maximum number of iterations allowed. If so, one needs to terminate the algorithm and notify the user.

2.3. Minimax Control Chart

The Minimax control chart developed by Sepulveda [6], and as discussed in [13] is similar to the charts proposed by [14] and [15]. The minimax control chart uses the minimum and maximum standardized sample means to make the decision if the process should be considered in control or out of control. However, the minimax chart uses both lower and upper control limits on both the maximum and minimum standardized sample means. This is facilitated by the development of the capability to determine the value of the joint density function of the maximum and minimum standardized sample means. This not only facilitates a method for setting the control limits, but also allows for the comparison of the performance of the minimax chart relative to other charts through computation of the out-of-control average run length.

Minimax control chart is used to standardize all *p* means and to monitor the maximum and the minimum of those standardized sample means. To do this, the sample average vector $\underset{\sim}{\bar{X}} = (\bar{X}_1, \bar{X}_2, \cdots, \bar{X}_p)$ is calculated and its elements are standardized using the expression:

$$\underset{\sim}{Z} = \frac{\sqrt{n}(\underset{\sim}{\bar{X}} - \underset{\sim}{\mu})}{\sigma} \tag{2.6}$$

where μ is the population mean and σ is the standard deviation. The vector $\underset{\sim}{Z} = [Z_i],\ i = 1, 2, \cdots, p$ is now defined as the standardized sample mean vector. The maximum sample mean (Z_p) is defined as the maximum of the elements of the vector *Z*, that is, $Z_{[p]} = \max(Z_i)$, Also, the minimum standardized sam-

ple mean ($Z_{[1]}$) is defined as the minimum of the elements of the vector *Z*.

The control limits that was proposed by [6] is modified to solve for both upper and lower of maximum and upper and lower of minimum as given in the expression below:

$$\begin{aligned} UCL_{[p]} &= \left\{\tau : \int_{-\infty}^{\tau}\cdots\int_{-\infty}^{\tau} f(Z)\mathrm{d}z = 1-\alpha\right\} \\ LCL_{[p]} &= \left\{\tau : \int_{-\infty}^{\tau}\cdots\int_{-\infty}^{\tau} f(Z)\mathrm{d}z = \alpha\right\} \\ UCL_{[1]} &= \left\{\tau : 1-\int_{\tau}^{\infty}\cdots\int_{\tau}^{\infty} f(Z)\mathrm{d}z\right\} \\ LCL_{[1]} &= \left\{\tau : 1-\int_{\tau}^{\infty}\cdots\int_{\tau}^{\infty} f(Z)\mathrm{d}z = \alpha\right\} \end{aligned} \quad (2.7)$$

3. Results

The data for this research work were collected from the production line of a manufacturing company that produces soft drinks. The samples were drawn from the lines on each variable of the production. The data are secondary and multivariate in nature. The data had five variables which are: X_1 = Contents in ml, X_2 = Brev brix, X_3 = pressure, X_4 = Gas volume (CO_2) and X_5 = Temperature. Thus, $\underset{\sim}{X} = \{X_1, X_2, \cdots, X_n\}$. We assumed that the variables are normally distributed since we are dealing with continuous data. The multivariate normal distribution was integrated numerically using Simpson's one third rule. Simpson's rule is a numerical method that approximates the value of a definite integral by using quadratic polynomials. This approach was applied to the multivariate normal distribution to obtain a non-linear polynomial (NLP) function. This (NLP) function overcomes the problem of obtaining the joint probability distribution needed for the control limits of both the maximum ($Z_{[p]}$) and the minimum ($Z_{[1]}$) statistic. This method was used to determine the position of the five control limits of the chart stated in Equation (2.4). In other to obtain the control limits, an algorithm was developed and implemented on *C* language to fit the polynomial function in the form $Z = 0.0024x^5 + 0.000005x^4 - 0.0444x^3 - 0.00006x^2 + 0.3805x + 0.4988$. Using the obtained polynomial equation, the algorithm in 2.2.1 was then used to obtain the control limits for both the minimum and the maximum statistics. The numerical solution for the control limits using the developed algorithm is presented in the Appendix. The control limits for minimum and maximum statistics for the five variables under consideration are presented in **Table 1**.

Using the obtained control limits in **Table 1**, the process under study was tested for stability. To test for the stability of the process, Equation (2.6) was used to transform the data to obtain the minimum and the maximum values for the five variables. The obtained minimum and maximum values are presented in **Table 2**.

Table 1. The upper and lower control limit for both maximum and minimum statistics.

$UCL_{[p]}$	$LCL_{[p]}$	$UCL_{[1]}$	$LCL_{[1]}$
2.4185	1.954	3.0306	2.7195
–2.9458	–1.3148	–3.877	–3.3942

Table 2. The maximum and the minimum values.

Maximum	0.018725	0.021426	0.021987	0.022794	0.0357959
Minimum	0.005012	–0.00226	–0.03127	–0.03031	–0.00954

4. Discussion of Result

The values in **Table 2** are arranged from the lowest to the highest. Thus minimum of $Z_{[p]}$ is 0.018725, and maximum of $Z_{[p]}$ is 0.0357959. Also the minimum of $Z_{[1]}$ is –0.031271 and the maximum of $Z_{[1]}$ is 0.005012. Comparing these values with the control limit in **Table 1**, the result shows that the minimum and maximum values obtained are within the control limits. Hence, the production process under consideration can be adjudged as being stable.

5. Conclusions

Minimax multivariate control chart is another sensitive multivariate control chart that has upper and lower control limits for both maximum and the minimum statistics for monitoring a multivariate process. The paper has addressed the use of numerical solution for obtaining the control limits of the minimax control chart as an alternative to the use of joint probability distribution.

6. References

[1] H. Hotelling, "Multivariable Quality Control—Illustrated by the Air Testing of Sample Bombsights," In: C. Eisenhart, M. W. Hastay and W. A. Wallis, Eds., *Techniques of Statistical Analysis*, McGraw Hill, New York, 1947, pp. 111-184.

[2] W. H. Woodall and M. M. Ncube, "Multivariate Cusum Quality Control Procedures," *Technometrics*, Vol. 27, No. 3, 1985, pp. 285-292. doi:10.2307/1269710

[3] C. A. Lowry, W. H. Woodall, C. W. Champ and S. E. Rigdon, "A Multivariate Exponentially Weighted Moving Average Control Chart," *Technometrics*, Vol. 34, No. 1, 1992, p. 46. doi:10.2307/1269551

[4] G. C. Runger, J. B. Keats, D. C. Montgomery and R. D. Scranton, "Improving the Performance of the Multivariate Exponentially Weighted Moving Average Control Chart," *Quality and Reliability International*, Vol. 15, No.

3, 1996, pp. 161-166. doi:10.1002/(SICI)1099-1638(199905/06)15:3<161::AID-QRE215>3.0.CO;2-V

[5] C. M. Mastrangelo, G. C. Runger and D. C. Montgomery, "Statistical Process Monitoring with Principal Components," *Quality and Reliability International*, Vol. 12, No. 3, 1996, pp. 203-210. doi:10.1002/(SICI)1099-1638(199605)12:3<203::AID-QRE12>3.0.CO;2-B

[6] A. Sepulveda, "The Minimax Control Chart for Multivariate Quality Control," Dissertation, Department of Industrial and Systems Engineering, Virginia Polytechnic Institute and State University, Blacksburg, 1996.

[7] N. M. Patrikalakis and T. Maekawa, "Shape Interrogation for Computer Aided Design and Manufacturing," Springer-Verlag, Heidelberg, 2002.

[8] E.C. Sherbrooke and N. M. Patrikalakis, "Computation of the Solutions of Nonlinear Polynomial Systems," *Computer Aided Geometric Design*, Vol. 10, No. 5, 1993, pp. 379-405. doi:10.1016/0167-8396(93)90019-Y

[9] S. M. Rump, "Ten Methods To Bound Multiple Roots of Polynomials," *Journal of Computational and Applied Mathematics*, Vol. 156, No. 2, 2003, pp. 403-432. doi:10.1016/S0377-0427(03)00381-9

[10] .M. McNamee, "A Bibliography On Roots of Polynomials," *Journal of Computational and Applied Mathematics*, Vol. 47, No. 3, 1993, pp. 391-394. doi:10.1016/0377-0427(93)90064-I

[11] H. S. Wilf, "A Global Bisection Algorithm for Computing the Zeros of Polynomials in the Complex Plane," *Journal of the Association for Computing Machinery*, Vol. 25, No. 3, 1978, pp. 415-420. doi:10.1145/322077.322084

[12] A. C. David, L. John and O. Donal, "Ideals, Varieties and Algorithms: An Introduction to Computational Algebraic Geometry and Commutative Algebra," Springer, 2nd Edition, Berlin, 1996.

[13] J. Rehmert, "A Performance Analysis of the Minimax Multivariate Quality Control Chart," M.Sc. Dissertation, Department of Industrial and Systems Engineering, Virginia Polytechnic Institute and State University, Blacksburg, 1997.

[14] A. J. Hayter and K. L. Tsui, "Identification and Quantification in Multivariate Quality Control Problems," *Journal of Quality Technology*, Vol. 26, 1994, pp. 197-208.

[15] N. H. Timm, "Multivariate Quality Control Using Finite Intersection Tests," *Journal of Quality Technology*, Vol. 28, 1996, pp. 233-243.

Appendix: Numerical Solution

The numerical solutions for the control limits is

$$Z(x) = 0.0024X^5 + 5\times10^{-5}X^4 - 0.444X^3 - 6\times10^{-5}X^2 + 0.3805X + 0.4988$$

The multiple integral of Equation (2.6) is solved below:

$$\int\left(0.0024X^5 + 5\times10^{-5}X^4 - 0.444X^3 - 6\times10^{-5}X^2 + 0.3805X + 0.4988\right)\mathrm{d}x =$$

$$\frac{0.0024X^6}{6} + \frac{5\times10^{-6}X^5}{5} - \frac{0.444X^4}{4} - \frac{6\times10^{-5}X^3}{3} + \frac{0.3805X^2}{2} + 0.4988X$$

$$\int\left(\frac{0.0024X^6}{6} + \frac{5\times10^{-6}X^5}{5} - \frac{0.444X^4}{4} - \frac{6\times10^{-5}X^3}{3} + \frac{0.3805X^2}{2} + 0.4988\right)\mathrm{d}x =$$

$$\frac{0.0024X^7}{7\times6} + \frac{5\times10^{-6}X^6}{6\times5} - \frac{0.444X^5}{5\times4} - \frac{6\times10^{-5}X^4}{4\times3} + \frac{0.3805X^3}{3\times2} + \frac{0.4988X^2}{1\times2}$$

$$\int\left(\frac{0.0024X^7}{7\times6} + \frac{5\times10^{-6}X^6}{6\times5} - \frac{0.444X^5}{5\times4} - \frac{6\times10^{-5}X^4}{4\times3} + \frac{0.3805X^3}{3\times2} + \frac{0.4988X^2}{1\times2}\right)\mathrm{d}x =$$

$$\frac{0.0024X^8}{7\times6\times8} + \frac{5\times10^{-6}X^7}{6\times5\times7} - \frac{0.444X^6}{5\times4\times6} - \frac{6\times10^{-5}X^5}{4\times3\times5} + \frac{0.3805X^4}{3\times2\times4} + \frac{0.4988X^3}{1\times2\times3}$$

$$\frac{0.0024X^9}{7\times6\times8\times9} + \frac{5\times10^{-6}X^8}{6\times5\times7\times8} - \frac{0.444X^7}{5\times4\times6\times7} - \frac{6\times10^{-5}X^6}{4\times3\times5\times6} + \frac{0.3805X^5}{3\times2\times4\times5} + \frac{0.4988X^4}{1\times2\times3\times4}$$

The possible solutions for the numerical algorithm of the multiple integral are given below.

-7.5249

$-4.2219 - 4.8351i$

$-4.2219 + 4.8351i$

-2.9458

$3.1708\times10^3x^5 + 2.0783\times10^2x^4 - 0.95)$, *roots*:

$0.24197 - 2.5085i$

$0.24197 + 2.5085i$

2.4185

$8.0042 - 4.6104i$

$8.0042 + 4.6104i$

$7.9366\times10^{-7}x^9 + 2.9763\times10^{-9}x^8 - 5.2857\times10^{-5}x^7 - 1.6667\times10^{-7}x^6 +$

-7.5651

$-4.223 - 4.7726i$

$-4.223 + 4.7726i$

-1.3148

$3.1708\times10^{-3}x^5 + 2.0783\times10^{-2}x^4 - 0.05)$, *roots*:

$5.8498\times10^{-2} - 1.2355i$, *roots*

$5.8498\times10^{-2} + 1.2355i$

1.1954

$8.0048 - 4.6049i$

$8.0048 + 4.6049i$

$$1-\sqrt{2*3.141592654}-(7.9366\times10^{-7}x^{9}+2.9763\times10^{-9}x^{8}-5.2857\times10^{-5}x^{7}-$$
$$-7.4507$$
$$-4.2262-4.928i$$
$$-4.2262+4.928i$$
$$-3.877$$
$$1.6667\times10^{-7}x^{6}+3.1708\times10^{-3}x^{5}+2.0783\times10^{-2}x^{4}))-0.95),\ root:$$
$$0.36978-3.1125i$$
$$0.36978+3.1125i$$
$$3.0306$$
$$8.0031-4.6195i$$
$$8.0031+4.6195i$$
$$1-(\sqrt{2*3.141592654}-(7.9366\times10^{-7}x^{9}+2.9763\times10^{-9}x^{8}-5.2857\times10^{-5}x^{7}-$$
$$-74962$$
$$-4.2229-4.8741i$$
$$-4.2229+4.8741i$$
$$-3.3942$$
$$1.6667\times10^{-7}x^{6}+3.1708\times10^{-3}x^{5}+2.0783\times10^{-2}x^{4}))-0.05,\ roots:$$
$$0.30276-2.8096i$$
$$0.30276+2.8096i$$
$$2.7195$$
$$8.0037-4.614i$$
$$8.0037+4.614i$$

Applied Mathematics, 2011, 2, 1546-1550
doi:10.4236/am.2011.212220 Published Online December 2011 (http://www.SciRP.org/journal/am)

Test of Generating Function and Estimation of Equivalent Radius in Some Weapon Systems and Its Stochastic Simulation

Famei Zheng
School of Mathematical Science, *Huaiyin Normal University*, *Huai'an*, *China*
E-mail: *hysyzfm*@163.*com*, 16032@*hytc.edu.cn*, *hssky*10@163.*com*
Received November 16, 2011; *revised December* 6, 2011; *accepted December* 14, 2011

Abstract

We discuss three-dimensional uniform distribution and its property in a sphere; give a method of assessing the tactical and technical indices of cartridge ejection uniformity in some type of weapon systems. Meanwhile we obtain the test of generating function and the estimation of equivalent radius. The uniformity of distribution is tested and verified with ω^2 test method on the basis of stochastic simulation example.

Keywords: Uniform Distribution in a Sphere, Weapon Systems, Generating Function, Equivalent Radius, Stochastic Simulation

1. Introduction

Uniform distribution is very important in the probability statistics, many scholars pay attention to it. The following questions have been explored: the estimate of interval length about uniform distribution in [*a*,*b*] [1,2], the estimate of regional area about two dimension uniform distribution in a rectangle [3], the estimate of cuboid volume about three dimension uniform distribution [4], the estimate of regional area about two-dimensional uniform distribution in a circle [5,6], estimate of radius on three-dimensional uniform distribution in a sphere [7]. In addition, many scholars get useful test statistics and limit theorems [8-12]. In this paper, basing on some articles [13-18], according to t the indices of cartridge ejection uniformity in some type of weapon systems, we give the test of generating function and the estimation of equivalent radius by simulation example.

Definition 1 [7]. If (X,Y,Z) is three-dimensional continuous random variable, its probability density function is

$$f(x,y,z)=\begin{cases}\dfrac{3}{4\pi R_0^3}, & (x,y,z)\in G,\\ 0 & (x,y,z)\notin G.\end{cases} \tag{1.1}$$

where $G=\left\{(x,y,z)\middle|x^2+y^2+z^2<R_0^2\right\}, R_0>0$, then we call that (X,Y,Z) obeys uniform distribution in $G=\left\{(x,y,z)\middle|x^2+y^2+z^2<R_0^2\right\}$, recorded as $(X,Y,Z)\sim U(G)$.

Give a transformation

$$\begin{cases}x=r\sin\varphi\cos\theta\\ y=r\sin\varphi\sin\theta\\ z=r\cos\varphi\end{cases}(0<r<R_0,0<\varphi<\pi,0<\theta<2\pi) \tag{1.2}$$

The probability density function of three-dimensional *r.v.* (R,Φ,Θ) is

$$h(r,\varphi,\theta)=f(r\sin\varphi\cos\theta,r\sin\varphi\sin\theta,r\cos\varphi)\left|\frac{\partial(x,y,z)}{\partial(r,\varphi,\theta)}\right| \tag{1.3}$$

in which $0<r<R_0, 0<\varphi<\pi, 0<\theta<2\pi$, $\dfrac{\partial(x,y,z)}{\partial(r,\varphi,\theta)}$ is Jacobi determinant of the transformation (1.2), and

$$\begin{aligned}\frac{\partial(x,y,z)}{\partial(r,\varphi,\theta)}&=\begin{vmatrix}\dfrac{\partial x}{\partial r} & \dfrac{\partial x}{\partial\varphi} & \dfrac{\partial x}{\partial\theta}\\ \dfrac{\partial y}{\partial r} & \dfrac{\partial y}{\partial\varphi} & \dfrac{\partial y}{\partial\theta}\\ \dfrac{\partial z}{\partial r} & \dfrac{\partial z}{\partial\varphi} & \dfrac{\partial z}{\partial\theta}\end{vmatrix}\\ &=\begin{vmatrix}\sin\varphi\cos\theta & r\cos\varphi\cos\theta & -r\sin\varphi\sin\theta\\ \sin\varphi\sin\theta & r\cos\varphi\sin\theta & r\sin\varphi\cos\theta\\ \cos\varphi & -r\sin\varphi & 0\end{vmatrix}\\ &=r^2\sin\varphi\end{aligned} \tag{1.4}$$

Therefore the probability density function of (R,Φ,Θ) is

$$h(r,\varphi,\theta)=\begin{cases}\dfrac{3r^2\sin\varphi}{4\pi {R_0}^3}, & 0<r<R_0, 0<\varphi<\pi, 0<\theta<2\pi\\ 0, & \text{otherwise}\end{cases} \tag{1.5}$$

Theorem 1. If the marginal density functions of $r.v.$ (R,Φ,Θ) about R,Φ,Θ are $h_1(r)$, $h_2(\varphi)$, $h_3(\theta)$, then

1) $h_1(r)=\begin{cases}\dfrac{3r^2}{R_0^3}, & 0<r<R_0,\\ 0, & \text{otherwise.}\end{cases}$

2) $h_2(\varphi)=\begin{cases}\dfrac{1}{2}\sin\varphi, 0<\varphi<\pi,\\ 0, & \text{otherwise.}\end{cases}$

3) $h_3(\theta)=\begin{cases}\dfrac{1}{2\pi}, & 0<\theta<2\pi,\\ 0, & \text{otherwise.}\end{cases}$

Proof. According to (1.5) and the definition of marginal density function, we have

$$\begin{aligned}h_1(r)&=\int_0^{\pi}\int_0^{2\pi}h(r,\varphi,\theta)\mathrm{d}\varphi\mathrm{d}\theta\\ &=\int_0^{\pi}\int_0^{2\pi}\frac{3r^2\sin\varphi}{4\pi R_0^3}\mathrm{d}\varphi\mathrm{d}\theta=2\pi\times\frac{3r^2}{4\pi {R_0}^3}\int_0^{\pi}\sin\varphi\mathrm{d}\varphi\\ &=2\pi\times\frac{3r^2}{4\pi {R_0}^3}\times 2=\frac{3r^2}{{R_0}^3},\end{aligned}$$

where $0<r<R_0$,

$$\begin{aligned}h_2(\varphi)&=\int_0^{R_0}\int_0^{2\pi}h(r,\varphi,\theta)\mathrm{d}r\mathrm{d}\theta=\int_0^{R_0}\int_0^{2\pi}\frac{3r^2\sin\varphi}{4\pi {R_0}^3}\mathrm{d}r\mathrm{d}\theta\\ &=2\pi\times\frac{3\sin\varphi}{4\pi R_0^3}\int_0^{R_0}r^2\mathrm{d}r=\frac{1}{2}\sin\varphi,\end{aligned}$$

where $0<\varphi<\pi$,

$$\begin{aligned}h_3(\theta)&=\int_0^{R_0}\int_0^{\pi}h(r,\varphi,\theta)\mathrm{d}r\mathrm{d}\varphi=\int_0^{R_0}\int_0^{\pi}\frac{3r^2\sin\varphi}{4\pi {R_0}^3}\mathrm{d}r\mathrm{d}\varphi\\ &=\frac{3}{4\pi R_0^3}\int_0^{R_0}r^2\mathrm{d}r\int_0^{\pi}\sin\varphi\mathrm{d}\varphi=\frac{3}{4\pi {R_0}^3}\times\frac{1}{3}{R_0}^3\times 2\\ &=\frac{1}{2\pi},\end{aligned}$$

where $0<\theta<2\pi$.

Corollary 1 [7]. If $r.v.$ (R,Φ,Θ) is defined by (1.5), then three $r.v.$ R,Φ,Θ are independent each other.

Corollary 2. If $r.v.$ (R,Φ,Θ) is defined by (1.5), the marginal distribution function of $r.v.$ (R,Φ,Θ) about R,Φ,Θ are $H_1(r),H_2(\varphi),H_3(\theta)$, then

$$H_1(r)=\begin{cases}0, & r\le 0\\ \dfrac{r^3}{R_0^3}, & 0<r<R_0\\ 1, & r\ge R_0\end{cases},$$

$$H_2(\varphi)=\begin{cases}0, & \varphi\le 0\\ \dfrac{1}{2}(1-\cos\varphi), & 0<\varphi<\pi\\ 1, & \varphi\ge\pi\end{cases},$$

$$H_3(\theta)=\begin{cases}0, & \theta\le 0\\ \dfrac{\theta}{2\pi}, & 0<\theta<2\pi\\ 1, & \theta\ge 2\pi\end{cases}.$$

Proof. According to theorem 1, we can get it easily.

Corollary 3. If $E(R)=\mu$, $Var(R)=\sigma^2$, then the probability of cartridges falling into a ball with radius μ is about 42.2%, and the probability of cartridges falling into a sphere with radius $\mu+\sigma$ is about 84.0%.

Proof. By the definition of Mathematical expectation, we have

$$\mu=E(R)=\int_0^{R_0}rh_1(r)\mathrm{d}r=\frac{3}{4}R_0 \tag{1.6}$$

$$E(R^2)=\int_0^{R_0}r^2h_1(r)\mathrm{d}r=\int_0^{R_0}\frac{3r^4}{R_0^3}\mathrm{d}r=\frac{3}{5}R_0^2 \tag{1.7}$$

then

$$\sigma^2=D(R)=E(R^2)-E^2(R)=\frac{3}{5}R_0^2-\frac{9}{16}R_0^2=\frac{3}{80}R_0^2$$

and $\sigma=\dfrac{\sqrt{15}}{20}R_0$, then the probability of cartridges falling into a sphere with radius μ is about

$$H_1(\mu)=H_1\left[E(R)\right]=H_1\left[\frac{3}{4}R_0\right]\approx 42.2\% \tag{1.8}$$

then the probability of cartridges falling into a sphere with radius $\mu+\sigma$ is about

$$H_1\left(\mu+\sigma\right)=H_1\left(\frac{3}{4}R_0+\frac{\sqrt{15}}{20}R_0\right)\approx 84.0\% \tag{1.9}$$

2. Test of Generating Distribution Function

Usually there are χ^2 test method, ω^2 test method and Cole Moge Rove test method (K test method) [17] to test distribution function. Here, we use ω^2 test method, we want to know the sub-sample is uniform distribution or not. Because the locations of any cartridges are ascertained by three-dimensional $r.v.$ (R,Φ,Θ), so we should

test them one by one, test $R \sim H_1(r)$, $\Phi \sim H_2(\varphi)$, $\Theta \sim H_3(\theta)$. We give testing hypotheses H_0

$$H_0 : F(x) = \Phi_0(x)$$

where $F(x)$ is generating distribution function, $\Phi_0(x)$ is known distribution function, and $\varphi_0(x)$ is the derivative of $\Phi_0(x)$.

Tests for generating function should be independent, $y_{(1)}, y_{(2)}, \cdots, y_{(n)}$ is the sequent sub-sample of the test, under hypotheses H_0 is correct, the statistic

$$n\omega^2 = \frac{1}{12n} + \sum_{i=1}^{n}\left[\Phi_0(y_{(i)}) - \frac{2i-1}{2n}\right]^2 \tag{2.1}$$

is Smirnov distribution. For the given confidence level α, according to the Table 10 in [17], we obtain the boundary value z_α of $n\omega^2$, in which $P(n\omega^2 > z_\alpha) = \alpha$. Then (z_α, ∞) is rejection region of the hypotheses H_0, when $n\omega^2 > z_\alpha$, we reject H_0, if $n\omega^2 \le z_\alpha$, we should accept H_0.

3. Estimation of Equivalent Radius

On the supposition that N is the number of cartridges from a shrapnel, n is the actual observed number of cartridges within a certain region near the centre of dispersion. When calculating equivalent radius, we presume all the cartridges are found. The distances from any cartridges to the dispersion centre point A are recorded as $r_i (i = 1, 2, \cdots, n)$, let $\bar{r} = \frac{1}{n}\sum_{i=1}^{n} r_i$. According to the properties of density function $h_1(r)$, we know that R obeys uniform distribution in a ball with radius

$r_{n0} (0 < r_{n0} < R_0)$, $E(R) = \frac{3}{4} r_{n0}$ (by 1.6), owing to

$$E(\bar{r}) = E\left(\frac{1}{n}\sum_{i=1}^{n} r_i\right) = \frac{1}{n}\sum_{i=1}^{n}\int_0^{r_{n0}} r_i \frac{3r_i^2}{r_{n0}^3} dr_i = \frac{3}{4} r_{n0} \tag{3.1}$$

so $\hat{r}_{n0}$ is a unbiased estimate of r_{n0} [7]. on the basis of the properties of distribution function, let $\varphi = \pi, \theta = 2\pi$, we have $H(r) = H(r, \varphi, \theta)\Big|_{\theta = 2\pi}^{\varphi = \pi}$, let $N \to \infty$, (N is amount of test cartridges)，then

$$\lim_{N\to\infty} H(r, \varphi, \theta)\Big|_{\theta = 2\pi}^{\varphi = \pi} = \lim_{N\to\infty} \frac{n}{N} = \frac{r_{n0}^3}{R_0^3} \tag{3.2}$$

Therefore let $\hat{R}_0 = \sqrt{\frac{N}{n}}\hat{r}_{n0}$, that is $\hat{R}_0 = \frac{4}{3n}\sqrt{\frac{N}{n}}\sum_{i=1}^{n} r_i$, and

$$D(\hat{R}_0) = \frac{16N}{9n^2} D(r_i) \tag{3.3}$$

As well as by (1.7), $D(r_i) = \frac{3}{80} r_{n0}^2$, substitute into (3.3), we obtain

$$\begin{aligned} D(\hat{R}_0) &= \frac{16N}{9n^2} D(r_i) = \frac{16N}{9n^2} \times \frac{3}{80} r_{n0}^2 = \frac{N r_{n0}^2}{15n^2}, \\ \sigma(\hat{R}_0) &= \frac{\sqrt{15N}\, r_{n0}}{15n} \end{aligned} \tag{3.4}$$

Based on Formula (3.4), if N is large enough, when $n \to N$, $\sigma(\hat{R}_0)$ becomes small enough. In order to decrease estimating error of equivalent radius R_0, sample size is large enough.

4. Stochastic Simulation

In order to verify the correctness of above methods, we give a simulation example. For some type of weapon systems, assuming the tactical technical requirements, the cartridges from single shrapnel should be more evenly scattered in a ball with equivalent radius (120 ± 20) m, launching a shrapnel, the number of cartridges is N = 400, measuring the coordinates of one hundred cartridges near the dispersion centre (n = 100), they were produced by computer simulation basing on uniform requirements in a sphere, *i.e.* (r, φ, θ) were produced by stochastic simulation according to the following formulas

$$\begin{gathered} r = \sqrt[3]{H_1(r)}\, r_{n0}, \varphi = \arccos\left[1 - 2H_2(\varphi)\right], \\ \theta = 2\pi H_3(\theta) \end{gathered} \tag{4.1}$$

where, $r_{n0} = 60$, $H_1(r)$, $H_2(\varphi)$, $H_3(\theta)$ are random number produced by stochastic simulation in (0,1), coordinates for cartridges as below **Table 1**, and the MATLAB program as below,

```
>> clear
for k=1:100
      r=rand(1,3);
            x=60*sqrt(r(1));
            y=acos(-2*r(2)+1);
            z=2*pi*r(3);
[x, y, z]
 end
>>clear
for k=1:100
a=(x^2-((2*k-1)/200))^2;
b=(y^2/3600-((2*k-1)/200))^2;
c=(z^2/3600-((2*k-1)/200))^2;
[a, b, c]
end

>> clear
for k=1:100
s=1/1200+sum(a);
u=1/1200+sum(b);
v=1/1200+sum(c);
[s u v]
End
```


Table 1. Polar coordinates points of fall for cartridges.

$(r/m, \varphi/rad, \theta/rad)$			$(r/m, \varphi/rad, \theta/rad)$			$(r/m, \varphi/rad, \theta/rad)$			$(r/m, \varphi/rad, \theta/rad)$		
57.8262	1.1283	0.0936	56.9007	1.7096	0.0811	55.0439	0.4464	5.2025	47.7960	0.6985	5.5996
58.8251	1.3574	1.8108	33.8961	1.4923	1.9503	43.4513	2.1067	5.7655	33.1923	2.1410	3.0668
41.6750	1.5768	5.1315	19.1279	1.4612	4.8952	45.6907	2.4810	0.7106	48.3936	1.3183	6.2367
45.5454	2.0309	6.1921	54.1207	0.6013	1.9308	47.0793	1.1287	5.1026	51.7387	2.2742	2.3455
46.6895	1.1728	0.1093	48.7537	1.4576	5.8226	50.8327	1.0500	5.7070	15.1818	0.4352	3.3389
31.8301	0.6831	5.1484	39.0650	1.3001	4.2644	33.6245	2.6167	0.9827	56.5426	1.7679	1.1391
30.8478	1.4572	3.9025	43.0160	1.1647	0.4668	7.5595	0.7407	0.7672	55.7802	2.6869	3.1535
48.6323	1.5043	3.5198	14.0717	2.3512	0.4442	55.4707	2.6500	4.7922	53.2184	1.1347	2.6528
53.9209	0.2431	1.5331	57.6967	2.1165	0.0748	48.0499	1.9865	4.5352	46.3803	2.4616	4.1494
44.1604	1.9052	5.1648	57.1905	2.6896	1.4275	35.8438	2.3398	4.0941	26.1303	0.6488	4.2330
42.6194	2.0355	1.6537	38.0081	1.6869	3.2440	28.1616	0.9503	4.7375	56.1754	0.5168	6.0149
39.4989	1.1188	4.7350	49.7335	0.2389	2.8790	32.3887	1.4809	4.1670	34.6740	1.0105	1.2057
57.2477	1.0742	4.1444	32.5254	1.7644	4.4183	44.4830	0.5776	5.5512	45.8214	2.6183	0.6987
51.3376	2.0009	1.3452	50.4480	2.2554	3.6600	44.4939	2.3493	1.7103	14.1080	0.5078	3.5506
37.3488	2.1746	3.7831	41.5086	2.8378	3.1994	22.4951	1.6951	2.6352	40.5506	1.0797	6.0897
59.5588	2.9061	3.8007	52.2026	0.9810	0.4668	58.8127	1.2010	1.3383	57.3967	3.0969	0.1489
51.7199	1.5174	4.1438	57.1376	1.9904	1.2139	31.8798	1.3179	0.2237	56.5065	0.9570	5.4676
36.7509	2.5075	1.1523	49.6781	1.6150	2.3851	43.6260	2.3973	0.5102	41.5920	1.5676	0.1690
52.7956	1.4728	3.9992	59.6074	2.6175	1.7367	40.6554	1.3123	5.3445	57.5123	1.1385	3.2641
52.3921	2.2256	1.0700	55.5081	2.0117	4.8437	33.1399	0.5499	2.1375	46.9686	1.9237	1.2083
30.7568	2.2887	3.3904	32.0629	0.9956	1.9723	57.8563	0.9268	2.9292	49.4790	2.7288	4.4969
16.9386	0.8401	3.9169	56.4546	1.4698	4.0099	41.1545	0.4487	5.7416	51.0491	2.1332	1.5752
38.4027	1.3570	4.3096	34.6080	0.8558	6.1990	54.1232	1.7046	1.4363	52.2896	1.9094	5.8679
29.3040	1.6124	4.2556	51.6795	2.7865	3.1598	44.6063	0.7133	5.4161	51.0684	0.7404	0.8621
24.6450	2.0222	5.5091	52.4759	1.2780	5.9546	44.2010	1.6150	4.1255	52.8935	0.6280	3.2773

According to the data in **Table 1** and methods in this paper, using above MATLAB program, we obtain

$$n\omega_r^2 = 0.0888, n\omega_\varphi^2 = 0.0425, n\omega_\theta^2 = 0.0749$$

$$\hat{R}_0 = 117.4909, \sigma(\hat{R}_0) = 3.0984$$

Take conspicuous level $\alpha = 10\%$, seeing the Table 10 in [17], we obtain the boundary value $z_\alpha = 0.3472$ for $n\omega^2$. Because $n\omega_r^2$, $n\omega_\varphi^2$, $n\omega_\theta^2$ are less than 0.3472, so we consider that cartridges obeys uniform distribution in a sphere.

5. References

[1] G. S. Chen, "Interval Estimate of the Interval Length on Uniform Distribution," *Pure and Applied Mathematics*, Vol. 22, No. 3, 2006, pp. 349-354.

[2] H. B. Zhang, "The Shortest Confidence Interval of the Interval Length on Uniform Distribution," *Journal of Xiaogan University*, Vol. 27, No. 3, 2007, pp. 52-55.

[3] Z. J. Liu, "Estimate of Rectangle Region Area on Two Dimensional Uniform Distribution," *College Mathematics*, Vol. 23, No. 4, 2007, pp. 155-159.

[4] Z. J. Liu, "Estimate of Cuboid Volume on Three-Dimensional Uniform Distribution," *Statistics and Decision*, No. 5, 2007, pp. 23-24.

[5] Z. X. Wang, "Parameter Estimation of Two-Dimensional Uniform Distribution in a Circle," *College Mathematics*, Vol. 24, No. 2, 2008, pp. 150-152.

[6] W. Q. Jin, D. S. Cui and B. Deng, "On the Testing and Estimation of Uniform Distribution in a Circle," *Acta Armamentarii*, Vol. 22, No. 4, 2001, pp. 468-472.

[7] F. M. Zheng, "Estimate of Radius on Three-Dimensional Uniform Distribution in a Sphere," *Mathematics in Practice and Theory*, Vol. 40, No. 14, 2010, pp. 166-170.

[8] Y. X. Liu and P. Cheng, "Uniform Distribution of Ball PPCM Test Statistic on Dimension and Sample Size Berry-Esseen Boundary and LIL," *China Science Bulletin*, Vol. 43, No. 13, 2005, pp. 1452-1453.

[9] S. R. Xie, "Two Types of Stay Limit Theorems of Non-Stationary Gaussian Process," *Science in China*, *Series A*, Vol. 23, No. 4, 1993, pp. 369-376.

[10] Z. S. Hu and C. Su, "Limit Theorems for the Number and Sum of Near-Maxima for Medium Tails," *Statistics & Probability Letters*, Vol. 63, No. 3, 2003, pp. 229-237. doi:10.1016/S0167-7152(03)00085-3

[11] Y. Qi, "Limit Distributions for Products of Sums," *Statistics & Probability Letters*, Vol. 62, No. 1, 2007, pp. 93-100. doi:10.1016/S0167-7152(02)00438-8

[12] G. Rempala and J. Wesolowski, "Asymptotics for Products of Sums and U-Statistics," *Electronic Communications in Probability*, Vol. 7, No. 7, 2002, pp. 47-54.

[13] K. T. Fang, J. Q. Fan, H. Jin, *et al.*, "Statistical Analysis of Directional Date," *Journal of Application of Statistics and Management*, Vol. 9, No. 2, 1990, pp. 59-65.

[14] M. D. Troutt, W. K. Pang and S. H. Hou, "Vertical Density Representation and Its Applications," World Scientific Publishing Co. Pte. Ltd, Singapore, 2004. doi:10.1142/9789812562616

[15] Z. S. Wei, "Probability Theory and Mathematical Statistics," Higher Education Press, Beijing, 1983.

[16] S. M. Berman, "Extreme Sojourns of a Gaussian Process with a Point of Maximum Variance," *Probability Theory and Related Fields*, Vol. 74, 1987, pp. 113-124. doi:10.1007/BF01845642

[17] C. P. Pan and Z. J. Han, "Probability and Statistic of Weapon Test," National Defence Industry Press, Beijing, 1979.

[18] N. I. Sidnyaev and K. S. Andreytseva, "Independence of the Residual Quadratic Sums in the Dispersion Equation with Noncentral χ^2-Distribution," *Applied Mathematics*, Vol. 2, No. 2, 2011, pp. 1303-1308.

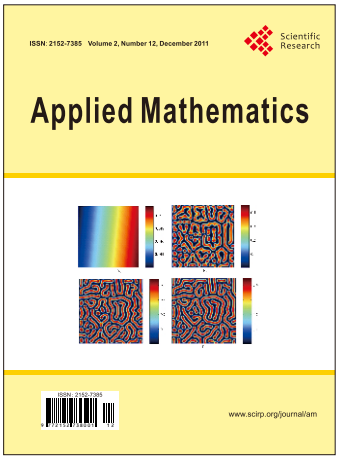

Call for Papers

Applied Mathematics (AM)

ISSN Print: 2152-7385 ISSN Online: 2152-7393
http://www.scirp.org/journal/am

Applied Mathematics **(AM)** is an international journal dedicated to the latest advancement of applied mathematics. The goal of this journal is to provide a platform for scientists and academicians all over the world to promote, share, and discuss various new issues and developments in different areas of applied mathematics.

Subject Coverage

All manuscripts must be prepared in English, and are subject to a rigorous and fair peer-review process. Accepted papers will immediately appear online followed by printed hard copy. The journal publishes original papers including but not limited to the following fields:

- Applied Probability
- Applied Statistics
- Approximation Theory
- Chaos Theory
- Combinatorics
- Complexity Theory
- Computability Theory
- Computational Methods in Mechanics and Physics
- Continuum Mechanics
- Control Theory
- Cryptography
- Discrete Geometry
- Dynamical Systems
- Elastodynamics
- Evolutionary Computation
- Financial Mathematics
- Fuzzy Logic
- Game Theory
- Graph Theory
- Information Theory
- Inverse Problems
- Mathematical Biology
- Mathematical Chemistry
- Mathematical Economics
- Mathematical Physics
- Mathematical Psychology
- Mathematical Sociology
- Matrix Computations
- Neural Networks
- Nonlinear Processes in Physics
- Numerical Analysis
- Operations Research
- Optimal Control
- Optimization
- Ordinary Differential Equations
- Partial Differential Equations
- Probability Theory
- Statistical Finance
- Stochastic Processes
- Theoretical Statistics

We are also interested in: 1) Short Reports—2-5 page papers where an author can either present an idea with theoretical background but has not yet completed the research needed for a complete paper or preliminary data; 2) Book Reviews—Comments and critiques.

Notes for Intending Authors

Submitted papers should not have been previously published nor be currently under consideration for publication elsewhere. Paper submission will be handled electronically through the website. All papers are refereed through a peer review process. For more details about the submissions, please access the website.

Website and E-Mail

http://www.scirp.org/journal/am **E-mail: am@scirp.org**

Applied Mathematics, 2011, 2, 1425-1550
Published Online December 2011 in SciRes (http://www.SciRP.org/journal/am/).

TABLE OF CONTENTS

Volume 2 Number 12 **December 2011**

